Bulletin 244

AUSTRALIA

Geology of the Bunger Hills–Denman Glacier region, East Antarctica

J.W. Sheraton, R.J. Tingey, R.L. Oliver & L.P. Black

AGSO
AUSTRALIAN GEOLOGICAL SURVEY ORGANISATION

AUSTRALIAN GEOLOGICAL SURVEY ORGANISATION
DEPARTMENT OF PRIMARY INDUSTRIES AND ENERGY

BULLETIN 244

Geology of the Bunger Hills–Denman Glacier region, East Antarctica

J.W. SHERATON[1], R.J. TINGEY[2], R.L. OLIVER[3] & L.P. BLACK[1]

[1] *Division of Regional Geology & Minerals, AGSO*
[2] *Division of Environmental Geoscience & Groundwater, AGSO*
[3] *Department of Geology & Geophysics, University of Adelaide*

AUSTRALIAN GOVERNMENT PUBLISHING SERVICE
CANBERRA

ISSN 0084–7089

ISBN 0644 452471

Editor: Ian Hodgson
Cover design and figures prepared by AGSO Cartographic Services Unit unless otherwise indicated
Prepared for publication by Lin Kay

Produced by the Australian Government Publishing Service.

***Front-cover illustration*:**

View of eastern Thomas Island, looking southeast towards the northeastern Bunger Hills and the polar plateau beyond. In the foreground are dolerite dykes cutting interlayered orthogneiss and paragneiss, whereas Black Island (top right) consists mainly of gabbro of the Booth Peninsula Batholith. Note tide cracks around the small bay in the foreground.

Contents

Tables

Figures

Abstract

The Bunger Hills area, which forms part of the East Antarctic Shield, consists predominantly of granulite-facies orthogneiss (pyroxene-quartz-feldspar gneiss), with subordinate mafic granulite and garnet, sillimanite, and cordierite-bearing paragneiss. The igneous precursors of granodioritic orthogneiss crystallised about 1500–1700 Ma ago, whereas late Archaean (2640 Ma) tonalitic orthogneiss occurs in the Obruchev Hills, in the southwest of the area. Metamorphism reached a peak of about 750–800°C and 5–6 kb (M_1) 1190±15 Ma ago (U-Pb zircon age) and was accompanied by the first of three ductile deformation events (D_1). Voluminous, mainly mantle-derived plutonic rocks were emplaced between 1170 (during D_3) and 1150 Ma. They range in composition from gabbro, through quartz gabbro, quartz monzogabbro, and quartz monzodiorite, to granite. Abundant dolerite dykes, of at least four chemically distinct groups, were intruded at about 1140 Ma. Their intrusion was associated with the formation of shear zones, indicating at least limited uplift; all subsequent deformation was of brittle-ductile or brittle type. Alkaline mafic dykes were emplaced 500 Ma ago.

Marked geochronological similarities with the Albany Mobile Belt of Western Australia suggest that high-grade metamorphism in both areas was the result of continental collision between the Archaean Yilgarn Craton of Australia and the East Antarctic Shield. However, Gondwana reconstructions and the composition of the plutonic rocks suggest that the Bunger Hills metamorphics may have formed in an Andean-type continental arc, with the actual collision zone having been to the east of the present Bunger Hills.

Exposures west of the Denman Glacier are also mainly granulite-facies gneiss, intruded by a variety of mafic to felsic plutonic rocks. They differ from the Bunger Hills in being partly derived from Archaean protoliths (~3000 Ma), in lacking isotopic evidence for a Mesoproterozoic high-grade event, and in not being intruded by dolerite dyke swarms. They also show evidence of much more extensive 500-600 Ma (Pan-African) metamorphism and plutonism (syenite to granite), and in this regard they are comparable with the Leeuwin Block metamorphics of southwestern Australia, although these were derived from significantly younger protoliths (T_{DM}^{Nd} model ages: 1100–1500 Ma).

If this early Palaeozoic activity was also a consequence of continental collision, it would explain the markedly different geological history of the terranes on either side of the Denman Glacier and could account for the final uplift of the Bunger Hills. However, the compressional tectonic regime implicit in the collision hypothesis was followed by an extensional regime, which, in southwestern Australia, eventually resulted in the formation of the Perth Basin rift zone. This structure is aligned with the Denman Glacier trough on our preferred Gondwana reconstruction, suggesting that it may have extended well to the south before the breakup of Gondwana.

Introduction

The Bunger Hills lie near the ice-bound coast of East Antarctica at about longitude 100°E (Fig. 1). They are separated from the Southern Ocean by the Shackleton Ice Shelf, but a direct sub-ice connection is indicated by tide cracks around the larger bodies of water and by the presence of seals. An area of low rocky hills and glacially deepened valleys with many lakes (Fig. 2), they occupy about 300 km^2 and have a maximum elevation of 165 m. Generally, areas of low relief and valley bottoms are mantled with locally derived rock debris and glacial deposits of probable late Quaternary age (Fig. 3). Nevertheless, the Bunger Hills and adjacent islands (Fig. 4), together with the Obruchev Hills, about 30 km to the southwest (Fig. 5), form a well-exposed section (~1500 km^2) of the Precambrian East Antarctic Shield in a region of generally poor outcrop. All other outcrops in the region are small and isolated.

The Bunger Hills were first sighted from Watson Bluff, about 60 km away on the western side of the Denman Glacier, by members of the western party of Douglas Mawson's 1911–14 Australasian Antarctic Expedition (Mawson 1915; Nockolds 1940), who named them the Hordern Islands (now Cape Hordern) after Mr Samuel Hordern, a Sydney businessman and major benefactor of the expedition. However, the area was not visited until 13 February 1947, when a Martin Mariner flying boat of Byrd's 1946–7 US Navy Expedition 'Operation Highjump', piloted by Lieutenant Commander David E. Bunger, landed on a marine inlet in the central part of the 'oasis'. Its discovery was greeted with somewhat lurid publicity and the term 'Shangri-la' was very mistakenly applied, although Bunger described the hills that now bear his name as 'a land of blue and green lakes and brown hills in an otherwise limitless expanse of ice' (Bertrand 1967; Rose 1980). Bunger's party landed near Geologov Island; however, no scientific observations were made, although a few rock specimens were collected.

The first geological studies of the Bunger Hills were made in 1956–7 by Soviet Antarctic Expedition scientists, a detailed, mainly petrological, account being given by Ravich et al. (1968). The Soviet 'Oasis' base, on the northern side of Algae Lake, was later used by the Polish Antarctic Expedition, and renamed 'Dobrowolski'.

In January 1986, Australian National Antarctic Research Expeditions (ANARE) personnel set up a summer field camp, Edgeworth David Base (named after Professor Tannatt William Edgeworth David, an Australian geologist with Shackleton's 1907–9 British National Antarctic Expedition), on the western side of the Bunger Hills (Fig. 6). In the six-week season, good logistic support and reasonable weather enabled most of the region's bedrock outcrops to be examined. Geologists R.J. Tingey and J.W. Sheraton of the then Bureau of Mineral Resources (now Australian Geological Survey Organisation) visited all significant outcrops in the Bunger Hills–Obruchev Hills area, and made brief visits to most of the generally small outcrops on the western side of the Denman Glacier

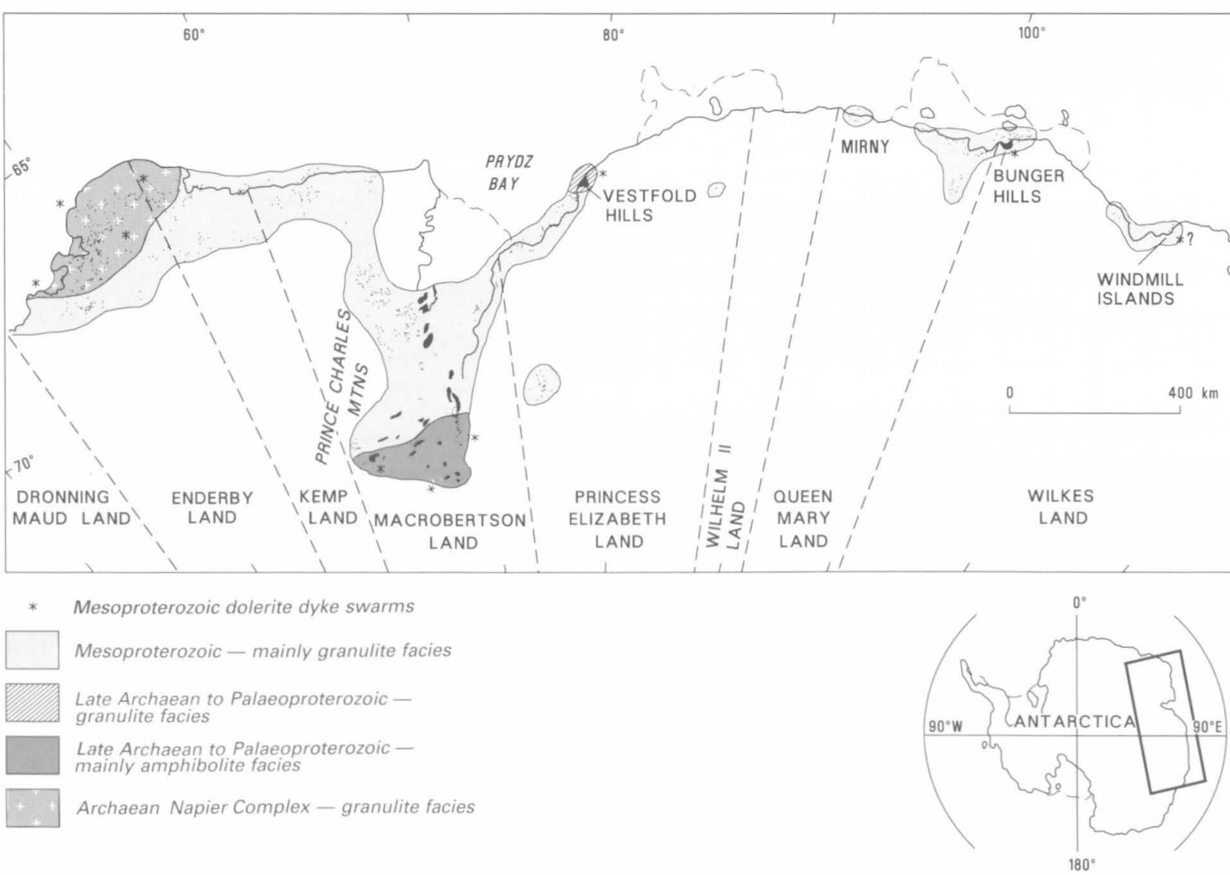

Figure 1. Part of East Antarctica, showing metamorphic complexes and outcrops (black). Mesoproterozoic metamorphics in the northern part of the southern Prince Charles Mountains are greenschist to amphibolite facies; metamorphic rocks of similar age in Enderby and Kemp Lands are termed Rayner Complex. Palaeo- to Mesoproterozoic dolerite dyke swarms are present in all the Archaean complexes, as well as in the Bunger Hills area and possibly the Windmill Islands.

as far west as 98°E. During the same period, geologists from the Universities of Melbourne (P. Marsh, K. Stüwe, and C.J.L. Wilson) and Adelaide (P. Ding) made detailed structural and petrological studies of the main Bunger Hills outcrops (Stüwe & Powell 1989a; Stüwe & Wilson 1990; Ding & James 1991).

It was intended that the 1986 field season would be the first of three consecutive summer programs in the area, but unusually heavy pack ice in 1987 prevented the ANARE support ship 'M.S. Nella Dan' from getting close enough to

Figure 2. East end of Algae Lake, looking west across the Bunger Hills. Note the essentially concordant summit levels, mostly between 100 and 150m high. Outcrops in the foreground are mainly felsic orthogneiss.

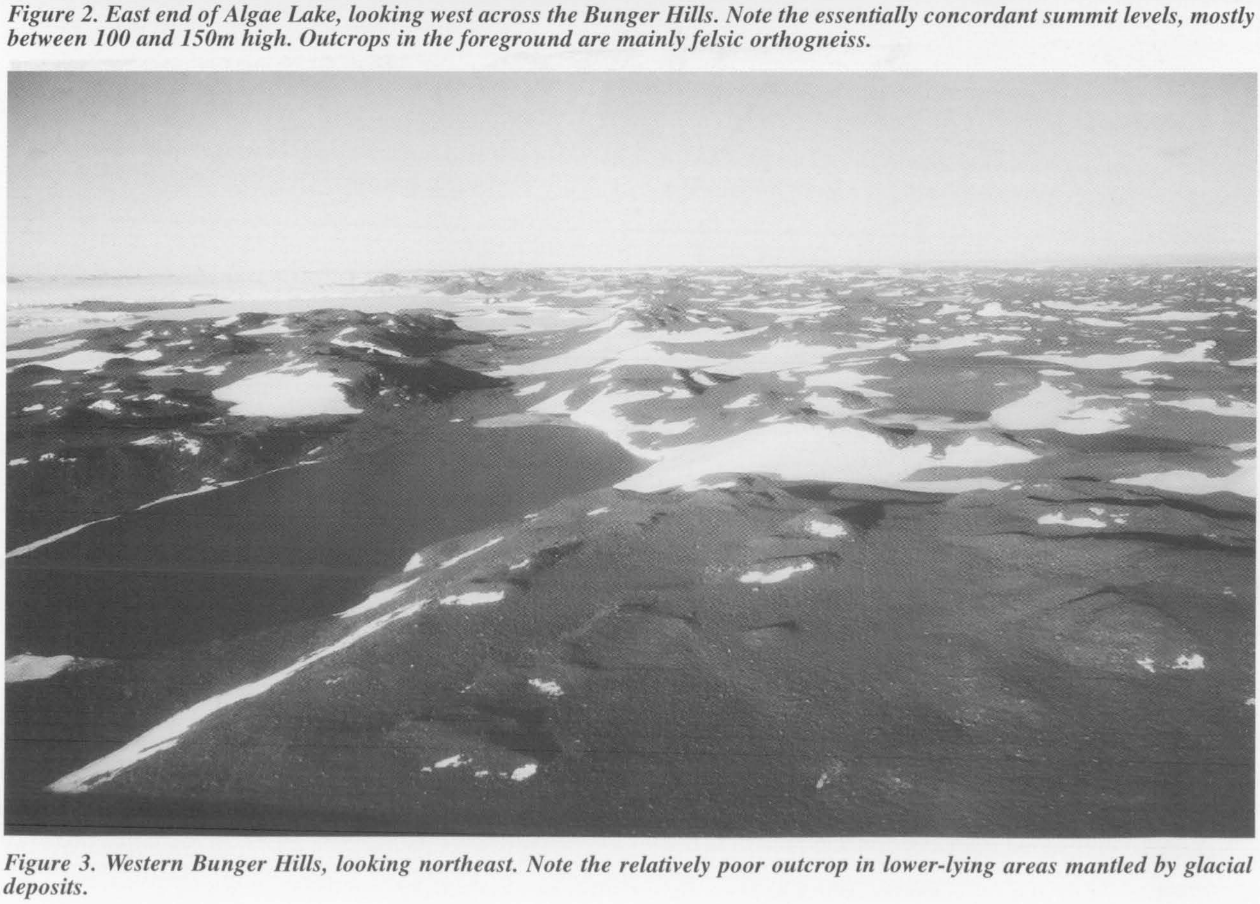

Figure 3. Western Bunger Hills, looking northeast. Note the relatively poor outcrop in lower-lying areas mantled by glacial deposits.

the coast to fly off personnel and stores to the base camp. The severe conditions developed because a large grounded iceberg prevented the normal summer dispersal of sea ice. Further operations in the area were consequently postponed indefinitely.

This *Bulletin*, therefore, presents the results of only one season's field work in the Bunger Hills–Denman Glacier region. However, the field observations have been complemented by the first detailed geochemical and geochronological studies of the region. In this account, the geology of the Bunger Hills–Obruchev Hills area is described separately from that of the area west of the Denman Glacier (and the isolated Mounts Amundsen and Sandow), because of the significant lithological differences between them. An attempt is also made to correlate the geological history with that of once contiguous parts of Gondwana.

The igneous rock classification of Streckeisen (1976) is used in this *Bulletin*. Mineral abbreviations used are given in Table 1. Most names of geographic features are those used on the 1992 AUSLIG 1:50 000 satellite image map of the Bunger Hills, and many of these differ from names used on an earlier (1988) topographic map of the area and in previous publications.

Table 1. Mineral abbreviations used in this Bulletin.

Act,	actinolite	Gt,	garnet	Pig,	pigeonite
Bi,	biotite	Hb,	hornblende	Pl,	plagioclase
Cd,	cordierite	Kf,	K-feldspar	Px,	pyroxene
Cor,	corundum	Mp,	mesoperthite	Qz,	quartz
Cp,	clinopyroxene	Ol,	olivine	Sa,	sapphirine
En,	enstatite	Op,	orthopyroxene	Si,	sillimanite
Fd,	feldspar	Phl,	phlogopite	Sp,	spinel

Figure 4. Booth Peninsula, looking east towards the icecap. The island in the foreground consists mainly of gabbroic rocks of the Booth Peninsula batholith cut by felsic veins. Most of the more distant outcrops are of quartz monzodioritic to granitic composition.

Figure 5. Northeastern Obruchev Hills, predominantly composed of tonalitic orthogneiss. A dolerite dyke crops out in the foreground and continues along the small valley.

Figure 6. Edgeworth David Base, on the northwestern coast of the Bunger Hills.

Bunger Hills–Obruchev Hills area

The Bunger Hills–Obruchev Hills area extends northeastwards for about 150 km from Cape Jones, on the eastern side of the Denman Glacier, to the northern islands of the Highjump Archipelago (Fig. 7). The Bunger Hills proper are the most extensive area of continuous outcrop (~300 km^2), but there are also good outcrops on the islands and peninsulas imme-

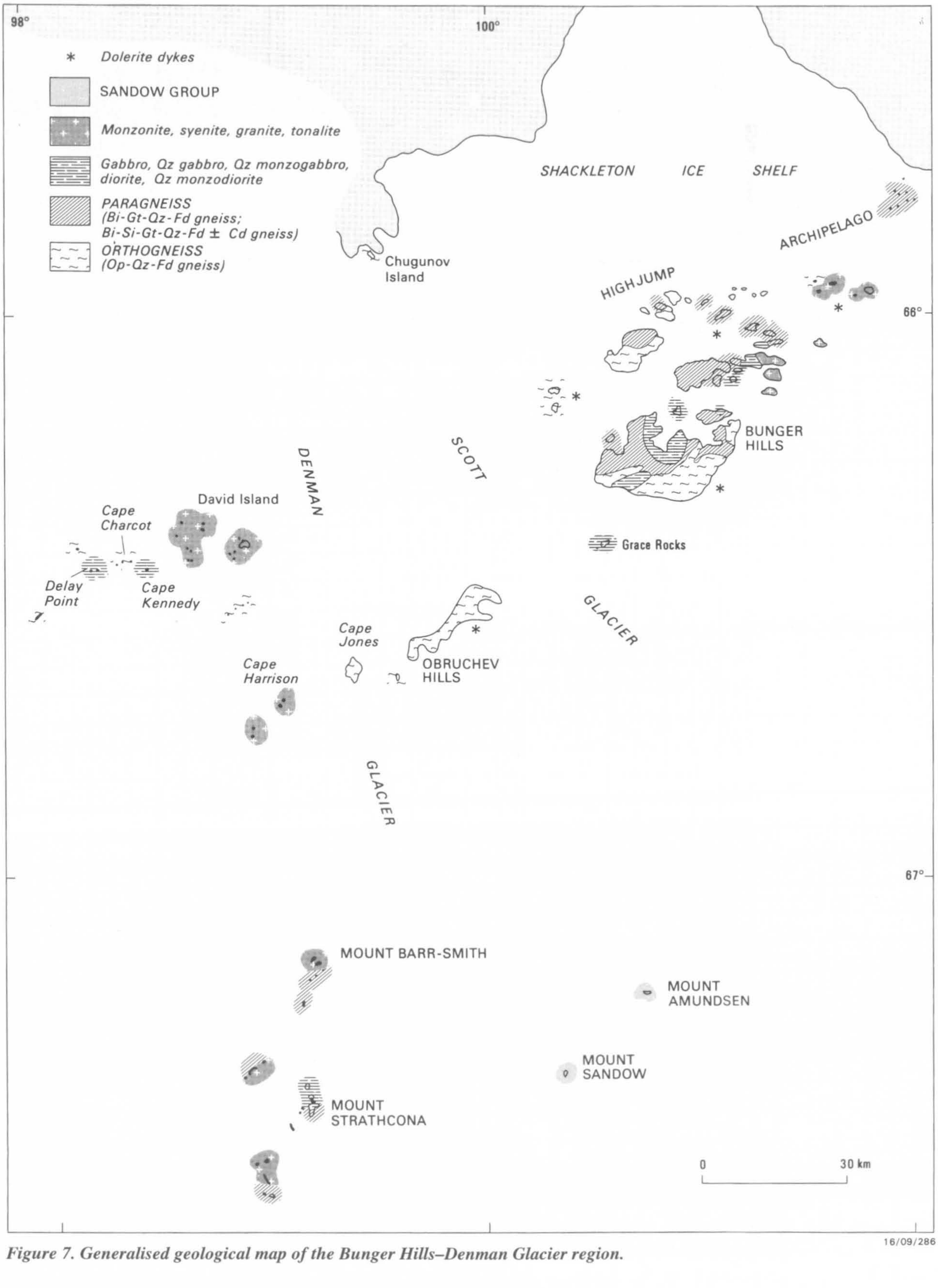

Figure 7. Generalised geological map of the Bunger Hills–Denman Glacier region.

diately to the north and in the Obruchev Hills.

The area consists almost entirely of granulite-facies metamorphic rocks of both igneous and sedimentary origin, together with a voluminous suite of plutonic rocks, ranging from gabbro to granite (Fig. 8), and abundant dolerite dykes. The field relations, petrography and geochemistry of these rocks are described in the following sections.

Metamorphic rocks

Pyroxene-quartz-feldspar gneiss

Massive pyroxene-quartz-feldspar gneiss (predominantly felsic orthogneiss: Ꝑp on geological map) makes up most of Cape Jones, the Obruchev Hills and Taylor Islands, and much of Currituck and Dieglman Islands and the southeastern part of the Bunger Hills (Figs 9, 10). Elsewhere, it is a relatively minor component of layered supracrustal rocks — predominantly garnet-quartz-feldspar gneiss and aluminous metasediments.

Major constituents are pleochroic orthopyroxene (up to 15%), quartz (mostly 15–40%) and feldspar (mostly 50–65%). Small amounts (generally less than 3%) of reddish-brown biotite are common and clinopyroxene occurs in some layers, particularly the more mafic ones; other layers contain minor greenish-brown hornblende or garnet. Opaque minerals, apatite, and zircon are ubiquitous accessory phases; monazite is less common, and allanite and rutile are rare.

In much orthogneiss the only feldspar is plagioclase (commonly antiperthitic andesine, rarely calcic oligoclase or sodic labradorite); such a tonalitic variety (distinguished as Ꝑpp) predominates at Cape Jones, the southern and central Obruchev Hills, Taylor Islands, and the southeastern Bunger Hills. Elsewhere, more potassic (granodioritic to granitic) orthogneiss is interlayered with tonalitic orthogneiss and metasediments. This gneiss generally contains both calcic oligoclase-sodic andesine antiperthite and K-feldspar (orthoclase or microcline

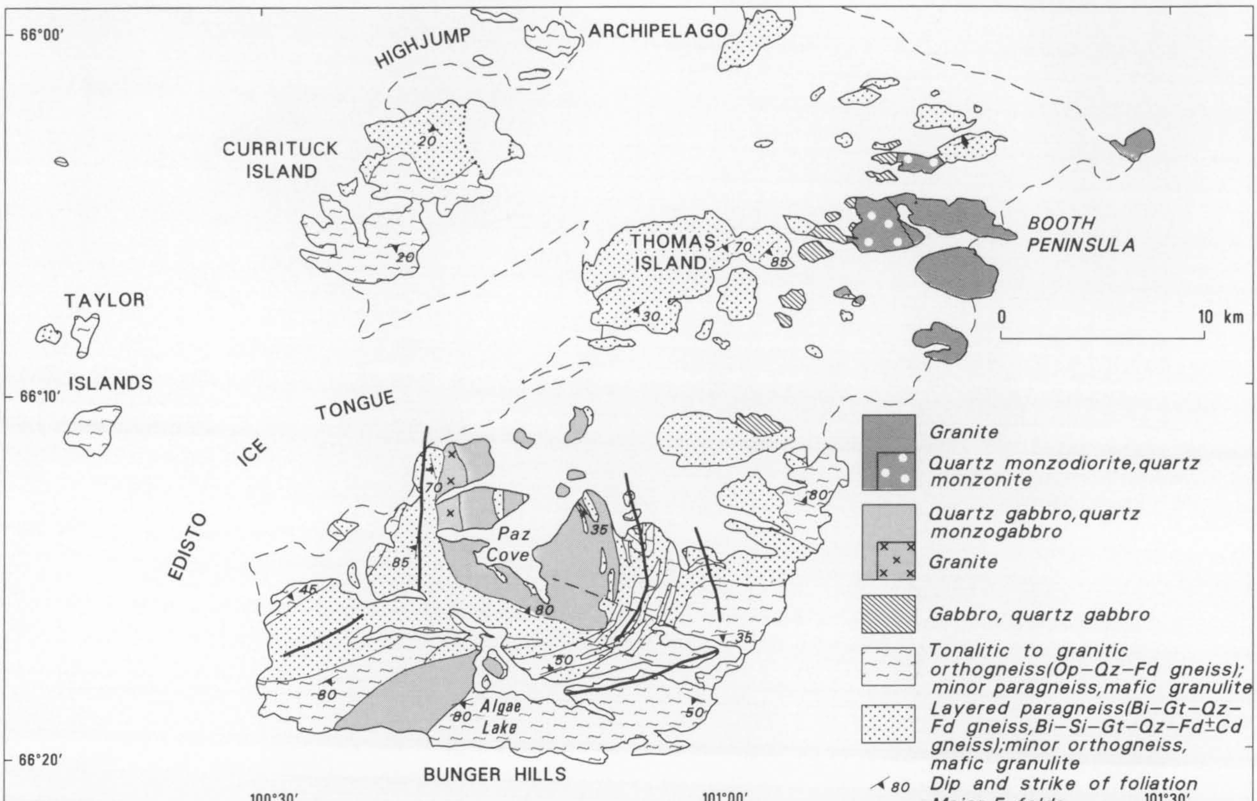

Figure 8. Generalised geological map of the main outcrops in the Bunger Hills area (in part after Stüwe & Wilson, 1990).

Figure 9. Massive felsic orthogneiss (orthopyroxene–quartz–feldspar gneiss); Currituck Island.

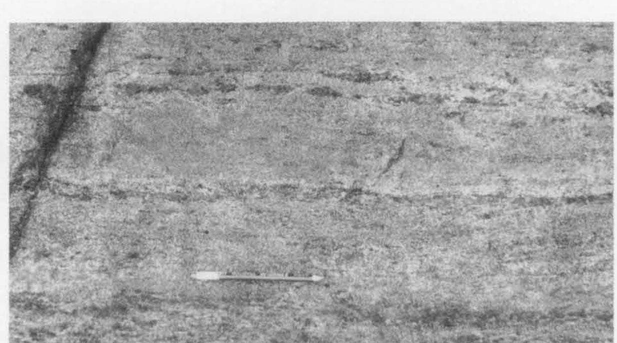

Figure 10. Massive felsic orthogneiss; Currituck Is. Mafic layers are predominantly of orthopyroxene with minor biotite.

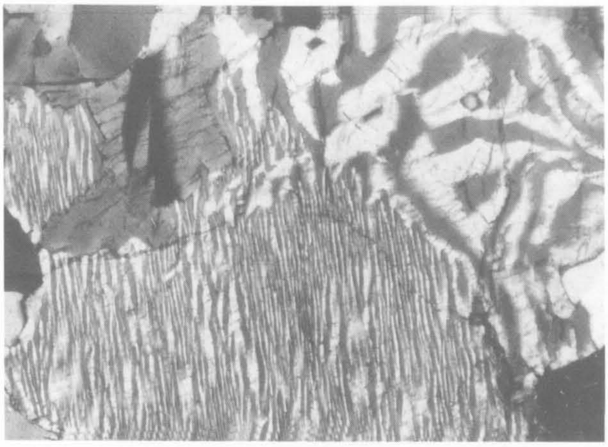

Figure 11. Mesoperthite in orthopyroxene–quartz–feldspar gneiss; southeastern Curritick Island. AGSO registered sample number 86285602; cross-polarised light; width of field: 1mm.

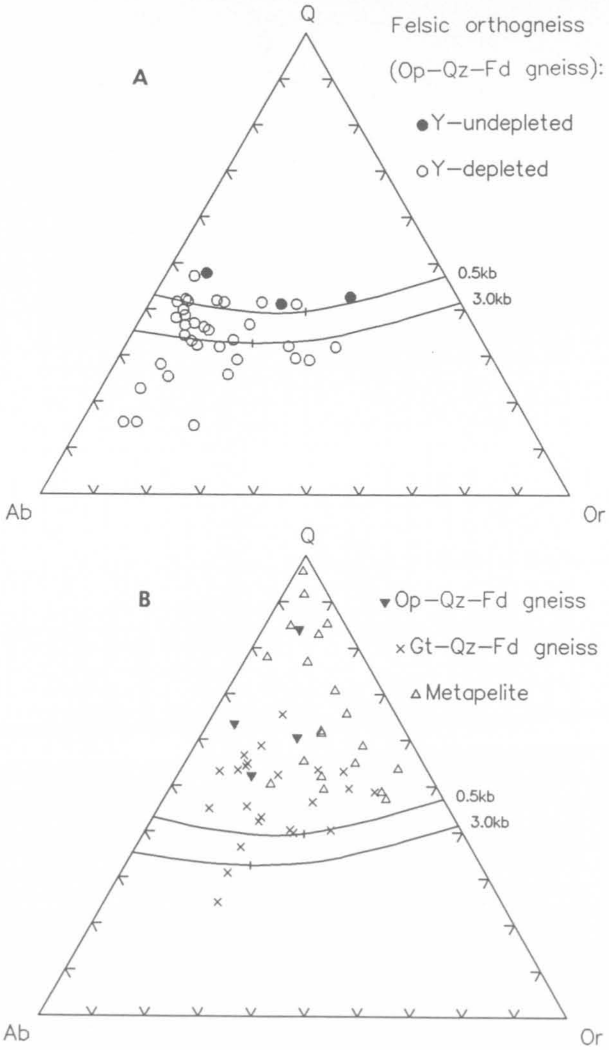

Figure 12. Normative Q–Ab–Or diagrams for A, felsic orthogneisses, and B, paragneisses and metapelites from the Bunger Hills area, showing quartz–feldspar field boundaries and positions of quaternary isobaric minima at 0.5 and 3.0kb P_{H2O} (after Tuttle & Bowen 1958). Depleted, mostly orthopyroxene-bearing orthogneisses have relatively low Y and HREE contents and are predominantly of tonalitic, trondhjemitic, or granodioritic composition. Most garnet (and a few orthopyroxene) -bearing gneisses (as well as the metapelites) plot well inside the quartz field, consistent with a sedimentary origin.

perthite), although a few rocks have only one feldspar, approaching mesoperthite in composition (Fig. 11). Texture is commonly granoblastic inequigranular interlobate (Winkler 1979), and most gneiss has only a weak foliation, defined by elongated mineral aggregates. However, some rocks contain late-crystallised biotite with a markedly preferred orientation, and some leucogneiss contains lenticular quartz aggregates.

Many samples show evidence of retrograde metamorphism, including partial or complete alteration of orthopyroxene to a yellowish-brown iddingsite-like material, in some cases with rims of colourless clinoamphibole. In others, orthopyroxene is replaced by fine-grained aggregates of biotite, quartz, and, less commonly, carbonate. Feldspar, particularly plagioclase, may show sericitic alteration, and biotite may be partly chloritised.

Retrogression is particularly extensive in the southeast of the Bunger Hills, where orthopyroxene is almost entirely altered to fine-grained brownish-green to reddish-brown biotite and quartz, with minor epidote and/or pale green amphibole. Such alteration appears to predate the formation of iddingsite, as some altered orthopyroxene grains have cores of iddingsite surrounded by secondary biotite. In a few rocks, small amounts of sphene are present, apparently replacing ilmenite.

Chemical data (Table 2) indicate an igneous origin for most of the gneiss, but it is often difficult to establish whether gneiss represents intrusive or extrusive rocks. However, massive, poorly layered orthogneiss, such as that in the Obruchev Hills, is probably of intrusive origin, whereas at least some of that interlayered with supracrustal rocks may well be metamorphosed felsic extrusives, although some layers (commonly of granite, s.s., composition) are locally cross-cutting and clearly represent small syn-metamorphic melt bodies.

The predominance of sodic orthogneiss (tonalite, granodiorite and minor quartz diorite) is emphasised by plots of normative compositions (Figs 12A, 13A). The orthogneiss is either Di-normative or only slightly (< 1%) C-normative (Fig. 14) and is thus equivalent to the I-type granitoid of Chappell & White (1974) — derived by partial melting of igneous precursors. Most is depleted in Y and, presumably, heavy rare-earth elements (HREE) (Table 2, Fig. 15). Such Y-depleted orthogneiss is thought to represent new continental crust derived by partial melting of a mafic source, leaving residual hornblende and/or garnet (Sheraton & Black 1983; Sheraton et al. 1985; Martin 1993). Derivation from a feldspar-poor mafic source (such as subducted hydrated oceanic crust), rather than more felsic crustal rocks, would also explain its high Sr (Fig. 16) and lack of a significant negative Sr anomaly on spidergrams (Fig. 17). Similar Y-depleted tonalitic to granodioritic orthogneiss is also common in other parts of the East Antarctic Shield (e.g. the Archaean Napier Complex of Enderby Land (Sheraton et al. 1987c) and the Vestfold Hills of Princess Elizabeth Land (Sheraton & Collerson 1984)).

Experimental studies by Beard & Lofgren (1991) have shown that dehydration melting (i.e. no added water) of amphibolite at 1–6.9 kb will produce metaluminous to slightly peraluminous tonalitic to granodioritic melts; however, under these conditions, the residues after melt extraction consist predominantly of plagioclase and pyroxene, which is inconsistent with the absence of Sr anomalies in the Bunger Hills orthogneiss. In contrast, water-saturated melting produces strongly peraluminous melts with low Fe and Mg, and the residues are amphibole-rich and plagioclase-poor. These data, therefore, suggest that melting at intermediate water pressures would be most likely to produce metaluminous or slightly peraluminous tonalitic liquids without a significant negative Sr anomaly.

Alternatively, dehydration melting under higher pressures, at which garnet rather than plagioclase would be a major residual phase, is possible, particularly as only a relatively

Table 2. Chemical analyses of representative felsic gneisses from Bunger Hills area.

Sample no.	*86285938*	*86285807*	*86285695*	*86285958*	*86285600*	*86286235*	*86285904*	*86285643*	*86285604*	*86285844*
Locality	*5km SW of Dobrowolski*	*Obruchev Hills NE*	*Obruchev Hills SW*	*W end of Lake Dolgoe*	*Currituck Island SE*	*5km S of Dobrowolski*	*1km S of Edgeworth David*	*Thomas Island SW*	*Currituck Island SE*	*Saturn Island*
Lithology	*Bi-Op-Qz-Pl gneiss*	*Op-Qz-Pl gneiss*	*Cp-Op-Qz-Pl gneiss*	*Bi-Cp-Op-Qz-Pl gneiss*	*Op-Qz-Mp gneiss*	*Op-Qz-Pl gneiss*	*Op-Pl-Qz-Kf gneiss*	*Bi-Op-Qz-Pl gneiss*	*Op-Qz-Kf gneiss*	*Bi-Op-Pl-Kf-Qz gneiss*
Classif.	*Depleted quartz diorite*	*Depleted tonalite*	*Depleted tonalite*	*Depleted tonalite*	*Depleted granodiorite*	*Depleted granodiorite*	*Depleted granite*	*Undepleted tonalite*	*Undepleted granite*	*Paragneiss*
SiO_2	55.40	72.70	66.10	61.30	71.10	70.60	70.80	68.00	74.10	79.60
TiO_2	0.64	0.28	0.50	0.82	0.33	0.29	0.29	0.59	0.48	0.17
Al_2O_3	19.48	14.75	15.94	15.11	14.83	15.15	15.31	14.33	11.48	10.74
Fe_2O_3	1.87	0.75	1.33	0.84	1.04	1.18	0.75	2.54	1.39	0.62
FeO	5.55	0.85	2.91	6.46	1.42	1.02	0.84	2.76	1.85	1.12
MnO	0.13	0.02	0.07	0.11	0.03	0.02	0.02	0.09	0.05	0.03
MgO	3.93	0.82	2.09	3.95	0.94	0.89	0.51	1.52	1.25	0.94
CaO	7.05	3.59	5.25	7.01	2.90	1.93	1.90	3.90	1.32	1.32
Na_2O	3.79	4.29	4.00	2.51	3.99	5.35	3.80	3.61	2.05	2.16
K_2O	0.76	0.70	0.85	0.96	2.83	1.88	4.85	0.85	5.37	2.67
P_2O_5	0.30	0.04	0.14	0.13	0.13	0.05	0.08	0.15	0.08	0.04
LOI	1.07	0.53	0.70	0.86	0.55	0.80	0.55	0.83	0.55	0.67
Rest	0.23	0.26	0.24	0.25	0.21	0.20	0.34	0.20	0.23	0.19
Total	**100.20**	**99.58**	**100.12**	**100.31**	**100.30**	**99.36**	**100.04**	**99.37**	**100.20**	**100.27**
O=S	0.01	0.01	0.02	0.03	0.01	0.00	0.00	0.02	0.01	0.01
Total	**100.19**	**99.57**	**100.10**	**100.28**	**100.29**	**99.36**	**100.04**	**99.35**	**100.19**	**100.26**
	C.I.P.W. norms									
Q	6.77	36.03	24.45	19.39	29.24	26.76	25.31	32.57	36.45	52.10
C	0.32	0.50	–	–	0.24	0.92	0.55	0.74	0.09	1.99
Or	4.49	4.14	5.02	5.67	16.72	11.11	28.66	5.02	31.73	15.78
Ab	32.07	36.30	33.85	21.24	33.76	45.27	32.15	30.55	17.35	18.28
An	33.02	17.55	23.03	27.13	13.54	9.25	8.90	18.37	6.03	6.29
Di	–	–	1.72	5.63	–	–	–	–	–	–
Hy	17.61	2.56	7.91	17.06	3.60	2.67	1.75	5.95	4.66	3.66
Mt	2.71	1.09	1.93	1.22	1.51	1.71	1.09	3.68	2.02	0.90
Il	1.22	0.53	0.95	1.56	0.63	0.55	0.55	1.12	0.91	0.32
Ap	0.71	0.09	0.33	0.31	0.31	0.12	0.19	0.36	0.19	0.09
mg	55.8	63.2	56.1	52.1	54.1	60.9	52.0	49.5	54.6	59.9
	Trace elements in parts per million									
Ba	609	704	554	537	765	958	1696	361	920	768
Rb	6	2	2	36	60	15	83	8	180	59
Sr	483	828	618	196	352	227	549	185	132	224
Pb	11	6	6	11	10	15	46	13	22	34
Th	1	11	<1	6	7	5	35	1	6	<1
U	0.5	<0.5	<0.5	1.0	0.5	0.5	0.5	0.5	1.0	<0.5
Zr	79	148	99	92	163	194	219	322	316	102
Nb	8	1	3	5	3	2	5	4	6	1
Y	22	2	8	18	6	2	3	26	17	7
La	29	46	15	27	35	34	60	21	39	37
Ce	54	75	29	53	59	58	100	45	63	62
Nd	23	20	13	23	18	16	27	19	19	18
Sc	21	6	14	27	7	5	5	15	8	7
V	85	22	71	165	23	23	18	46	22	19
Cr	74	6	50	62	11	4	4	12	5	25
Ni	17	12	26	29	9	3	4	9	7	18
Cu	9	17	23	31	19	4	12	16	5	11
Zn	99	24	52	62	26	27	31	60	35	24
Sn	1	<1	<1	1	<1	<1	<1	<1	1	1
Ga	24	15	18	19	16	17	18	17	12	11
S	300	300	500	700	200	100	<100	500	200	200
K/Rb	1050	2910	3530	221	392	1040	485	882	248	376
Rb/Sr	0.012	0.002	0.003	0.184	0.170	0.066	0.151	0.043	1.36	0.263
Ce/Y	2.5	37	3.6	2.9	9.8	29	33	1.7	3.7	8.9
Th/U	2	>22	–	6	14	10	70	2	6	–
Nb/Nb*	0.33	0.03	0.16	0.19	0.06	0.05	0.05	0.19	0.07	0.02
Sr/Sr*	0.99	1.41	2.31	0.41	0.73	0.50	0.70	0.45	0.26	0.45

mg = atomic $100Mg/(Mg+Fe^{2+})$. Nb/Nb* = Nb/(0.5(K+La)) and Sr/Sr* = Sr/(0.5(Ce+Nd)), where all element concentrations are normalised to estimated primordial mantle abundances (Fig. 17).

Sample no.	*86285961*	*86286262*	*86285871*	*86285825*
Locality	*W end of Lake Dolgoe*	*Samoylov-icha Islands*	*Aviatorov Peninsula S*	*1km E of Edgeworth David*
Lithology	*Bi-Gt-Pl-Qz-Kf gneiss*	*Gt-Bi-Pl-Kf-Qz gneiss*	*Gt-Op-Pl-Kf-Qz gneiss*	*Bi-Gt-Kf-Qz gneiss*
Classif.	*Orthogneiss*	*Paragneiss*	*Paragneiss*	*Paragneiss*
SiO_2	73.70	72.60	69.00	75.60
TiO_2	0.13	0.74	0.93	0.53
Al_2O_3	14.41	12.37	12.80	11.28
Fe_2O_3	0.19	1.69	1.16	0.35
FeO	1.67	3.06	4.97	3.32
MnO	0.03	0.12	0.10	0.08
MgO	0.61	1.67	2.24	1.39
CaO	1.58	2.06	2.37	0.33
Na_2O	3.25	2.53	2.11	1.26
K_2O	4.06	1.57	3.38	5.65
P_2O_5	0.07	0.03	0.15	0.04
LOI	0.34	0.73	0.55	0.42
Rest	0.18	0.21	0.36	0.24
Total	**100.22**	**99.38**	**100.12**	**100.49**
O=S	0.00	0.00	0.03	0.01
Total	**100.22**	**99.38**	**100.09**	**100.48**
	C.I.P.W. norms			
Q	33.91	43.60	32.69	41.67
C	1.96	2.84	1.72	2.59
Or	23.99	9.28	19.97	33.39
Ab	27.50	21.41	17.85	10.66
An	7.38	10.02	10.78	1.38
Di	–	–	–	–
Hy	4.27	7.37	12.39	8.53
Mt	0.28	2.45	1.68	0.51
Il	0.25	1.41	1.77	1.01
Ap	0.17	0.07	0.36	0.09
mg	39.4	49.3	44.5	42.7
	Trace elements in parts per million			
Ba	932	657	1011	778
Rb	69	32	80	157
Sr	247	308	122	148
Pb	25	12	12	22
Th	9	5	21	20
U	0.5	1.0	1.5	1.0
Zr	55	232	442	259
Nb	3	8	40	6
Y	18	14	95	33
La	27	27	95	46
Ce	56	56	197	86
Nd	20	19	82	32
Sc	5	10	12	8
V	7	94	67	61
Cr	7	123	0	72
Ni	4	32	20	14
Cu	5	14	23	12
Zn	16	44	115	33
Sn	<1	1	<1	<1
Ga	16	12	22	12
S	<100	<100	600	200
K/Rb	488	407	351	299
Rb/Sr	0.279	0.104	0.66	0.106
Ce/Y	3.1	4.0	2.1	2.6
Th/U	18	5	14	20
Nb/Nb*	0.05	0.24	0.44	0.06
Sr/Sr*	0.52	0.66	0.07	0.20

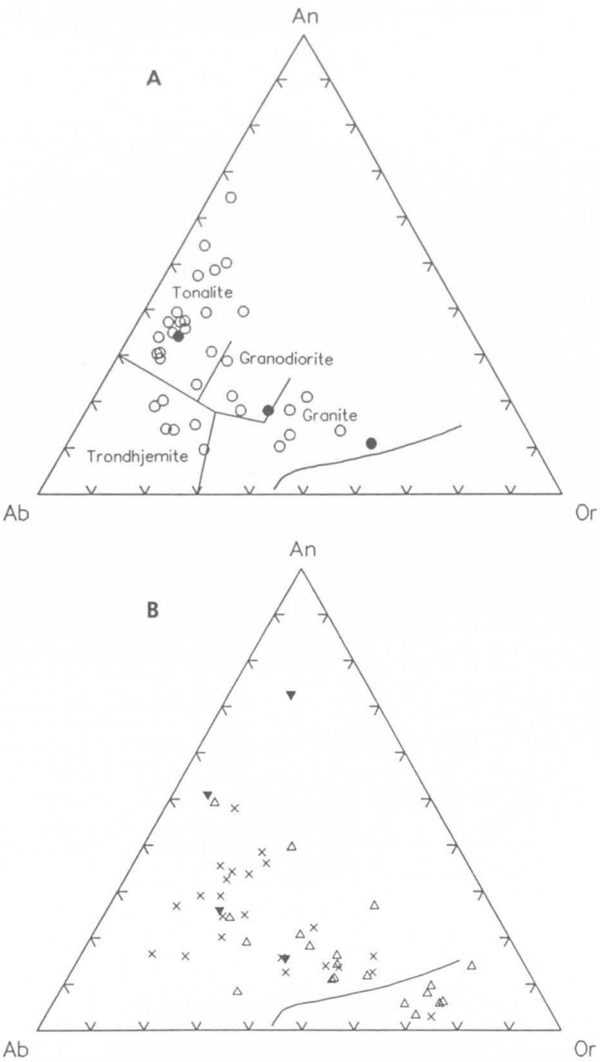

Figure 13. Normative Ab–Or–An diagrams for A, felsic orthogneisses and B, paragneisses and metapelites from the Bunger Hills area, showing plagioclase–alkali feldspar field boundary at 1.0kb P_{H2O} projected onto the Ab–Or–An face of the tetrahedron (after James & Hamilton 1969). The compositional fields are essentially those of O'Connor (1965), except that granite and quartz monzonite are combined as granite. Symbols as in Figure 12.

moderate pressure (~10 kb) is required (Wolf & Wyllie 1994). Rapp et al. (1991) have shown experimentally that the degree of melting required to produce tonalitic melts increases with pressure, so that, if melt segregation is most effective for such higher degrees of melting (20–35%), an origin by melting of a garnet-rich source (eclogite or garnet amphibolite) is most likely.

Negative Nb anomalies are characteristic of subduction-related magmatism and probably result from the stability of residual Ti oxide minerals (ilmenite, rutile, sphene, or perovskite) under hydrous melting conditions (Saunders et al. 1980, 1991; Tarney & Weaver 1987). The role of fractional crystallisation is difficult to assess, but the lack of correlation of Sr anomaly with SiO_2 indicates that fractionation of plagioclase was not a dominant factor. Various degrees of partial melting were probably of greater importance (cf. Sheraton & Black 1983; Sheraton & Collerson 1984).

Only minor orthogneiss appears to belong to the Y-undepleted suite of Sheraton & Black (1983). This is thought to represent partial melts at relatively low P_{H2O} of predominantly

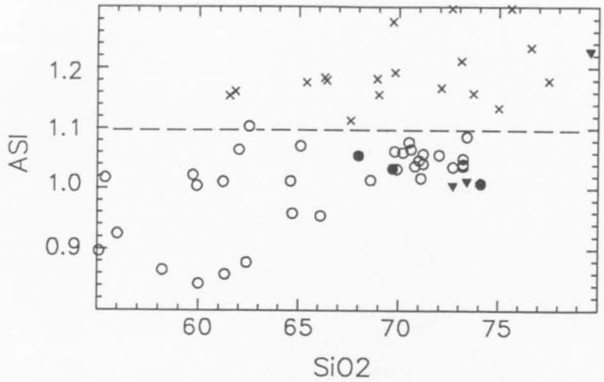

Figure 14. Plot of alumina saturation index (ASI = molecular $Al_2O_3/(Na_2O+K_2O+CaO-3.33P_2O_5)$) against SiO_2 for felsic gneisses from the Bunger Hills area. The dashed line separates the fields of I-type (igneous-derived) and S-type (sedimentary-derived) granitoids (after Chappell & White 1974). Garnet-bearing gneisses (mostly paragneisses) are distinctly more peraluminous than orthopyroxene-bearing orthogneisses. Symbols as in Figure 12.

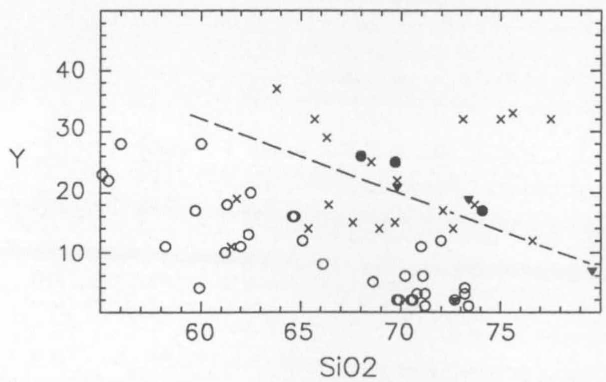

Figure 15. Plot of Y against SiO_2 for for felsic gneisses from the Bunger Hills area. Dashed line indicates the approximate boundary between fields of Y-depleted and undepleted orthogneisses of the Napier Complex, Enderby Land (after Sheraton & Black 1983). Symbols as in Figure 12.

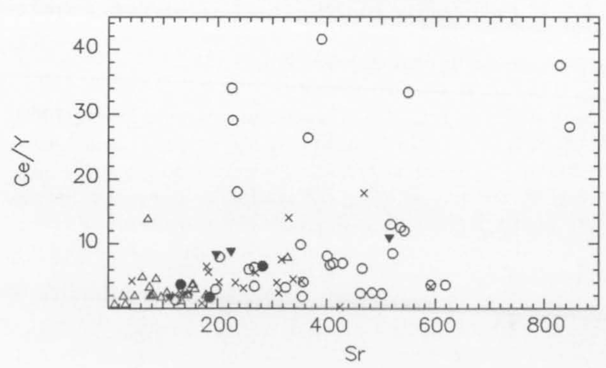

Figure 16. Plot of Ce/Y against Sr for felsic gneisses from the Bunger Hills area. Y-depleted orthogneisses commonly have high Sr and Ce/Y, consistent with derivation by partial melting of a hornblende(±garnet)-bearing mafic source. Symbols as in Figure 12.

felsic crustal rocks, and tends to have lower Ce/Y and Sr (Fig. 16), but higher Zr and Nb. Its spidergrams are generally more irregular than those of the Y-depleted suite and are

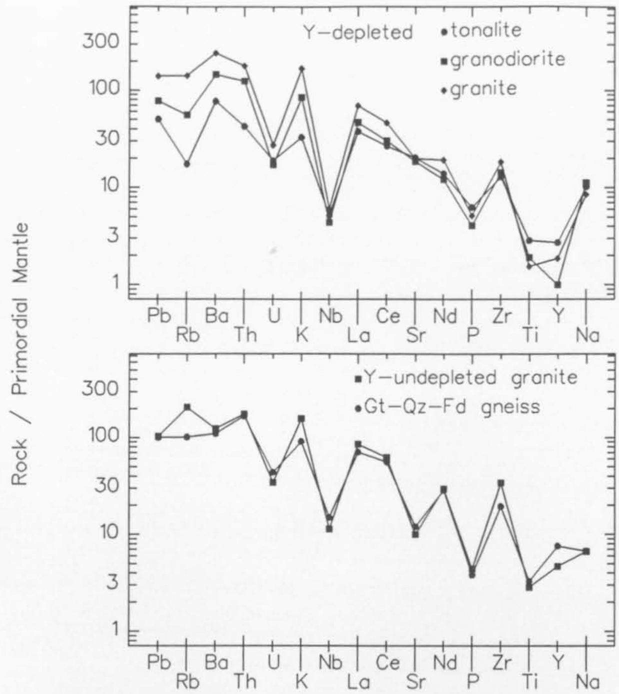

Figure 17. Primordial mantle-normalised incompatible element abundance patterns (spidergrams) for average felsic gneisses from the Bunger Hills area. Normalising values (Pb, 0.20; Rb, 0.63; Ba, 6.91; Th, 0.092; U, 0.022; K, 230; Nb, 0.71; La, 0.70; Ce, 1.81; Sr, 20.9; Nd, 1.35; P, 95; Zr, 11.1; Ti, 1270; Y, 4.52; Na, 2890ppm) after Sun & McDonough (1989). Y-depleted orthogneisses do not have significant Sr anomalies, whereas Y-undepleted orthogneisses have marked negative Sr anomalies, consistent with partial melting of felsic crustal rocks.

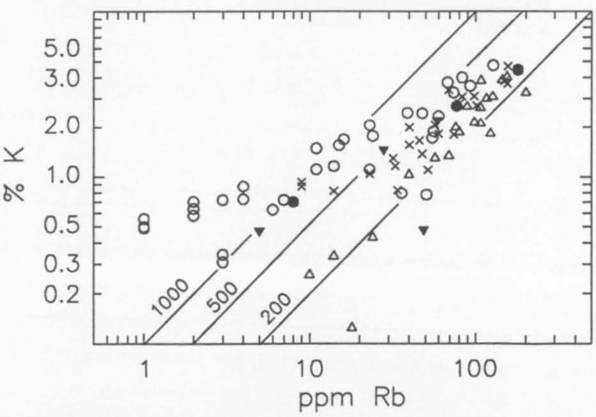

Figure 18. Plot of K against Rb for felsic gneisses and metapelites from the Bunger Hills area. Lines of constant K/Rb ratio are indicated. Symbols as in Figure 12.

characterised by marked negative Sr anomalies, but no Y anomalies (Fig. 17). A negative Sr anomaly would be produced by partial melting with major residual plagioclase or by plagioclase fractionation (Tarney et al. 1987; Sheraton & Black 1988).

Some orthopyroxene-quartz-feldspar gneiss samples plot well within the quartz field on a Q-Ab-Or diagram (Fig. 12B) and may well be of sedimentary origin. One such rock, which contains about 8 per cent clinopyroxene and unusually calcic plagioclase ($\sim An_{70}$), probably has calc-silicate affinities.

Very low Rb/Sr (average of 15 Y-depleted tonalites is

0.026), high K/Rb (up to 4000: Fig. 18) and low U (Fig. 17) of much orthogneiss are consistent with loss of large-ion lithophile elements (LILE) during high-grade metamorphism. Th/U ranges up to very high values (~100), much greater than the estimated crustal average (~3.8: Taylor & McLennan 1985). Such LILE depletion during granulite-facies metamorphism is well established (Lambert & Heier 1968; Tarney et al. 1972; Rollinson & Windley 1980), although geochemical data indicate preferential loss of K and Rb from tonalitic gneiss which does not contain significant amounts of a phase, such as K-feldspar, capable of retaining these elements (cf. Tarney & Windley 1977; Cohen et al. 1991). However, the marked compositional similarity, apart from LILE (Fig. 17), of all Y-depleted orthogneiss samples (tonalite to granite) suggests variable interaction of the magma — during generation, transport, or, less likely, emplacement — with an LILE-rich fluid phase (Sheraton et al. 1985). Such a fluid, probably subduction-derived, may be important in the generation of syn-orogenic (calc-alkaline) granitic magma (Tarney & Saunders 1979; Pearce et al. 1984), and addition of LILE would enhance the negative Nb anomaly. Nevertheless, the extremely low Rb content of the tonalitic orthogneiss would be difficult to explain without some degree of metamorphic depletion (Rb/Sr is commonly even less than the estimated primordial mantle value ~0.03: Sun & McDonough 1989). The linear trend on an AFM diagram (Fig. 19) suggests equilibration of mafic minerals (predominantly orthopyroxene) during metamorphism.

A Y-depleted granodioritic orthogneiss from near Lake Dolgoe has given an ion-microprobe U-Pb zircon age of 1699^{+19}_{-14}, whereas a tonalitic orthogneiss from the Obruchev Hills gave a late Archaean conventional U-Pb zircon age of 2641^{+16}_{-14} Ma (Sheraton et al. 1992); both are interpreted as emplacement ages, and show evidence for isotopic resetting during high-grade metamorphism at about 1000–1050 Ma. A quartz-rich (~40%) orthopyroxene-quartz-feldspar gneiss from Thomas Island that gave an ion-microprobe emplacement age of 1521±29 Ma is probably an orthogneiss (Y-undepleted granodiorite) that has undergone some degree of metamorphic differentiation. It has produced the most precise estimate of the age of high-grade metamorphism (1190±15 Ma: Sheraton et al. 1992). T^{Nd}_{DM} model ages of these three orthogneisses range from 1970 to 2470 Ma (Table 8).

Mafic granulite

Mafic granulite is interlayered with both felsic orthogneiss and metasediments throughout the area. Individual layers are rarely more than a few metres thick, but reach 20 m or so in places. Some are boudinaged (Fig. 20) and, hence, too small to be distinguished at the scale of the map. Most probably represent metamorphosed mafic intrusives (e.g., dykes), but their texture is granoblastic and mostly equigranular polygonal (Fig. 21). Locally discordant bodies, which clearly represent younger dykes, are discussed later.

Most mafic granulite contains colourless to pale green diopside or augite (10–20%), pink to pale green pleochroic orthopyroxene (10–20%), andesine-labradorite (An_{40-60}, rarely up to An_{70}; typically 50-60%), opaque minerals (up to 5%), and minor apatite. Representative analyses of pyroxenes are given in Table 3. Up to 30 per cent of primary greenish-brown hornblende may be present, and up to 5 per cent of reddish-brown biotite occurs in many layers. In some cases, the biotite defines a marked foliation. Quartz is a minor constituent of some granulite, although rarely in association with primary hornblende. Zircon is a rare accessory.

A few layers with little or no clinopyroxene may be classified as norite (Fuller Island) or leuconorite (southeast of Paz Cove). Scapolite occurs in a boudinaged layer at Raketa Island. Retrograde effects, particularly evident in the southeastern Bunger Hills, include replacement of pyroxene by colourless to pale green amphibole and, to a lesser extent, biotite.

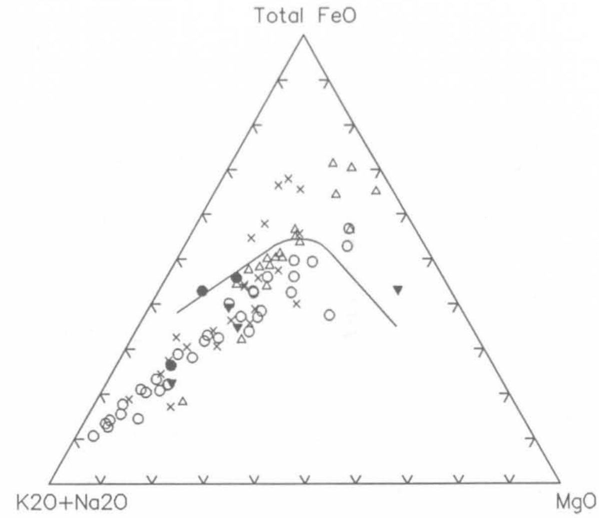

***Figure 19.** A (Na_2O+K_2O) – F (total FeO) – M (MgO) diagram for felsic gneisses and metapelites from the Bunger Hills area. Line divides the tholeiitic (upper) and calc-alkaline fields of Irvine & Baragar (1971). Symbols as in Figure 12.*

***Figure 20.** Mafic granulite boudins in migmatitic garnet–cordierite–sillimanite paragneiss; Saturn Island.*

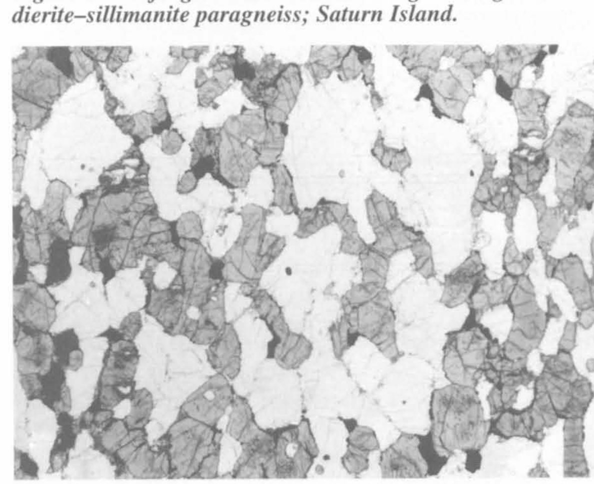

***Figure 21.** Granoblastic equigranular–polygonal texture in mafic granulite (orthopyroxene, clinopyroxene, plagioclase, and minor hornblende and opaque minerals); Foster Island. Sample 86285914; width of field: 7mm.*

Ultramafic rocks

Ultramafic layers and, more commonly, pods are widespread, but volumetrically insignificant. The most common varieties are hornblende pyroxenite and pyroxene hornblendite, containing various amounts of clinopyroxene, orthopyroxene and pale brown hornblende. Other bodies contain abundant biotite or phlogopite, and olivine or plagioclase may also be present. Minor phases include opaque minerals and spinel. A subconcordant, but clearly intrusive, body at Zabytyy Island consists almost entirely of pale green clinopyroxene, with only minor plagioclase, orthopyroxene, and phlogopite. It has an adcumulus texture.

Garnet-quartz-feldspar gneiss

Layered, garnet-bearing felsic gneiss (*Ᵽsl*) occurs throughout the Bunger Hills and adjacent islands (including the northeast Highjump Archipelago), but is rare in the Obruchev Hills. It is commonly associated with aluminous metasediments (Figs 22–24), and most is probably of sedimentary origin. However, some massive, locally discordant leucogneiss of granitic composition, with only minor garnet, is clearly of intrusive igneous origin.

Figure 22. Interlayered orthogneiss and paragneiss; southeastern corner of Algae Lake. Height of cliff about 80m.

Almandine-pyrope garnet (2–15%), reddish-brown biotite (up to 6%), quartz (30–50%), perthite (up to 50%), plagioclase (commonly An_{25-40}: up to 50%) and minor opaque minerals and zircon occur in most rocks. Small amounts of apatite, rutile, monazite, corundum, spinel, and sillimanite may also be present. Some layers contain orthopyroxene (Table 3), which is often partly altered to iddingsite or fine-grained biotite. Some gneiss contains up to 80 per cent quartz. In contrast to the felsic orthogneiss (orthopyroxene-quartz-feldspar gneiss), garnet-bearing gneiss is mostly relatively potassic, with K-feldspar being the dominant feldspar. However, some contains only antiperthite, and apparently corresponds to the biotite-garnet-plagioclase gneiss group of Ravich et al. (1968).

Most garnet-bearing gneiss samples plot in the quartz field on the Q-Ab-Or diagram (Fig. 12B), consistent with a sedimentary origin, although those plotting near the granite minimum may well represent partial melts. This contrasts with the abundance of garnet leucogneiss of intrusive igneous origin in the Napier Complex (Sheraton & Black 1983). Garnet-bearing orthogneiss is significantly C-normative (Table 2, Fig. 14) and therefore corresponds to the S-type (sedimentary-derived) granitoid of Chappell & White (1974). Garnet gneiss in general has lower Ce/Y and Sr than orthopyroxene-bearing orthogneiss (Fig. 16) and more irregular spidergrams with marked negative Sr anomalies (Fig. 17). Such patterns are typical of felsic igneous rocks formed by intracrustal melting and of clastic sedimentary rocks derived from them (Tarney et al. 1987). K/Rb tends to be lower, for a given K content, than those of the orthopyroxene-bearing gneiss (Fig. 18).

Aluminous metasediments

Aluminous metasediments (metapelites) (*Ᵽsm*) crop out with garnet-quartz-feldspar gneiss in much of the Bunger Hills and nearby islands (Figs 22–24). They characteristically contain significant amounts of sillimanite and cordierite (Figs 25, 26). Garnet (usually 5–25%), sillimanite (up to 10%), reddish-brown biotite (up to 10%), cordierite (up to 25%), commonly antiperthitic oligoclase-andesine (up to 25%), quartz (25–50%), perthite (up to 45%), opaque minerals (magnetite + ilmenite: up to 3%), and minor dark green or brownish-green spinel are prominent constituents. Accessory minerals comprise zircon, rutile, corundum, monazite, and rare apatite and ?chevkinite. Some layers contain orthopyroxene, generally rather altered. Cordierite is partly replaced by pinite and/or biotite. Corundum occurs in association with opaque oxides and spinel (Figs 27, 28), which are often intergrown. Spinel, sillimanite, biotite and quartz all occur as inclusions in garnet. Many of the metapelites have a marked foliation, defined by aligned biotite or sillimanite grains (Fig. 25).

Typical assemblages are:

- garnet + sillimanite ± biotite + K-feldspar + plagioclase + quartz,
- garnet + sillimanite + cordierite ± biotite + K-feldspar + plagioclase + quartz, and
- garnet + cordierite + biotite + K-feldspar + plagioclase + quartz.

Figure 23. Layered orthopyroxene–quartz–feldspar gneiss, garnet–quartz–feldspar gneiss, and metapelite; Aviatorov Peninsula. Felsic boudins at right. Height of cliff about 50m.

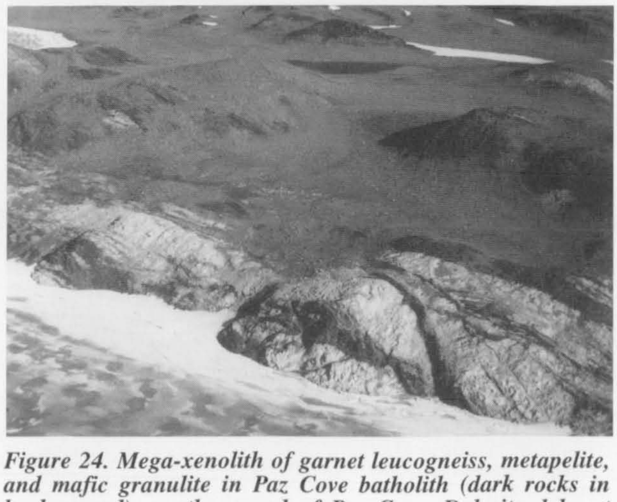

Figure 24. Mega-xenolith of garnet leucogneiss, metapelite, and mafic granulite in Paz Cove batholith (dark rocks in background); southern end of Paz Cove. Dolerite dyke at bottom right.

In many rocks, biotite is clearly secondary, but in others it appears to be primary. The assemblage

- garnet + cordierite + orthopyroxene + biotite + K-feldspar + plagioclase + quartz

is restricted mainly to migmatitic metasediments adjacent to the Booth Peninsula batholith. A few rocks (e.g. from Thomas Island and Krylatyy Peninsula) contain spinel + quartz, either in contact, or separated only by thin rims of cordierite, sillimanite, or garnet (Figs 27, 29). Stüwe & Powell (1989a) have suggested that the assemblages (with quartz and feldspar):

- garnet + cordierite + spinel + spinel + ilmenite, and
- garnet + sillimanite + spinel + ilmenite + rutile

were originally more widely distributed in the metapelites, although in most cases spinel is rimmed by a massive reaction corona of garnet, cordierite, or sillimanite (Figs 30–32). Coexisting sillimanite and orthopyroxene have not been found, and sapphirine was noted in only one sample from moraine in the central Bunger Hills, in association with biotite, cordierite, orthopyroxene, and minor antiperthite (i.e. a silica-deficient assemblage).

Near the large intrusive bodies of the central Bunger Hills and Booth Peninsula, aluminous gneiss is particularly strongly migmatised, with extensive development of granitic leucosome containing irregular, often diffuse layers and schlieren of aluminous melanosome (Fig. 33). Much of this migmatitic gneiss is relatively rich in cordierite (10–25%), with lesser amounts of garnet, sillimanite, biotite, and spinel, as well as quartz and feldspar. Typical exposures are west of Paz Cove,

Table 3. Representative analyses of minerals in felsic gneisses (samples 1–4,8) and mafic granulites (samples 5–7) from Bunger Hills area, and felsic gneiss (sample 9) from Cape Charcot, Denman Glacier area. Sample details are given in Table 23.

	1 *86285679*		*2* *86285979*		*3* *86286056*		*4* *86286072*		*5* *86285984*		
	Op	*Gt*	*Op*	*Gt*	*Op*	*Gt*	*Op*	*Gt*	*Op*	*Gt*	*Cp*
SiO_2	51.74	39.22	51.54	38.16	49.94	38.08	10.54	38.90	51.61	38.27	52.24
TiO_2	–	–	–	–	0.17	–	0.18	–	–	–	0.16
Al_2O_3	4.89	21.84	2.07	20.94	4.61	21.19	4.77	21.73	1.27	20.77	2.58
FeO^+	22.77	26.84	29.59	30.49	27.79	30.83	24.21	27.58	28.32	28.21	12.13
MnO	0.23	1.03	0.30	0.99	0.28	1.11	0.42	1.02	0.34	1.19	–
MgO	21.20	9.60	16.73	5.66	17.39	7.01	19.41	9.19	16.95	4.30	10.56
CaO	–	1.44	0.28	3.41	–	1.55	0.16	1.67	0.55	7.25	21.83
Na_2O	–	0.19	0.31	0.30	–	0.24	0.30	0.21	0.18	–	0.55
Total	**100.83**	**100.17**	**100.83**	**99.95**	**100.18**	**100.02**	**99.99**	**100.30**	**99.24**	**99.99**	**100.05**
O	6	12	6	12	6	12	6	12	6	12	6
Si	1.905	3.009	1.966	3.011	1.900	2.993	1.898	2.995	1.992	3.020	1.970
Al^{iv}	0.095	–	0.034	–	0.100	0.007	0.102	0.005	0.008	–	0.030
Al^{vi}	0.117	1.975	0.059	1.948	0.107	1.956	0.109	1.968	0.050	1.932	0.085
Ti	–	–	–	–	0.005	–	0.005	–	–	–	0.005
Fe	0.701	1.722	0.944	2.012	0.884	2.026	0.760	1.776	0.914	1.863	0.383
Mn	0.007	0.067	0.010	0.067	0.009	0.074	0.013	0.066	0.011	0.079	–
Mg	1.163	1.098	0.951	0.665	0.986	0.821	1.086	1.054	0.975	0.506	0.594
Ca	–	0.118	0.012	0.289	–	0.131	0.007	0.138	0.023	0.613	0.882
Na	–	0.029	0.023	0.046	–	0.037	0.022	0.031	0.014	–	0.040
Total	**3.989**	**8.018**	**3.999**	**8.038**	**3.992**	**8.044**	**4.003**	**8.034**	**3.986**	**8.013**	**3.988**
mg	62.4	38.9	50.2	24.8	52.7	28.8	58.8	37.2	51.6	21.4	60.8

+ Total Fe as FeO. mg = atomic 100Mg/(Mg+totalFe).

	6 *86285859*		*7* *86285956*		*8* *86286012*		*9* *86285893*	
	Op	*Cp*	*Op*	*Cp*	*Op*	*Cp*	*Op*	*Cp*
SiO_2	53.27	52.76	53.25	52.56	53.46	53.71	53.73	54.17
TiO_2	0.10	0.15	–	0.16	–	–	–	–
Al_2O_3	1.49	2.25	1.24	2.54	0.76	1.71	0.52	0.90
FeO^+	22.60	9.18	22.60	10.43	22.23	8.19	25.62	9.38
MnO	0.91	0.30	0.75	0.20	0.69	0.16	0.55	0.14
MgO	20.80	12.85	21.38	12.56	21.84	13.29	19.48	13.74
CaO	0.66	21.76	0.55	21.12	0.40	21.95	0.62	21.38
Na_2O	0.18	0.53	0.19	0.57	0.15	0.69	–	0.50
Total	**100.02**	**99.79**	**99.96**	**100.14**	**99.53**	**99.70**	**100.53**	**100.21**
O	6	6	6	6	6	6	6	6
Si	1.987	1.971	1.986	1.963	1.998	1.996	2.015	2.009
Al^{iv}	0.013	0.029	0.014	0.037	0.002	0.004	–	–
Al^{vi}	0.053	0.070	0.031	0.075	0.032	0.071	0.023	0.039
Ti	0.003	0.004	–	0.005	–	–	–	–
Fe	0.705	0.287	0.705	0.326	0.695	0.255	0.804	0.291
Mn	0.029	0.010	0.024	0.006	0.022	0.005	0.018	0.005
Mg	1.156	0.716	1.189	0.699	1.217	0.736	1.089	0.760
Ca	0.026	0.871	0.022	0.845	0.016	0.874	0.025	0.850
Na	0.013	0.039	0.014	0.041	0.011	0.050	–	0.036
Total	**3.984**	**3.995**	**3.994**	**3.997**	**3.991**	**3.991**	**3.973**	**3.989**
mg	62.1	71.4	62.8	68.2	63.7	74.3	57.5	72.3

Thomas Island, Fuller Island, and the islands north and south of Booth Peninsula (e.g. Miles and Obryvistyy Islands).

The metapelites were clearly derived from more mature sediments than most of the garnet-quartz-feldspar gneiss. They are richer in quartz, tend to be more potassic (higher Or/Ab: Figs 12, 13), and are more depleted in CaO and Sr (Table 4, Fig. 16). There is a reasonably good correlation of the observed mineral assemblages in the various metasedimentary rocks with those predicted from a modified AFM diagram (Fig. 34). None of the metapelite samples has such high K/Rb as the more extreme orthogneiss values, even for

Figure 25. Garnet–sillimanite–quartz–K-feldspar paragneiss (metapelite), showing sillimanite-rich layers with minor biotite passing around partly rotated garnets with sieve-like texture; southwestern Thomas Island. Sample 86285636; width of field: 15mm.

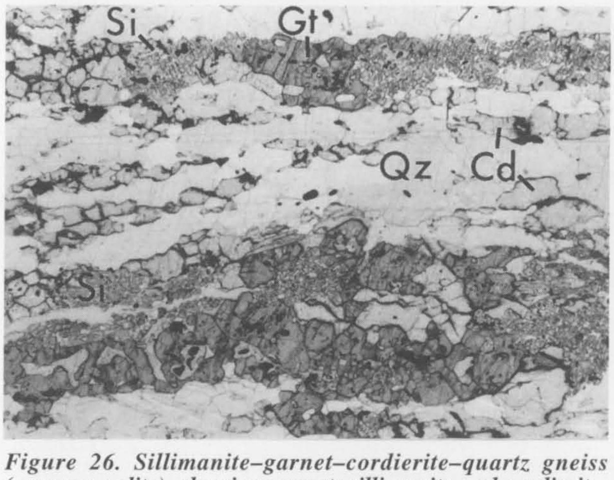

Figure 26. Sillimanite–garnet–cordierite–quartz gneiss (psammo-pelite), showing garnet+sillimanite and cordierite-rich layers; southeastern Paz Cove. Sample 86285885; width of field: 8mm. Mineral abbreviations as in Table 1.

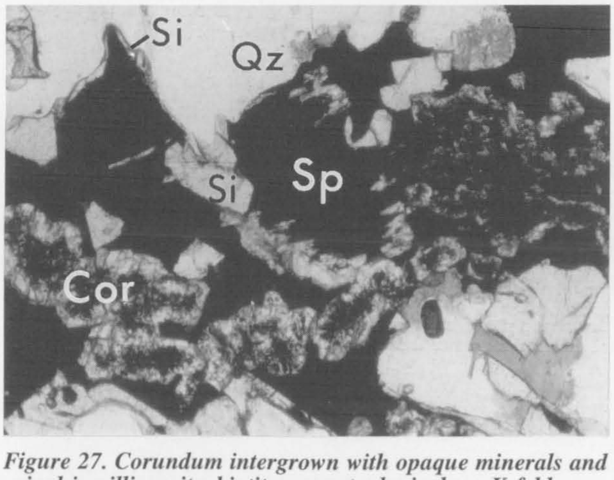

Figure 27. Corundum intergrown with opaque minerals and spinel in sillimanite–biotite–garnet–plagioclase–K-feldspar–quartz metapelite; northern Thomas Island. Spinel is separated from quartz by only a thin rim of sillimanite. Sample 86285631; width of field: 1.5mm.

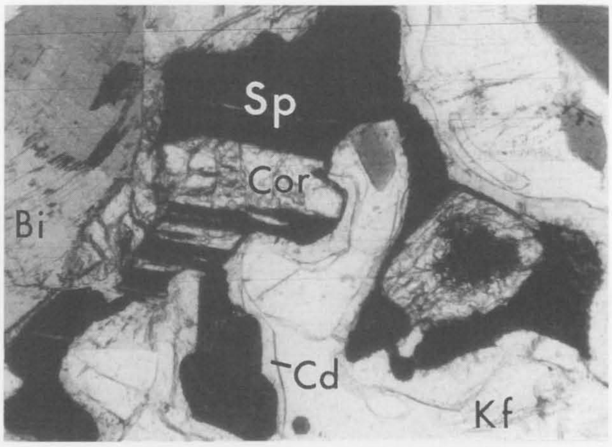

Figure 28. Corundum intergrown with opaque minerals and spinel in cordierite–biotite–sillimanite–garnet–K-feldspar–quartz metapelite; northern Thomas Island. Sample 86285634; width of field: 0.8mm.

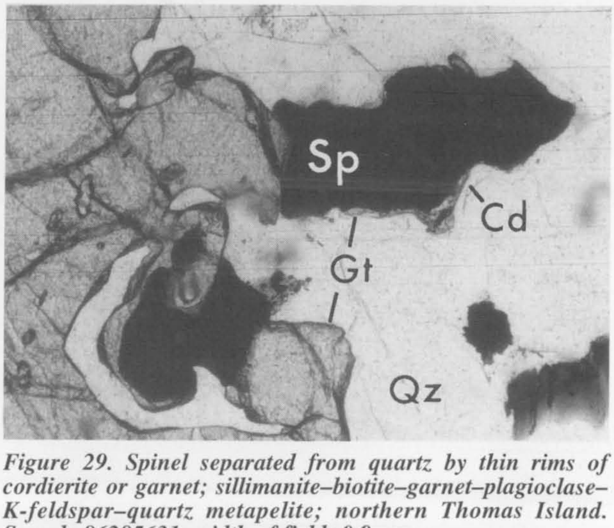

Figure 29. Spinel separated from quartz by thin rims of cordierite or garnet; sillimanite–biotite–garnet–plagioclase–K-feldspar–quartz metapelite; northern Thomas Island. Sample 86285631; width of field: 0.9mm.

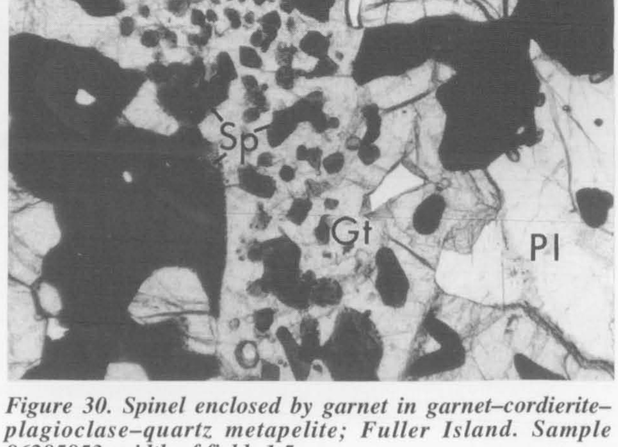

Figure 30. Spinel enclosed by garnet in garnet–cordierite–plagioclase–quartz metapelite; Fuller Island. Sample 86285853; width of field: 1.5mm.

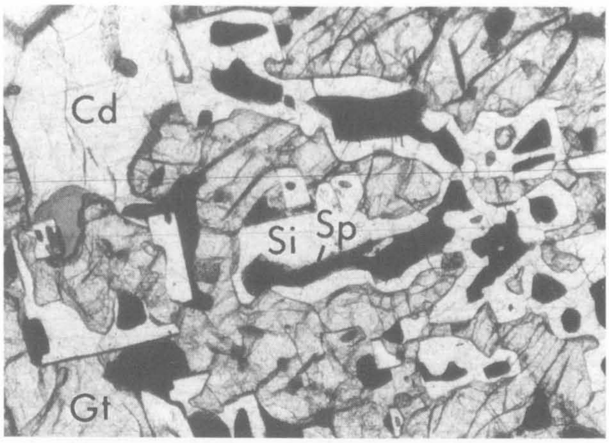

Figure 31. Spinel rimmed by sillimanite, enclosed by garnet, in garnet–sillimanite–cordierite–plagioclase–K-feldspar–quartz metapelite; Saturn Island. Sample 86285842; width of field: 1.2mm.

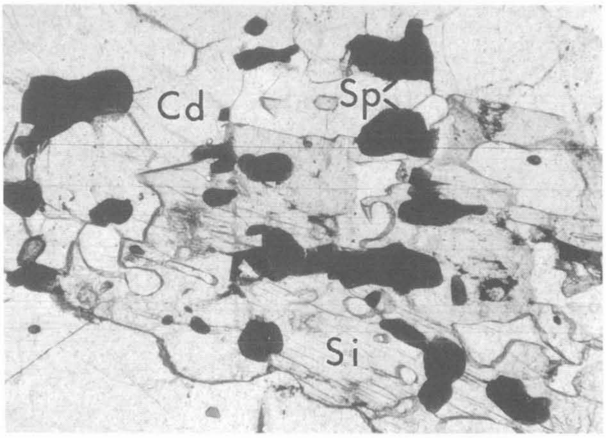

Figure 32. Spinel enclosed by sillimanite and cordierite in sillimanite–garnet–cordierite–plagioclase–K-feldspar–quartz metapelite; Zabytyy Island. Sample 86286248; width of field; 1.2mm.

Figure 33. Migmatitic garnet–cordierite–quartz–feldspar paragneiss, showing partial melt bodies; west of Paz Cove.

low K contents (Fig. 18), which suggests that the high ratios of many of the orthogneiss samples may partly reflect high primary igneous values, rather than being entirely due to metamorphic depletion of LILE.

Quartzite

Impure quartzite is a minor component of the layered metasediments (garnet gneiss and metapelite) already discussed.

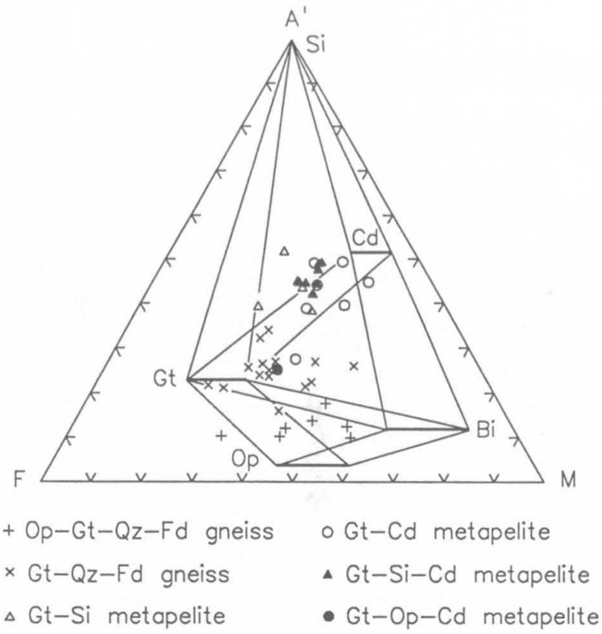

Figure 34. Modified A'FM diagram for paragneisses and metapelites from the Bunger Hills area. A' = Al_2O_3–(K_2O+Na_2O+CaO), F = total Fe as FeO, M = MgO (all as molecular proportions). Mineral abbreviations as in Table 1.

Apart from quartz (up to 90%), subordinate garnet, sillimanite, K-feldspar, plagioclase, biotite, and orthopyroxene may be present. Ravich et al. (1968) described a layer of garnet quartzite 150 m thick at Grace Rocks, but this was not examined in 1986.

Calc-silicate rocks and marble

These occur in association with other metasedimentary rocks throughout the Bunger Hills and adjacent islands, but are only of minor volume. They form concordant, mostly boudinaged, layers with individual boudins averaging a few metres long. Ravich et al. (1968) described these rocks in detail and recognised several major variants. Marble and diopside-forsterite marble are widespread and contain subordinate quartz, plagioclase, scapolite, phlogopite, spinel, sphene, amphibole, garnet, and apatite. Scapolite-diopside, diopside, and plagioclase-diopside rocks are the commonest of the calc-silicates, and form layers and boudins, as well as marginal zones to the marbles. Scapolite-diopside rocks generally contain 10–35 per cent quartz and 5–15 per cent carbonate. Plagioclase is mainly sodic bytownite (An_{69-82}). Minor phases in the calc-silicate rocks are sphene, spinel, phlogopite, apatite, opaque minerals, and rare garnet.

Certain two-pyroxene and two-pyroxene-plagioclase rocks, in which diopside is more abundant than orthopyroxene, should probably be classified as calc-silicate, rather than the igneous pyroxenite described above. Alteration of calc-silicate bodies in retrograde zones has locally resulted in the formation of phlogopite-tremolite schist.

Igneous rocks

Mafic to felsic plutonic rocks

Three intrusive bodies (charnockites of Ravich et al. 1968), 5–20 km across, crop out in the Bunger Hills: the Algae Lake pluton and the Paz Cove and Booth Peninsula batholiths. They clearly postdate the peak of the high-grade metamorphism and were probably emplaced during or after the third major deformation (D_3). Contacts are mostly subconcordant and commonly indistinct, and may be transitional in places. How-

Figure 35. Intrusive contact of Paz Cove batholith with felsic orthogneiss; Vertoletnyy Peninsula. (University of Melbourne photograph).

Figure 36. Gneiss xenoliths in foliated granitic intrusive; Bunger Hills. (University of Melbourne photograph).

ever, there are many clear examples of cross-cutting contacts (Fig. 35) and xenoliths of country rocks are present locally (Fig. 36). All three bodies are characterised by the presence of orthopyroxene, with lesser amounts of clinopyroxene, biotite, and hornblende. Their composition ranges from gabbro to granite, and at least three geochemically distinct suites (gabbroic, granitic, and quartz monzodioritic) are present (Sheraton et al. 1992).

The Algae Lake pluton and Paz Cove batholith crop out over about 20 and 80 km^2, respectively, although the former may be much larger if it extends under the Apfel Glacier to the isolated Grace Rocks, about 10 km to the south. These two bodies were termed the Lake Figure and Fishtail Gulf plutons, respectively, by Sheraton et al. (1992), but have been (informally) renamed to reflect the official AUSLIG nomenclature of geographic features. Pluton is used for a single, compositionally coherent intrusion, whereas batholith refers to a composite body comprising two or more compositionally distinct, genetically unrelated components. The Algae Lake pluton consists of quartz gabbro and quartz monzogabbro, grading locally into quartz monzonite (*Ᵽgh*). Most of the Paz Cove batholith is compositionally similar, but granite (*Ᵽgo*) crops out on the western side, on Vertoletnyy and Krylatyy Peninsulas.

The Booth Peninsula batholith (Charnockite Peninsula pluton of Sheraton et al. 1992) is the largest (at least 300 km^2) and compositionally most varied body. It makes up most of Booth, Geomorfologov, and Countess Peninsulas and nearby islands, and part of Miles Island (Fig. 37). It is generally more felsic than the other two bodies (quartz monzodiorite to quartz monzonite (*Ᵽgi*), and granite (*Ᵽgc*), but also includes a significant proportion of gabbro and quartz gabbro (*Ᵽgr*).

Contacts between the various plutonic rock types are difficult to map in detail as they are generally indistinct and most rocks have the dark reddish-brown colour typical of outcrops of 'charnockitic' intrusions. In general, the more felsic varieties postdate the more mafic, although locally they grade into one another. Emplacement of the Paz Cove and Booth Peninsula batholiths, in particular, was accompanied

Figure 37. Outcrops of orthopyroxene granite of the Booth Peninsula batholith; eastern Booth Peninsula, looking southwest.

by widespread migmatisation of the metasedimentary country rocks.

Gabbroic rocks. The Algae Lake pluton and Paz Cove batholith are petrographically very similar, although the latter is interlayered with country rock gneiss (predominantly metasediments) towards the contact, and also contains blocks of gneiss hundreds of metres long, such as near the southeastern corner of Paz Cove (Fig. 24). Both bodies consist predominantly of quartz gabbro or leucogabbro and quartz monzogabbro, grading into quartz monzonite or granodiorite. The presence of labradorite and pyroxene is consistent with these rocks being termed gabbros (strictly gabbronorites) rather than diorites, although their association with more felsic rocks is more typical of diorites.

Texture is hypidiomorphic or allotriomorphic granular to intergranular (Figs 38, 39), and myrmekitic intergrowths are common. Most rocks are medium-grained (0.2–2 mm) and relatively equigranular, although some contain plagioclase crystals up to 5 mm across. Rocks near the contacts, particularly in the Paz Cove intrusion, have a foliation defined by oriented biotite grains and plagioclase laths (Figs 40, 41). Nevertheless, the texture is essentially igneous (intergranular), rather than a superimposed metamorphic one.

The gabbroic rocks comprise greenish-brown pargasitic or hastingsitic hornblende (Leake 1978) (up to 6%), reddish-

Table 4. Chemical analyses of representative aluminous metasediments from Bunger Hills area.

Sample no.	*86285995*	*86285659*	*86285868*	*86285852*	*86285691*	*86285963*	*86285607*	*86285645*
Locality	*Raketa Island*	*Thomas Island E*	*Aviatorov Peninsula S*	*Fuller Island*	*1km S of Edgeworth David*	*6km S of Edgeworth David*	*Currituck Island*	*Thomas Island NW*
Lithology	*Op-Gt-Qz-Pl gneiss*	*Gt-Cd pelite*	*Bi-Gt-Cd pelite*	*Sp-Gt-Cd pelite*	*Cd-Gt-Bi-Si pelite*	*Si-Gt-Cd pelite*	*Si-Gt pelite*	*Bi-Gt-Pl quartzite*
SiO_2	68.50	66.30	66.50	57.40	66.30	70.00	56.30	82.50
TiO_2	0.44	0.95	0.92	1.34	0.82	0.93	1.54	0.94
Al_2O_3	13.55	16.24	14.08	20.81	16.73	15.46	23.45	6.35
Fe_2O_3	1.34	2.83	1.01	5.43	2.80	0.97	3.49	0.73
FeO	7.56	4.32	6.24	8.01	4.18	5.71	7.79	4.55
MnO	0.33	0.24	0.12	0.44	0.16	0.09	0.11	0.09
MgO	3.35	2.46	3.38	4.46	2.64	3.61	3.09	1.96
CaO	1.10	0.87	0.52	0.50	0.55	0.24	2.07	0.90
Na_2O	2.52	1.74	0.90	0.59	0.80	0.25	1.00	0.41
K_2O	1.12	3.22	4.87	0.40	3.70	1.24	0.31	0.52
P_2O_5	0.02	0.03	0.03	0.02	0.04	0.03	0.05	0.03
LOI	0.45	0.84	1.17	0.91	1.15	1.07	0.76	0.55
Rest	0.12	0.26	0.30	0.18	0.33	0.17	0.24	0.20
Total	**100.40**	**100.30**	**100.04**	**100.49**	**100.20**	**99.77**	**100.20**	**99.73**
O=S	0.00	0.00	0.02	0.01	0.03	0.01	0.01	0.04
Total	**100.40**	**100.30**	**100.02**	**100.48**	**100.17**	**99.76**	**100.19**	**99.69**
mg	44.1	50.4	49.1	49.8	53.0	53.0	41.4	43.4
	Trace elements in parts per million							
Ba	295	881	962	109	1063	379	244	143
Rb	9	89	155	14	127	40	10	24
Sr	135	145	133	62	158	31	82	27
Pb	11	31	21	4	19	5	7	4
Th	2	1	3	1	18	3	7	5
U	0.5	1.0	1.5	<0.5	1.0	1.0	<0.5	<0.5
Zr	149	357	297	217	241	240	265	192
Nb	4	10	10	4	10	8	19	13
Y	25	29	36	5	32	31	32	19
La	32	35	25	14	48	11	33	19
Ce	55	58	40	24	94	19	66	35
Nd	17	16	13	8	34	8	28	14
Sc	11	14	15	16	14	15	26	10
V	44	102	116	212	95	131	194	118
Cr	43	119	96	217	104	99	430	75
Ni	7	34	19	64	39	26	52	21
Cu	1	7	22	19	29	22	13	18
Zn	31	77	76	143	58	64	75	47
Sn	<1	2	<1	<1	2	<1	1	<1
Ga	12	21	18	39	21	21	32	7
S	100	100	500	200	600	200	200	900
K/Rb	1030	300	261	237	242	257	257	180
Rb/Sr	0.067	0.61	1.17	0.23	0.80	1.29	0.12	0.89
Ce/Y	2.2	2.0	1.1	4.8	2.9	0.61	2.1	1.8
Th/U	4	1	2	>2	18	3	>14	>10
Nb/Nb*	0.13	0.17	0.13	0.33	0.14	0.37	0.92	0.80
Sr/Sr*	0.30	0.32	0.40	0.31	0.20	0.18	0.14	0.09

mg = atomic $100Mg/(Mg+Fe^{2+})$.

Figure 38. Biotite–clinopyroxene–orthopyroxene gabbro (gabbronorite, s.s.) from the Booth Peninsula batholith, showing typical intergranular texture; Black Island, southeast of Thomas Island. Sample 86285846; cross-polarised light; width of field: 8mm.

Figure 39. Clinopyroxene–biotite–orthopyroxene quartz gabbro from the Paz Cove batholith, showing intergranular texture and randomly orientated biotite grains (top centre); east of Paz Cove. Sample 86286242; cross-polarised light; width of field: 10mm.

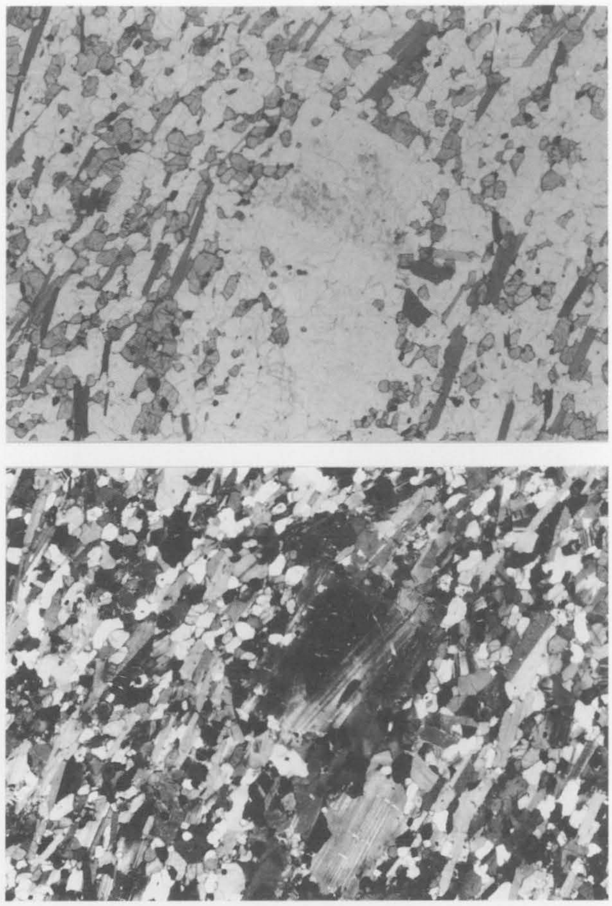

Figure 40. Strongly foliated biotite–clinopyroxene–orthopyroxene quartz monzogabbro, showing essentially intergranular texture with strongly aligned biotite grains and plagioclase laths, and zoned plagioclase phenocrysts; Krylatyy Peninsula. Sample 86286084; cross-polarised light in lower photo; width of field: 5mm.

brown biotite (up to 6%), augite ($Ca_{45}Mg_{36}Fe_{19}$ to $Ca_{42}Mg_{22}Fe_{36}$: 2–6%), pale pink to green pleochroic orthopyroxene ($Ca_2Mg_{55}Fe_{43}$ to $Ca_2Mg_{30}Fe_{68}$: 6-20%), quartz (4-18%), perthitic K-feldspar (up to 30%), zoned plagioclase (mostly An_{50-65}, with some grains to An_{73}: 35–75%), ilmenite + magnetite (1–3%), and minor apatite and zircon. Quartz monzogabbro, grading into quartz monzonite, contains less orthopyroxene (6–12%) and plagioclase (35–55%), and more quartz (10–18%) and K-feldspar (10–30%) than quartz gabbro. Such rocks predominate at Grace Rocks.

Representative analyses of mafic minerals are given in Table 5. Biotite is mostly of late crystallisation and randomly orientated in the centres of the plutons, but more or less aligned near the margins. It is mostly intergrown with quartz, suggesting replacement of early pyroxene (Fig. 42). Hornblende commonly forms large poikilitic grains up to 5 mm across. Plagioclase may be slightly zoned, and K-feldspar is strongly perthitic and commonly poikilitic. Near the northern end of the peninsula east of Paz Cove and, more particularly, on Geologov Island, the quartz gabbro/quartz monzogabbro contains small irregular lenses or schlieren (about 1 cm thick and tens of cms across) of somewhat coarser grained granite (Fig. 43). Such rocks have granodioritic bulk compositions. The granitic lenses contain only minor orthopyroxene and hornblende (Fig. 44), and possibly represent a residual liquid which segregated from the crystallising magma during emplacement.

Gabbro and quartz gabbro crop out in a belt 15 km long, from Fuller Island to western Miles Island, on the western side of the Booth Peninsula batholith. They are petrographically similar to the more mafic components of the Algae Lake and Paz Cove intrusions, and consist of biotite (2–5%), diopside ($Ca_{46}Mg_{36}Fe_{18}$: 5–15%), hypersthene ($Ca_1Mg_{56}Fe_{43}$: 15–20%), K-feldspar (up to 5%), quartz (up to 8%), plagioclase (An_{50-65}: 55–60%), ilmenite + magnetite (1–3%), and minor apatite. Greenish-brown hornblende is present locally, partly replacing pyroxene.

Pressure-temperature (P-T) estimates for the gabbroic and other plutonic rocks, obtained by a variety of methods, are given in Table 6. The two-pyroxene geothermometers of Wood & Banno (1973) and Wells (1977) give temperatures of 800-900°C, in reasonable agreement with the Al^{iv}-in-amphibole thermometer of Blundy & Holland (1990) and the higher of the values obtained by the Ti-in-biotite method of Luhr et al. (1984). However, the graphical two-pyroxene thermometer of Lindsley (1983) gives temperatures of 700–800°C (Fig. 45).

Pressure estimates are mostly between 5 and 7 kb, using the Al-in-amphibole geobarometer of Johnson & Rutherford (1989) and clinopyroxene-plagioclase-quartz equilibria (Ellis, 1980). Pressures calculated using the Al-in-amphibole barometer of Schmidt (1992) tend to be higher (6.7–7.7 kb), but this calibration was carried out under water-saturated conditions and is not, therefore, strictly applicable to the

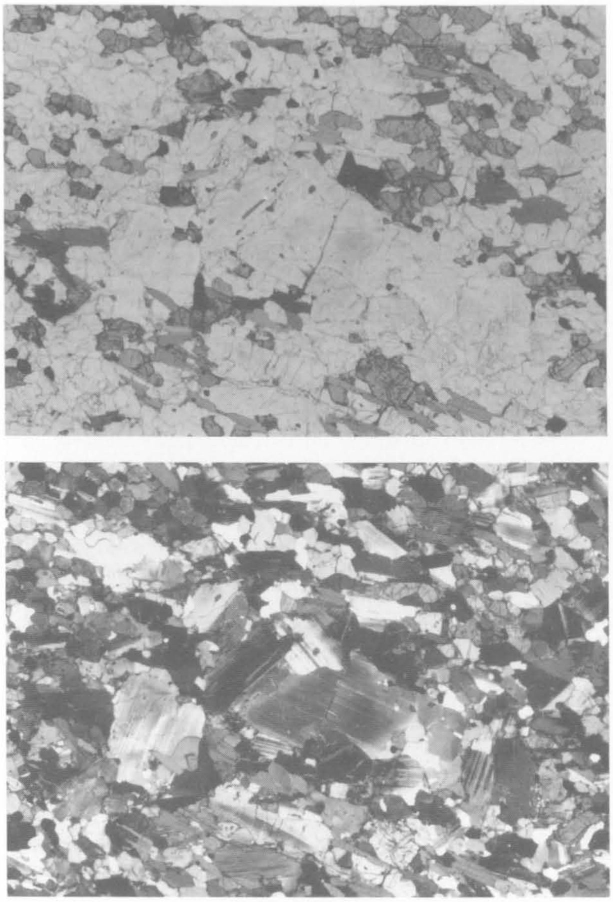

Figure 41. Moderately foliated clinopyroxene–biotite–orthopyroxene quartz monzogabbro, showing intergranular texture with some alignment of biotite and plagioclase grains; Krylatyy Peninsula. Larger plagioclase grains are zoned. Sample 86286083; cross-polarised light in lower photo; width of field: 7mm.

Figure 42. Randomly orientated intergrowth of biotite and quartz replacing pyroxene (mostly orthopyroxene) in clinopyroxene–biotite–orthopyroxene quartz gabbro; east of Paz Cove. Sample 86286242; width of field; 8mm.

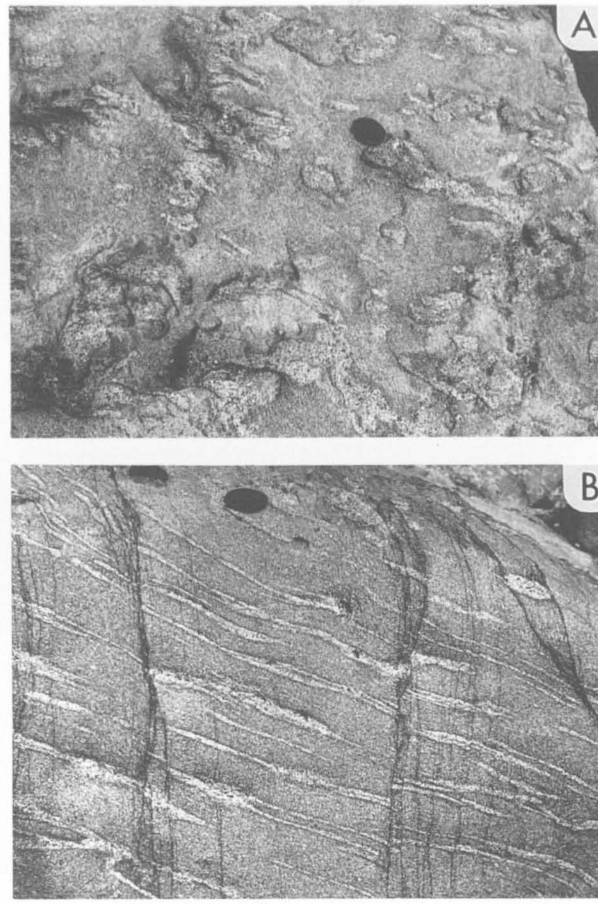

Figure 43. Small lensoid bodies of orthopyroxene–hornblende granite, possibly representing a residual liquid, in clinopyroxene–hornblende–orthopyroxene quartz monzogabbro; Geologov Island. A, View approximately parallel to foliation. B, Cross-section.

Figure 44. Lens of orthopyroxene–hornblende granite in clinopyroxene–hornblende–orthopyroxene quartz monzogabbro; Geologov Island. The granite is relatively coarse grained. Sample 86286218; width of field: 16mm.

Bunger Hills rocks. Garnet granite (86286088) gives a pressure of 4.1 kb (at 850°C) using the garnet-orthopyroxene-plagioclase-quartz barometer of Perkins & Chipera (1985), but the solubility of Al_2O_3 in orthopyroxene coexisting with garnet does not give sensible results. The equation of Harley & Green (1982) gives 18.5 kb at 850°C, whereas that of Harley (1984b) gives negative pressures. This is probably due to the very Fe-rich compositions of the minerals in this rock and extremely high Kd^{Gt-Op}_{Fe-Mg} (~100) values involved (see discussion in Harley 1984b).

Taken together, the data are consistent with emplacement of all three bodies about 20 km deep in the crust during the waning stages of granulite-facies metamorphism, followed by slow cooling and re-equilibration.

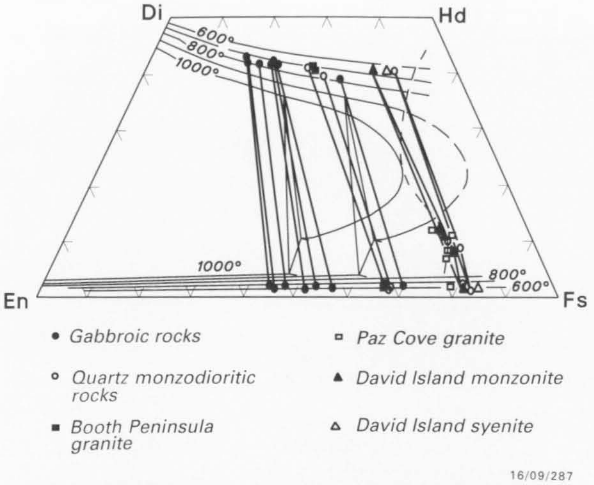

Figure 45. Pyroxene compositions for Bunger Hills and David Island plutonic rocks plotted on the graphical geothermometer of Lindsley (1983) for a pressure of 5kb. Pigeonites plot near the boundary of the 'forbidden zone' (short-dashed line), pyroxene relations to the right of which are metastable with respect to augite+olivine+silica, and have bulk compostions consistent with crystallisation at 800–850°C. Note that pyroxene end-members are corrected for non-quadrilateral components (see Lindsley, 1983).

Most rocks from the Algae Lake pluton (including Grace Rocks) and Paz Cove batholith, as well as the more mafic components of the Booth Peninsula batholith, apparently form a single suite ranging from gabbro to quartz monzogabbro (Table 7, Fig. 46). They are relatively evolved (*mg* = atomic $100Mg/(Mg+Fe^{2+})$ = 28-67, SiO_2 51.0–59.6%) and show a marked tholeiitic Fe-enrichment trend on an AFM diagram (Fig. 47). Normative compositions show a wide range of SiO_2-saturation (Fig. 48) and a trend displaced towards the Or apex on an Ab-Or-An diagram (Fig. 49). Such trends are typical of plutonic rocks in other Antarctic granulite terranes, including the late Archaean Crooked Lake Gneiss in the Vestfold Hills (Sheraton & Collerson 1984) and the Mesoproterozoic Mawson Charnockite (Sheraton 1982).

High P_{CO2}, as is commonly inferred for granulite terranes (Wendlandt 1981), and high An content (James & Hamilton 1969) both tend to result in fractionation trends characterised by high Or/Ab; granitic minimum melts become poorer in quartz at high pressures (Huang & Wyllie 1975). K/Rb does not approach the very high values of some country rock orthogneiss, although the least evolved gabbro and quartz gabbro samples tend to have higher ratios than the other gabbroic rocks (Fig. 50). Pt (<0.5 ppb), Pd (0.5–0.9 ppb), and Au (<1.0–2.0 ppb) are all very low (Sheraton et al. 1992), consistent with the S-saturated (300–1400 ppm S) nature of the magmas (Hamlyn & Keays 1986).

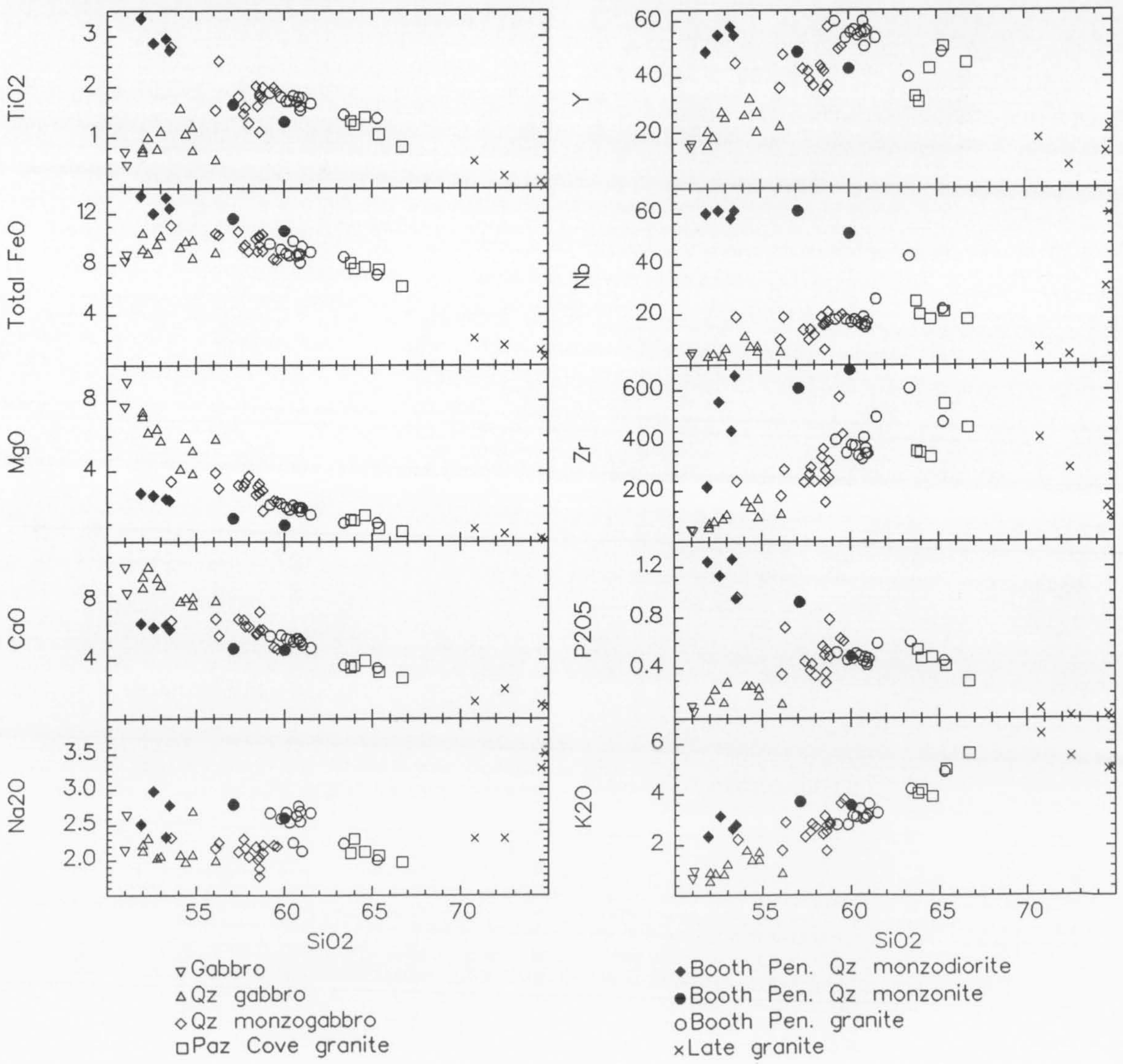

Figure 46. SiO_2 variation diagrams for Bunger Hills plutonic rocks.

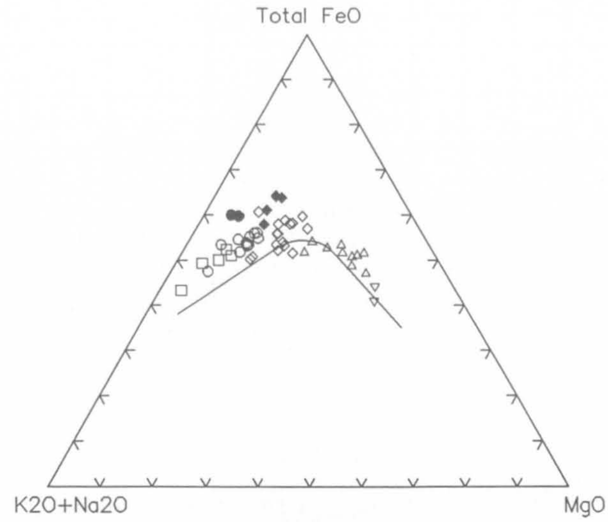

Figure 47. A-F-M diagram for Bunger Hills plutonic rocks, showing the early Fe-enrichment (tholeiitic) trend of the gabbroic rocks. Boundary between tholeiitic and calc-alkaline fields after Irvine & Baragar (1971). Symbols as in Figure 46.

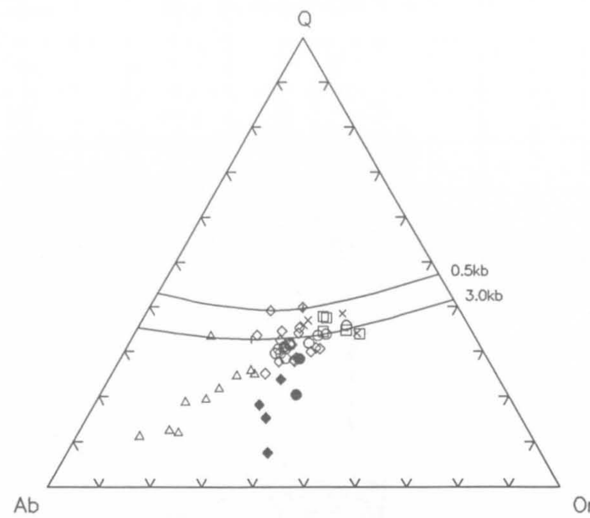

Figure 48. Normative Q-Ab-Or diagram for Bunger Hills plutonic rocks, showing the distinct trend defined by the quartz monzodioritic rocks of the Booth Peninsula batholith. Quartz-feldspar field boundaries after Tuttle & Bowen (1958). Symbols as in Figure 46.

Essentially continuous variation trends (Figs 46–50) and near-constant incompatible element ratios (Fig. 51) for most of the gabbroic rocks are consistent with a common origin and suggest that fractional crystallisation was important in their petrogenesis. Fractionation of orthopyroxene, clinopyroxene, plagioclase, and minor ilmenite can explain most of the chemical variations, as well as differences in the generally very similar spidergrams (Fig. 52). However, petrogenetic modelling by Sheraton et al. (1992) has shown that significant fractionation of olivine (or an Ol-normative mineral such as biotite or hornblende), for which there is no petrographic evidence, would also be required. Moreover, trends of normative Hy and Di, as well as alumina-saturation, for individual rock types on SiO_2 variation diagrams tend to be oblique to the overall trends (Fig. 53), and some elements, such as P_2O_5, show significant variation for a given SiO_2 content (Fig. 46). Such features probably reflect differences in the degree and/or conditions of melting and imply that the gabbro, quartz gabbro and quartz monzogabbro were derived from distinct parent magmas. Nevertheless, REE data are consistent with virtually all of the gabbroic rocks having been derived by partial melting of a similar mantle source with only relatively small variations in the amount of residual (or fractionating) clinopyroxene (Sheraton et al. 1992).

Ratios of LILE, LREE, and HFSE (high field strength elements: P, Nb, Zr, Ti, etc.), which, for sub-alkaline mafic rocks at least, are essentially incompatible during partial melting or fractionation processes, should reflect those of the source region. Many such ratios are indeed essentially constant over the whole compositional range of the gabbroic rocks (Fig. 51), and hence should approximate those of the mantle source. HFSE ratios (P/Zr, Nb/Zr) are close to estimated primordial mantle (PM) values (Sun & McDonough 1989), whereas the source appears to have been strongly enriched in LREE and particularly LILE.

It is very unlikely, in view of the near-constant LILE/HFSE ratios, that this enrichment was due to AFC (assimilation-fractional crystallisation) processes (DePaolo 1981). However, the significant scatter for many of these elements could be due to crustal contamination, source heterogeneity, or both. Source heterogeneity is suggested by the higher Nb/Zr (and possibly K/Zr) of the two gabbro samples, and the significant differences in P/Zr may reflect an irregular distribution of apatite in the mantle source (Menzies & Wass 1983). Negative Nb anomalies on the spidergrams (Fig. 52) are characteristic of subduction-related magmatism, and metasomatic enrichment of the subcontinental lithosphere in LILE and LREE — ultimately derived by partial melting of subducted oceanic crust, probably with a sedimentary component — could produce the required Nb-poor mantle (Tarney & Weaver 1987; Nelson & McCulloch 1989; Sun & McDonough 1989). Very low Th and U (Fig. 52) may be a result of these elements having migrated in hydrous fluids (Smithson & Heier, 1971) towards the upper parts of the intrusions, which have since been removed by erosion.

Isotopic data are consistent with derivation of the gabbroic rocks from a heterogeneous long-enriched mantle source (initial $^{87}Sr/^{86}Sr = Sr_i = 0.7091$-$0.7144$, ε_{Nd} -9.4: Table 8). The very high Sr_i and low ε_{Nd} values are, presumably, of crustal origin, but whether they entirely reflect subduction-related mantle-enrichment processes or are partly due to more direct crustal contamination is uncertain. Nevertheless, a T^{Nd}_{DM} model age of 2310 Ma for a quartz monzogabbro, if taken at face value, suggests that source enrichment may have been coeval with continental crust formation (Table 8). Quartz monzogabbro from both the Algae Lake and Paz Cove bodies has given indistinguishable conventional zircon U-Pb ages of 1171±3 and 1170±4 Ma, respectively (Sheraton et al. 1992).

Granitic rocks. Medium to coarse-grained, slightly porphyritic, garnet-orthopyroxene granite crops out on the western side of the Paz Cove batholith. Unlike the gabbroic rocks, the granite does not have a distinct foliation. It comprises iron-rich orthopyroxene ($Ca_2Mg_{20}Fe_{78}$: 4–7%), almandine-rich garnet (up to 10%), quartz (20–30%), plagioclase ($An_{40\text{-}45}$: 25–35%), perthite (25–40%), and minor ilmenite, magnetite, iron-rich augite, hornblende, biotite, apatite, and zircon. Orthopyroxene contains exsolution lamellae of clinopyroxene, and some grains have compositions near $Ca_8Mg_{18}Fe_{74}$ (Table 5), suggesting inversion of original pigeonite.

Some garnet occurs as symplectitic rims around orthopyroxene (Fig. 54) and may have formed during near-isobaric cooling, although there is no significant compositional difference between primary and secondary garnet. The distribution of garnet is markedly irregular, both in hand specimens and

Table 5. Representative analyses of minerals from Bunger Hills plutonic rocks.

	Booth Peninsula Qz gabbro (86285845)			*Algae Lake Qz gabbro (86285944)*				*Paz Cove Qz monzogabbro (86286245)*			*Booth Peninsula Qz monzodiorite (86286052)*		
	Op	*Cp*	*Bi*	*Op*	*Cp*	*Hb**	*Bi*	*Op*	*Cp*	*Hb**	*Op*	*Cp*	*Hb**
SiO_2	52.29	52.12	34.78	51.39	51.04	41.29	35.30	48.13	49.04	40.14	49.25s	49.97	40.74
$TiO2_2$	0.09	0.28	5.27	0.09	0.26	1.94	2.91	0.14	0.27	1.67	0.12	0.22	1.76
Al_2O_3	1.15	2.19	13.93	1.20	2.20	11.70	15.88	0.88	2.02	11.90	0.75	1.51	11.40
FeO^+	26.52	10.78	15.75	30.47	13.60	18.62	18.60	39.42	21.20	23.87	38.31	19.87	22.72
MnO	0.70	0.34	0.05	0.74	0.31	0.15	0.08	1.28	0.66	0.21	0.98	0.48	0.20
MgO	19.14	12.48	12.97	16.40	10.99	8.85	11.81	9.20	7.09	5.40	10.35	8.17	6.01
CaO	0.92	21.94	0.03	0.56	21.00	11.08	0.07	0.97	18.75	11.04	0.96	19.24	11.15
Na_2O	0.00	0.37	0.00	0.02	0.38	1.16	0.02	0.02	0.28	1.20	0.02	0.26	1.15
K_2O	0.00	0.00	9.92	0.00	0.00	2.10	9.51	0.00	0.00	1.76	0.00	0.00	1.63
Cr_2O_3	0.03	0.02	0.10	0.00	0.03	0.00	0.00	0.00	0.00	0.00	0.00	0.00	0.00
BaO	–	–	–	–	–	–	0.16	–	–	–	–	–	–
F	–	–	0.04	–	–	–	0.12	–	–	–	–	–	–
Cl	–	–	0.07	–	–	–	0.06	–	–	–	–	–	–
Total	**100.84**	**100.52**	**92.81**	**100.87**	**99.80**	**96.89**	**94.52**	**100.04**	**99.31**	**97.19**	**100.74**	**99.72**	**96.76**
O	6	6	22	6	6	23	22	6	6	23	6	6	23
Si	1.973	1.951	5.416	1.974	1.947	6.283	5.431	1.966	1.945	6.242	1.979	1.959	6.333
Al^{iv}	0.027	0.049	2.557	0.026	0.053	1.717	2.569	0.034	0.055	1.758	0.021	0.041	1.667
Al^{vi}	0.024	0.048	–	0.028	0.046	0.382	0.311	0.008	0.039	0.423	0.015	0.029	0.422
Ti	0.003	0.008	0.617	0.003	0.007	0.222	0.337	0.004	0.008	0.195	0.004	0.006	0.206
Fe^3	–	–	–	–	–	0.528	–	–	–	0.556	–	–	0.448
Fe^2	0.837	0.337	2.051	0.979	0.434	1.841	2.393	1.347	0.703	2.547	1.287	0.652	2.505
Mn	0.022	0.011	0.007	0.024	0.010	0.019	0.010	0.044	0.022	0.028	0.033	0.016	0.026
Mg	1.076	0.696	3.011	0.939	0.625	2.008	2.709	0.560	0.419	1.252	0.620	0.478	1.393
Ca	0.037	0.880	0.005	0.023	0.858	1.807	0.012	0.042	0.797	1.839	0.041	0.808	1.857
Na	0.000	0.027	0.000	0.001	0.028	0.342	0.006	0.002	0.022	0.362	0.002	0.020	0.347
K	0.000	0.000	1.971	0.000	0.000	0.408	1.866	0.000	0.000	0.349	0.000	0.000	0.323
Cr	0.001	0.001	0.012	0.000	0.001	0.000	0.000	0.000	0.000	0.000	0.000	0.000	0.000
Ba	–	–	–	–	–	–	0.010	–	–	–	–	–	–
F	–	–	0.020	–	–	–	0.058	–	–	–	–	–	–
Cl	–	–	0.018	–	–	–	0.016	–	–	–	–	–	–
Total	**4.000**	**4.007**	**15.685**	**3.997**	**4.010**	**15.557**	**15.728**	**4.009**	**4.010**	**15.550**	**4.001**	**4.009**	**15.527**
mg	56.2	67.4	59.5	49.0	59.0	52.2	53.1	29.4	37.3	32.9	32.5	42.3	35.7

\+ Total Fe as FeO. mg = atomic 100 Mg/(Mg+total Fe), or 100 Mg/(Mg+Fe^{2+}) for hornblende.
* Fe^{3+} in hornblendes calculated assuming total cations (excluding Ca, Na, and K) = 13.

	Booth Peninsula Qz monzonite (86285972)			*Booth Peninsula Granite (86285828)*			*Paz Cove Granite (86286088)*				
	Op	*Pig*	*Cp*	*Op*	*Cp*	*Hb**	*Op*	*Pig*	*Hb**	*Bi*	*Gt*
SiO_2	47.30	47.63	49.15	48.33	49.91	40.88	47.52	47.53	39.52	35.66	37.58
TiO_2	0.07	0.10	0.16	0.12	0.18	2.16	0.13	0.10	1.74	4.65	0.07
Al_2O_3	0.50	0.49	1.09	0.84	1.59	11.88	0.43	0.49	11.35	12.91	20.35
FeO^+	45.29	43.00	24.67	37.60	18.82	21.58	44.53	41.78	26.52	27.30	32.67
MnO	1.37	1.27	0.58	1.02	0.53	0.23	0.63	1.23	0.08	0.09	1.31
MgO	5.05	4.69	3.95	10.76	8.47	6.47	5.60	4.75	4.18	5.79	0.83
CaO	0.61	3.05	19.94	0.78	19.77	11.24	1.20	3.88	10.83	0.01	7.78
Na_2O	0.02	0.04	0.27	0.02	0.29	1.27	0.02	0.07	1.54	0.02	0.00
K_2O	0.00	0.00	0.00	0.00	0.00	1.72	0.00	0.00	1.60	9.43	0.00
Cr_2O_3	0.00	0.00	0.00	0.00	0.00	0.00	0.00	0.00	0.00	0.00	0.00
BaO	–	–	–	–	–	–	–	–	–	0.05	–
F	–	–	–	–	–	–	–	–	–	1.00	–
Cl	–	–	–	–	–	–	–	–	–	0.27	–
Total	**100.21**	**100.27**	**99.81**	**99.47**	**99.56**	**97.43**	**100.06**	**99.83**	**97.36**	**97.18**	**100.59**
O	6	6	6	6	6	23	6	6	23	22	12
Si	1.987	1.990	1.978	1.966	1.955	6.298	1.988	1.989	6.213	5.511	3.021
Al^{iv}	0.013	0.010	0.022	0.034	0.045	1.702	0.012	0.011	1.787	2.352	–
Al^{vi}	0.012	0.014	0.030	0.006	0.028	0.455	0.009	0.013	0.317	–	1.929
Ti	0.002	0.003	0.005	0.004	0.005	0.250	0.004	0.003	0.206	0.540	0.004
Fe^3	–	–	–	–	–	0.319	–	–	0.619	–	–
Fe^2	1.591	1.502	0.830	1.279	0.617	2.460	1.558	1.462	2.868	3.528	2.197
Mn	0.049	0.045	0.020	0.035	0.018	0.030	0.022	0.044	0.011	0.012	0.089
Mg	0.316	0.292	0.237	0.652	0.495	1.486	0.349	0.296	0.980	1.334	0.099
Ca	0.027	0.137	0.860	0.034	0.830	1.855	0.054	0.174	1.824	0.002	0.670
Na	0.002	0.003	0.021	0.002	0.022	0.379	0.002	0.006	0.469	0.006	0.000
K	0.000	0.000	0.000	0.000	0.000	0.338	0.000	0.000	0.321	1.859	0.000
Cr	0.000	0.000	0.000	0.000	0.000	0.000	0.000	0.000	0.000	0.000	0.000
Ba	–	–	–	–	–	–	–	–	–	0.003	–
F	–	–	–	–	–	–	–	–	–	0.489	–
Cl	–	–	–	–	–	–	–	–	–	0.071	–
Total	**3.999**	**3.996**	**4.002**	**4.011**	**4.014**	**15.573**	**3.998**	**3.998**	**15.615**	**15.705**	**8.101**
mg	16.6	16.3	22.2	33.8	44.5	37.7	18.3	16.8	25.5	27.4	4.3

Table 6. Summary of pressure–temperature estimates for Bunger Hills and David Island plutonic rocks.

	1	*2*	*3*	*4*	*5*	*6*	*7*
Algae Lake	°C				kb		
Quartz gabbro (5944)*	863	816	709	907	5.5	7.0	6.1
Quartz monzogabbro (5937)	875	831	840	–	–	–	7.2
Quartz monzogabbro (5953)	851	807	842	–	–	–	8.0
Quartz monzogabbro (5962)	861	810	785	912	5.5	7.1	7.9
Paz Cove							
Quartz gabbro (6082)	901	853	777	–	–	–	4.5
Quartz monzogabbro (6245)	878	816	–	881	6.1	7.7	7.2
Granite (6088)**	–	–	673	845	5.4	6.9	–
Booth Peninsula							
Quartz gabbro (5845)	825	805	841	–	–	–	6.7
Quartz monzodiorite (6051)	874	813	–	850	5.7	7.2	5.9
Quartz monzodiorite (6052)	876	814	–	860	5.6	7.2	6.7
Quartz monzonite (5972)	817	789	–	–	–	–	3.9
Granite (5828)	851	798	–	855	5.5	7.0	6.5
Granite (5837)	843	793	–	835	5.2	6.7	5.9
David Island							
Monzonite (6015)	839	799	–	794	4.5	6.0	–
Syenite (6024)	825	794	–	784	4.2	5.6	1.3

* All sample numbers are prefixed '8628'
**A pressure of 4.1kb (garnet–orthopyroxene–plagioclase–quartz barometer of Perkins & Chipera (1985), using the Fe end-member) was obtained at 850°C.

1. Wells (1977).
2. Wood & Banno (1973).
3. Luhr & others (1984).
4. Blundy & Holland (1990), assuming pressures in column 5.
5. Johnson & Rutherford (1989).
6. Schmidt (1992).
7. Ellis (1980), assuming 850°C.

outcrops, and some parts of the intrusion are virtually garnet-free.

The eastern part of the Booth Peninsula batholith, including the small nunataks 5 km east and 20 km ENE of Miles Island, is predominantly of granitic composition, grading locally into quartz monzonite. The rocks are massive, relatively coarse-grained (1–6 mm), melanocratic, and commonly contain poikilitic K-feldspar phenocrysts about 10 mm long. They comprise augite ($Ca_{44}Mg_{25}Fe_{31}$: 1–3%), hastingsitic or pargasitic hornblende (up to 3%), orthopyroxene (near $Ca_2Mg_{32}Fe_{66}$: 5–10%), quartz (15–25%), plagioclase (An_{40-49}: 20–40%), orthoclase or microcline perthite (20–45%), ilmenite + magnetite (1–2%), and minor biotite, apatite, and zircon.

Granite at the nunataks 5 km east of Miles Island is more potassic than elsewhere (40–45% K-feldspar), and there is more extensive shearing, recrystallisation and alteration of pyroxene. Orthopyroxene commonly shows exsolution of clinopyroxene, both as thin lamellae and large blebs (Fig. 55).

The original presence of pigeonite in the Paz Cove granite indicates a crystallisation temperature of about 830°C at 5 kb (or slightly higher temperatures at higher pressures) (Lindsley 1983), in general agreement with temperatures derived for both granitic plutons by other methods (Fig. 45, Table 6).

The granitic rocks plot on continuations of the gabbroic suite trends for most elements (Table 7, Figs 46–51), although the Booth Peninsula granite has higher Na_2O and K/Rb, and defines a more Ab-rich trend on the Ab-Or-An diagram (Fig. 49). Incompatible element/Zr ratios are generally similar, but some (e.g., P/Zr and Ce/Zr) are slightly lower (Fig. 51); Sr_i values (0.7115–0.7147: Table 8) are also comparable to those of the gabbroic rocks. Spidergrams are very similar to those of the quartz monzogabbroic rocks, apart from slightly greater depletion in Sr, Ti, and P (Fig. 52), which can be attributed to plagioclase, ilmenite, and apatite fractionation, respectively. This suggests an ultimate derivation from a similar source (?mantle) to that of the gabbroic suite, but significant compositional differences (e.g. trends of normative components) preclude the granitic and gabbroic rocks being comagmatic (Sheraton et al. 1992).

Although there is no compelling evidence for a major crustal component having been involved in the petrogenesis of the granitic rocks (most of which are only slightly more siliceous than the quartz monzogabbro), some crustal contamination is possible. In particular, the presence of garnet in some of the relatively siliceous Paz Cove granite samples could reflect assimilation of garnet-bearing metasedimentary country rocks, which show evidence of migmatisation and mobilisation. Alternatively, crystallisation of garnet could have been compositionally dependent, as these granites have relatively low *mg* (18–30) and are peraluminous, or close to it (Fig. 53).

Quartz monzodioritic rocks.

The central parts of Miles Island and Booth Peninsula consist of massive slightly porphyritic quartz monzodiorite and quartz monzonite. Poikilitic greenish-brown hastingsitic or pargasitic hornblende (1–5%), iron-rich augite ($Ca_{44}Mg_{25}Fe_{31}$ to $Ca_{44}Mg_{12}Fe_{44}$: up to 6%), iron-rich orthopyroxene ($Ca_2Mg_{32}Fe_{66}$ to $Ca_3Mg_{15}Fe_{82}$: 10–15%), orthoclase or microcline perthite (20–35%), slightly zoned plagioclase (An_{39-50}: 30–50%), opaque minerals (mostly ilmenite: 2–4%), and minor biotite, apatite, allanite, and zircon are present. Some orthopyroxene grains with exsolved clinopyroxene have pigeonitic bulk compositions ($Ca_8Mg_{16}Fe_{76}$: Table 5). Euhedral zircon and apatite are relatively abundant.

In some places, retrogression has resulted in replacement of pyroxene by fine-grained aggregates of biotite, colourless to pale green amphibole, quartz, and minor carbonate, or by yellowish-brown iddingsite. Secondary garnet locally formed along small shear zones.

As in the Paz Cove granite, pigeonite compositions indicate original crystallisation temperatures of at least 820°C, although Ca-rich clinopyroxene and orthopyroxene compositions indicate significantly lower temperatures using Lindsley's (1983) method (Fig. 45).

Rocks of this suite differ in composition from the gabbroic and granitic rocks in a number of important respects (Table 7). They plot on distinct trends on many SiO_2 variation diagrams (Fig. 46), have different normative compositions (Figs 48, 49), and have higher K/Rb (Fig. 50). Large variations in ratios such as Nb/Zr and P/Zr (Fig. 51) are probably at least partly due to source heterogeneity, although variation trends imply fractionation of plagioclase, apatite, and ilmenite, in addition to K-feldspar and pyroxene (Sheraton et al. 1992).

The quartz monzodioritic rocks were apparently derived from a much more Nb-rich source (Nb/Zr up to 4 x PM) than either of the other suites (Fig. 51). This is reflected in the absence of significant Nb anomalies on the spidergrams (Fig. 52), and suggests a source component similar to that of ocean-island basalt (OIB) (Sun & McDonough 1989). Pearce et al. (1984) and Brown et al. (1984) have shown that within-plate granitoids commonly have high Nb (and other HFSE), whereas syn-collisional granitoids have much higher LILE/HFSE ratios.

The degree of LILE enrichment of the source is difficult to estimate in such evolved (*mg* 17–30) rocks, but was apparently similar to, or somewhat less than, that of the gabbroic

Table 7. Chemical analyses of repesentative rocks from Algae Lake, Paz Cove, and Booth Peninsula intrusions.

Sample no.	*86285968*	*86285845*	*86286082*	*86285944*	*86285953*	*86285937*	*86286083*	*86286245*	*86285933*	*86286051*	*86285972*
Lithology	*Bi-Hb-Cp-Op gabbro*	*Bi-Cp-Op quartz gabbro*	*Cp-Op quartz gabbro*	*Hb-Cp-Op quartz gabbro*	*Bi-Cp-Op quartz monzogab.*	*Bi-Cp-Op quartz monzogab.*	*Cp-Bi-Op quartz monzogab.*	*Hb-Cp-Op quartz monzogab.*	*Hb-Op quartz monzogab.*	*Hb-Cp-Op quartz monzodior.*	*Hb-Cp-Op quartz monzonit*
Intrusion	*Booth Pen.*	*Booth Pen.*	*Paz Cove*	*Algae Lake*	*Algae Lake*	*Algae Lake*	*Paz Cove*	*Paz Cove*	*Algae Lake*	*Booth Pen.*	*Booth Pen.*
SiO_2	51.10	52.30	52.80	54.80	53.60	56.10	58.00	58.80	59.60	53.30	60.00
TiO_2	0.47	0.99	0.76	0.73	2.79	1.54	1.29	1.99	1.91	2.95	1.31
Al_2O_3	16.42	17.12	16.27	18.67	15.78	15.34	15.39	3.64	14.46	13.88	13.93
Fe_2O_3	0.81	1.38	0.93	1.52	2.85	3.61	1.28	2.43	2.68	2.94	2.57
FeO	8.09	7.56	8.68	7.05	8.54	7.18	7.86	8.17	5.94	10.62	8.33
MnO	0.19	0.17	0.19	0.16	0.21	0.24	0.19	0.21	0.17	0.26	0.20
MgO	9.08	6.14	6.34	3.81	3.43	3.92	3.71	1.74	2.28	2.43	0.94
CaO	8.53	10.23	9.46	8.15	6.63	6.74	6.23	6.00	4.72	6.34	4.64
Na_2O	2.65	2.30	2.02	2.68	2.32	2.17	2.05	2.10	2.20	2.33	2.60
K_2O	0.98	0.82	0.79	1.37	2.22	1.78	2.71	2.87	3.79	2.64	3.56
P_2O_5	0.06	0.22	0.12	0.17	0.96	0.35	0.34	0.78	0.61	1.26	0.49
LOI	1.64	1.08	1.26	1.07	0.80	0.90	0.88	0.91	1.20	0.79	1.00
Rest	0.26	0.30	0.27	0.34	0.49	0.38	0.35	0.44	0.50	0.63	0.51
Total	**100.28**	**100.61**	**99.89**	**100.52**	**100.62**	**100.25**	**100.28**	**100.08**	**100.06**	**100.37**	**100.08**
O=F,S	0.02	0.05	0.04	0.05	0.07	0.05	0.02	0.06	0.06	0.08	0.05
Total	**100.26**	**100.56**	**99.85**	**100.47**	**100.55**	**100.20**	**100.26**	**100.02**	**100.00**	**100.29**	**100.03**
	C.I.P.W. norms										
Q	–	3.45	5.00	7.36	10.97	14.61	13.35	18.91	18.07	10.99	6.97
C	–	–	–	–	–	–	–	–	–	–	–
Or	5.79	4.85	4.67	8.10	13.12	10.52	16.01	16.96	22.40	15.60	21.04
Ab	22.42	19.46	17.09	22.68	19.63	18.36	17.35	17.77	8.62	19.72	22.00
An	30.01	33.97	32.99	34.87	26.09	26.86	4.79	9.32	18.39	19.62	15.82
Di	9.70	12.58	10.85	3.70	0.44	3.53	3.25	4.56	0.86	3.06	3.46
Hy	19.19	20.53	24.68	18.42	17.42	16.12	19.21	2.11	11.10	17.18	11.92
Ol	9.02	–	–	–	–	–	–	–	–	–	–
Mt	1.17	2.00	1.35	2.20	4.13	5.23	1.86	3.52	3.89	4.26	3.73
Il	0.89	1.88	1.44	1.39	5.30	2.92	2.45	3.78	3.63	5.60	2.49
Ap	0.14	0.52	0.28	0.40	2.27	0.83	0.81	1.85	1.44	2.98	1.16
mg	66.7	59.1	56.6	49.1	41.7	49.3	45.7	27.5	40.6	29.0	16.7
	Trace elements in parts per million										
Ba	248	439	465	690	1156	848	1129	1293	1369	2120	1914
Rb	26	15	16	31	50	48	85	80	110	44	34
Sr	272	361	274	572	484	389	346	348	343	453	401
Pb	6	7	6	11	16	13	16	17	25	14	8
Th	0.66	0.82	1.14	2.59	3.49	4	5.32	1.50	8.58	1.35	0.40
U	0.40	<0.5	1.0	0.53	1.01	0.5	0.78	<0.5	1.25	1.0	0.5
Zr	46	76	86	92	238	181	237	252	427	438	680
Nb	5	4	3	5	19	10	12	21	20	58	52
Y	16	18	27	20	45	36	37	58	51	58	43
La	11.6	16.8	15.5	30.0	56.7	38	47.1	59.4	72.9	71.7	31.2
Ce	23.9	34.7	30.2	55.2	118	79	93.7	129	144	146	67.8
Nd	11.0	18.9	14.4	24.9	65.0	37	42.7	65.9	67.0	69.6	34.6
Sm	2.30	3.39	3.19	4.34	12.0	–	8.62	12.8	13.2	13.0	7.28
Eu	0.84	1.20	1.12	1.54	3.33	–	2.13	3.15	2.92	4.14	3.89
Tb	0.49	0.48	0.70	0.61	1.53	–	1.20	1.84	1.66	1.78	1.30
Yb	1.56	1.62	2.54	1.93	3.30	–	3.07	4.50	3.80	4.66	4.21
Lu	0.27	0.24	0.42	0.31	0.53	–	0.50	0.73	0.64	0.71	0.69
Sc	33	35	36	28	27	30	25	28	21	32	19
V	144	212	156	120	207	194	143	138	140	111	27
Cr	510	133	168	55	65	71	61	2	32	3	<2
Ni	49	33	11	22	10	17	5	3	5	<2	<2
Cu	19	25	14	17	23	28	12	11	14	18	17
Zn	90	79	86	89	149	105	111	137	122	156	121
Sn	–	–	<1	1	<1	<1	<1	<1	2	<1	<1
Ga	16	18	16	22	21	18	18	20	19	18	21
S	500	1000	900	1100	500	500	500	600	300	900	700
F	–	–	–	–	1000	600	–	600	1000	800	300
K/Rb	313	454	410	367	369	308	265	298	286	498	869
Rb/Sr	0.096	0.042	0.058	0.054	0.103	0.123	0.245	0.230	0.321	0.097	0.085
Ce/Y	1.5	2.2	1.3	3.2	2.98	2.19	2.92	2.48	3.14	3.00	1.63
Th/U	1.7	>2	1	4.9	3.5	8	6.8	>3	6.9	1	1
K/Zr	177	90	76	124	77	82	95	95	74	50	43
P/Zr	5.7	13	6.1	8.1	18	8.4	6.3	13	6.2	13	3.1
Nb/Zr	0.11	0.05	0.03	0.05	0.080	0.055	0.051	0.083	0.047	0.13	0.076
Nb/Nb*	0.25	0.19	0.15	0.14	0.33	0.24	0.20	0.30	0.23	0.77	0.85
Sr/Sr*	1.22	1.04	0.96	1.12	0.41	0.52	0.40	0.28	0.25	0.33	0.61

mg = atomic $100Mg/(Mg+Fe^{2+})$.

Sample no.	*86286060*	*86286088*	*86285837*	*86285828*	*86285975*
Lithology	*Op granite*	*Hb-Op-Gt granite*	*Hb-Cp-Op granite*	*Cp-Op granite*	*Bi-Hb-Op granite*
Intrusion	*Paz Cove*	*Paz Cove*	*Booth Pen.*	*Booth Pen.*	*Booth Pen.*
SiO_2	64.00	66.70	59.20	60.90	63.40
TiO_2	1.25	0.81	1.88	1.62	1.45
Al_2O_3	13.92	13.25	14.01	13.71	13.56
Fe_2O_3	1.85	1.82	2.13	1.82	1.76
FeO	5.98	4.58	7.70	7.14	7.00
MnO	0.15	0.12	0.17	0.15	0.17
MgO	1.19	0.58	2.09	1.93	1.06
CaO	3.59	2.74	5.59	5.19	3.65
Na_2O	2.30	1.97	2.67	2.55	2.24
K_2O	4.16	5.61	2.79	3.15	4.20
P_2O_5	0.47	0.29	0.52	0.44	0.60
LOI	0.78	0.68	0.66	1.12	0.72
Rest	0.42	0.49	0.38	0.39	0.46
Total	**100.06**	**99.64**	**99.79**	**100.11**	**100.27**
O=F,S	0.02	0.01	0.02	0.03	0.04
Total	**100.04**	**99.63**	**99.77**	**100.08**	**100.23**
	C.I.P.W. norms				
Q	23.07	25.42	16.37	18.40	22.34
C	0.23	–	–	–	0.13
Or	24.58	33.15	16.49	18.61	24.82
Ab	19.46	16.67	22.59	21.58	8.95
An	14.74	10.74	18.00	16.66	14.19
Di	–	0.83	5.35	5.25	–
Hy	10.63	6.81	12.09	11.36	11.96
Ol	–	–	–	–	–
Mt	2.68	2.64	3.09	2.64	2.55
Il	2.37	1.54	3.57	3.08	2.75
Ap	1.11	0.69	1.23	1.04	1.42
mg	26.2	18.4	32.6	32.5	21.3
	Trace elements in parts per million				
Ba	1973	2740	1356	1436	1774
Rb	100	150	59	70	65
Sr	294	277	259	247	304
Pb	21	26	17	19	15
Th	1.01	1.41	2.04	1.54	0.91
U	0.50	<0.5	1.0	0.87	0.64
Zr	351	451	404	370	606
Nb	20	18	18	16	43
Y	31	45	60	56	40
La	46.4	50.5	47.2	42.7	40.1
Ce	94.8	103	105	92.2	79.0
Nd	51.0	51.9	58.1	50.6	40.6
Sm	9.28	10.2	12.1	10.5	8.02
Eu	3.12	3.64	3.02	2.80	3.05
Tb	1.17	1.35	1.95	1.67	1.18
Yb	1.99	3.98	5.06	4.53	3.35
Lu	0.32	0.65	0.76	0.73	0.55
Sc	21	17	24	24	18
V	70	12	139	120	38
Cr	8	<2	17	15	2
Ni	3	<2	5	5	<2
Cu	19	12	14	15	13
Zn	102	98	114	106	109
Sn	<1	<1	<1	<1	1
Ga	18	17	19	19	20
S	400	200	500	600	400
F	–	–	–	–	400
K/Rb	345	310	393	374	536
Rb/Sr	0.34	0.54	0.228	0.283	0.214
Ce/Y	3.39	2.44	1.92	1.80	2.13
Th/U	2.0	>3	2	1.8	1.4
K/Zr	98	103	57	71	58
P/Zr	5.8	2.8	5.6	5.2	4.3
Nb/Zr	0.057	0.040	0.045	0.043	0.071
Nb/Nb*	0.26	0.18	0.29	0.25	0.58
Sr/Sr*	0.31	0.28	0.25	0.27	0.39

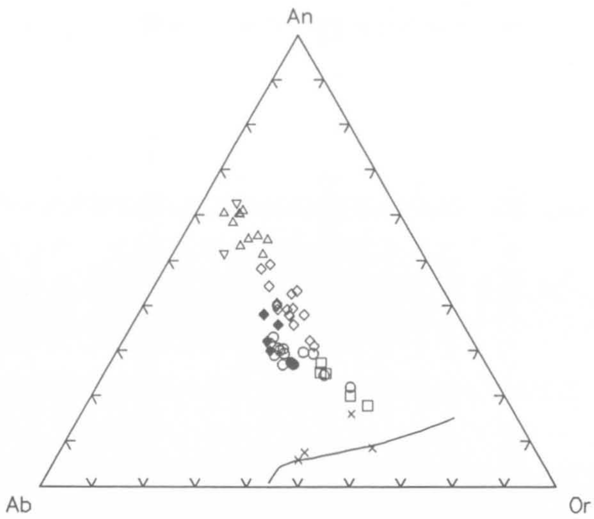

Figure 49. Normative Ab-Or-An diagram for Bunger Hills plutonic rocks, showing the distinct trends of the quartz monzodioritic and granitic rocks of the Booth Peninsula batholith. Plagioclase-alkali feldspar field boundary after James & Hamilton (1969). Symbols as in Figure 46.

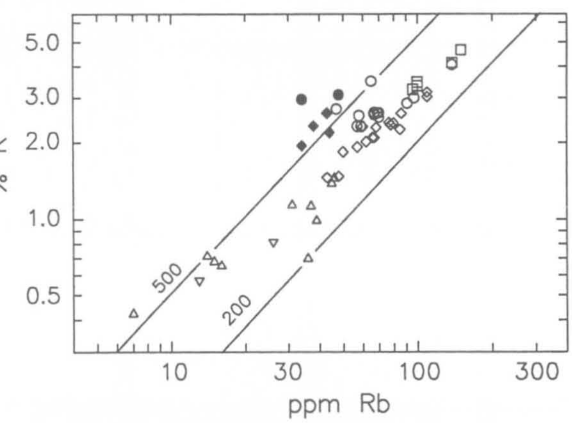

Figure 50. Plot of K against Rb for Bunger Hills plutonic rocks, showing high K/Rb ratios of quartz monzodioritic rocks. Lines of constant K/Rb are indicated. Symbols as in Figure 46.

suite. Limited isotopic data (Sr_i 0.7074–0.7082, ε_{Nd} –3.5) also imply a less-enriched source (or, possibly, less crustal contamination). Quartz monzodiorite from Booth Peninsula has given a zircon U-Pb age of 1151±4 Ma (Sheraton et al. 1992), significantly younger than the gabbroic rocks. However, estimated depths of emplacement are mostly very similar (5–6 kb: Table 6).

Felsic dykes and minor intrusions

Late-stage dykes, mainly felsic, intrude the Booth Peninsula batholith. They intrude all the main rock types, including the gabbro, and the country rock gneiss on nearby islands (e.g. Mars and Husky Dog Islands). Usually 0.1–2 m thick, the dykes are petrographically and chemically similar to the plutonic rocks, but tend to be finer-grained. They include quartz monzodiorite, quartz monzonite, granodiorite, and granite. For example, orthopyroxene quartz gabbro or diorite dykes on Mars Island are probably related to the quartz monzodioritic suite. They have characteristically high Nb (Table 9), but appear to have been depleted in alkalies, possibly by a

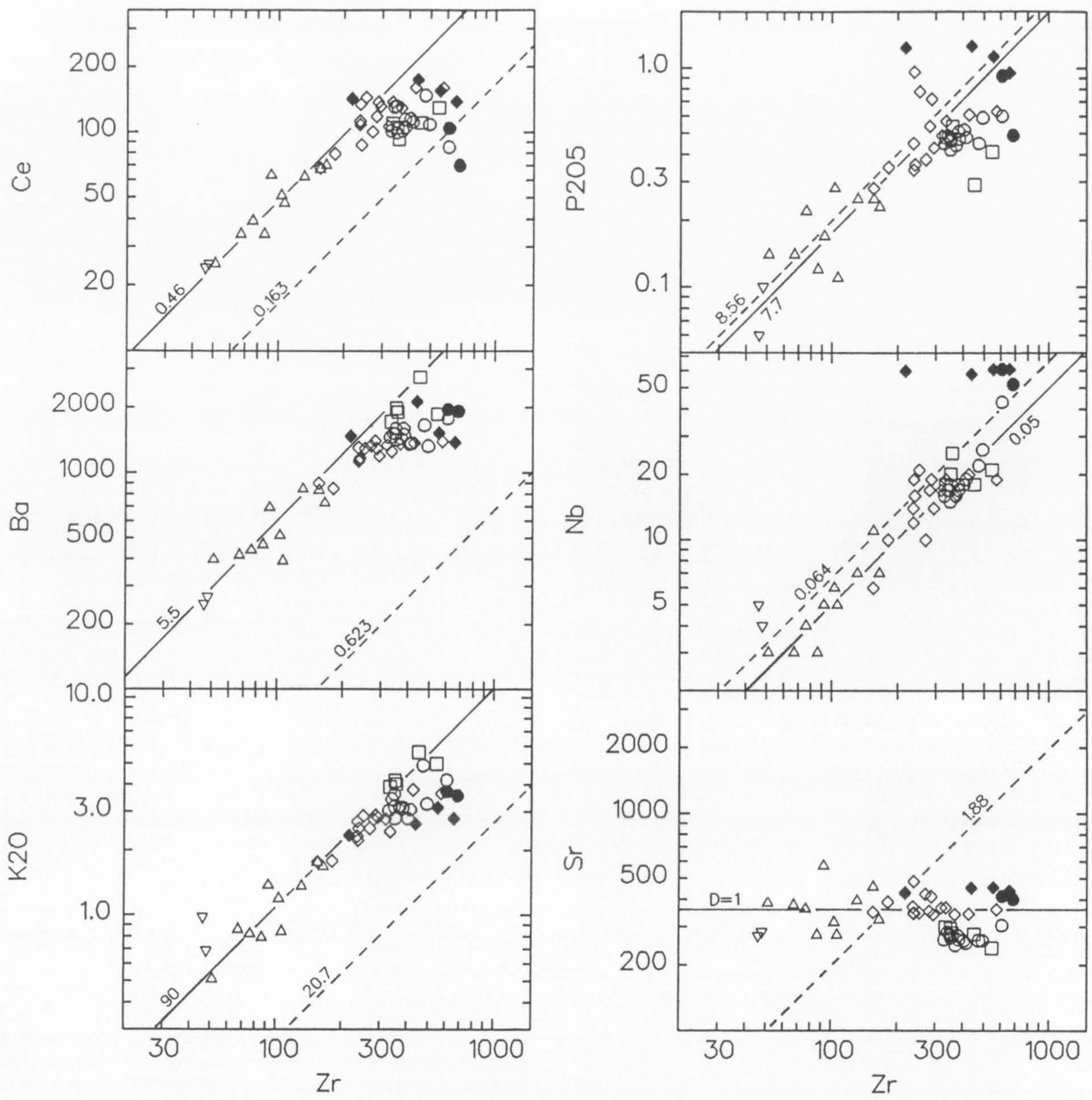

Figure 51. Logarithmic plots of various incompatible elements against Zr for Bunger Hills plutonic rocks. Solid lines of unit slope are those of constant element/Zr ratio, the values of which are indicated. Trends which approximate to such lines, e,g., the gabbroic rocks for most elements, imply that bulk distribution coefficients (D) were close to zero. However, for Sr, D (given by 1-S, where S is the slope) was about 1, reflecting plagioclase fractionation. Dashed lines represent estimated primordial mantle ratios (after Sun & McDonough 1989). See text for further discussion. Symbols as in Figure 46.

late-magmatic fluid. A monzodiorite dyke at Booth Peninsula also has high Nb (Table 9). Many dykes are relatively leucocratic granitic aplites, with less than 5 per cent total mafic minerals. In some, orthopyroxene is largely replaced by iddingsite or fine-grained biotite.

Felsic dykes are not common in the main Bunger Hills, but subconcordant layers of white to pink garnet leucogranite are associated with migmatitic paragneiss adjacent to the Paz Cove batholith. Small bodies, up to a few tens of metres across, of coarse-grained pink granite, grading into pegmatite, are widespread, and those that contain altered orthopyroxene, are probably genetically related to the plutonic rocks. On Geomorfologov Peninsula such pink granite is cut by dolerite dykes, whereas at the eastern end of Thomas Island similar granite clearly postdates syn-plutonic mafic granulite dykes.

Other small bodies of pink granite (e.g. Currituck Island) contain well-crystallised muscovite and dark brown biotite, in addition to quartz, oligoclase, and microcline. These may represent a younger intrusive phase, but no evidence has been found to indicate their age relative to the dolerites. All of the analysed pink granites have high SiO_2 (>70%), are slightly C-normative and have near-minimum melt compositions (Table 9, Figs 46, 48, 49, 53). They have the markedly irregular spidergrams typical of such granites (Fig. 56). However, two pink granites from within or near the Booth Peninsula batholith, which contain secondary biotite ± amphibole, plot on a continuation of the plutonic trend on an Ab-Or-An diagram (Fig. 49); in contrast, two biotite-muscovite granites

Table 8. Sr and Nd isotopic data for rocks from Bunger Hills–Obruchev Hills area.

Sample	Rock type	Locality	$^{87}Sr/^{86}Sr(T)$*	T^{Nd}_{DM}	$\varepsilon Nd(T)$*
86285807	Tonalitic orthogneiss	NE Obruchev Hills	0.70220	2470(2640**)	22.9
5960	Granodioritic orthogneiss	SW Bunger Hills	0.71074	2130	–9.6
5628	Granodioritic orthogneiss	Thomas Island	0.71039	1970	–7.5
5968	Gabbro	Booth Peninsula	0.71010		
6227	Quartz gabbro	SW Paz Cove	0.70907		
6245	Quartz monzogabbro	E of Paz Cove	0.71226		
5962	Quartz monzogabbro	W of Algae Lake	0.71435	2310	–9.4
6089	Granite	W of Paz Cove	0.71471		
5837	Granite	Countess Peninsula	0.71146		
6281	Granite	E of Miles Island	0.71167		
5815	Quartz monzodiorite	Booth Peninsula	0.70819	1840	–3.5
5972	Quartz monzonite	Booth Peninsula	0.70737		
5678	Group 1 dolerite	SW Bunger Hills	0.70493	1940	–0.7
5603	Group 2 high-Mg dolerite	Currituck Island	0.70391	1480	+2.4
6075	Group 4B dolerite	NE of Paz Cove	0.70312	1370	+3.9
5833	Group 4D dolerite	Geomorfologov Peninsula	0.70328	1430	+2.9
5811	Group 4E dolerite	NE Obruchev Hills	0.70298	1110	+6.3
6055	Alkali basalt	Miles Island	0.71679	2080	–17.2
5919	Trachybasalt	N Taylor Islands	0.70846	2290	–18.6

* Calculated at the emplacement age for the intrusive rocks (1170Ma for the gabbroic rocks, 1150Ma for quartz monzodioritic and granitic rocks, 1140Ma for dolerite dykes, and 500Ma for alkaline dykes), and 1160Ma for the country rocks.

The following parameters were used for model age calculations:
$(^{147}Sm/^{144}Nd)_{DM} = 0.225$ (**0.214), $(^{143}Nd/^{144}Nd)_{DM} = 0.51317$

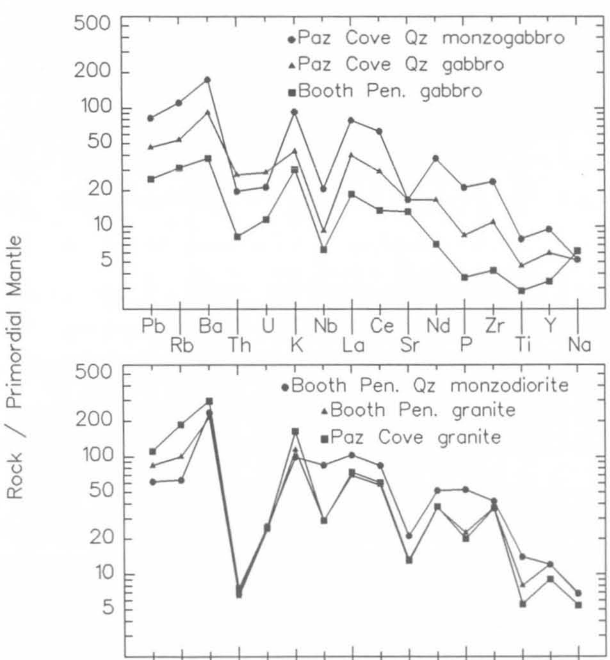

Figure 52. Spidergrams for average Bunger Hills plutonic rocks. The gabbroic rocks have very similar patterns, apart from Sr and Na (which reflect plagioclase fractionation), as do the granitic rocks. The quartz monzodioritic rocks have distinctive patterns without significant Nb anomalies.

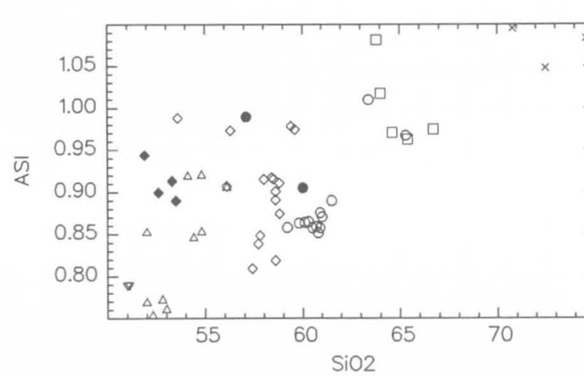

Figure 53. Plot of alumina saturation index against SiO_2 for Bunger Hills plutonic rocks. The trends for the quartz gabbros and quartz monzogabbros are oblique to the overall trend of increasing ASI with SiO_2. Symbols as in Figure 46.

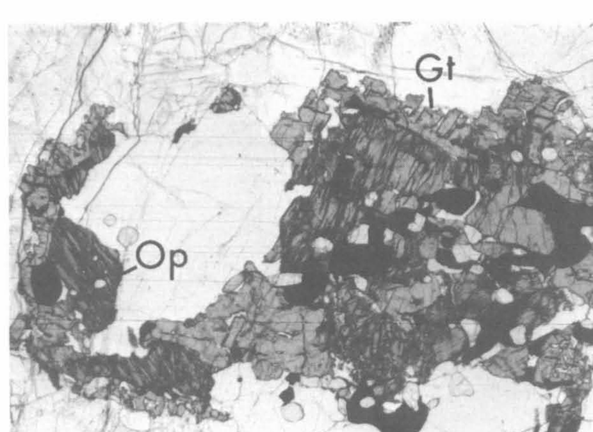

Figure 54. Growth of garnet around orthopyroxene in garnet-orthopyroxene granite of the Paz Cove batholith; Krylatyy Peninsula. Sample 86286088; width of field: 3.5mm.

from Currituck Island plot nearer the granite minimum and have much higher Rb, Pb, U, Nb and Ga, but lower Ba, Sr, and Zr.

A reddish-brown trachyte dyke, 30 cm thick, on Geologov Island has a spherulitic texture, and consists mainly of turbid alkali feldspar, with subordinate carbonate, ?quartz, opaque minerals, and biotite phenocrysts. It has a highly evolved chemical composition, showing extreme enrichment in Th, U, Pb, Zr, Nb, and REE (Table 9, Fig. 98). It does not appear

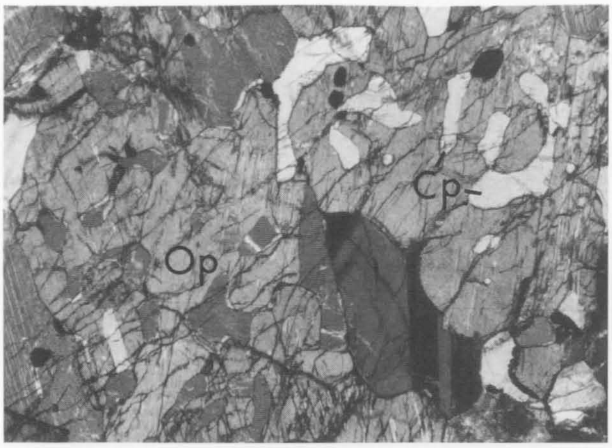

Figure 55. Exsolution of clinopyroxene, as fine lamellae and coarse blebs, from orthopyroxene in hornblende–clinopyroxene–orthopyroxene granite of the Booth Peninsula batholith; eastern Booth Peninsula. Sample 86285830; cross polarised light; width of field: 2.5mm.

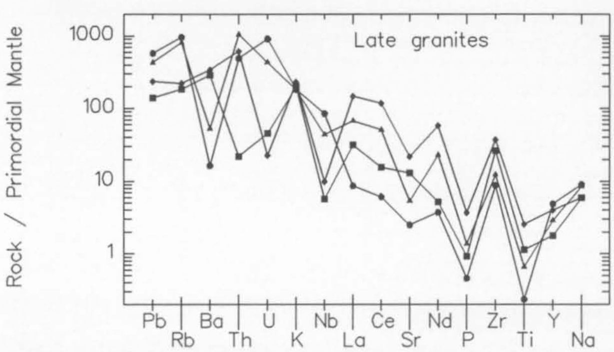

Figure 56. Spidergrams for late granites from the Bunger Hills area.

to be related to the trachyte dykes at Baldwin Rocks (see below), being slightly Ne and Ol-normative, and having higher *mg*, lower SiO_2, and a negative Nb anomaly.

Mafic dykes

Several distinct suites of mafic dykes are present in the Bunger Hills, comprising syn-plutonic mafic granulites and younger unmetamorphosed dykes, with compositions ranging from tholeiitic to alkaline. The most abundant younger dykes are dolerites, which, on geochemical criteria, have been put into four major groups (1–4). All except group 1 demonstrably post-date the plutonic bodies, but dyke intersections are rare, and it has not been possible to deduce a detailed emplacement sequence. These dykes have been described in detail by Sheraton et al. (1990).

Mafic granulite dykes. The oldest recognisable mafic dykes — excluding the concordant granulite layers already described, which may well also be of intrusive origin — comprise subconcordant, but locally cross-cutting, mafic granulite layers in gneiss and folded and boudinaged mafic granulite in the plutons.

Examples of the former are well exposed on Obryvistyy and Thomas Islands, where they are generally folded (Fig. 57). They consist of clinopyroxene (5–15%), greenish-brown hornblende (up to 15%), reddish-brown biotite (up to 15%), orthopyroxene (13–17%), plagioclase (An_{55-70}: 55–60%), opaque minerals (2–7%), and minor quartz and apatite. Their texture is granoblastic (Figs 58, 59). Similar, locally discordant

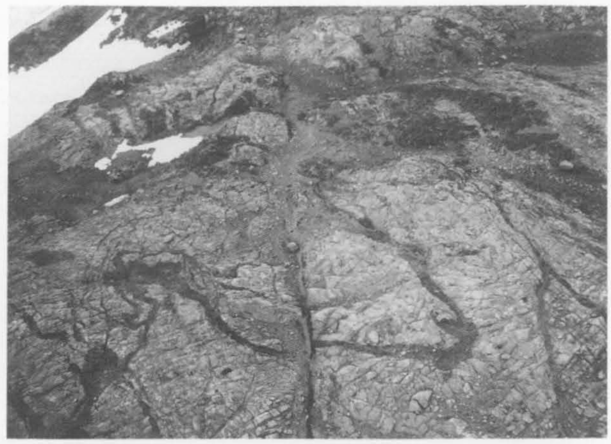

Figure 57. Folded, sudconcordant mafic granulite dykes cutting migmatitic garnet-quartz-feldspar gneiss; Obryvistyy Island. Width of view: about 100m.

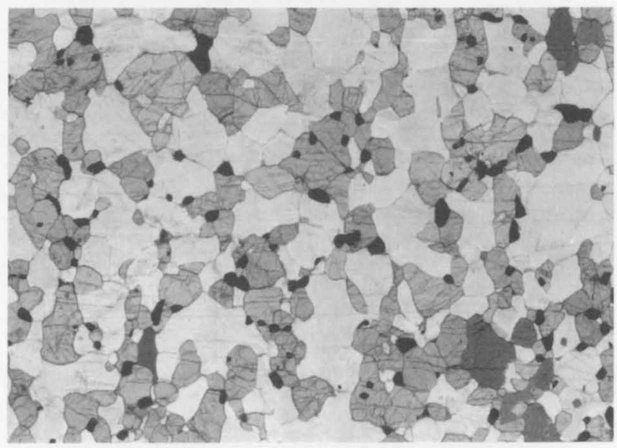

Figure 58. Subconcordant mafic granulite (hornblende, clinopyroxene, orthopyroxene, plagioclase) dyke, showing granoblastic texture; east end of Algae Lake. Sample 86286203; width of field: 6.5mm.

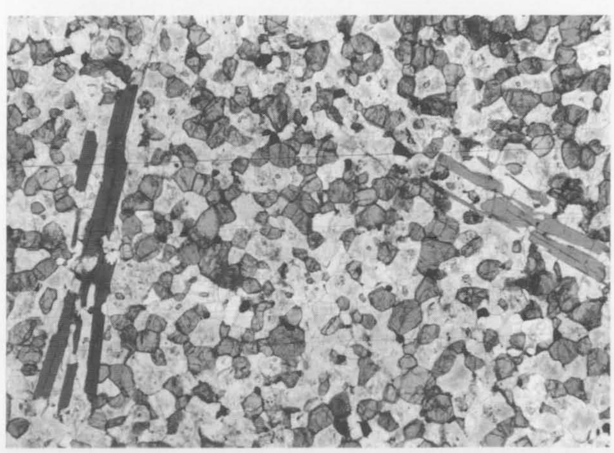

Figure 59. Discordant mafic granulite (biotite, clinopyroxene, orthopyroxene, plagioclase) dyke, with large randomly orientated biotite grains; southern Thomas Island. Sample 86285640; width of field: 4.5mm.

two-pyroxene granulite layers in the northeastern Highjump Archipelago contain several percent of garnet, which forms irregular aggregates and rims around pyroxene grains.

Deformed mafic dykes, up to a few metres thick, which intrude the plutonic rocks of the Booth Peninsula area also have a granoblastic texture, but some contain strongly zoned igneous plagioclase phenocrysts; one consists mainly of andesine-labradorite and greenish-brown hornblende with only minor altered pyroxene. They are probably syn-plutonic, and are of similar age to or, possibly, younger than the subconcordant metadykes elsewhere.

Virtually all the analysed metamorphosed dykes are subalkaline olivine or quartz tholeiites (Table 10, Figs 60, 61). Their varied composition implies that they do not represent a single suite, although much of the variation, for LILE in particular, is probably due to metamorphism.

A hornblende granulite dyke (86285970) cutting quartz monzonite at Booth Peninsula is unusual in not having a negative Nb anomaly. In terms of less-mobile incompatible elements (REE, and HFSE: Zr, Nb, P, Ti, Y), it is quite similar to the group 1 dolerites (see below), and may be related to these rather than to the gabbroic plutons of the area. The slightly Ne-normative composition of this dyke may be due to enrichment in alkalies during emplacement, possibly from the still-crystallising plutonic country rocks.

Flat-lying dolerites (group 1). A small group of sill-like dolerites, generally less than 1 m thick, crops out mainly in the southwestern Bunger Hills. It appears to be the oldest essentially unmetamorphosed suite of mafic dykes and may be contemporaneous with some of the plutonic rocks. The dolerites are cut by alkali basalt dykes. Texture is usually intergranular, with randomly orientated plagioclase laths, but granular pyroxene. Most dykes contain zoned plagioclase and clinopyroxene phenocrysts (Fig. 62), and spherulitic intergrowths of pyroxene are present locally (Fig. 63). Like dolerites of similar texture in the Vestfold Hills (Collerson & Sheraton 1986) and Napier Complex (Sheraton & Black 1981), these dykes were probably emplaced deep in the crust not long after the high-grade metamorphism. They contain reddish-brown biotite (up to 2%), pyroxene (35–40%), zoned andesine (55–60%), ilmenite + magnetite (2–4%), and minor secondary amphibole, apatite, and carbonate. In contrast to most of the other dolerites, pyroxene is generally quite fresh, and consists predominantly of clinopyroxene (augite and pigeonite), with up to 10 per cent of Ca-rich orthopyroxene ($Ca_5Mg_{73}Fe_{22}$ to $Ca_5Mg_{56}Fe_{39}$), commonly in the form of composite grains with overgrowths of augite (Fig. 63). Pigeonite is also unusually calcic ($Ca_{14}Mg_{65}Fe_{21}$ to $Ca_{15}Mg_{53}Fe_{32}$), whereas augite has relatively low Ca (Table 11, Fig. 64), indicating crystallisation temperatures of at least 1200°C and pressures more than 10 kb (Lindsley 1983). Such high P-T conditions clearly reflect magmatic crystallisation, and the pyroxenes have presumably survived through rapid cooling of the very thin dykes.

Most group 1 dykes are subalkaline in terms of an alkalies-SiO_2 plot (Fig. 65), but only marginally tholeiitic on an AFM diagram (Fig. 66). They are mostly slightly Q-normative, although two are Ol-normative (Fig. 67). Group 1 dykes tend

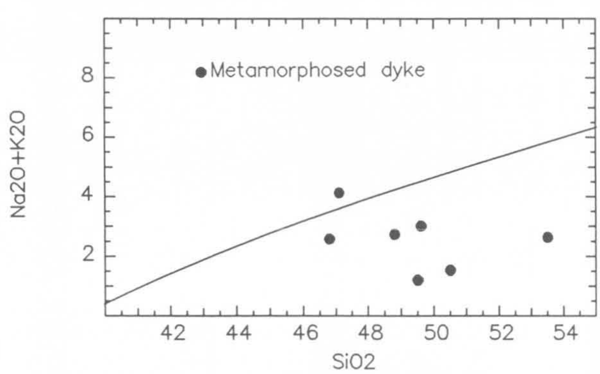

Figure 60. Alkalies-SiO_2 plot for metamorphosed mafic dykes from the Bunger Hills area. Boundary between alkaline (upper) and subalkaline fields after Irvine & Baragar (1971).

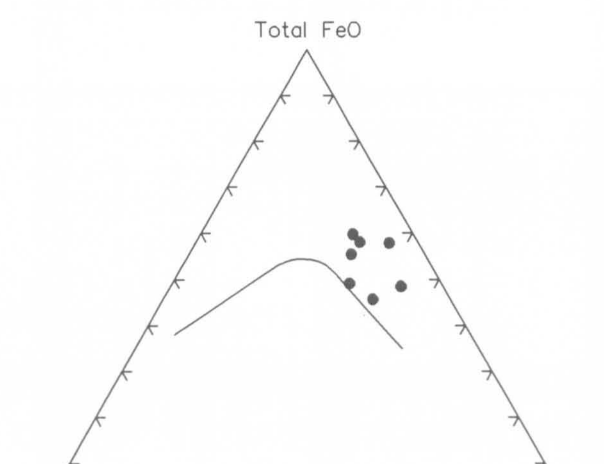

Figure 61. A-F-M diagram for metamorphosed mafic dykes from the Bunger Hills area. Boundary between tholeiitic and calc-alkaline (plus alkaline) fields after Irvine & Baragar (1971). Symbols as in Figure 60.

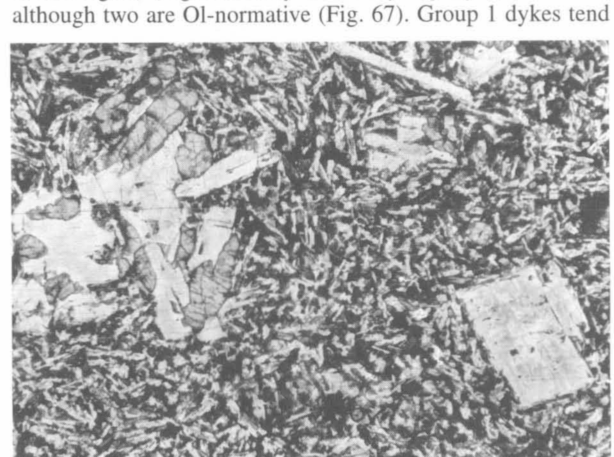

Figure 62. Group 1 dolerite dyke, with plagioclase and clinopyroxene phenocrysts in a fine-grained intergranular groundmass (glomeroporphyritic texture); south of Edgeworth David Base. Sample 86285905; width of field: 3.6mm.

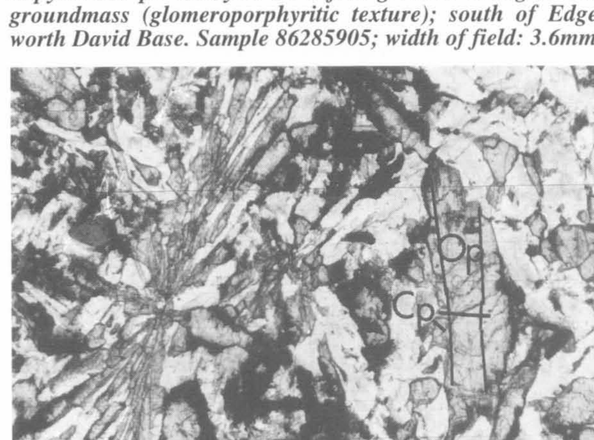

Figure 63. Group 1 dolerite dyke, showing spherulitic clinopyroxene and microphenocryst of orthopyroxene with clinopyroxene overgrowth; west of Lake Dolgoe. Sample 86285682; width of field: 2.0mm.

Table 9. Chemical analyses of mafic to felsic dykes and minor granitic intrusives from Bunger Hills area.

Sample no.	*86285827*	*86286266*	*86286256*	*86285834*	*86286041*	*86285617*	*86285676*	*86286222*
Locality	*Booth Peninsula E*	*Mars Island*	*Husky Dog Island*	*Geomorfologov Peninsula*	*Thomas Island E*	*Currituck Island W*	*Currituck Island W*	*Geologov Island*
Lithology	*Hb–Op monzodiorite dyke*	*Cp–Op Qz gabbro dyke*	*Op granite dyke*	*Hb–Bi granite*	*Bi granite*	*Bi–Mus granite*	*Bi–Mus granite*	*Trachyte dyke*
Intrusion	*Booth Pen.*	*Booth Pen.*	*Booth Pen.*					
SiO_2	47.50	50.70	64.60	72.50	70.80	74.80	74.60	58.70
TiO_2	1.88	3.46	1.15	0.24	0.54	0.05	0.14	0.43
Al_2O_3	15.76	13.27	13.24	13.98	13.86	13.56	13.63	18.01
Fe_2O_3	6.29	4.97	5.04	0.47	1.19	0.50	0.69	1.98
FeO	11.82	12.20	3.78	1.17	1.07	0.25	0.59	2.41
MnO	0.33	0.36	0.16	0.03	0.04	0.03	0.03	0.11
MgO	2.04	2.28	0.80	0.47	0.75	0.12	0.19	1.09
CaO	6.02	7.79	3.47	2.01	1.18	0.77	0.98	1.74
Na_2O	3.17	1.72	2.15	2.31	2.31	3.51	3.31	5.04
K_2O	2.58	0.81	3.68	5.49	6.38	5.05	5.02	6.71
P_2O_5	1.41	0.89	0.46	0.02	0.08	0.01	0.03	0.19
H_2O+	–	–	–	–	–	–	–	0.72
H_2O-	–	–	–	–	–	–	–	0.14
CO_2	–	–	–	–	–	–	–	2.25
LOI	0.87	1.07	1.05	0.78	1.02	0.83	0.96	–
Rest	0.62	0.44	0.45	0.33	0.48	0.14	0.19	0.59
Total	**100.29**	**99.96**	**100.03**	**99.80**	**99.70**	**99.62**	**100.36**	**100.11**
O=F,S	0.11	0.08	0.02	0.00	0.01	0.00	0.00	0.02
Total	**100.18**	**99.88**	**100.01**	**99.80**	**99.69**	**99.62**	**100.36**	**100.09**
	C.I.P.W. norms							
Q	0.84	15.44	30.15	32.46	29.45	33.25	33.68	–
C	0.18	–	0.51	0.63	1.20	0.94	1.04	–
Or	15.25	4.79	21.75	32.44	37.70	29.84	29.66	39.65
Ab	26.82	14.55	18.19	19.55	19.55	29.70	28.01	41.02
An	20.65	26.10	14.21	9.84	5.33	3.75	4.67	6.70
Ne	–	–	–	–	–	–	–	0.88
Di	–	5.73	–	–	–	–	–	0.57
Hy	19.10	16.01	3.17	2.59	2.03	0.32	0.81	–
Ol	–	–	–	–	–	–	–	3.46
Mt	9.12	7.21	7.31	0.68	1.73	0.72	1.00	2.87
Il	3.57	6.57	2.18	0.46	1.03	0.09	0.27	0.82
Ap	3.34	2.11	1.09	0.05	0.19	0.02	0.07	0.45
mg	23.5	25.0	27.4	41.7	55.5	46.1	36.5	44.6
	Trace elements in parts per million							
Ba	1264	745	2140	1976	2360	113	363	92
Rb	33	6	60	116	140	604	507	344
Sr	375	487	315	269	455	52	111	114
Pb	11	6	11	28	47	115	86	175
Th	<1	<1	<1	2	56	45	96	273
U	1.5	1.0	0.5	1.0	0.5	20	9.5	40
Zr	711	271	560	290	411	97	137	1593
Nb	59	58	20	4	7	60	31	112
Y	75	64	34	8	18	22	13	53
La	78	33	32	22	103	6	47	453
Ce	176	77	62	28	214	11	92	794
Nd	87	48	28	7	78	5	31	208
Sc	30	33	20	7	6	4	5	5
V	17	129	29	9	33	<2	3	11
Cr	<2	6	<2	<2	<2	<2	<2	<2
Ni	<2	4	<2	<2	3	2	2	<2
Cu	24	20	17	3	26	<1	3	2
Zn	204	165	106	25	21	16	15	64
Sn	<1	<1	<1	<1	<1	7	6	–
Ga	25	20	17	15	11	30	28	19
S	1200	1630	400	100	200	<100	100	500
F	1200	–	–	–	–	–	–	–
K/Rb	649	1120	509	393	378	69	82	162
Rb/Sr	0.088	0.012	0.190	0.43	0.31	11.6	4.6	3.0
Ce/Y	2.3	1.2	1.8	3.5	12	0.50	7.1	15
Th/U	–	–	–	2	110	2.3	10	6.8
K/Zr	30	25	55	157	129	432	304	35
P/Zr	8.7	14	3.6	0.3	0.8	0.4	1.0	0.52
Nb/Zr	0.083	0.21	0.036	0.014	0.017	0.62	0.23	0.70
Nb/Nb*	0.81	2.14	0.32	0.05	0.05	0.89	0.35	0.35
Sr/Sr*	0.22	0.60	0.55	1.25	0.25	0.51	0.14	0.02

mg = atomic 100Mg/(Mg+Fe^{2+}).

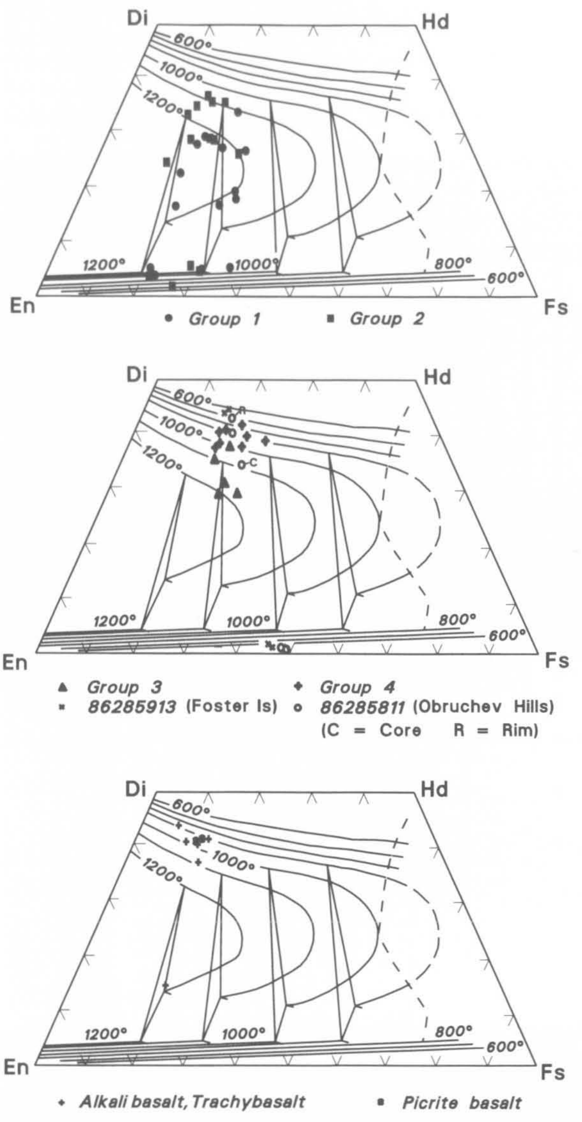

Figure 64. Pyroxene compositions for Bunger Hills mafic dykes, plotted on the graphical geothermometer of Lindsley (1983) for a pressure of 5kb. Most compositions reflect magmatic crystallisation, but some groups 3 and 4 dykes show equilibration at metamorphic temperatures.

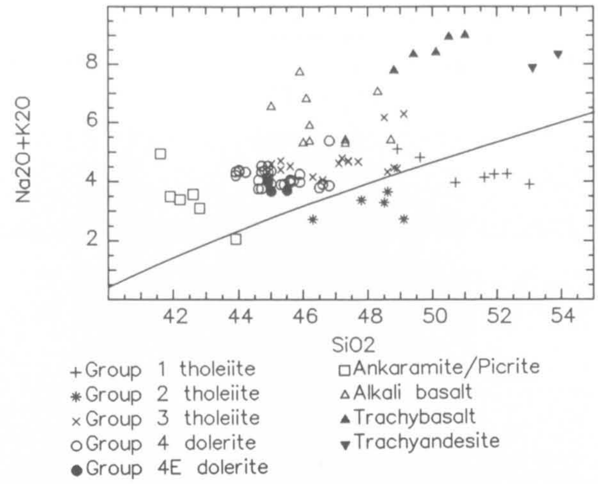

Figure 65. Alkalies-SiO_2 plot for Bunger Hills mafic dykes. Boundary between alkaline and subalkaline fields after Irvine & Baragar (1971).

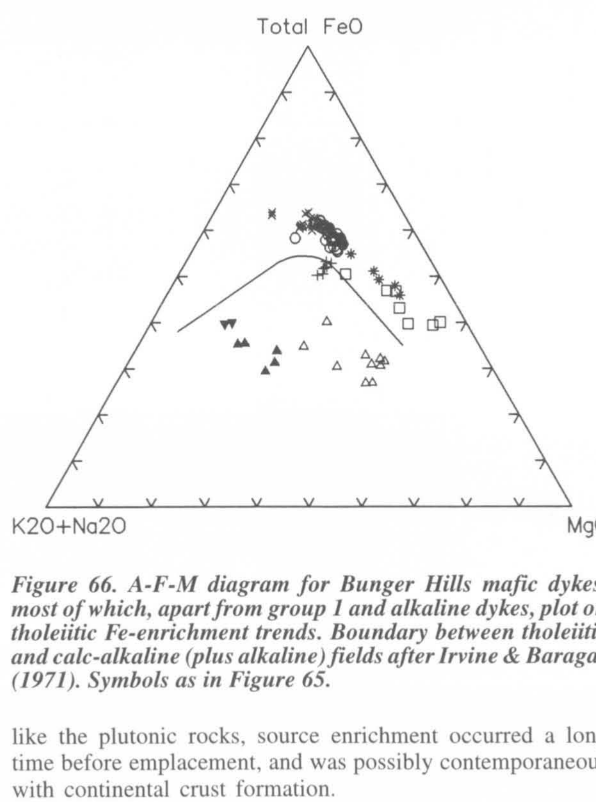

Figure 66. A-F-M diagram for Bunger Hills mafic dykes, most of which, apart from group 1 and alkaline dykes, plot on tholeiitic Fe-enrichment trends. Boundary between tholeiitic and calc-alkaline (plus alkaline) fields after Irvine & Baragar (1971). Symbols as in Figure 65.

to have relatively high SiO_2 (Table 12), and K/Zr, Ba/Zr, Ce/Zr, Sr/Zr, Nb/Zr and P/Zr are all significantly higher than the other dyke suites (Fig. 68); in contrast to most other dyke suites, essentially constant Sr/Zr precludes significant plagioclase fractionation. Spidergrams are relatively irregular (fractionated) and unusual in having positive Nb and Sr anomalies (Fig. 69). Sheraton et al. (1990) argued that the high LILE/Zr ratios and Sr_i values (0.7049–0.7053) and relatively low ε_{Nd} (–0.7) can be better explained by derivation from an enriched lithospheric mantle source rather than direct crustal assimilation, although some degree of contamination is quite possible. Ratios of many incompatible elements (particularly LREE and some HFSE) are thus considered to approximate those of the mantle source. In particular, a positive Nb anomaly suggests the presence of a Nb-rich OIB-like (?asthenospheric) source component (Sun & McDonough 1989). In this respect, and in their degree of LILE enrichment (Figs 68, 69), group 1 dykes are similar to the quartz monzodioritic plutonic rocks, and may, indeed, be of similar age.

A T_{DM}^{Nd} model age of 1940 Ma (Table 8) indicates that, like the plutonic rocks, source enrichment occurred a long time before emplacement, and was possibly contemporaneous with continental crust formation.

Magnesian dolerite dykes (group 2). Rare north-west-trending magnesian dolerites of variable thickness also contain significant amounts of orthopyroxene. Most have a hypidiomorphic granular or intergranular texture; finer grained dykes have a partly variolitic groundmass and contain phenocrysts of clinopyroxene (some with pigeonite or orthopyroxene cores) and olivine (Fig. 70). The typical assemblage is orthopyroxene (up to 10%), olivine (Fo_{87-61}: up to 15%), clinopyroxene (35–50%), zoned labradorite-andesine (An_{55-35}: 40–55%), ilmenite + magnetite (2–5%) and minor biotite, hornblende and apatite. Clinopyroxene comprises augite ($Ca_{43}Mg_{39}Fe_{18}$ or $Ca_{32}Mg_{44}Fe_{24}$) and subcalcic augite ($Ca_{20}Mg_{63}Fe_{17}$) (Table 11).

A dyke on Currituck Island (86285603) is unusual in having a poikilitic texture, and containing about 30 per cent orthopyroxene (about $Ca_4Mg_{70}Fe_{26}$) and 5 per cent biotite, but no olivine (Fig. 71). Like the group 1 dykes, pyroxene compositions indicate igneous crystallisation temperatures of the order of 1200°C, but with partial re-equilibration at about 1000–1050°C during cooling (Fig. 64, Table 23).

Group 2 dykes are relatively little-evolved olivine tholeiites (mg^* = atomic $100Mg/(Mg+0.85Fe_{total}$ = 54–67) (Figs 65–67). They are characterised by high MgO, Cu, Cr, and Ni (Table 12) and low P/Zr (Fig. 68). In contrast to the group 1 dykes,

Table 10. Chemical analyses of mafic granulite dykes from Bunger Hills area.

Sample no.	*86286045*	*86286044*	*86285970*	*86286040*	*86285640*	*86285984*	*86285996*
Locality	*Obryvistyy Island*	*Obryvistyy Island*	*Booth Peninsula W*	*Thomas Island E*	*Thomas Island S*	*Highjump Archipelago NE*	*Highjump Archipelago NE*
Lithology	*Cp–Op–Pl granulite*	*Cp–Bi–Op–Pl granulite*	*Px–Hb–Pl granulite*	*Cp–Bi–Op–Pl granulite*	*Cp–Op–Pl granulite*	*Gt–Hb–Cp–Op–Pl granulite*	*Op–Hb–Cp Pl granulite*
SiO_2	46.80	53.50	47.10	49.50	50.50	48.80	49.60
TiO_2	2.32	1.16	1.61	1.53	0.51	1.91	1.84
Al_2O_3	15.32	14.47	15.47	16.69	17.46	13.50	14.64
Fe_2O_3	4.40	1.35	1.61	3.93	1.89	2.62	2.71
FeO	9.66	6.97	10.17	9.13	7.55	11.90	9.53
MnO	0.25	0.16	0.19	0.19	0.18	0.22	0.19
MgO	7.28	7.09	7.90	8.03	8.30	6.88	6.63
CaO	9.96	7.48	9.05	8.67	11.00	11.18	11.01
Na_2O	2.21	1.15	2.99	0.91	1.33	2.36	2.45
K_2O	0.36	1.48	1.13	0.29	0.20	0.37	0.56
P_2O_5	0.62	1.60	0.32	0.24	0.05	0.21	0.16
LOI	1.09	1.21	2.20	0.91	1.00	0.70	0.83
Rest	0.42	2.00	0.33	0.28	0.28	0.27	0.39
Total	**100.69**	**99.62**	**100.07**	**100.30**	**100.25**	**100.92**	**100.54**
O=S	0.08	0.25	0.04	0.04	0.06	0.03	0.09
Total	**100.61**	**99.37**	**100.03**	**100.26**	**100.19**	**100.89**	**100.45**
	C.I.P.W. norms						
Q	–	14.51	–	6.19	3.29	–	–
C	–	1.21	–	–	–	–	–
Or	2.13	8.75	6.68	1.71	1.18	2.19	3.31
Ab	18.70	9.73	24.53	7.70	11.25	19.97	20.73
An	30.82	26.66	25.45	40.60	41.08	25.15	27.30
Ne	–	–	0.42	–	–	–	–
Di	11.98	–	14.21	0.69	10.72	23.96	21.64
Hy	20.60	27.66	–	35.50	28.07	16.34	17.66
Ol	5.59	–	19.67	–	–	4.75	1.84
Mt	3.29	1.98	2.81	3.06	2.24	3.45	2.89
Il	4.41	2.20	3.06	2.91	0.97	3.63	3.49
Ap	1.47	3.79	0.76	0.57	0.12	0.50	0.38
mg	52.8	64.5	58.8	57.1	65.3	50.3	53.7
	Trace elements in parts per million						
Ba	400	8730	385	293	197	114	172
Rb	6	84	21	20	4	2	13
Sr	342	2380	371	173	234	199	306
Pb	9	12	4	8	4	4	5
Th	<1	10	2	<1	<1	<1	<1
U	<0.5	1.5	<0.5	1.0	0.5	0.5	<0.5
Zr	266	406	140	110	29	112	121
Nb	20	14	24	10	<1	9	8
Y	33	32	25	31	22	32	28
La	36	94	23	19	6	15	12
Ce	76	199	41	44	16	32	32
Nd	36	88	21	22	8	18	19
Sc	41	31	35	41	30	49	37
V	291	171	198	252	160	413	309
Cr	94	245	246	88	270	126	163
Ni	56	110	135	110	23	63	55
Cu	58	172	28	76	47	74	83
Zn	121	108	102	103	70	113	94
Ga	20	15	16	19	16	18	19
As	<0.5	<0.5	<0.5	<0.5	<0.5	<0.5	<0.5
S	1700	5000	900	900	1160	700	1810
K/Rb	498	146	447	120	415	1540	358
Rb/Sr	0.018	0.035	0.057	0.116	0.017	0.010	0.042
Ce/Y	2.3	6.2	1.6	1.4	0.73	1.0	1.1
K/Zr	11.2	30.3	67.0	21.9	57	27	38
P/Zr	10	17	10	9.5	7.5	8.2	5.8
Nb/Zr	0.075	0.034	0.17	0.10	<0.03	0.08	0.07
Nb/Nb*	0.87	0.21	0.92	0.75	~0.1	0.73	0.60
Sr/Sr*	0.48	1.30	0.93	0.41	1.52	0.61	0.92

mg = atomic 100Mg/(Mg+0.85Fe(total)).

Table 11. Representative analyses of mafic minerals in dolerite dykes from Bunger Hills area.

	Group 1 *86285682*				*Group 1* *86285964*		*Group 2* *86285603*		*Group 2* *86285655*	
	Op	*Pig* *(core)*	*Pig* *(rim)*	*Cp*	*Op*	*Cp*	*Op*	*Cp*	*Cp*	*Ol*
SiO_2	51.80	53.26	51.84	51.90	50.77	49.16	52.85	51.71	49.08	38.48
TiO_2	0.47	0.30	0.30	0.63	0.21	1.29	0.57	0.76	1.50	–
Al_2O_3	1.90	2.77	2.00	3.49	2.62	1.50	2.86	4.79	5.89	–
FeO^+	19.70	12.77	19.49	11.52	22.48	13.20	17.31	9.10	12.30	20.56
MnO	0.28	0.18	0.39	0.20	0.32	0.28	0.13	–	0.14	0.17
MgO	22.17	22.69	17.93	16.27	19.75	12.07	23.54	16.45	14.68	40.04
CaO	2.14	6.81	7.24	15.55	2.05	17.96	2.57	16.59	15.80	0.14
Na_2O	0.25	0.38	0.40	0.61	0.23	0.80	–	0.54	0.59	–
K_2O	–	–	–	–	–	–	–	–	–	–
Cr_2O_3	–	0.18	–	–	0.25	0.18	–	0.22	–	–
Total	**98.71**	**99.34**	**99.60**	**100.18**	**98.68**	**100.43**	**99.85**	**100.15**	**99.98**	**99.39**
O	6	6	6	6	6	6	6	6	6	4
Si	1.943	1.944	1.954	1.919	1.931	1.850	1.933	1.895	1.833	0.999
Al^{iv}	057	0.056	0.046	0.081	0.069	0.150	0.067	0.105	0.167	–
Al^{vi}	027	0.063	0.043	0.071	0.049	0.094	0.056	0.102	0.092	–
Ti	0.013	0.008	0.008	0.018	0.006	0.037	0.016	0.021	0.042	–
Fe	0.618	0.390	0.614	0.356	0.715	0.415	0.529	0.279	0.384	0.446
Mn	0.009	0.005	0.013	0.006	0.010	0.009	0.004	–	0.004	0.004
Mg	1.240	1.234	1.007	0.897	1.120	0.677	1.283	0.899	0.818	1.549
Ca	0.086	0.266	0.293	0.616	0.083	0.724	0.101	0.651	0.632	0.004
Na	0.018	0.027	0.029	0.044	0.017	0.059	–	0.038	0.043	–
K	–	–	–	–	–	–	–	–	–	
Cr	–	0.005	–	–	0.007	0.005	–	0.006	–	–
Total	**4.011**	**3.999**	**4.008**	**4.009**	**4.007**	**4.019**	**3.990**	**3.996**	**4.016**	**3.001**
mg	66.7	76.0	62.1	71.6	61.0	62.0	70.8	76.3	68.0	77.6

+ Total Fe as FeO. mg = atomic 100Mg/(Mg+total Fe).

	Group 3A *86285913*		*Group 3A* *86285948*	*Group 3B* *86285998*	*Group 4A* *86285864*		*Group 4B* *86286075*	*Group 4D* *86285833*	*Group 4E* *86285811*		
	Op	*Cp*	*Cp*	*Cp*	*Cp*	*Ol*	*Cp*	*Cp*	*Op*	*Cp*	*Hb*
SiO_2	50.73	53.09	51.30	51.33	48.28	35.59	51.33	48.74	51.11	51.15	40.98
TiO_2	–	0.25	0.78	0.93	2.47	–	1.26	2.05	–	0.93	2.02
Al_2O_3	1.02	1.40	2.54	3.33	4.92	0.14	3.57	5.17	1.07	3.00	12.97
FeO^+	27.68	9.96	13.56	13.24	12.49	36.53	10.80	12.31	29.31	13.73	17.06
MnO	0.86	0.36	0.28	0.31	0.18	0.51	–	0.13	0.92	0.39	–
MgO	17.55	12.67	14.82	15.53	12.13	26.80	14.21	11.29	16.41	13.15	8.79
CaO	0.49	22.50	16.05	15.07	18.92	–	18.70	20.31	0.31	17.23	11.71
Na_2O	0.16	0.56	0.51	0.47	0.61	–	0.71	0.66	0.20	0.62	2.13
K_2O	–	–	–	–	–	–	–	–	–	–	1.68
Cr_2O_3	–	–	–	0.13	–	–	–	–	–	–	–
Total	**98.50**	**100.79**	**99.83**	**100.34**	**99.98**	**99.56**	**100.59**	**100.66**	**99.33**	**100.19**	**97.33**
O	6	6	6	6	6	4	6	6	6	6	23
Si	1.977	1.976	1.927	1.911	1.828	1.000	1.903	1.835	1.986	1.925	6.243
Al^{iv}	0.023	0.024	0.073	0.089	0.172	–	0.097	0.165	0.014	0.075	1.757
Al^{vi}	0.024	0.037	0.039	0.057	0.047	0.005	0.059	0.064	0.035	0.058	0.571
Ti	–	0.007	0.022	0.026	0.070	–	0.035	0.058	–	0.026	0.231
Fe	0.902	0.310	0.426	0.412	0.395	0.859	0.335	0.388	0.953	0.432	2.174
Mn	0.028	0.011	0.009	0.010	0.006	0.012	–	0.004	0.030	0.012	–
Mg	1.020	0.703	0.830	0.862	0.684	1.123	0.786	0.634	0.951	0.737	1.996
Ca	0.021	0.897	0.646	0.601	0.767	–	0.743	0.820	0.013	0.695	1.911
Na	0.012	0.041	0.037	0.034	0.045	–	0.051	0.048	0.015	0.045	0.628
K	–	–	–	–	–	–	–	–	–	–	0.326
Cr	–	–	–	0.004	–	–	–	–	–	–	–
Total	**4.006**	**4.007**	**4.008**	**4.005**	**4.015**	**2.998**	**4.009**	**4.015**	**3.997**	**4.005**	**15.839**
mg	53.1	69.4	66.1	67.7	63.4	56.7	70.1	62.0	50.0	63.1	47.9

spidergrams show marked negative Nb, Sr, and P anomalies (Fig. 69). Lower LILE/Zr and Sr_i (0.7039-0.7040) and higher ε_{Nd} (+2.4) imply derivation from a distinct, less-enriched mantle source (Sheraton et al. 1990).

Dolerite dykes (groups 3 and 4). By far the most abundant dykes are northwest-trending dolerites, which are up to 50 m thick, though commonly much thinner (Figs 72, 73); chilled margins are common. They occur throughout the Bunger Hills area and Obruchev Hills, but have not been found west of the Denman Glacier. At least some postdate the magnesian dolerites.

Two major groups (3 and 4) and at least 10 subgroups can be distinguished on composition, but, petrographically, all are typical dolerites with fine to medium-grained (0.1–2 mm) intergranular or, rarely, subophitic texture (Figs 74, 75). Many are plagioclase-phyric, whereas olivine and clinopyroxene phenocrysts are rare.

These dolerites typically contain reddish-brown biotite (2–6%), opaque minerals (5–10%), pink augite ($Ca_{40}Mg_{40}Fe_{20}$ to $Ca_{44}Mg_{34}Fe_{22}$ or about $Ca_{33}Mg_{42}Fe_{25}$: 20-–0%), reddish-clouded labradorite-andesine (An_{68-38}: 50–60%), and minor apatite, carbonate, and, in some rocks, K-feldspar. Olivine (Fo_{57-40}: up to 15%) is largely confined to groups 4A-C dolerites, and minor quartz to some group 3 dykes. Opaque minerals comprise ilmenite (as discrete grains and intergrown with hematite or magnetite), titanomagnetite, magnetite, and rare pyrite.

Augite is commonly partly altered to pale green actinolitic or hastingsitic amphibole and greenish-brown or reddish-brown biotite. Olivine may be replaced by ferruginous serpentine with rims of pale green to colourless clinoamphibole. Such alteration may be partly deuteric, but some is clearly associated with late shearing or, in the southeastern Bunger Hills, with a regional retrograde metamorphism.

A granoblastic plagioclase-phyric group 3A dyke (86285913) from Foster Island contains about 14 per cent each of orthopyroxene ($Ca_1Mg_{52}Fe_{47}$) and salite ($Ca_{47}Mg_{37}Fe_{16}$), and may have crystallised relatively deep in the crust.

Dolerites in the Obruchev Hills (group 4E) contain relatively abundant greenish-brown hornblende (ferroan pargasite: up to 20%), reddish-brown biotite (4–8%) and opaque minerals (8–10%), but less (~15%) augite (zoned from $Ca_{37}Mg_{40}Fe_{23}$ to $Ca_{43}Mg_{36}Fe_{17}$). Much of the hornblende and biotite is clearly secondary, but many well-crystallised grains may be primary; clinopyroxene is clouded with exsolved Fe-Ti oxide. Plagioclase is strongly zoned. Minor primary orthopyroxene is present in some dykes, and secondary metamorphic orthopyroxene ($Ca_{0.6}Mg_{50}Fe_{49}$) forms granular rims around amphibole (Fig. 76). Patches of carbonate are present locally.

Clinopyroxene is generally more calcic than that in groups 1 and 2 dykes (Table 11), and its equilibration temperatures were presumably lower. Estimates of minimum temperature range from igneous values (1100–1200°C) down to about 800°C (Fig. 64), consistent with relatively slow cooling of these mostly thick dykes deep in the crust. Coexisting orthopyroxene and clinopyroxene in a group 4E dolerite from the Obruchev Hills (86285811) and a group 3A dyke from Foster Island (86285913) give clear metamorphic temperatures of 700–800°C (Fig. 64, Table 23).

Textural evidence (symplectitic orthopyroxene + plagioclase coronas) suggests that this metamorphism was a discrete post-emplacement event (uplift?) in the Obruchev Hills, but it is not clear whether the two-pyroxene assemblage in the Foster Island dyke crystallised directly from magma during emplacement deep in the crust or during later recrystallisation. The presence of zoned plagioclase phenocrysts is more consistent with the former, although country rocks in the area are cut by shear zones and considerably recrystallised. Possibly, dyke emplacement and shearing were contemporaneous, as can be demonstrated elsewhere in the Bunger Hills.

Groups 3 and 4 dolerites are chemically rather varied, but nevertheless share many compositional features. Each group has been subdivided into five subgroups. Group 3 dykes comprise strongly Hy-normative (generally >9%) olivine tholeiites and subordinate quartz tholeiites, whereas group 4

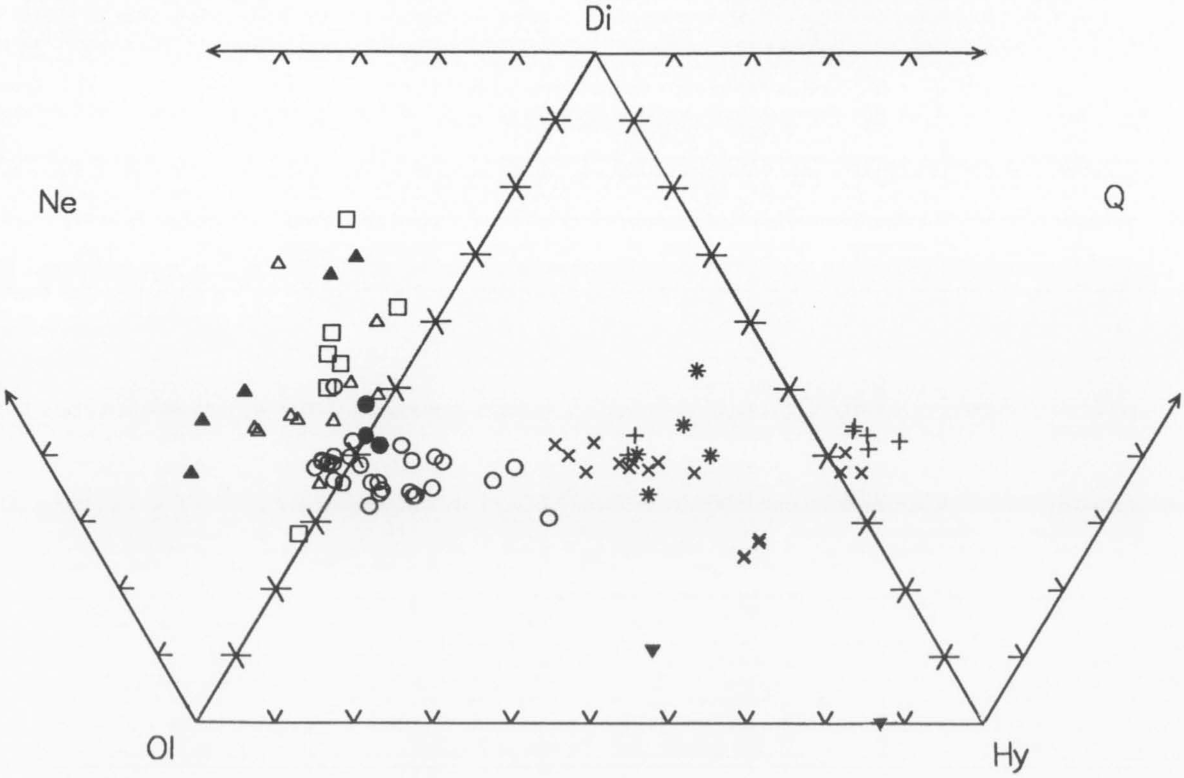

Figure 67. Normative Q-Hy-Di-Ol-Ne diagram for Bunger Hills mafic dykes. Symbols as in Figure 65.

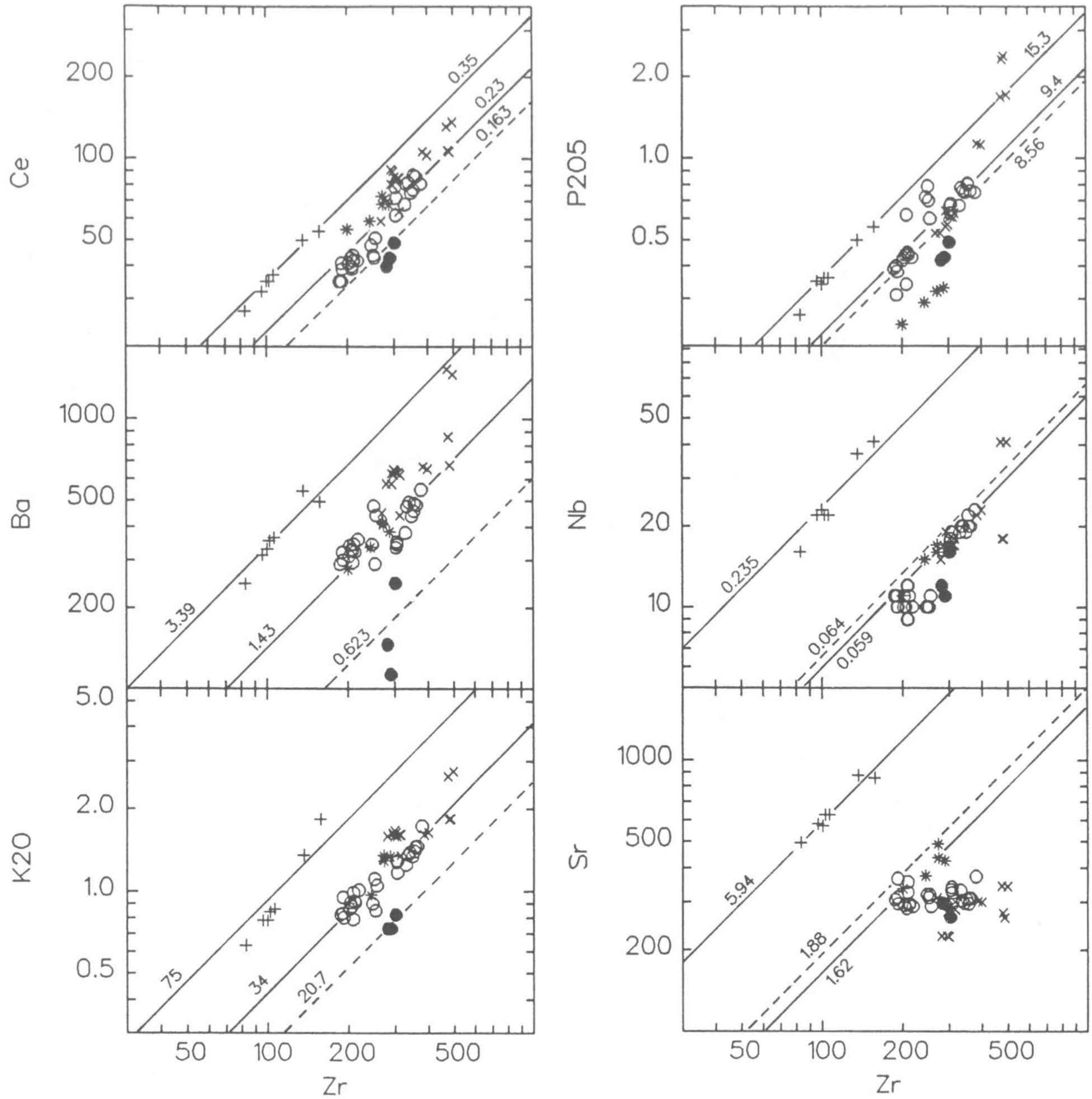

Figure 68. Logarithmic plots of incompatible elements against Zr for Bunger Hills dolerite dykes. Estimated ratios for groups 1 and 4 dykes, and for primordial mantle (dashed lines) are indicated. Symbols as in Figure 65.

dykes are only slightly (<4%) Hy or Ne-normative transitional dolerites (Table 12, Fig. 67). In spite of this, all samples plot in the alkaline field on an alkalies-SiO_2 plot (Fig. 65), but show a classic tholeiitic Fe-enrichment trend on an AFM diagram (Fig. 66). Group 4 dolerites are more strongly Ol-normative and tend to have higher *mg** values (40–51) than group 3 tholeiites (*mg** 27–46).

Similar incompatible element/Zr ratios (Fig. 68) are consistent with derivation from generally similar mantle source regions, although significant differences between subgroups, reflected in systematic differences in the relevant spidergrams (Fig. 69), imply the involvement of a range of parent magmas.

Nearly all these dykes have marked negative Sr and Nb anomalies, and most have negative Th anomalies. The Sr anomalies of group 3 dykes are generally larger than those of group 4, owing to more extensive plagioclase fractionation. The importance of plagioclase (in addition to clinopyroxene and olivine) fractionation is confirmed by the near-constant Sr content with decreasing *mg** and increasing Zr, indicating a bulk distribution coefficient for Sr of about 1 (Fig. 68).

Sheraton et al. (1990) concluded that most of the gross chemical variation can be explained by a combination of partial melting and fractional crystallisation processes. In addition, the magmas were derived from a heterogeneous mantle source. P/Zr shows particularly large variations (Figs 68, 69), suggestive of various amounts of apatite in the source, as has been postulated for mantle beneath southeastern Australia (Menzies & Wass 1983). Group 4E dolerites from the Obruchev Hills have distinctively low incompatible element/Zr ratios (Fig. 68), implying an origin from unenriched or even depleted mantle.

Isotopic data are also consistent with the involvement of at least two source components in the genesis of groups 3 and 4 dykes. These range from slightly depleted (Sr_i 0.7029,

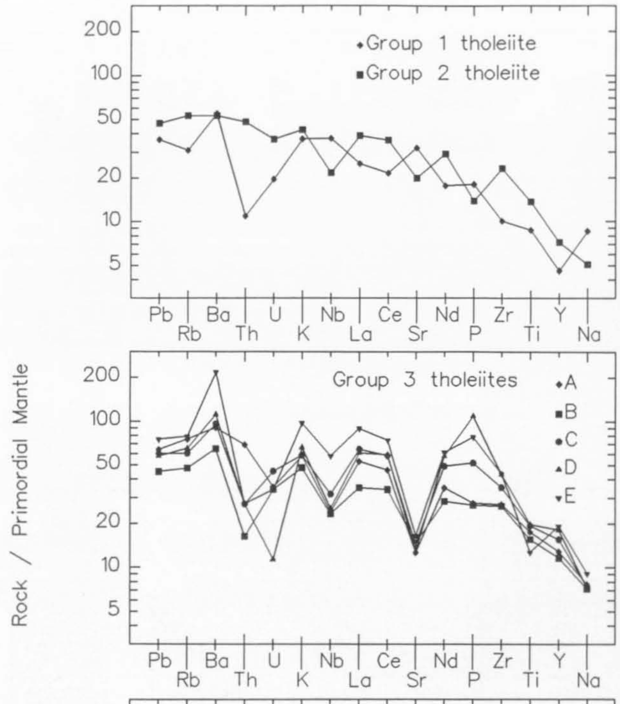

Figure 69. Spidergrams for average groups 1 to 4 dolerite dykes from the Bunger Hills area. Groups 3 and 4 have generally similar patterns, although variably modified by fractionation of plagioclase, in particular. Groups 1 and 2 patterns are quite different, group 1 having small positive Nb and Sr anomalies.

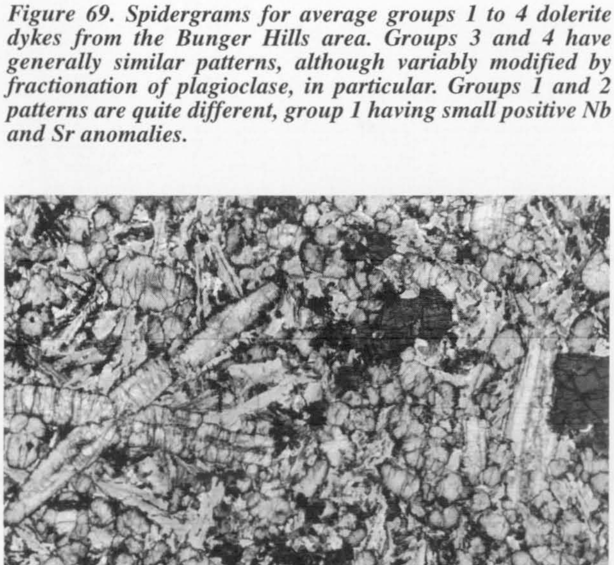

Figure 70. Group 2 magnesian dolerite dyke, showing olivine (dark grey) and clinopyroxene microphenocrysts in a fine-grained intergranular (locally spherulitic) groundmass; eastern Thomas Island. Sample 86285655; width of field: 5mm.

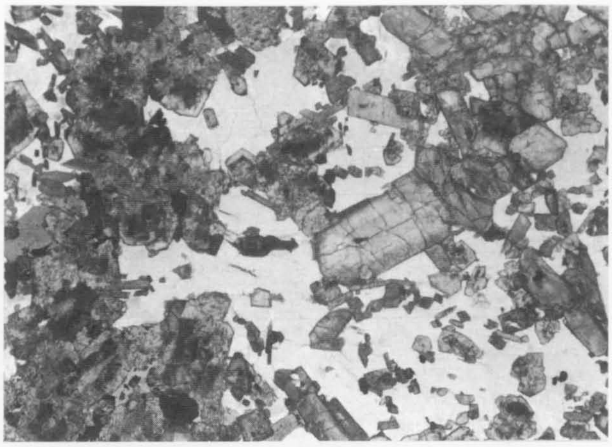

Figure 71. Group 2 magnesian dolerite dyke, showing poikilitic texture with reddish-clouded subhedral orthopyroxene, subordinate clinopyroxene, and minor biotite, enclosed in plagioclase oikocrysts; southeastern Currituck Island. Sample 86285603; width of field: 6mm.

ε_{Nd} +6.3) for group 4E to moderately enriched (Sr_i 0.7046 to 0.7053) for group 3A (Table 8). Thus, a depleted (asthenospheric?) component may have been variably mixed with an enriched lithospheric component, probably containing subducted crustal material and/or long-term enriched (late Archaean or Palaeoproterozoic) mantle. However, significant differences in HFSE ratios preclude simple two-component mixing, and require a more complex source chemistry.

Quite good correlations of Sr_i with both SiO_2 and Q-saturation (i.e. normative Q minus the Q deficiency of Ol and Ne) can be explained either by a modest (maximum of 5–10%) degree of crustal contamination — with a granitic melt or a siliceous LILE and ^{87}Sr-rich fluid phase — in AFC magma chambers or by segregation over a large depth of magma derived from variably enriched mantle source regions. Sheraton et al. (1990) preferred the second alternative as being the simpler, in view of the abundant evidence for LILE and LREE heterogeneity of the mantle sources of dykes and other mafic intrusives in the Bunger Hills and elsewhere. But, clearly, some degree of crustal contamination cannot be entirely ruled out.

The small range of Rb/Sr for individual subgroups means that whole-rock Rb-Sr isochrons are imprecise. However, the most precise ages (1220±80 Ma for group 3A, 1110±160 Ma for group 4E: Sheraton et al. 1990) are consistent with the 1150–1170 Ma age of the plutonic rocks they intrude. The best estimate of emplacement age of groups 3 and 4 dykes (and probably also group 2), deduced from these Rb-Sr data and a Sm-Nd mineral isochron age (1120±40 Ma) for a group 4D dyke, is about 1140 Ma (Sheraton et al. 1990). Mineral isochrons reflect partial resetting during later geological activity, probably about 500 Ma ago.

Picrite and ankaramite dykes. Rare, mostly thin and northwest to west-northwest-trending alkaline picrite and ankaramite dykes crop out in the Bunger Hills. Their age is unknown, but probably similar to that of the dolerites. They have an intergranular to granular or poikilitic texture and some dykes contain plagioclase + carbonate ocelli (Fig. 77).

The ankaramites contain reddish-brown biotite or phlogopite (up to 15%), rather cloudy olivine, commonly partly replaced by serpentine (5–20%), brown or reddish-brown kaersutite or ferroan pargasite (up to 30%), clinopyroxene (20–50%), albitic plagioclase (15–30%), opaque minerals (intergrown ilmenite and magnetite, and minor sulphides: up to 10%) and minor apatite and carbonate (Fig. 78).

Picrites differ in having more olivine (~ Fo_{72}: 22%) and less clinopyroxene (diopside, $Ca_{46}Mg_{42}Fe_{12}$: ~22%) (Table 13). A very altered, flat-lying picrite (86286085) at Krylatyy Peninsula contains relict olivine in a groundmass of pale reddish phlogopite, colourless amphibole, carbonate, chlorite, and opaque minerals.

The rock classification of Irvine & Baragar (1971) used

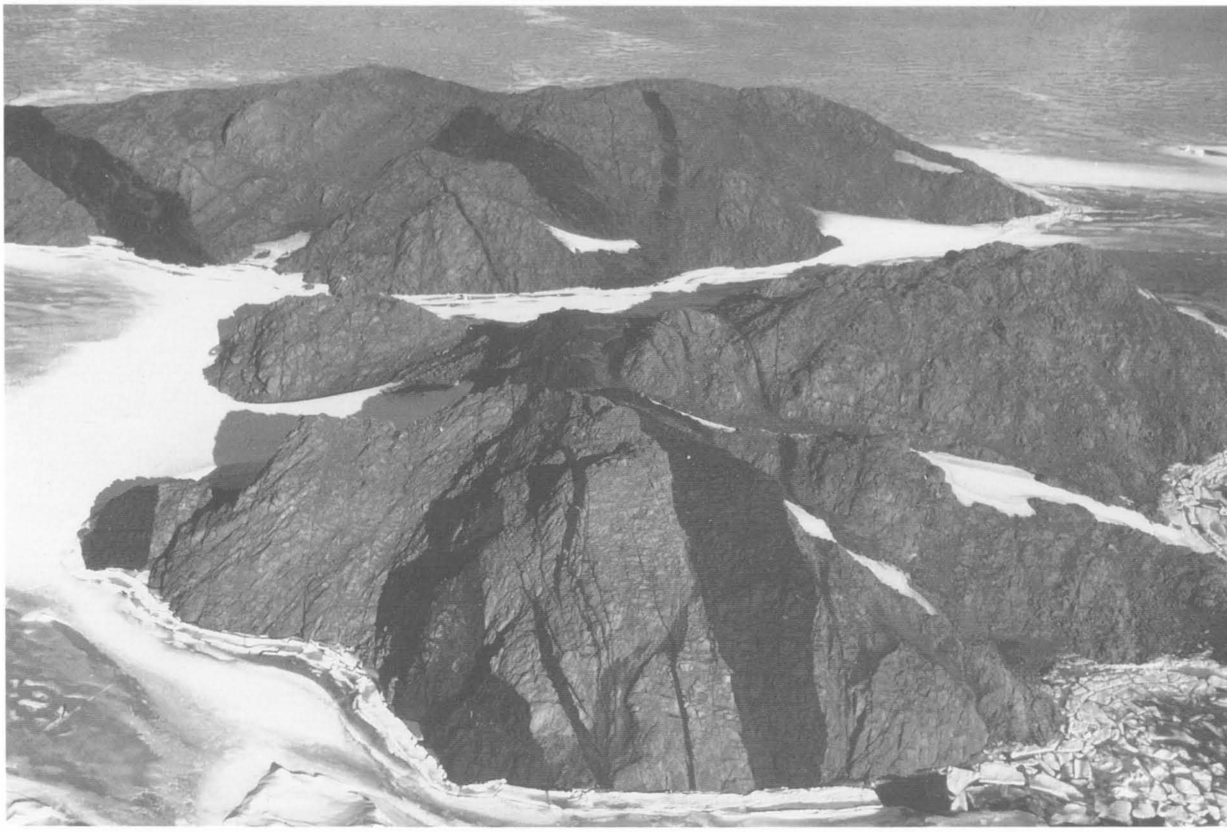

Figure 72. Group 4 dolerite dykes cutting migmatitic paragneiss; Saturn Island.

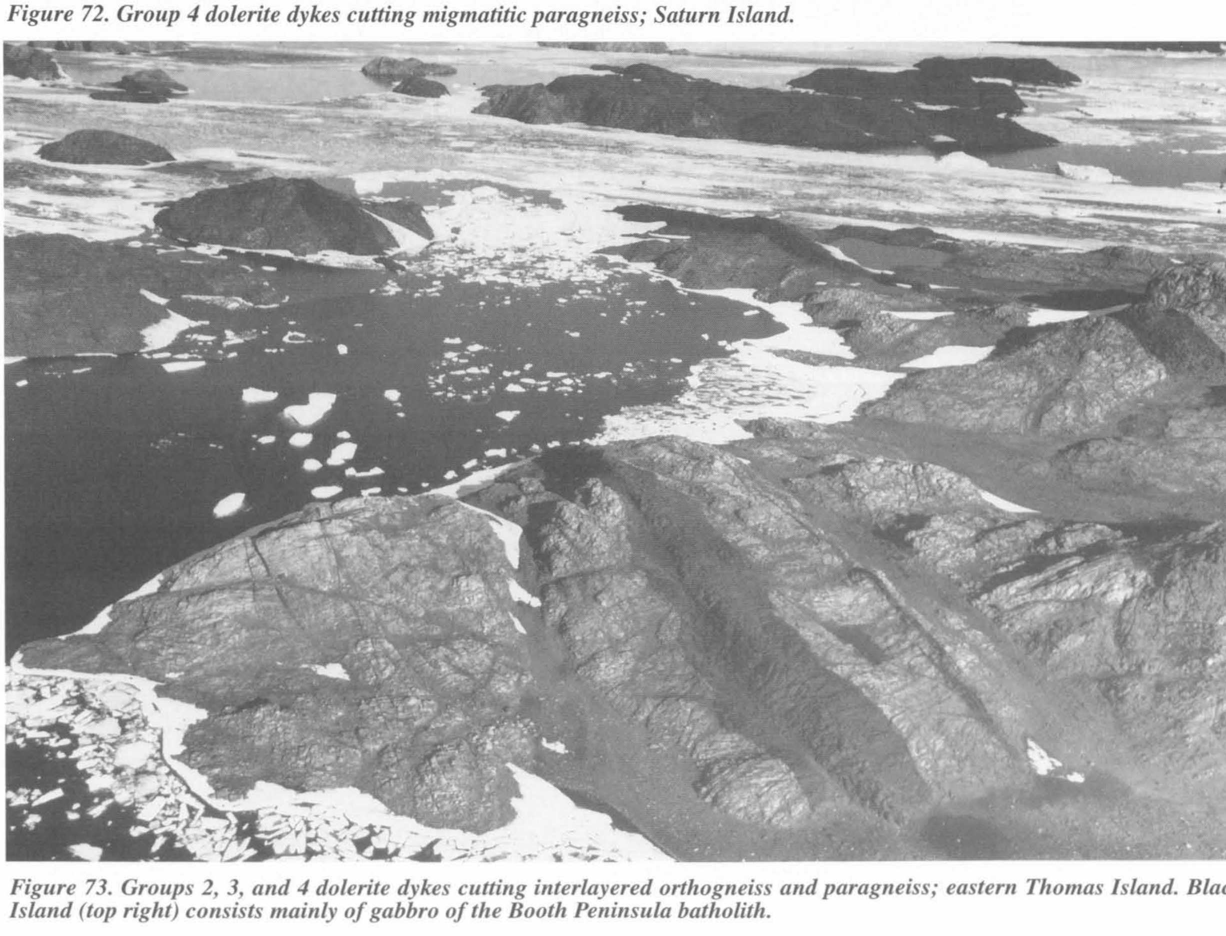

Figure 73. Groups 2, 3, and 4 dolerite dykes cutting interlayered orthogneiss and paragneiss; eastern Thomas Island. Black Island (top right) consists mainly of gabbro of the Booth Peninsula batholith.

Table 12. Chemical analyses of representative dolerite dykes from Bunger Hills–Obruchev Hills area.

Sample no.	*86285964*	*86285682*	*86286201*	*86285654*	*86285936*	*86285913*	*86286054*	*86285660*	*86286219*	*86286260*
Locality	*1km N of Edgeworth David*	*W of Lake Dolgoe*	*E end of Algae Lake*	*Thomas Island E*	*5km SW of Dobrowolski*	*Foster Island*	*Miles Island E*	*Thomas Island E*	*Geologov Island*	*Liberty Islands S*
Lithology	*Olivine tholeiite*	*Quartz tholeiite*	*High–Mg olivine tholeiite*	*High–Mg olivine tholeiite*	*Quartz tholeiite*	*Olivine tholeiite*	*Olivine tholeiite*	*Olivine tholeiite*	*Olivine tholeiite*	*Quartz tholeiite*
Classif.	*Group 1*	*Group 1*	*Group 2*	*Group 2*	*Group 3A*	*Group 3A*	*Group 3B*	*Group 3C*	*Group 3D*	*Group 3E*
SiO_2	49.60	52.30	46.30	48.60	48.80	47.40	46.60	45.30	45.00	49.10
TiO_2	2.11	1.72	2.76	3.32	3.67	3.74	3.08	4.06	4.19	2.67
Al_2O_3	14.63	15.20	10.64	11.74	14.25	15.81	14.92	13.59	12.25	13.23
Fe_2O_3	3.21	2.66	3.53	3.41	3.38	5.62	5.49	3.62	2.78	5.14
FeO	8.10	8.03	10.39	10.67	10.84	8.68	9.07	12.44	13.81	11.10
MnO	0.16	0.15	0.19	0.19	0.22	0.21	0.23	0.27	0.29	0.29
MgO	5.98	5.49	12.08	7.69	4.80	4.09	5.78	4.95	4.64	2.86
CaO	8.10	8.51	8.23	9.64	7.90	8.23	8.57	8.48	8.37	6.28
Na_2O	3.46	3.42	1.75	2.30	2.87	3.08	2.74	2.79	2.75	3.54
K_2O	1.35	0.84	0.97	1.35	1.59	1.59	1.31	1.61	1.84	2.75
P_2O_5	0.50	0.36	0.29	0.32	0.53	0.62	0.53	1.13	2.40	1.71
LOI	2.46	1.31	2.04	1.01	1.02	0.71	1.29	1.17	0.98	0.76
Rest	0.50	0.33	0.72	0.40	0.47	0.44	0.48	0.52	0.52	0.60
Total	**100.16**	**100.32**	**99.89**	**100.64**	**100.34**	**100.22**	**100.09**	**99.93**	**99.82**	**100.03**
O=S,Cl	0.09	0.05	0.13	0.03	0.10	0.08	0.11	0.11	0.11	0.11
Total	**100.07**	**100.27**	**99.76**	**100.61**	**100.24**	**100.14**	**99.98**	**99.82**	**99.71**	**99.92**
	C.I.P.W. norms									
Q	–	1.71	–	–	0.13	–	–	–	–	–
Or	7.98	4.96	5.73	7.98	9.40	9.40	7.74	9.51	10.87	16.25
Ab	29.28	28.94	14.81	19.46	24.29	26.06	23.19	23.61	23.27	29.95
An	20.40	23.64	18.31	17.72	21.30	24.62	24.54	19.80	15.65	12.09
Ne	–	–	–	–	–	–	–	–	–	–
Di	13.58	13.37	16.69	22.96	12.00	10.16	12.03	12.43	8.54	6.74
Hy	10.71	19.33	19.62	16.09	20.07	10.25	9.77	8.40	17.95	15.59
Ol	7.28	–	12.58	4.51	–	6.39	10.27	10.27	4.57	4.96
Mt	2.66	2.52	3.28	3.32	3.35	3.32	3.39	3.79	3.94	3.80
Il	4.01	3.27	5.24	6.30	6.97	7.10	5.85	7.71	7.96	5.07
Ap	1.18	0.85	0.69	0.76	1.26	1.47	1.26	2.68	5.68	4.05
mg	53.3	52.5	65.1	54.0	42.0	38.4	46.4	39.8	37.4	27.6
	Trace elements in parts per million									
Ba	543	354	336	415	579	651	452	669	676	1457
Rb	25	15	27	38	48	45	31	38	41	51
Sr	877	627	375	490	225	288	312	303	263	343
Pb	7	3	8	11	13	13	9	12	12	15
Th	2	1	5	4	6	6	2	2	2	2
U	0.5	0.5	1.0	0.5	<0.5	0.5	0.5	0.5	<0.5	0.5
Zr	136	102	243	270	279	297	268	384	483	496
Nb	37	22	15	17	15	16	16	22	18	41
Y	22	22	31	34	57	56	49	70	81	88
La	24	16	21	33	31	42	23	47	41	63
Ce	50	35	59	73	72	90	59	106	106	136
Nd	32	22	36	44	41	51	38	67	78	82
Sc	17	19	25	30	27	25	27	29	34	21
V	113	117	288	348	281	226	290	282	202	29
Cr	142	116	978	383	50	28	77	28	2	<0.2
Ni	75	46	598	122	53	33	54	27	8	<0.2
Cu	32	28	126	87	36	50	41	34	33	22
Zn	129	111	116	109	142	141	123	148	170	179
Ga	20	19	19	21	21	21	20	24	20	23
As	<0.5	<0.5	<0.5	<0.5	<0.5	<0.5	<0.5	<0.5	<0.5	<0.5
S	1670	980	2630	410	2030	1560	2230	2080	2190	2030
Cl	495	245	140	225	120	165	135	175	105	345
K/Rb	448	465	298	295	275	293	351	352	373	448
Rb/Sr	0.029	0.024	0.072	0.078	0.213	0.156	0.100	0.125	0.156	0.149
Ce/Y	2.3	1.6	1.9	2.2	1.26	1.61	1.20	1.51	1.31	1.55
K/Zr	82	68	33	41	47	44	41	35	32	46
P/Zr	16	15	5.2	5.2	8.3	9.1	8.6	13	22	15
Nb/Zr	0.27	0.22	0.062	0.063	0.054	0.054	0.060	0.057	0.037	0.083
Nb/Nb*	1.26	1.17	0.65	0.50	0.42	0.38	0.56	0.49	0.41	0.61
Sr/Sr*	1.64	1.68	0.61	0.64	0.31	0.32	0.49	0.27	0.22	0.24

mg = atomic 100Mg/(Mg+0.85Fe(total)).

Sample no.	86285877	86286097	86286075	86285966	86286050	86285839	86285977	86285803
Locality	2km SE of Dobrowolski	Bunger Hills SE	Paz Cove NE	1km N of Edgeworth David	Miles Island W	Saturn Island	Booth Peninsula W	Obruchev Hills C
Lithology	Olivine dolerite	Olivine dolerite	Olivine dolerite	Olivine dolerite	Olivine dolerite	Olivine dolerite	Olivine dolerite	Olivine dolerite
Classif.	Group 4A	Group 4A	Group 4B	Group 4B	Group 4C	Group 4D	Group 4D	Group 4E
SiO_2	45.60	45.30	44.70	44.90	46.60	44.20	44.90	45.00
TiO_2	3.05	3.25	3.30	4.00	2.59	3.70	3.98	3.34
Al_2O_3	16.83	15.92	15.65	15.27	15.68	15.01	14.18	15.04
Fe_2O_3	3.97	3.35	2.69	4.20	2.91	3.94	2.13	4.79
FeO	9.04	11.05	11.90	11.54	10.32	11.75	14.02	10.16
MnO	0.18	0.20	0.21	0.22	0.21	0.24	0.25	0.24
MgO	5.84	6.07	6.91	5.66	6.11	5.73	5.43	6.71
CaO	8.79	8.50	8.98	8.48	8.75	8.27	8.32	9.03
Na_2O	3.15	3.01	2.96	3.01	2.92	3.06	2.89	2.94
K_2O	0.83	0.88	0.79	1.11	0.99	1.25	1.40	0.73
P_2O_5	0.40	0.44	0.62	0.79	0.34	0.67	0.81	0.43
LOI	2.05	1.85	1.11	0.62	1.70	1.69	1.12	0.82
Rest	0.42	0.38	0.46	0.44	0.70	0.51	0.53	0.29
Total	**100.15**	**100.20**	**100.28**	**100.24**	**99.82**	**100.02**	**99.96**	**99.52**
O=S,Cl	0.10	0.08	0.13	0.10	0.24	0.12	0.12	0.04
Total	**100.05**	**100.12**	**100.15**	**100.14**	**99.58**	**99.90**	**99.84**	**99.48**
	C.I.P.W. norms							
Q	–	–	–	–	–	–	–	–
Or	4.90	5.20	4.67	6.56	5.85	7.39	8.27	4.31
Ab	26.65	25.47	24.56	25.47	24.71	24.29	24.45	24.88
An	29.33	27.33	27.08	24.88	26.75	23.53	21.58	25.69
Ne	–	–	0.26	–	–	0.87	–	–
Di	9.62	9.90	11.06	9.99	11.92	10.90	12.00	13.46
Hy	1.08	3.04	–	2.79	6.57	–	3.56	0.74
Ol	16.13	16.34	19.88	16.20	12.71	18.43	15.20	18.25
Mt	3.05	3.40	3.46	3.70	3.13	3.70	3.85	3.50
Il	5.79	6.17	6.27	7.60	4.92	7.03	7.56	6.34
Ap	0.95	1.04	1.47	1.87	0.81	1.59	1.92	1.02
mg	49.3	47.5	50.3	43.7	49.8	44.0	41.7	49.3
	Trace elements in parts per million							
Ba	322	330	295	478	327	380	458	113
Rb	15	18	14	16	15	29	32	7
Sr	313	285	327	312	356	332	297	295
Pb	6	6	6	5	6	9	9	3
Th	<1	<1	<1	<1	1	1	3	<1
U	0.5	0.5	1.0	<0.5	<0.5	0.5	1.0	0.5
Zr	191	206	208	250	208	329	354	289
Nb	10	10	9	10	12	19	22	11
Y	39	42	40	44	36	54	60	51
La	15	13	15	16	16	28	32	12
Ce	41	43	40	44	39	68	77	43
Nd	26	25	28	31	24	43	50	30
Sc	24	26	25	25	27	28	31	32
V	207	253	218	266	261	313	316	323
Cr	62	73	68	49	72	46	71	106
Ni	95	84	93	60	55	53	43	71
Cu	35	42	50	38	42	38	40	48
Zn	109	125	105	130	107	144	153	122
Ga	20	21	20	20	21	22	23	22
As	<0.5	<0.5	<0.5	0.5	<0.5	<0.5	0.5	<0.5
S	2030	1570	2450	2040	4720	2350	2380	670
Cl	155	75	135	70	165	235	160	85
K/Rb	459	406	468	576	548	358	363	866
Rb/Sr	0.048	0.063	0.043	0.051	0.042	0.087	0.108	0.024
Ce/Y	1.1	1.0	1.0	1.0	1.1	1.3	1.3	0.84
K/Zr	36	35	32	37	40	32	33	21
P/Zr	9.1	9.3	13	14	7.1	8.9	10	6.5
Nb/Zr	0.052	0.049	0.043	0.040	0.058	0.058	0.062	0.038
Nb/Nb*	0.55	0.56	0.51	0.45	0.58	0.63	0.64	0.71
Sr/Sr*	0.71	0.65	0.73	0.63	0.87	0.46	0.36	0.61

here is based on chemical composition and, therefore, gives a more consistent nomenclature for compositionally similar rocks than would a petrographic classification. However, the more hornblende-rich dykes would be classified as spessartites on the scheme of Streckeisen (1979).

Chemically, these dykes form a heterogeneous group of alkaline (Ne-normative) magnesian rocks (Table 14, Figs 65, 67). The two picrites are strongly Ol-normative and probably represent near-primary liquids (*mg'* = atomic 100Mg/(Mg+0.8Fe_{total}) = 73-75, high Cr and Ni), although the altered sample has apparently lost Na_2O. The ankaramites are more evolved (*mg'* 58–75) and more strongly Di and Ne-normative, but have lower LILE contents and presumably represent higher degree melts. Both dyke types have many chemical features in common with group 1 dolerites, despite being much more SiO_2-undersaturated. They plot in the tholeiite field on an AFM diagram (Fig. 66) and do not have Nb anomalies (Fig. 79). Hence, they were presumably also derived from an enriched mantle source with a major Nb-rich OIB-type component (Sheraton et al. 1990).

Alkali basalt and trachybasalt dykes. These are the youngest dyke suite, cropping out mainly in the south-western Bunger Hills and Taylor Islands. Most are less than 1 m thick and their predominant trend is east-west.

Alkali basalts are commonly porphyritic, with olivine (Fo_{87-77}: 5–15%) and diopside ($Ca_{48}Mg_{44}Fe_8$: 5-20%) phenocrysts in a fine-grained groundmass of brown or reddish-brown biotite (rarely up to 25%), alkali feldspar, oligoclase (An_{30-20}) and minor clinopyroxene, pale green amphibole, magnetite, pyrite, apatite and carbonate (Fig. 80). Olivine is wholly or partly replaced by mixtures of yellowish serpentine,

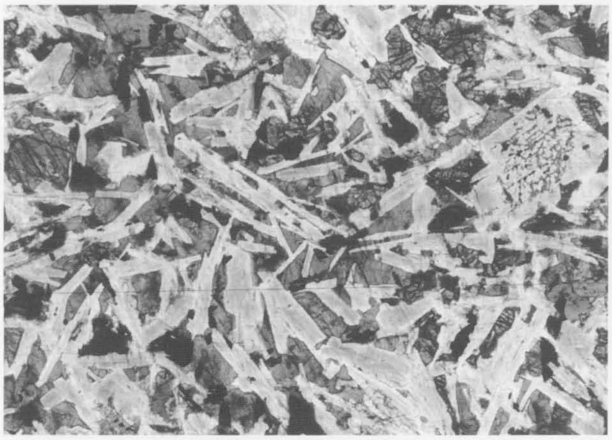

Figure 74. Group 4 dolerite dyke (olivine, clinopyroxene, plagioclase), showing subophitic to intergranular texture; east of Paz Cove. Minor reddish-brown biotite is associated with Fe-Ti oxides. Sample 86285872; width of field: 6mm.

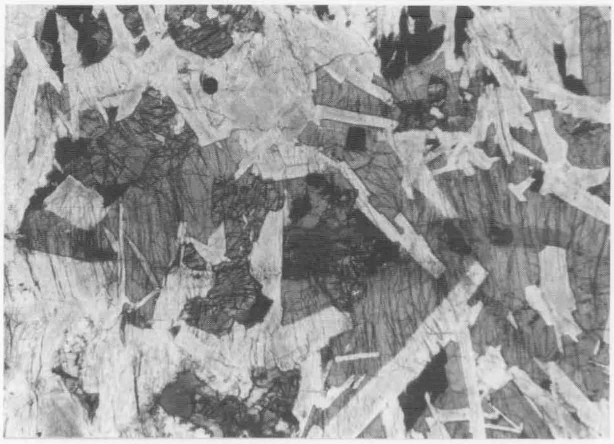

Figure 75. Relatively coarse-grained group 4 dolerite dyke (olivine, clinopyroxene, plagioclase), showing subophitic to intergranular texture; northeastern Paz Cove. Sample 86286075; width of field: 7mm.

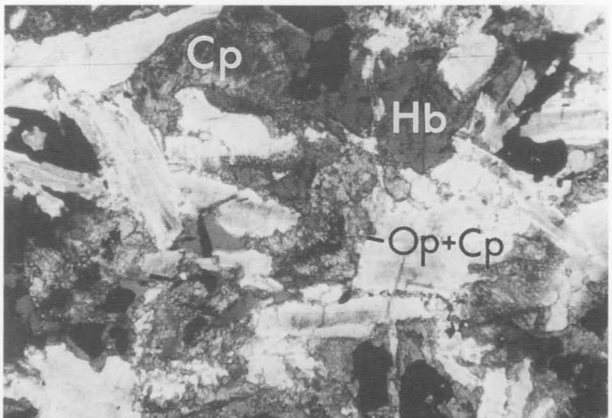

Figure 76. Group 4E dolerite dyke, showing possibly primary hornblende and biotite, as well as clinopyroxene, with secondary granular orthopyroxene and clinopyroxene; northeastern Obruchev Hills. Sample 86285811; width of field: 1.8mm.

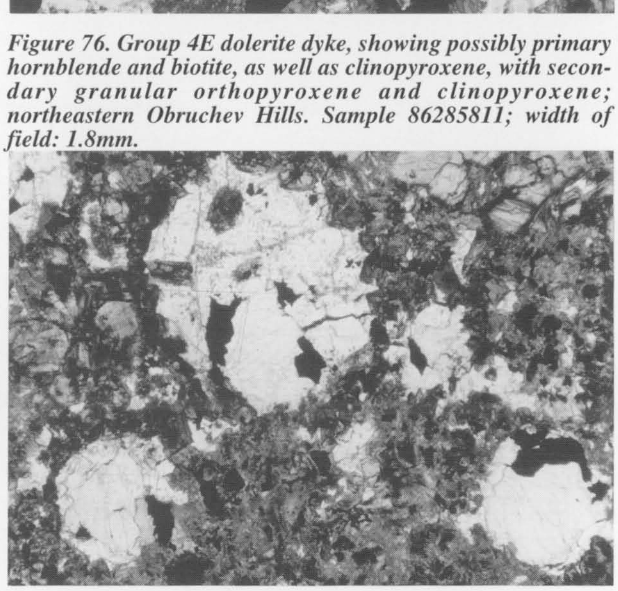

Figure 77. Plagioclase+carbonate-rich ocelli in ankaramite (spessartite-kersantite) dyke; southwest of Edgeworth David Base. Groundmass consists of olivine, clinopyroxene, biotite, hornblende, plagioclase, and opaque minerals. Sample 86285688; width of field: 3.0mm.

Figure 78. Ankaramite (spessartite) dyke, showing slightly zoned subhedral clinopyroxene, olivine (darker grey), fine-grained reddish-brown hornblende, and plagioclase, with a locally poikilitic texture; east of Edgeworth David Base. Sample 86285824; width of field: 3.2mm.

chlorite, talc, colourless clinoamphibole, opaque minerals and carbonate, probably as a result of deuteric alteration. Some plagioclase is replaced by scapolite. Some dykes contain carbonate ± quartz ocelli.

A chemically similar dyke (86285918) from the northern Taylor Islands contains comparatively well crystallised dark brown biotite (20%) and pale green actinolite (25%), as well as fine-grained granular feldspar. Some of the actinolite forms aggregates which probably replace original clinopyroxene (and possibly olivine) phenocrysts. Representative analyses of mafic minerals are given in Table 13.

Trachybasalts contain phenocrysts of zoned labradorite-andesine (An_{60-47}, with K-feldspar rims: 5–10%), as well as diopside ($Ca_{47}Mg_{40}Fe_{13}$, some with pigeonite ($Ca_{12}Mg_{68}Fe_{20}$) cores: 4–10%) and olivine (Fo_{78-71}: 4%), in an intergranular groundmass of feldspar (mainly alkali feldspar), greenish-brown actinolite or reddish-brown pargasitic amphibole, dark brown biotite, pyrite (partly altered to goethite), apatite and quartz (Figs 81, 82). Two such dykes from the Taylor Islands contain poikilitic aggregates of biotite (20–25%) and actinolite (13–17%) (Fig. 83). These presumably replaced clinopyroxene or olivine, but nevertheless appear to be of magmatic rather than deuteric or metamorphic origin.

The extent of replacement of original anhydrous minerals by hydrous phases was probably a function of cooling rate, as well as the water content of the magma. Hence, in the

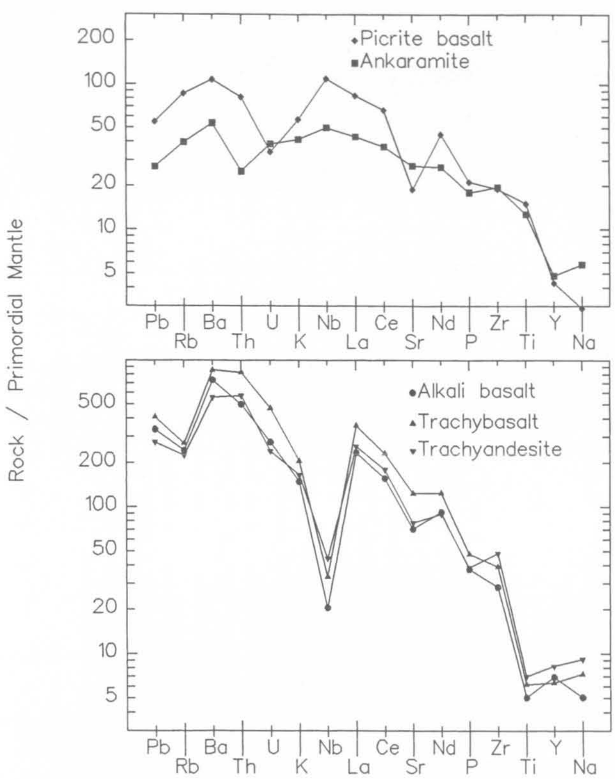

Figure 79. Spidergrams for average Bunger Hills alkaline dykes.

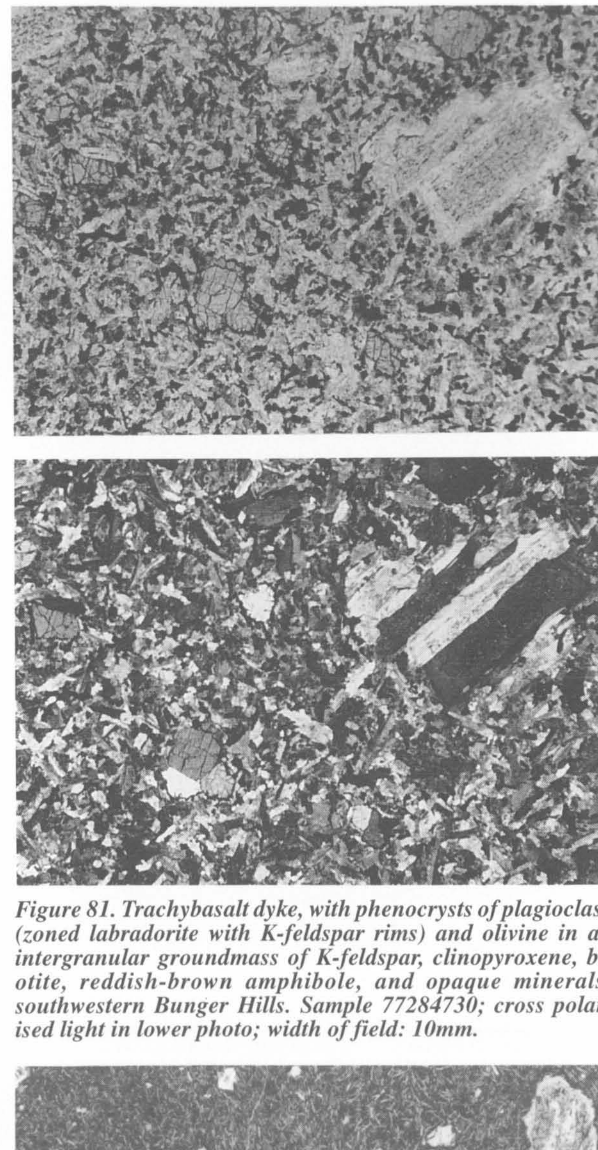

Figure 81. Trachybasalt dyke, with phenocrysts of plagioclase (zoned labradorite with K-feldspar rims) and olivine in an intergranular groundmass of K-feldspar, clinopyroxene, biotite, reddish-brown amphibole, and opaque minerals; southwestern Bunger Hills. Sample 77284730; cross polarised light in lower photo; width of field: 10mm.

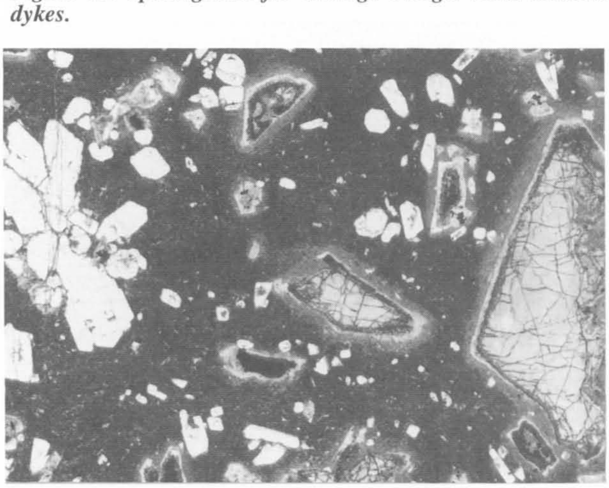

Figure 80. Alkali basalt dyke, with clinopyroxene (white) and slightly altered olivine phenocrysts; northern Taylor Islands. Sample 86285922; width of field: 7mm.

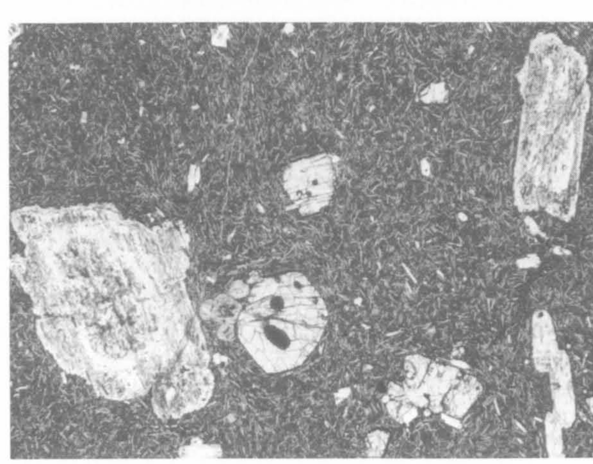

Figure 82. Trachybasalt dyke, with zoned plagioclase and olivine phenocrysts in a fine-grained, locally trachytic groundmass; southwestern Bunger Hills. Sample 86285952; width of field: 11mm.

Table 13. Representative analyses of mafic minerals in alkaline dykes from Bunger Hills area.

	Picrite 86285954				*Alkali basalt 86285912*		*Alkali basalt 86285918*		*Trachybasalt 86285949*			*Trachybasalt 86285919*
	Cp	*Ol*	*Hb**	*Phl*	*Cp*	*Ol*	*Act**	*Bi*	*Pig*	*Cp*	*Ol*	*Act**
SiO_2	51.73	37.88	46.28	36.78	53.02	40.23	56.25	36.72	54.11	49.56	38.78	53.57
TiO_2	1.09	–	1.36	2.16	0.53	–	–	2.08	0.31	1.72	–	–
Al_2O_3	3.45	–	7.60	15.80	2.47	0.14	0.87	14.29	1.95	5.11	0.09	3.11
FeO^+	6.80	25.27	14.36	11.49	4.58	12.48	7.49	14.53	12.57	7.38	20.77	10.84
MnO	–	0.52	0.20	–	–	0.19	0.15	–	0.18	–	0.24	–
MgO	14.74	36.14	13.29	18.48	15.80	46.96	18.98	15.61	24.35	13.63	39.89	16.40
CaO	21.52	0.20	10.86	–	23.42	0.21	12.79	–	6.17	22.54	0.16	12.52
Na_2O	0.72	–	2.54	0.47	–	–	0.21	0.20	0.31	0.36	–	0.57
K_2O	–	–	0.35	9.21	–	–	–	9.07	–	–	–	0.22
Cr_2O_3	–	–	0.11	–	0.31	–	–	–	0.71	0.23	–	–
Total	**100.05**	**100.01**	**96.95**	**94.38**	**100.44**	**100.20**	**96.73**	**92.50**	**100.66**	**100.53**	**99.94**	**97.23**
O	6	4	23	22	6	4	23	22	6	6	4	23
Si	1.909	1.007	6.810	5.459	1.936	0.996	7.952	5.640	1.946	1.836	1.001	7.675
Al^{iv}	0.091	–	1.190	2.541	0.064	0.004	0.048	2.360	0.054	0.164	–	0.325
Al^{vi}	0.059	–	0.129	0.224	0.042	–	0.098	0.227	0.029	0.059	0.003	0.200
Ti	0.030	–	0.150	0.241	0.015	–	–	0.241	0.008	0.048	–	–
Fe^3	–	–	0.532	–	–	–	0.018	–	–	–	–	0.082
Fe^2	0.210	0.558	1.235	1.426	0.140	0.258	0.867	1.866	0.378	0.229	0.448	1.216
Mn	–	0.012	0.025	–	–	0.004	0.018	–	0.006	–	0.005	–
Mg	0.811	1.423	2.916	4.088	0.860	1.733	3.999	3.574	1.305	0.752	1.535	3.502
Ca	0.851	0.006	1.713	–	0.916	0.006	1.937	–	0.238	0.895	0.005	1.922
Na	0.052	–	0.724	0.134	0.023	–	0.057	0.060	0.022	0.026	–	0.158
K	–	–	0.065	1.744	–	–	–	1.776	–	–	–	0.041
Cr	–	–	0.013	–	0.009	–	–	–	0.020	0.007	–	–
Total	**4.012**	**2.999**	**15.502**	**15.856**	**4.003**	**3.002**	**14.994**	**15.744**	**4.005**	**4.015**	**2.997**	**15.121**
mg	79.4	71.8	70.2	74.1	86.0	87.0	82.2	65.7	77.5	76.7	77.4	74.2

		Trachybasalt 77284730			
	Bi	*Cp*	*Ol*	*Hb**	*Bi*
SiO_2	36.54	46.93	37.11	39.72	33.70
TiO_2	2.37	1.91	–	3.89	8.22
Al_2O_3	14.00	6.91	–	11.98	13.64
FeO^+	16.97	8.89	26.53	14.16	22.38
MnO	–	–	0.32	0.28	0.25
MgO	14.48	12.70	35.88	11.48	8.87
CaO	–	22.18	0.16	11.77	–
Na_2O	0.30	0.40	–	2.14	0.18
K_2O	9.07	–	–	2.32	9.72
Cr_2O_3	–	–	–	–	–
Total	**93.72**	**99.93**	**100.00**	**97.73**	**96.96**
O	22	6	4	23	22
Si	5.612	1.766	0.987	6.008	5.207
Al^{iv}	2.388	0.234	–	1.992	2.484
Al^{vi}	0.146	0.073	–	0.144	–
Ti	0.273	0.054	–	0.442	0.955
Fe^3	–	–	–	0.074	–
Fe^2	2.179	0.280	0.590	1.717	2.892
Mn	–	–	0.007	0.036	0.032
Mg	3.314	0.712	1.423	2.587	2.043
Ca	–	0.894	0.005	1.907	–
Na	0.089	0.029	–	0.628	0.054
K	1.778	–	–	0.447	1.915
Cr	–	–	–	–	–
Total	**15.780**	**4.042**	**3.012**	**15.982**	**15.582**
mg	60.3	71.8	70.7	60.1	41.4

+ Total Fe as FeO. mg = atomic 100Mg/(Mg+total Fe), or 100Mg/($Mg+Fe^{2+}$) for amphibole (Act, Hb).

* Fe^{3+} in amphiboles calculated assuming total cations (excluding Ca, Na, and K) = 13.

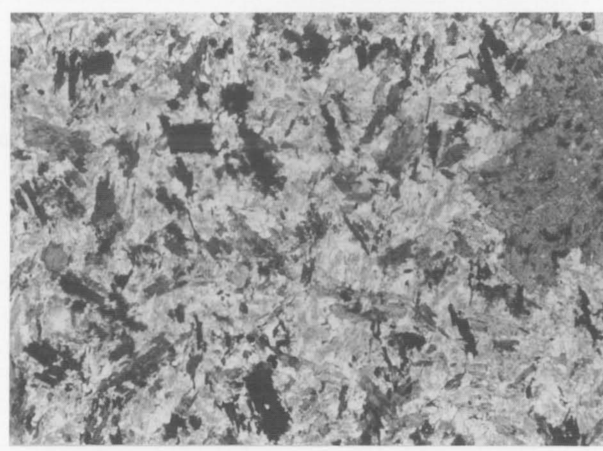

Figure 83. Trachybasalt dyke, with poikilitic aggregates of pale green actinolite and dark brown biotite in a K-feldspar-rich groundmass; northern Taylor Islands. Sample 86285919; width of field: 5.5mm.

presumably more rapidly cooled, finer grained dykes, clinopyroxene and olivine phenocrysts have not reacted substantially with the residual hydrous liquid, although the abundance of biotite in the groundmass attests to the high water content of the magma.

Two even more evolved trachyandesite dykes contain only zoned calcic andesine (10%) phenocrysts, together with K-feldspar, dark brown biotite (8–10%), green amphibole (up to 8%) and minor opaque minerals, quartz and apatite.

Clinopyroxene has a much more restricted range of composition in these dykes than in the dolerites, and mostly indicates crystallisation at at least 900–1000°C (1200° for pigeonite cores) (Fig. 64), consistent with rapid quenching after emplacement.

The more biotite and amphibole-rich of these dykes would be classified as lamprophyre (minette or vogesite, respectively)

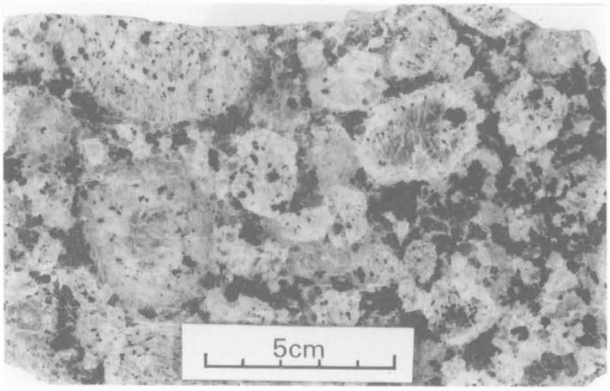

Figure 84. Small boulder (cobble) of rapakivi granite from moraine, showing rounded K-feldspar phenocrysts rimmed by altered plagioclase.

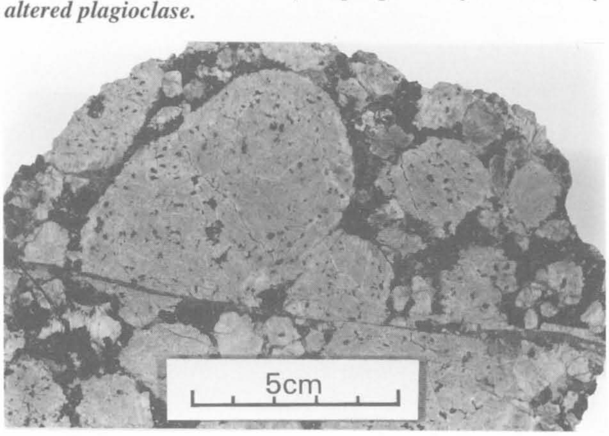

Figure 85. Small boulder of rapakivi granite from moraine, showing pink rounded K-feldspar crystals, partly mantled by green epidotised plagioclase. Many of the smaller feldspar crystals are altered plagioclase. The boulder is cut by a small mylonite zone.

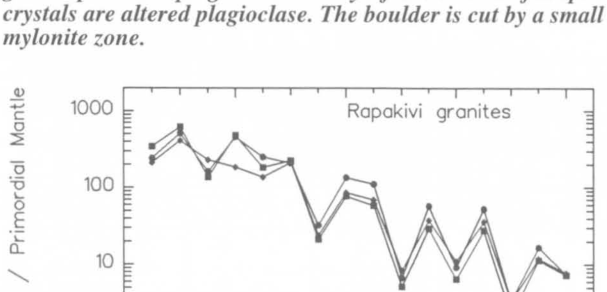

Figure 86. Spidergrams for rapakivi granites from moraines in the Bunger Hills area.

on the criteria of Streckeisen (1979) and Rock (1984). However, because of the secondary nature of much of these minerals, the presence of plagioclase phenocrysts in some dykes, and the chemical similarity of olivine + clinopyroxene-phyric dykes to biotite + amphibole-rich ones, the chemical classification of Irvine & Baragar (1971) is used here. In terms of the total alkali silica (TAS) classification of volcanic rocks (Le Maitre 1984), these dykes range from basanite, through trachybasalt and phonotephrite, to basaltic trachyandesite (shoshonite).

The alkali basalt and trachybasalt dykes are Ne-normative and strongly enriched in alkalies, particularly K_2O (Table 14, Figs 65–67). The former are little evolved (normative Ol 13–26%, *mg'* 65-80), whereas the latter are more fractionated (Ol 9–14%, *mg'* 54-67). The Hy-normative trachyandesites are even more evolved (Ol 2–5%, *mg'* 43–44). All these dykes have very high incompatible element contents (especially Pb, K, Ba, Rb, Sr, Th, U, and LREE), and spidergrams show strong and increasing enrichment in most elements from Zr to Ba, large negative Nb anomalies and relatively low Rb (Fig. 79).

Much of the chemical variation can be explained by fractionation of clinopyroxene and olivine and probably, in the most evolved dykes, plagioclase, together with different conditions and/or degrees of partial melting. The similarity of the spidergrams suggests derivation from similar source regions, although the Hy-normative trachyandesites, at least, probably formed from a distinct parent magma which segregated under relatively high P_{H_2O} or low pressure conditions (Sheraton et al. 1990). However, significant variations in some incompatible element ratios and Sr_i values, which form two distinct groupings (0.7074–0.7085, 0.7147–0.7168: Table 8) that do not correlate with bulk composition, preclude melting of a homogeneous source. Nevertheless, the high Sr_i and low $\varepsilon_{Nd}(-18.6, -17.2)$ are consistent with derivation from long-term, variably enriched mantle. The large negative Nb anomalies suggest a major LILE-rich (slab-derived?) component in the source. An alkali basalt and a trachybasalt have indistinguishable mineral-whole-rock Rb-Sr isochron ages of 502±12 and 502±7 Ma, respectively, interpreted as crystallisation ages. Moreover, $^{87}Sr/^{86}Sr$ ratios of these two dykes converge to the same value at 2426 Ma, and T^{Nd}_{DM} model ages are 2290 and 2080 Ma, respectively. These values resemble T^{Nd}_{DM} model ages of the country rocks (Table 8), suggesting that metasomatism of the source of the alkaline dykes (and possibly also the plutonic rocks) was contemporaneous with formation of continental crust in the area.

Rapakivi granite and felsic volcanics

A distinctive megacrystic granite, commonly with a rapakivi texture, occurs in moraines in much of the Bunger Hills area. It has not been found in situ, so its age relations with the other units are unknown. It is most common in the western Bunger Hills and at Grace Rocks, suggesting a sub-glacial source to the south or southeast, rather than east.

The granite is characterised by pink poikilitic K-feldspar megacrysts, up to 6 cm across, commonly rounded and rimmed by pale green altered plagioclase (Figs 84, 85). There are smaller greenish phenocrysts of sericitised plagioclase, and the groundmass is rich in biotite and hornblende. The granite contains dark greenish-brown hornblende (up to 4%), dark brown biotite (1–5%), quartz (25–35%), sodic andesine or oligoclase, locally with albite rims (20–35%), microcline (25–50%) and minor opaque minerals, apatite, zircon, sphene and, in one rock, fluorite.

Alteration is extensive; plagioclase is sericitised and biotite is chloritised. Up to 2 per cent of secondary pale green clinoamphibole may replace original pyroxene, and sphene rims opaque minerals. Small amounts of secondary epidote or clinozoisite, carbonate and muscovite may also be present. Other, strongly epidotised, granitic rocks have also been found in Bunger Hills moraines.

The rapakivi granite is moderately fractionated and marginally metaluminous or peraluminous (Table 15, Figs 89–91). The presence of hornblende and sphene, together with the mostly Di-normative compositions, is consistent with it being I-type (Chappell & White 1974), although relatively high REE and HFSE suggest anorogenic (A-type) affinities (Collins et al. 1982; Whalen et al. 1987), in common with most rapakivi granites (Rogers & Greenberg 1990). Like other rapakivi granites, it has the irregular spidergrams that are more typical of intracrustal than mantle-derived melts (large negative Nb, Sr, P, and Ti anomalies, but no Y depletion) (Fig. 86). There are no obvious chemical correlations with

Table 14. Chemical analyses of representative alkaline dykes from Bunger Hills area.

Sample no.	*86285954*	*86285823*	*86285688*	*86285677*	*86285918*	*86285919*	*86285952*	*86285931*
Locality	*Lake Poly–anskogo*	*1km E of Edgeworth David*	*2km SW of Edgeworth David*	*W of Lake Dolgoe*	*N Taylor Islands*	*N Taylor Islands*	*6km SW of Dobrowolski*	*S Taylor Islands*
Lithology	*Picrite basalt*	*Ankaramite*	*Ankaramite*	*Alkali olivine basalt*	*Alkali olivine basalt*	*Trachybasalt*	*Trachybasalt*	*Trachy-andesite*
SiO_2	42.60	43.90	41.90	46.10	48.30	50.10	51.00	53.90
TiO_2	2.40	1.82	2.68	0.93	1.10	1.16	1.42	1.50
Al_2O_3	8.79	7.33	10.41	12.96	14.29	15.31	18.12	18.41
Fe_2O_3	3.46	2.57	3.98	3.43	1.84	1.65	2.46	3.04
FeO	9.47	9.78	10.42	3.98	5.59	4.17	4.69	4.44
MnO	0.18	0.18	0.20	0.14	0.12	0.07	0.12	0.09
MgO	15.59	16.58	12.41	12.49	9.56	5.21	3.68	2.54
CaO	8.78	12.47	10.10	6.91	7.28	7.26	5.80	5.45
Na_2O	2.09	1.50	2.43	1.91	2.12	2.81	2.94	3.67
K_2O	1.47	0.55	1.06	4.89	4.92	5.59	6.06	4.68
P_2O_5	0.41	0.18	0.39	0.95	0.91	0.98	1.01	0.85
H_2O^+	1.95	0.49	0.79	1.88	1.45	0.92	0.93	0.52
H_2O^-	0.08	0.05	0.02	0.10	0.05	0.18	0.11	0.04
CO_2	1.77	1.60	2.17	1.68	0.67	2.25	0.36	0.04
Rest	0.70	0.63	0.67	1.58	1.08	1.69	1.26	1.06
Total	**99.74**	**99.63**	**99.63**	**99.93**	**99.28**	**99.35**	**99.96**	**100.23**
O=S,Cl	0.08	0.09	0.13	0.10	0.06	0.04	0.03	0.05
Total	**99.66**	**99.54**	**99.50**	**99.83**	**99.22**	**99.31**	**99.93**	**100.18**
	C.I.P.W. norms							
Or	8.69	3.25	6.26	28.90	29.07	33.03	35.81	27.66
Ab	8.98	5.93	8.23	4.79	11.15	15.65	18.91	31.05
An	10.26	11.64	14.37	12.35	14.95	12.65	18.35	19.94
Ne	4.71	3.66	6.68	6.16	3.68	4.40	3.23	–
Di	24.51	39.23	26.79	12.52	12.19	13.67	3.13	1.28
Hy	–	–	–	–	–	–	–	7.88
Ol	28.40	25.30	23.01	23.48	18.40	8.55	10.51	3.49
Mt	4.06	3.90	4.51	2.28	2.33	1.82	2.22	2.31
Il	4.56	3.46	5.09	1.77	2.09	2.20	2.70	2.85
Ap	0.97	0.43	0.92	2.25	2.16	2.32	2.39	2.01
mg	73.4	75.3	66.3	79.7	74.6	67.2	54.3	44.1
	Trace elements in parts per million							
Ba	1012	184	337	6060	4240	7220	5820	4050
Rb	43	10	22	213	189	107	212	145
Sr	517	329	629	1621	1280	4250	1729	1635
Pb	11	4	5	110	25	49	109	51
Th	6	<1	2	76	58	55	96	54
U	0.5	<0.5	<0.5	10	7.5	6.5	14	5.0
Zr	201	125	216	406	340	317	604	542
Nb	47	15	32	12	21	20	31	32
Y	22	16	21	39	25	22	36	37
La	57	13	34	166	118	242	322	182
Ce	114	35	75	301	212	401	532	319
Nd	57	22	34	140	102	167	207	124
Sc	29	34	27	18	20	12	14	12
V	309	286	321	126	127	110	150	121
Cr	734	1260	669	890	637	207	81	<2
Ni	503	534	339	363	194	180	40	22
Cu	70	127	88	42	46	76	63	31
Zn	112	82	114	76	71	88	92	95
Ga	16	14	20	11	14	16	18	20
As	0.50	<0.50	<0.50	2.00	<0.50	<0.50	3.00	2.50
S	1330	1780	2350	1050	890	480	570	350
Cl	685	255	410	2070	685	695	165	1500
K/Rb	284	457	400	191	216	434	237	268
Rb/Sr	0.083	0.030	0.035	0.131	0.148	0.025	0.123	0.089
Ce/Y	5.2	2.2	3.6	7.7	8.5	18	15	8.6
Th/U	12	–	>4	7.6	7.7	8.5	6.9	11
K/Zr	61	37	41	100	120	146	83	72
P/Zr	8.9	6.3	7.9	10	12	13	7.3	6.9
Nb/Zr	0.23	0.12	0.15	0.030	0.062	0.063	0.051	0.059
Nb/Nb*	0.98	1.10	1.04	0.08	0.17	0.10	0.13	0.21
Sr/Sr*	0.47	0.88	0.90	0.57	0.64	1.18	0.37	0.58

mg = atomic 100Mg/(Mg+0.8Fe(total)).

Table 15. Chemical analyses of rapakivi granites from moraines in Bunger Hills area.

Sample no.	*86285878*	*86286230*	*86286285*
Locality	*Moraine (2km SE of Dobrowol.)*	*Moraine (Grace Rocks)*	*Moraine*
Lithology	*Bi granite*	*Bi–Hb granite*	*Bi–Hb granite*
SiO_2	69.90	65.60	67.50
TiO_2	0.45	0.70	0.71
Al_2O_3	14.44	15.56	14.40
Fe_2O_3	0.44	1.04	1.16
FeO	1.94	3.02	3.18
MnO	0.04	0.07	0.07
MgO	0.99	0.73	0.76
CaO	1.36	2.79	2.38
Na_2O	2.83	3.00	2.89
K_2O	6.15	5.84	5.74
P_2O_5	0.14	0.24	0.20
LOI	1.31	0.69	0.86
Rest	0.27	0.35	0.34
Total	**100.26**	**99.63**	**100.19**
	C.I.P.W. norms		
Q	24.76	17.86	21.55
C	0.99	–	–
Or	36.34	34.51	33.92
Ab	23.95	25.39	24.45
An	5.83	11.74	9.37
Di	–	0.45	0.96
Hy	5.00	5.25	5.24
Mt	0.64	1.51	1.68
Il	0.85	1.33	1.35
Ap	0.33	0.57	0.47
mg	47.6	30.1	29.9
	Trace elements in parts per million		
Ba	947	1581	1117
Rb	389	259	322
Sr	107	176	139
Pb	68	42	48
Th	44	17	42
U	4.0	3.0	5.5
Zr	306	404	585
Nb	15	17	23
Y	51	54	75
La	54	60	94
Ce	106	126	200
Nd	40	51	78
Sc	7	12	11
V	22	32	35
Cr	2	3	<2
Ni	2	3	7
Cu	17	7	9
Zn	38	61	71
Sn	6	3	7
Ga	19	20	18
S	100	100	<100
K/Rb	131	187	148
Rb/Sr	3.64	1.47	2.32
Ce/Y	2.1	2.3	2.7
Th/U	11	5.7	7.6
K/Zr	167	120	81
P/Zr	2.0	2.6	1.5
Nb/Zr	0.049	0.042	0.039
Nb/Nb*	0.14	0.16	0.19
Sr/Sr*	0.12	0.16	0.08

mg = atomic $100Mg/(Mg+Fe^{2+})$.

any of the felsic intrusive rocks cropping out in the area, but the relative abundance of rapakivi granite erratics in the Bunger Hills area implies a significant sub-glacial occurrence.

Porphyritic felsic rocks of presumed volcanic origin also occur in moraines, notably at Chugunov Island (see below). The location of this island, between the seaward ends of the Denman and Scott Glaciers, suggests a source for these volcanics, like that of the rapakivi granite, to the south or southeast. They include pink to purple rhyolite with phenocrysts predominantly quartz and K-feldspar. One sample (86286034) contains corroded quartz (10%) and K-feldspar (5%) phenocrysts in a turbid, spherulitic quartzo-feldspathic groundmass with minor opaque minerals and hematite. Another coarser grained rhyolite (86286035) consists of greenish-brown hornblende (5%), quartz (25%), sericitised feldspar (mainly alkali feldspar: 70%) and minor opaque minerals, apatite and zircon. A few iddingsite pseudomorphs may be after pyroxene. Both rocks contain granophyric intergrowths of K-feldspar and quartz.

A third porphyry contains large (1–6 cm), altered pink poikilitic K-feldspar phenocrysts with green strongly sericitised rims, which suggest an affinity with the rapakivi granite, although the groundmass is much finer grained. There are also small greenish sericitised plagioclase and a few quartz phenocrysts, and the groundmass contains quartz, altered feldspar, colourless to pale green secondary amphibole, epidote, iddingsite pseudomorphs (after pyroxene?), and minor opaque minerals, hematite, apatite and zircon.

Denman Glacier Area

This study covered an area on the western side of the Denman Glacier. Similar in size to the Bunger Hills area, it extends from David Island in the north to Jones Rocks in the west and Mount Borzov about 140 km to the south (Fig. 7). However, outcrops are generally small and isolated. As only a few of the southern outcrops were visited in 1986, much of the following account relies on descriptions given by Nockolds (1940) and Ravich et al. (1968).

The predominantly granulite-facies metamorphic rocks exposed in this area are of somewhat different composition to those of the Bunger Hills, and there is only a relatively small proportion of clearly sedimentary origin. They are intruded by a wide variety of plutonic rocks, including a major batholith of syenitic to granitic composition at David Island. No unmetamorphosed dolerite dykes have been found, but rare mafic dykes may be related to mafic plutonic rocks. The geology of the isolated Chugunov Island, about 60 km northwest of the Bunger Hills, is also described in this section, although it is situated on the eastern side of the Denman Glacier terminus.

Metamorphic rocks

Felsic orthogneiss

Felsic orthogneiss (*Epg*) is the most abundant rock type at Jones Rocks, Cape Charcot, and Cape Gerlache, and also crops out at Hippo Island. It is commonly layered and ranges in composition from tonalite to granite.

Tonalitic gneiss predominates at Capes Charcot and Gerlache and contains orthopyroxene (5–7%), clinopyroxene (up to 7%), quartz (30–35%), oligoclase (50–60%) and minor primary reddish-brown biotite, greenish-brown hornblende, K-feldspar, opaque minerals, apatite and zircon. Orthopyroxene is partly altered to iddingsite or fine-grained biotite and amphibole. Nockolds (1940) reported more potassic orthopyroxene-bearing orthogneiss (with abundant orthoclase microperthite) at Cape Charcot, Hippo Island and Avalanche Cliff, west of Jones Rocks.

Strongly layered, fissile granitic orthogneiss, interlayered with impure quartzite at Jones Rocks, contains dark brown biotite crystals, which define a strong foliation. Much of the biotite, together with less abundant sieve-like aggregates of dark green hornblende (Fig. 132), appears to be secondary. Oligoclase, microcline and quartz are the other major constituents. Similar, strongly foliated biotite-quartz-feldspar gneiss occurs in locally derived rubble at isolated Chugunov Island. Minor orthopyroxene-biotite-quartz-K-feldspar-andesine gneiss is interlayered with garnet gneiss at Mount Borzov (Ravich et al. 1968).

A clinopyroxene-orthopyroxene-quartz-plagioclase gneiss (Table 16) from Cape Charcot belongs to the Y-depleted orthogneiss suite of Sheraton & Black (1983), and has a very similar composition to tonalitic orthogneiss in the Obruchev Hills and much of the Bunger Hills. It has given an ion-microprobe U-Pb zircon age of 3003 ± 8 Ma and apparently underwent at least two periods of metamorphism, at 2889 ± 9 and about 550–600 Ma (Black et al. 1992b).

Mafic rocks

Mafic granulite layers and boudins are interlayered with felsic gneiss at Jones Rocks, Cape Charcot and Hippo Island, and also occur at Chugunov Island. Greenish-brown hornblende and/or reddish-brown biotite are generally major constituents in addition to orthopyroxene, clinopyroxene and labradorite (Nockolds 1940).

Amphibolite (grading into hornblendite) boudins in felsic gneiss at Cape Gerlache contain dark green hornblende and lesser amounts of labradorite, clinopyroxene, brown biotite, magnetite and apatite (Ravich et al. 1968). Garnet amphibolite (with subordinate altered clinopyroxene and, possibly, or-

Table 16. Chemical analyses of felsic gneisses from Denman Glacier area.

Sample no.	*86285893*	*86286001*	*86285885*
Locality	*Cape Charcot*	*Mount Strathcona*	*Jones Rocks*
Lithology	*Cp–Op–Qz–Pl gneiss*	*Gt–Bi–Pl–Kf–Qz gneiss*	*Bi–Pl–Qz–Kf gneiss*
Classif.	*Depleted tonalite*	*Paragneiss*	*Paragneiss*
SiO_2	69.00	72.40	79.20
TiO_2	0.30	0.50	0.30
Al_2O_3	14.04	12.28	10.91
Fe_2O_3	1.01	0.67	0.13
FeO	2.65	3.25	.52
MnO	0.06	0.18	0.01
MgO	2.10	1.38	0.48
CaO	4.10	1.11	0.91
Na_2O	4.34	1.58	2.16
K_2O	1.02	5.19	4.93
P_2O_5	0.05	0.06	0.02
LOI	–	0.70	0.31
Rest	0.21	0.25	0.13
Total	**98.88**	**99.55**	**100.01**
	C.I.P.W. norms		
Q	27.33	36.84	44.99
C	–	2.19	0.41
Or	6.03	30.67	29.13
Ab	36.72	13.37	18.28
An	15.82	5.11	4.38
Di	3.43	–	–
Hy	7.19	8.36	1.56
Mt	1.46	0.97	0.19
Il	0.57	0.95	0.57
Ap	0.12	0.14	0.05
mg	58.5	43.1	62.2
	Trace elements in parts per million		
Ba	586	1191	577
Li	5	–	–
Rb	10	194	158
Sr	522	97	79
Pb	17	32	18
Th	<1	21	4
U	<0.5	1.0	0.5
Zr	175	229	145
Nb	2	9	6
Y	8	41	4
La	12	39	13
Ce	22	84	21
Nd	11	30	7
Sc	12	16	5
V	60	20	37
Cr	78	14	11
Ni	32	5	7
Cu	9	5	2
Zn	51	51	15
Sn	4	3	1
Ga	18	12	13
S	100	100	<100
K/Rb	847	222	259
Rb/Sr	0.019	2.00	2.00
Ce/Y	2.8	2.1	5.3
Th/U	–	21	8
Nb/Nb*	0.10	0.10	0.09
Sr/Sr*	2.46	0.14	0.45

mg = atomic $100Mg/(Mg+Fe^{2+})$.

thopyroxene) forms lenses and layers in granitic gneiss at Possession Rocks and Cape Harrison.

Nockolds (1940) described chlorite-epidote-albite rocks (with minor quartz, biotite and sphene) from Hippo Island, but their relation to other rock types is unknown. Mafic xenoliths ('metadolerite') in quartz diorite and quartz monzodiorite at Mount Strathcona (Ravich et al. 1968) may be related to the mafic plutons (see below). Similar xenoliths occur in granite at Mount Barr-Smith (Nockolds 1940).

Ultramafic rocks

Ultramafic subconcordant layers and boudins are widespread, but constitute only a minor component of the exposed rocks. Pods of orthopyroxene hornblendite at Jones Rocks contain subordinate clinopyroxene, reddish-brown biotite, and olivine (~5% of each). Phlogopite-olivine pyroxenite (websterite) and phlogopite lherzolite are interlayered with felsic gneiss at Cape Gerlache. They consist of pale reddish-brown phlogopite, olivine, clinopyroxene, orthopyroxene and minor pale brown hornblende and opaque minerals. Their texture is granoblastic polygonal. Hornblende pyroxenite and clinopyroxenite crop out at Hippo Island and Cape Charcot, respectively (Nockolds, 1940).

Garnet-quartz-feldspar gneiss

Garnet-bearing gneiss (*Ꝑsg* in part) is abundant only in the south of the area, notably at Mounts Borzov, Gist, and Strathcona. Garnet-biotite-quartz-feldspar gneiss of probable sedimentary origin, interlayered with impure quartzite on the southern side of Mount Strathcona (Table 16), contains various amounts of oligoclase-andesine and K-feldspar, as well as accessory opaque minerals, zircon, and monazite. Mounts Borzov and Gist were not visited in 1986, but according to Ravich et al. (1968) they are predominantly felsic gneiss with garnet (6%), biotite (11%), quartz (22%), and andesine (60%), minor magnetite, apatite and zircon, and secondary chlorite, sericite and carbonate. Gneiss at Mount Gist commonly has a cataclastic texture.

Metasediments

Rocks clearly of sedimentary origin (*Ꝑsg* in part) are much less abundant than in the Bunger Hills. However, impure quartzite crops out at Jones Rocks, Mount Barr-Smith, and Mount Strathcona. At the last two places, assemblages include

- garnet + biotite + plagioclase + quartz,
- muscovite + biotite + plagioclase + quartz,
- biotite + orthopyroxene + plagioclase + quartz, and
- muscovite + biotite + garnet + sillimanite + quartz.

The last was reported by Nockolds (1940).

Aluminous metasediments interlayered with garnet gneiss at Mount Gist comprise sillimanite (3–10%), garnet (up to 14%), biotite (10–12%), andesine (10–12%), K-feldspar (9–20%), quartz (50–55%) and minor opaque minerals (Ravich et al. 1968). Small diopside-rich calc-silicate pods occur at Jones Rocks.

Igneous rocks

Mafic to felsic plutonic rocks

Plutonic rocks form many of the outcrops west of the Denman Glacier. Like those in the Bunger Hills area, they have a wide range of composition — gabbro, diorite, quartz monzodiorite, tonalite, syenite, monzonite and granite. Some of the more felsic intrusions (e.g. granite at Cape Harrison, Possession Rocks and Mount Barr-Smith) are quite strongly deformed, but, since they apparently postdate the high-grade metamorphism, they are described in this section.

Gabbro and diorite of Cape Kennedy and Delay Point.

Both Cape Kennedy and Delay Point are largely gabbro or diorite. Intrusives at Cape Kennedy (*?Ꝑgb*) contain clinopyroxene (~1%), reddish-brown biotite (3%), orthopyroxene (16–18%) and sodic labradorite (80%), minor greenish-brown hornblende, quartz, apatite and opaque minerals, and secondary carbonate (Fig. 87). Much of the biotite forms overgrowths that partly replace orthopyroxene, but otherwise the latter is fresh. According to Streckeisen (1976), the presence of abundant orthopyroxene and relatively calcic plagioclase (>An_{50}) means that these rocks should be classified as leuconorite.

In contrast, intrusives at Delay Point (*?Ꝑgd*) have slightly more sodic plagioclase (~An_{48}), abundant biotite and hornblende, and only subordinate orthopyroxene (Fig. 88). Hence, they are termed diorite on the basis of the Streckeisen (1976) classification. The Delay Point diorite comprises reddish-brown biotite (8–9%), clinopyroxene (6–9%), brownish-green hornblende (2–10%), slightly zoned calcic andesine (65–78%) and minor orthopyroxene, opaque minerals, apatite, zircon and allanite. Clinopyroxene is partly replaced by pale green amphibole and orthopyroxene by iddingsite. Hornblende forms sieve-like aggregates or rims around clinopyroxene, also suggesting replacement of the latter, and allanite inclusions have pleochroic haloes. Texture is hypidiomorphic to allotriomorphic granular or intergranular. Myrmekitic intergrowths are common.

A quartz diorite dyke at Delay Point is finer grained and slightly porphyritic, with zoned andesine antiperthite phenocrysts. It contains more quartz and opaque minerals, whereas clinopyroxene is absent, although hornblende forms poikilitic

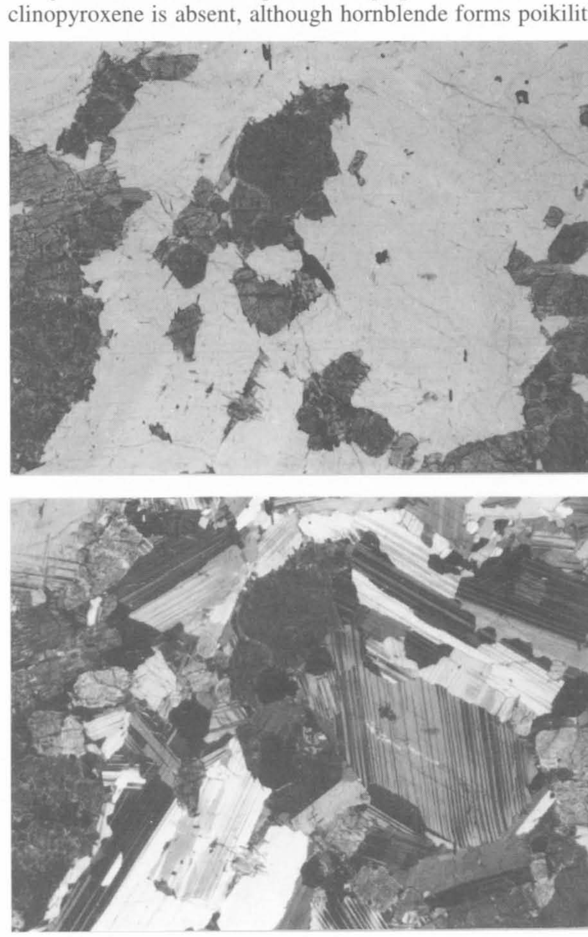

Figure 87. Leuconorite, showing orthopyroxexe with overgrowths of biotite, and intergranular texture; Cape Kennedy. Sample 86286030; cross-polarised light in lower photo; width of field 11mm.

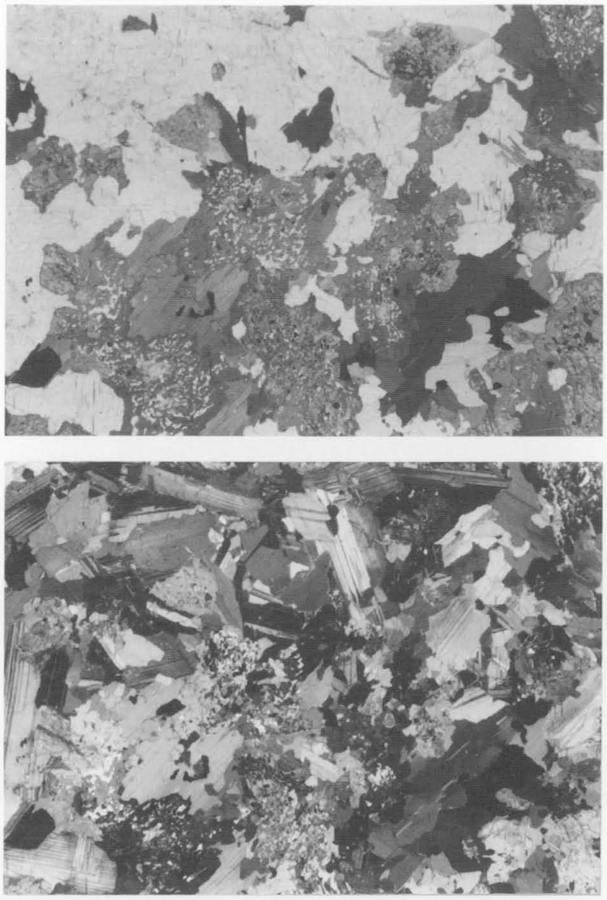

Figure 88. Biotite-hornblende quartz diorite, with pale greenish-brown hornblende rimming clinopyroxene and forming sieve-like aggregates with quartz, also probably after clinopyroxene; Delay Point. Sample 86285889; cross-polarised light in lower photo; width of field: 8mm.

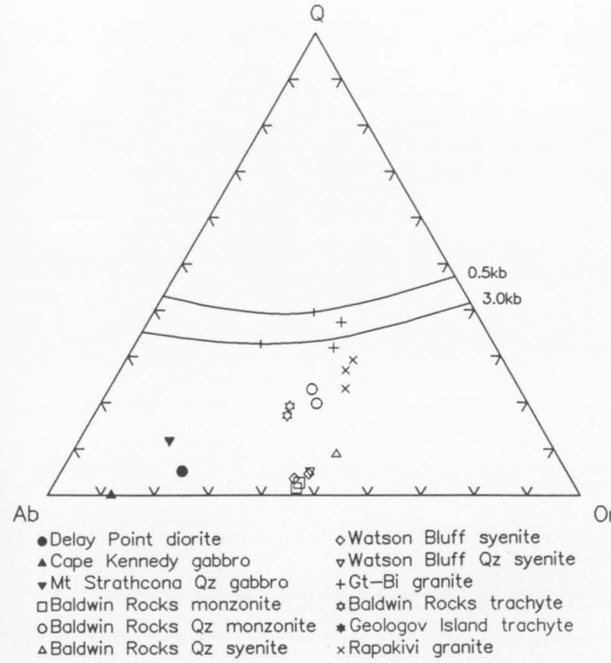

Figure 89. Normative Q-Ab-Or diagram for plutonic rocks from the Denman Glacier area, trachyte dykes, and rapakivi granites. Quartz-feldspar field boundaries after Tuttle & Bowen (1958).

grains and aggregates. A petrographically similar, but partly recrystallised, rock (termed metadolerite) of unknown field relations from Hippo Island (Nockolds 1940) may belong to the same intrusive suite.

Both the gabbro and diorite are marginally SiO_2-saturated (slightly Ol or Q-normative), although the former has higher *mg* (65–66) as well as higher SiO_2, and both are strongly Hy-normative, but relatively low in normative Di (Table 17, Figs 89, 90). In contrast to the Bunger Hills gabbroic rocks, an AFM plot suggests calc-alkaline, rather than tholeiitic, affinities (Fig. 91). The diorite is more strongly enriched in incompatible elements (particularly Ba, Sr, Zr, and LREE), but both intrusives were apparently derived from enriched mantle source regions. Both have a negative Nb anomaly, but the gabbro is unusual in having a marked positive Sr anomaly (Fig. 92) and is probably a plagioclase-rich cumulate. Hence, the gabbro and diorite apparently represent two genetically distinct magma types, neither of which is related to the Bunger Hills gabbroic rocks.

Quartz gabbro and monzodiorite of Mount Strathcona.

Much of Mount Strathcona is quartz gabbro and quartz monzodiorite (*?Ꝑgm*). Quartz gabbro from the large nunatak north of the summit resembles the Delay Point diorite, and consists of reddish-brown biotite (3%), green hornblende (20%), quartz (10%), sodic labradorite (65%), opaque minerals (2%) and minor apatite and zircon. Sieve-like aggregates of hornblende and quartz have probably replaced pyroxene. The texture is essentially allotriomorphic granular, but the rock is slightly deformed, showing strained quartz and minor recrystallisation.

According to Ravich et al. (1968), the eastern nunatak consists of clinopyroxene-biotite-orthopyroxene quartz monzodiorite, which contains lenticular xenoliths of metadolerite. The xenoliths consist mainly of clinopyroxene, orthopyroxene, biotite, and andesine-labradorite, but become more biotite and quartz-rich near their margins. Similar 'metadolerite' xenoliths in biotite granite at Mount Barr-Smith have relict igneous textures, but are largely recrystallised (Nockolds 1940). Most of the pyroxene is replaced by green hornblende, although some clinopyroxene and minor orthopyroxene survive.

On the basis of a single analysis, the Mount Strathcona quartz gabbro is significantly more evolved than the Delay Point and Cape Kennedy intrusives, having low *mg* (35), Cr, and Ni, although, conversely, SiO_2 is also lower (Table 17). In contrast to these other rocks, the AFM plot suggests a tholeiitic affinity (Fig. 91). Abundances of most incompatible elements (LILE, LREE and Zr) suggest derivation from a similarly enriched source to that of the Bunger Hills gabbroic rocks, but P, Ti and, particularly, Nb are considerably more enriched and there is no Nb anomaly (Fig. 92).

Tonalite of Mount Astronomicheskaya and Mount Gist.

Mount Astronomicheskaya, Mount Garan and part of Mount Gist consist of coarsely porphyritic, foliated biotite tonalite (*Ꝑgt*). It was not examined in 1986, but, according to Ravich et al. (1968), it comprises garnet (2%), orthopyroxene (3%), biotite (19%), quartz (35%), andesine (An_{40-45}: 40%) and minor magnetite, zircon and apatite. Plagioclase phenocrysts up to 10cm long make up about 15–20 per cent of the rock and their marked preferred orientation defines a foliation parallel to that of the enclosing paragneiss. Locally, up to 20 per cent orthoclase microperthite and 7 per cent garnet are present, and the tonalite grades into granodiorite or granite.

Table 17. Chemical analyses of plutonic rocks from Denman Glacier area.

Sample no.	*86286031*	*86285888*	*86285793*	*86286006*	*86286013*	*1172**
Locality	*Cape Kennedy*	*Delay Point*	*Mount Strathcona*	*Cape Harrison*	*Possession Rocks*	*Mount Gist*
Lithology	*Op leuco–gabbro*	*Hb–Cp–Bi diorite*	*Bi–Hb quartz gabbro*	*Gt–Pl–Qz–Kf granite gneiss*	*Gt–Bi–Qz–Pl–Kf gran-ite gneiss*	*Gt–Bi–Pl–Qz grano–diorite gn*
SiO_2	52.00	50.20	49.20	71.30	68.60	65.79
TiO_2	0.90	1.87	3.13	0.39	0.55	0.94
Al_2O_3	18.47	17.42	16.97	13.83	15.33	14.29
Fe_2O_3	1.39	2.64	2.99	0.49	0.63	1.46
FeO	6.64	5.77	10.28	2.71	2.43	5.30
MnO	0.12	0.12	0.21	0.08	0.03	0.26
MgO	7.08	4.30	3.10	0.29	0.68	1.52
CaO	7.72	8.68	8.76	2.15	2.40	3.48
Na_2O	3.32	3.41	2.79	2.55	2.87	2.31
K_2O	0.69	1.52	0.94	5.06	5.09	3.60
P_2O_5	0.14	1.25	0.40	0.14	0.17	0.28
LOI	1.57	2.31	1.29	0.26	0.58	0.79
Rest	0.34	0.84	0.28	0.37	0.29	–
Total	**100.38**	**100.33**	**100.34**	**99.62**	**99.65**	**100.19**
O=F,S	0.04	0.12	0.03	0.00	0.00	
Total	**100.34**	**100.21**	**100.31**	**99.62**	**99.65**	
	C.I.P.W. norms					
Q	–	2.09	3.94	30.60	25.34	26.42
C	–	–	–	0.58	1.14	0.94
Or	4.08	8.98	5.55	29.90	30.08	21.27
Ab	28.09	28.85	23.61	21.58	24.29	19.55
An	33.46	27.74	31.00	9.75	10.80	15.43
Di	3.19	5.80	8.26	–	–	–
Hy	24.93	13.44	15.20	4.80	4.78	11.24
Ol	0.66	–	–	–	–	–
Mt	2.02	3.83	4.33	0.71	0.91	2.12
Il	1.71	3.55	5.94	0.74	1.04	1.78
Ap	0.33	2.96	0.95	0.33	0.40	0.66
mg	65.5	57.0	35.0	16.0	33.3	33.8
	Trace elements in parts per million					
Ba	556	1947	463	1300	1090	
Rb	10	41	15	158	211	
Sr	876	1580	385	163	168	
Pb	7	28	7	62	40	
Th	1	9	1	66	47	
U	1.0	1.0	<0.5	1.0	1.5	
Zr	47	201	93	343	268	
Nb	4	18	18	17	13	
Y	8	35	21	102	30	
La	17	128	15	217	102	
Ce	32	266	33	407	253	
Nd	13	105	17	206	88	
Sc	19	24	36	16	8	
V	90	181	362	6	25	
Cr	145	39	5	<2	10	
Ni	80	32	8	<2	2	
Cu	18	25	19	4	7	
Zn	78	105	120	35	73	
Sn	<1	<1	<1	<1	<1	
Ga	19	22	22	20	22	
S	900	1100	600	<100	<100	
F	–	1600	–	–	–	
K/Rb	573	308	520	266	200	
Rb/Sr	0.011	0.026	0.039	0.97	1.26	
Ce/Y	4.0	7.6	1.6	4.0	8.4	
Th/U	1	9	>2	66	31	
K/Zr	122	63	84	122	158	
P/Zr	13	27	19	1.8	2.8	
Nb/Zr	0.09	0.09	0.19	0.050	0.049	
Nb/Nb*	0.23	0.21	0.92	0.10	0.11	
Sr/Sr*	3.07	0.67	1.20	0.04	0.08	

mg = atomic $100Mg/(Mg+Fe^{2+})$. * From Ravich et al. (1968).

There is a range of xenoliths, including garnet and sillimanite-bearing paragneiss (with fine-grained aggregates of spinel and corundum) like that of Mount Gist and Mount Borzov, as well as mafic granulite (amphibole-clinopyroxene-biotite-orthopyroxene- plagioclase) and biotite-orthopyroxene-quartz-feldspar gneiss.

South of Mount Astronomicheskaya (at Mount Garan?), the tonalite is interlayered with orthopyroxene-biotite-hornblende-plagioclase-quartz gneiss and biotite-diopside-plagioclase gneiss. Near contacts with the tonalite, the gneiss contains concordant veins of massive biotite leucotonalite.

Samples analysed by Ravich et al. (1968) have granodioritic bulk compositions (Table 17) and are markedly C-normative, consistent with partial melting of sedimentary precursors (i.e. S-type granitoids of Chappell & White 1974).

Granite of Cape Harrison, Possession Rocks and Mount Barr-Smith. Cape Harrison and Possession Rocks consist of massive foliated garnet-biotite granite (*Ꝑgg*) with subconformable layers of garnet aplite. It comprises garnet (1–4%), quartz (30–35%), sodic andesine (15–25%), perthite (35–45%) and minor opaque minerals, apatite and zircon. That at Cape Harrison also contains minor altered pyroxene and dark greenish-brown hornblende, whereas several percent of dark reddish-brown biotite is present in the Possession Rocks granite. Plagioclase is commonly sericitised and small amounts of secondary biotite, chlorite and iddingsite are present. There is a marked foliation, ranging from lenticular quartz aggregates (flaser structure) in the most deformed rocks to a weak preferred orientation of biotite in the least deformed.

Similar strongly deformed granite (augen gneiss), interlayered with impure quartzite on the southeastern outcrop of Mount Barr-Smith, has been extensively recrystallised. It contains about 4 per cent of reddish-brown biotite, but only minor garnet (Fig. 131). Nockolds (1940) noted that biotite granite around the summit area of Mount Barr-Smith contains mafic xenoliths (metadolerite) with relict igneous textures and reported quartz-tourmaline rocks on the southeastern spur.

Granite samples from Cape Harrison and Possession Rocks are chemically similar, and have compositions not far removed from minimum melts (Table 17, Figs 89, 90). They are C-normative and, like the tonalite described above, may be S-type. Spidergrams are markedly irregular (Fig. 93) and typical of partial melts of felsic crustal rocks (Tarney et al. 1987; Sheraton & Black 1988), although Th/U is unusually high.

Granite from Cape Harrison has given preliminary U-Pb zircon ion microprobe ages of about 1000 (presumably emplacement) and 500 Ma (L.P. Black, unpublished data).

Syenitic rocks of David Island. All the outcrops examined on David Island are relatively coarse-grained, commonly porphyritic, intrusives (*Ꞓg*), ranging in composition from syenite to quartz monzonite and granite. Although poorly exposed, the batholith therefore extends over at least 120 km^2.

Watson Bluff and nearby nunataks are syenite and quartz syenite, containing iron-rich orthopyroxene ($Ca_2Mg_{15}Fe_{83}$: 1–2%), iron-rich augite

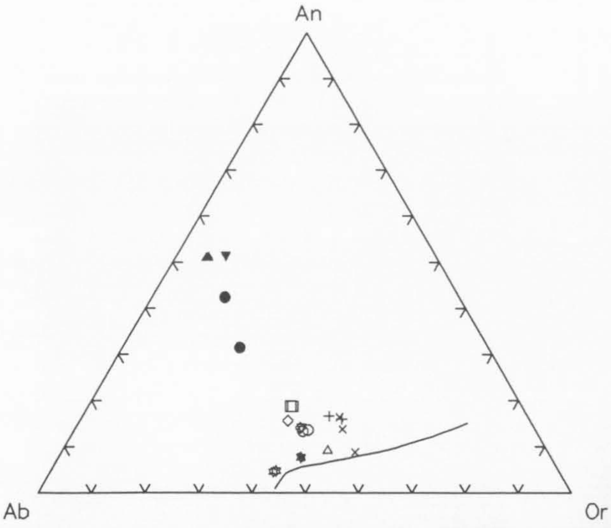

Figure 90. Normative Ab-Or-An diagram for plutonic rocks from the Denman Glacier area, trachyte dykes, and rapakivi granites. Plagioclase-alkali feldspar field boundary after James & Hamilton (1969). Symbols as in Figure 89.

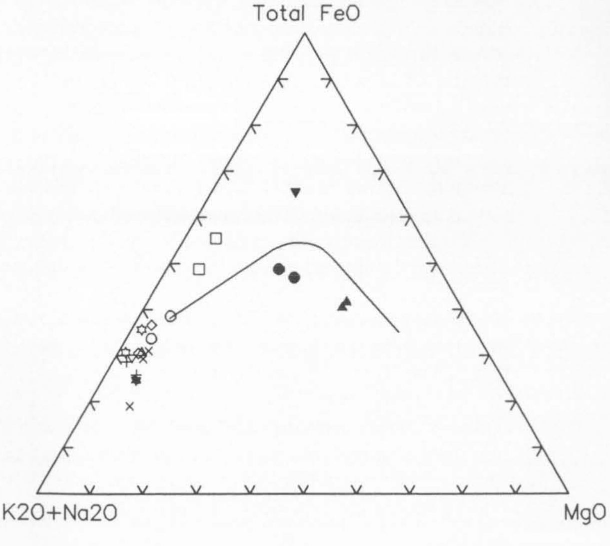

Figure 91. A-F-M diagram for plutonic rocks from the Denman Glacier area, trachyte dykes, and rapakivi granites. Boundary between tholeiitic and calc-alkaline fields after Irvine & Baragar (1971). Symbols as in Figure 89.

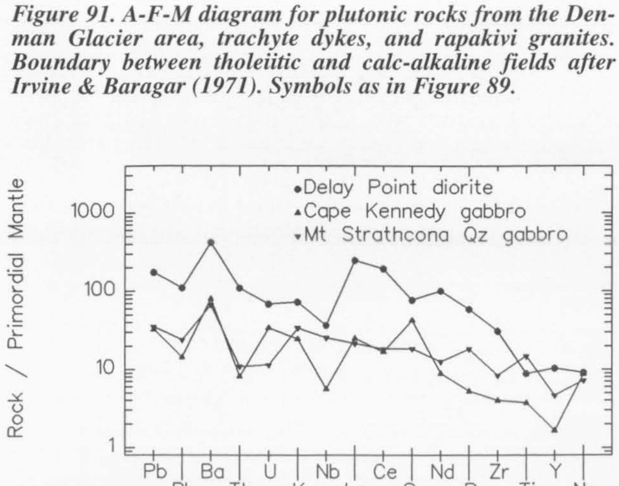

Figure 92. Spidergrams for average mafic plutonic rocks from the Denman Glacier area.

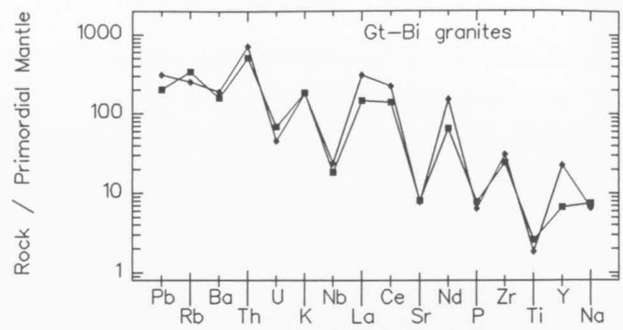

Figure 93. Spidergrams for garnet-biotite granites from Cape Harrison (diamond symbols) and Possession Rocks.

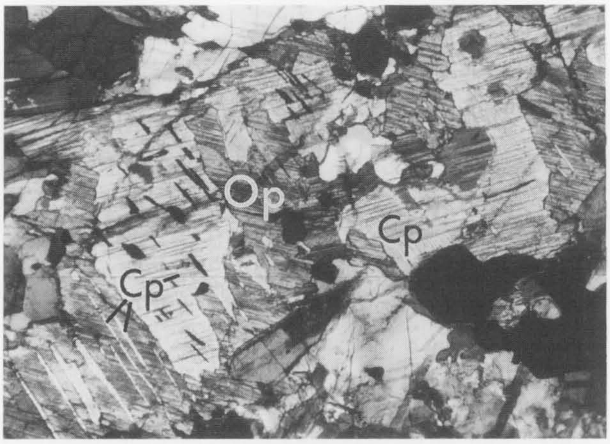

Figure 94. Exsolution of orthopyroxene from clinopyroxene and vice versa in orthopyroxene-clinopyroxene monzonite; Baldwin Rocks. Sample 86286015; cross-polarised light; width of field: 2.2mm.

($Ca_{43}Mg_{12}Fe_{45}$: up to 2%), dark greenish-brown hastingsitic hornblende (2–4%), quartz (4–12%), plagioclase (An_{20-30}, with albite rims: 15–20%) and perthite (60–70%), and minor dark brown biotite, ilmenite, apatite, zircon, yellowish-brown metamict allanite and dark reddish-brown metamict chevkinite or perrierite. Accessory minerals are unusually abundant; metamict allanite is commonly intergrown with opaque minerals, and chevkinite grains in hornblende have pleochroic haloes. The texture is allotriomorphic granular, medium to coarse grained (0.5–5 mm), and commonly porphyritic with coarsely perthitic orthoclase or microcline phenocrysts up to 20 mm long. Locally, there has been considerable cataclastic deformation (Ravich et al. 1968).

Monzonite, the predominant rock type at Baldwin Rocks, is petrographically similar to the syenite, except that orthopyroxene and clinopyroxene (3–5% each) and plagioclase (An_{20-30}: ~40%) are more abundant, whereas quartz (2–3%) and perthite (~45%) are less so. Up to two per cent of fayalite (Fo_6) is also present. As in the syenite, accessory minerals are unusually abundant, and include euhedral zircon and apatite grains up to 1mm long. Clinopyroxene and orthopyroxene show exsolution textures, including both thin lamellae and coarser lamellae and blebs (Fig. 94). Some grains have compositions suggesting inversion of original iron-rich pigeonite ($Ca_6Mg_{16}Fe_{78}$ - $Ca_{11}Mg_{17}Fe_{72}$) (Table 18). Greenish-brown hornblende commonly rims pyroxene, which is slightly altered to pale green or colourless amphibole.

Pink, porphyritic biotite-hornblende quartz monzonite (grading into quartz syenite and granite) crops out on the west side of David Island. Dark greenish-brown hornblende (2–8%) and dark brown biotite (3–5%) are the main mafic

Table 18. Representative analyses of minerals from David Island batholith.

	Baldwin Rocks Monzonite (86286015)					Watson Bluff Syenite (86286024)		
	Op	*Pig*	*Cp*	*Ol*	*Bi*	*Op*	*Cp*	*Hb**
SiO_2	48.19	48.65	50.07	30.35	34.09	47.29	49.24	40.08
TiO_2	0.10	0.12	0.15	0.02	4.66	0.12	0.14	2.05
Al_2O_3	0.00	0.40	0.73	0.00	13.29	0.25	0.67	9.62
FeO^+	44.74	41.09	23.63	66.14	30.54	44.60	25.56	28.59
MnO	0.97	0.96	0.48	1.29	0.17	1.33	0.67	0.37
MgO	5.73	5.35	4.96	2.28	3.58	4.52	3.99	2.92
CaO	0.79	4.38	19.96	0.04	0.03	1.06	19.25	10.34
Na_2O	0.00	0.04	0.33	0.00	0.04	0.02	0.35	1.76
K_2O	0.00	0.00	0.00	0.00	8.88	0.00	0.00	1.30
Cr_2O_3	0.00	0.00	0.00	0.00	0.00	0.00	0.00	0.00
BaO	–	–	–	–	0.43	–	–	–
F	–	–	–	–	0.00	–	–	–
Cl	–	–	–	–	0.01	–	–	–
Total	**100.52**	**100.99**	**100.31**	**100.12**	**95.72**	**99.19**	**99.87**	**97.03**
O	6	6	6	4	22	6	6	23
Si	2.006	1.998	1.991	1.007	5.530	2.005	1.986	6.390
Al^{iv}	–	0.002	0.009	–	2.470	0.000	0.014	1.610
Al^{vi}	0.000	0.017	0.025	0.000	0.071	0.012	0.018	0.198
Ti	0.003	0.004	0.004	0.000	0.568	0.004	0.004	0.246
Fe^3	–	–	–	–	–	–	–	0.579
Fe^2	1.557	1.412	0.786	1.835	4.143	1.581	0.862	3.233
Mn	0.034	0.033	0.016	0.036	0.023	0.048	0.023	0.050
Mg	0.356	0.328	0.294	0.113	0.866	0.286	0.240	0.694
Ca	0.035	0.193	0.850	0.001	0.005	0.048	0.832	1.766
Na	0.000	0.003	0.025	0.000	0.013	0.002	0.027	0.544
K	0.000	0.000	0.000	0.000	1.837	0.000	0.000	0.264
Cr	0.000	0.000	0.000	0.000	0.000	0.000	0.000	0.000
Ba	–	–	–	–	0.027	–	–	–
F	–	–	–	–	0.000	–	–	–
Cl	–	–	–	–	0.003	–	–	–
Total	**3.991**	**3.990**	**4.001**	**2.993**	**15.556**	**3.986**	**4.006**	**15.575**
mg	18.6	18.9	27.2	5.8	17.3	15.3	21.8	17.7

+ Total Fe as FeO. mg = atomic 100Mg/(Mg+total Fe), or 100Mg/(Mg+Fe^{2+}) for hornblende.
* Fe^{3+} in hornblende calculated assuming total cations (excluding Ca, Na, and K) = 13.

minerals. There is only a little altered pyroxene, although aggregates of hornblende and quartz in some rocks suggest replacement of original pyroxene. The quartz monzonite also contains quartz (10–25%), plagioclase (sodic oligoclase with albite rims: 15–35%), microcline perthite (35–50%), and minor opaque minerals, apatite, zircon, allanite, sphene and chevkinite or perrierite. K-feldspar phenocrysts are up to 4 cm long. Plagioclase is commonly sericitised, biotite is locally altered to chlorite and there has been minor recrystallisation. Metamict allanite, chevkinite and opaque minerals occur in unusual zoned intergrowths (Fig. 95). Representative analyses of chevkinite/perrierite and allanite are given in Table 19. Chevkinite/perrierite has been found in several other Antarctic intrusive rocks, including granite (Sheraton & Black 1988) and pegmatite (Grew & Manton 1979).

Equilibration temperatures of 825-840°C (Wells 1977) and 790–800°C (Wood & Banno 1973) estimated for the David Island batholith are similar to those (~800–830°C) derived from pigeonite compositions (Fig. 45) and comparable to estimates for intrusions in the Bunger Hills. Pressure estimates, although not very consistent, are all significantly lower than for the Bunger Hills (Table 6). The Johnson & Rutherford (1989) method gives 4.2–4.5 kb (equivalent to about 15 km depth), about 1.5 kb lower than Schmidt (1992), whereas the Ellis (1980) geobarometer gives a negative pressure for one sample (86286015) and a relatively low pressure (1.5kb) for the other (86286024). Inverted pigeonites from monzonite 86286015 plot very close to the boundary of the 'forbidden zone', in which pigeonite is replaced by augite + olivine + quartz (Lindsley 1983), at 5kb (Fig. 45), so that the higher pressures are probably more realistic. It is unlikely that fayalite crystallised at a significantly lower pressure than pigeonite (e.g. during emplacement), because both minerals appear to have crystallised at the same time.

All the syenitic rocks are characterised by high Al_2O_3, Na_2O, LILE, LREE and HFSE, but low FeO, MgO, CaO, Cr, Ni, V, Sc and *mg* values (17–27) (Table 20). Normative Q, Hy and Di tend to be low, but Pl and Or are high; trends on Q-Ab-Or and Ab-Or-An diagrams (Figs 89,90) are quite different

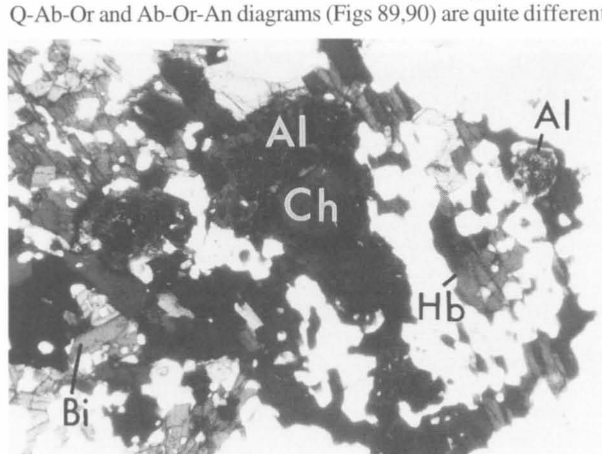

Figure 95. Zoned intergrowths of metamict chevkinite or perrierite (Ch) and allanite (Al), with opaque inclusions, in hornblende-biotite quartz syenite; 5 km southwest of Baldwin Rocks. Sample 86286021; width of field: 3mm.

Table 19. Representative analyses of chevkinite/perrierite and allanite from David Island batholith.

	1	2	3	4	5	6
SiO_2	20.45	19.87	20.34	19.86	30.84	31.11
TiO_2	18.35	18.49	18.30	17.07	1.53	1.88
Al_2O_3	1.50	1.43	1.06	0.07	14.55	14.23
FeO^+	10.39	10.38	10.25	10.06	15.15	16.07
MnO	–	0.01	–	1.01	0.25	0.35
MgO	0.18	0.44	0.44	0.49	0.41	0.38
CaO	2.94	3.43	3.19	3.20	9.81	9.65
UO_2	0.10	0.04	0.28	–	–	–
ThO_2	2.52	2.63	2.22	1.62	0.49	0.86
La_2O_3	11.22	11.11	12.05	23.76	7.33	7.74
Ce_2O_3	21.19	20.57	21.08	19.26	12.33	12.83
Pr_2O_3	2.46	1.59	1.88	2.46	1.15	1.24
Nd_2O_3	5.72	5.95	6.42	2.32	3.13	2.88
Sm_2O_3	0.98	0.16	1.71	–	0.27	–
Eu_2O_3	0.72	0.08	0.91	–	0.14	–
Gd_2O_3	–	–	–	–	0.26	–
Tb_2O_3	–	–	–	0.16	–	–
Er_2O_3	–	–	0.61	–	–	–
Yb_2O_3	–	–	0.41	0.06	0.05	0.18
Total	**98.72**	**96.18**	**101.15**	**101.40**	**97.69**	**99.40**
	Cations per 22 (chevkinite) or 25 (allanite) oxygens					
Si	4.182	4.126	4.131	4.118	6.050	6.035
Ti	2.823	2.887	2.794	2.662	0.225	0.274
Al	0.361	0.351	0.254	0.017	3.366	3.255
Fe	1.777	1.803	1.741	1.744	2.486	2.608
Mn	–	0.001	–	0.177	0.041	0.057
Mg	0.055	0.136	0.133	0.152	0.120	0.110
Ca	0.644	0.764	0.694	0.711	2.062	2.006
U	0.005	0.001	0.012	–	–	–
Th	0.117	0.125	0.103	0.076	0.022	0.038
La	0.847	0.851	0.903	1.817	0.530	0.554
Ce	1.586	1.563	1.567	1.463	0.885	0.912
Pr	0.183	0.120	0.139	0.186	0.083	0.087
Nd	0.418	0.442	0.466	0.172	0.219	0.199
Sm	0.069	0.011	0.120	–	0.018	–
Eu	0.050	0.006	0.063	–	0.009	–
Gd	–	–	–	–	0.017	–
Tb	–	–	–	0.011	–	–
Er	–	–	0.039	–	–	–
Yb	–	–	0.026	0.004	0.004	0.010
Total	**13.117**	**13.187**	**13.185**	**13.310**	**16.137**	**16.145**

+ Total Fe as FeO.

1–3. Chevkinite, syenite, Watson Bluff (86286024).
4. Chevkinite, syenite pegmatite, Bjorkedalen, Norway (Segelstad & Larsen, 1978).
5. Allanite, monzonite, Baldwin Rocks (86286015).
6. Allanite, syenite, Watson Bluff (86286024).

from those of the Bunger Hills plutonic rocks (Figs 48, 49).

Most of these rocks have highly irregular spidergrams showing strong enrichment in most incompatible elements (Fig. 96) and reflecting their highly fractionated nature. Many of their chemical features (e.g. high Nb, Zr and LREE; low *mg*) are characteristic of post-orogenic or anorogenic (A-type) granitoids, which are generally considered to have been derived by partial melting of lower crustal rocks (Collins et al. 1982; Whalen et al. 1987; Sheraton & Black 1988; Rogers & Greenberg 1990; Skjerlie & Johnston 1993). Such rocks have been termed 'within-plate granites' by Pearce et al. (1984).

Irregular spidergrams are typical of partial melts of plagioclase-rich crustal rocks, rather than mafic or ultramafic (i.e. mantle) sources (Tarney et al. 1987). The strong enrichment in many HFSE is explicable in terms of high-temperature partial melting of virtually anhydrous granulite-facies crustal rocks. For example, Zr is relatively soluble in high-temperature melts (Watson & Harrison 1983), although the solubility of P is much higher in peraluminous than metaluminous melts (Bea et al. 1992).

High Th/U (7–44) is also consistent with melting of a granulite-facies source. However, there seems to be no compelling reason to assume a refractory residual source, as suggested for A-type granitoids by Collins et al. (1982), because even the highest grade metamorphic terranes do not have particularly refractory compositions (Sheraton & Black 1988). Creaser et al. (1991) argued that A-type magmas may have been derived by melting of tonalitic to granodioritic source rocks which had not undergone previous melt depletion.

The strong depletion of Ba, Sr, P and Ti, relative to LREE and Zr, shown by the spidergrams suggests fractionation of feldspar (plagioclase and/or K-feldspar), apatite and a Ti oxide phase. Many of the chemical variations within the suite can be explained by fractionation of pyroxene, feldspar and, possibly, hornblende, as well as minor phases, but different degrees of melting were probably also important (Sheraton et al. 1992).

In contrast to most of the syenitic rocks, the two Baldwin Rocks monzonites have much less irregular spidergrams, which closely resemble, apart from higher Ba, those of the Bunger Hills quartz monzogabbro (Figs 52, 96). This suggests that they may have a similar origin, namely, direct partial melting (with subsequent fractionation) of an enriched mantle source. The possibility that the other syenitic rocks represent more strongly fractionated mantle, rather than crustal melts, therefore needs to be assessed.

The two available Sr_i ratios (0.7111 for a monzonite and 0.7122 for syenite: Table 21) are similar to those of the Bunger Hills gabbroic rocks and, like the very low ε_{Nd} (–14.4 and –13.1, respectively), might reflect derivation from a long-enriched mantle source. Many other alkaline (syenitic to granitic) plutonic complexes have chemical and isotopic characteristics that suggest fractionation of mafic magma with or without significant crustal contamination (see various papers in Fitton & Upton 1987; Zhao et al. 1995). Nevertheless, certain chemical features (higher Al_2O_3, Th, U and *mg*; lower P_2O_5 and P/Ce) mean that the more evolved syenitic rocks cannot have been derived by fractionation of a monzonitic parent magma. Hence, the possibility that they are genetically unrelated to the monzonites and were derived by melting of lower crustal rocks, as argued above, or at least include a major crustal component is quite feasible.

Syenite at Watson Bluff has given a conventional U-Pb zircon age of 516±1.5 Ma (Black et al. 1992b) which is broadly comparable to K-Ar ages (460, 470, and 560 Ma) quoted by Ravich et al. (1968).

Felsic dykes and minor intrusions

Dykes and subconcordant layers of granite and pegmatite are widespread, but their age is unknown. White to pink, slightly foliated medium to coarse-grained granite crops out at Jones Rocks, and pink aplite veins at Delay Point and Cape Kennedy. Such intrusives typically contain dark brown or reddish-brown biotite (2–5%), oligoclase (15–25%), quartz (~35%), microcline perthite (40–45%) and minor opaque minerals, apatite, zircon and monazite. Even-grained biotite granite occurs in rubble at Chugunov Island.

Trachyte dykes (syenite porphyry of Ravich et al. 1968) cut monzonite at Baldwin Rocks and consist of anorthoclase (~5%) and rare altered ferromagnesian phenocrysts (possibly pyroxene) in a trachytic groundmass of alkali feldspar, hematite, and minor carbonate and opaque minerals (Fig. 97). A few platy pseudomorphs may be after biotite. Little quartz was noted, but some cryptocrystalline material in the ground-

Table 20. Chemical analyses of syenitic rocks from David Island batholith.

Sample no.	*86286015*	*86286020*	*86286021*	*86286024*	*86286023*	*86286016*
Locality	*Baldwin Rocks*	*Baldwin Rocks W*	*Baldwin Rocks W*	*Watson Bluff*	*Watson Bluff*	*Baldwin Rocks*
Lithology	*Ol–Cp–Op monzonite*	*Hb–Bi quartz monzonite*	*Hb–Bi quartz syenite*	*Op–Cp–Hb syenite*	*Op–Cp–Hb quartz syenite*	*Trachyte dyke*
SiO_2	54.00	63.80	62.20	59.50	60.90	65.20
TiO_2	1.66	0.93	0.78	0.77	0.63	0.22
Al_2O_3	15.70	14.85	16.44	17.43	18.20	15.75
Fe_2O_3	2.20	1.37	1.76	1.50	1.33	3.16
FeO	9.66	4.78	3.44	4.76	3.38	1.73
MnO	0.18	0.09	0.11	0.12	0.09	0.12
MgO	1.25	0.92	0.73	0.56	0.49	0.21
CaO	4.61	2.72	2.17	3.13	2.93	0.72
Na_2O	3.62	3.52	3.92	4.22	4.37	4.79
K_2O	4.52	5.16	6.75	5.80	6.06	5.34
P_2O_5	0.77	0.32	0.16	0.19	0.14	0.02
H_2O^+	–	–	–	–	–	1.24
H_2O^-	–	–	–	–	–	0.41
CO_2	–	–	–	–	–	1.39
LOI	0.93	0.90	0.88	0.65	0.61	–
Rest	0.82	0.51	0.67	0.90	0.81	0.25
Total	**99.92**	**99.87**	**100.01**	**99.53**	**99.94**	**100.55**
O=F,S	0.03	0.01	0.03	0.02	0.00	0.01
Total	**99.89**	**99.86**	**99.98**	**99.51**	**99.94**	**100.54**
	C.I.P.W. norms					
Q	0.92	14.84	7.08	3.42	4.07	14.91
C	–	–	–	–	–	0.83
Or	26.71	30.49	39.89	34.27	35.81	31.56
Ab	30.63	29.79	33.17	35.71	36.98	40.53
An	13.24	9.48	7.33	11.49	12.15	3.44
Di	3.98	1.64	2.03	2.43	1.27	–
Hy	14.57	7.73	4.57	6.59	4.80	0.95
Mt	3.19	1.99	2.55	2.17	1.93	4.58
Il	3.15	1.77	1.48	1.46	1.20	0.42
Ap	1.82	0.76	0.38	0.45	0.33	0.05
mg	18.7	25.5	27.4	17.3	20.5	17.8
	Trace elements in parts per million					
Ba	4530	1908	1611	3010	3400	290
Rb	71	162	180	104	109	141
Sr	607	309	289	516	568	52
Pb	26	53	52	56	59	15
Th	2.80	38.7	96	108	76	30
U	0.77	4.16	3.5	2.30	2.5	2.5
Zr	601	806	1030	1082	969	541
Nb	34	51	30	48	38	132
Y	45	56	34	52	38	43
La	91.4	152	518	736	417	143
Ce	184	291	894	1020	747	230
Nd	88.0	126	284	408	249	83
Sm	15.8	20.8	–	46.8	–	–
Eu	7.66	3.86	–	5.76	–	–
Tb	1.72	2.21	–	3.39	–	–
Yb	3.28	4.39	–	3.85	–	–
Lu	0.55	0.74	–	0.61	–	–
Sc	26	13	19	12	12	2
V	<2	32	7	6	5	<2
Cr	<2	<2	<2	<2	<2	<2
Ni	<2	<2	<2	<2	<2	<2
Cu	10	6	2	4	3	6
Zn	137	110	70	121	89	73
Sn	<1	2	<1	<1	<1	–
Ga	25	25	19	25	24	20
S	700	200	200	100	100	145
F	–	–	400	300	–	–
K/Rb	528	264	311	463	462	314
Rb/Sr	0.117	0.52	0.62	0.202	0.192	2.7
Ce/Y	4.2	5.5	26	19	20	5.4
Th/U	3.6	9.3	27	47	30	12
K/Zr	62	53	54	45	52	82
P/Zr	5.6	1.7	0.68	0.77	0.63	0.16
Nb/Zr	0.057	0.063	0.029	0.044	0.039	0.24
Nb/Nb*	0.33	0.36	0.09	0.11	0.13	0.94
Sr/Sr*	0.34	0.11	0.04	0.06	0.09	0.03

mg = atomic $100Mg/(Mg+Fe^{2+})$.

Table 21. Sr and Nd isotopic data for rocks from Denman Glacier area.

Sample	*Rock type*	*Locality*	$^{87}Sr/^{86}Sr(T)$*	T^{Nd}_{DM}	$\varepsilon_{Nd}(T)$*
86285893	Tonalitic orthogneiss	Cape Charcot		3730**	-29.7
86286001	Gt-Bi paragneiss	Mount Strathcona	0.82352	2280	-17.7
86285890	Diorite dyke	Delay Point	0.71090	1750	-14.1
86286006	Gt granite	Cape Harrison	0.73040	1660	-8.1
86286015	Monzonite	Baldwin Rocks	0.71113	2010	14.4
86286024	Syenite	Watson Bluff	0.71221	1600	-13.9

* Calculated at the emplacement age for the syenitic intrusives (515Ma).

The following parameters were used for model age calculations:
$(^{147}Sm/^{144}Nd)_{DM}$ = 0.225 (**0.214), $(^{143}Nd/^{144}Nd)_{DM}$ = 0.51317

mass may be silica. Ravich et al. (1968) reported a K-Ar age of 330 Ma, possibly that of emplacement, for these dykes. Chemically, the trachytes bear some resemblance to the syenitic rocks, but are even more fractionated (lower TiO_2, MgO, CaO, P_2O_5, Ba, Sr and Sc) and slightly C-normative (Table 20, Figs 89–91). Spidergrams are highly irregular, but differ from those of the syenitic rocks in showing marked Ba depletion, which suggests extensive fractionation of K-feldspar, and in having no Nb anomalies (Fig. 98). There are also significant differences from the Geologov Island trachyte (see above), which is SiO_2-undersaturated (Ne and Ol-normative) and shows extreme enrichment in most incompatible elements except Ba (Fig. 98).

Mafic dykes

Mafic dykes are rare west of the Denman Glacier, but a few in the Delay Point-David Island area may be related to the gabbros and diorites of Cape Kennedy and Delay Point. One such dyke (quartz diorite) from Delay Point has already been described and a thin dyke (10 cm), petrographically similar, but finer grained and more melanocratic, intrudes quartz syenite at Baldwin Rocks on western David Island. It consists of clinopyroxene + minor orthopyroxene (5%), well-crystallised reddish-brown biotite (13%), poikilitic greenish-brown hornblende (25%), andesine (54%), opaque minerals (3%) and minor apatite, and contains a few strongly zoned plagioclase phenocrysts. In contrast, a mafic dyke at Cape Kennedy has, like the country rocks, an almost anhydrous assemblage-clinopyroxene (15%), orthopyroxene (15%), calcic andesine (62%), opaque minerals (7%) and minor apatite and reddish-brown biotite. Its texture is granoblastic, but there are a few plagioclase phenocrysts and irregular mafic schlieren of clinopyroxene and subordinate orthopyroxene.

Both these dykes were apparently emplaced at considerable depths in the crust, probably soon after the associated plutonic rocks. The Baldwin Rocks dyke appears to be alkaline (Table 22, Figs 99, 100), although this may reflect addition of alkalies during metamorphism (with crystallisation of hornblende and biotite), as most incompatible element contents (and *mg** value) are similar to those of the Hy-normative Cape Kennedy dyke.

Two dykes, one metre thick, at Cape Charcot have allotriomorphic granular to granoblastic inequigranular fabrics, which possibly represent much-recrystallised relict igneous textures. They contain clinopyroxene (10%), orthopyroxene (10%), reddish-brown biotite (~14%), greenish-brown hornblende (15–20%), calcic andesine (45–50%) and minor opaque minerals, apatite and carbonate. In terms of chemical composition, they are slightly Ne-normative alkali basalts or gabbros. They are much less evolved (high *mg**, Cr and Ni) and have higher Ba and Sr than the dykes described above (Table 22, Figs 99, 100). However, like most mafic intrusions in the Denman Glacier area, they have negative Nb anomalies and unusually high Ba/Rb (Fig. 101), suggesting an origin from generally similar enriched mantle source regions.

Figure 97. Trachyte dyke, with anorthoclase phenocrysts in a trachytic groundmass of alkali feldspar, hematite, and minor carbonate and opaque minerals; Baldwin Rocks. Sample 86286016; width of field: 3.6mm.

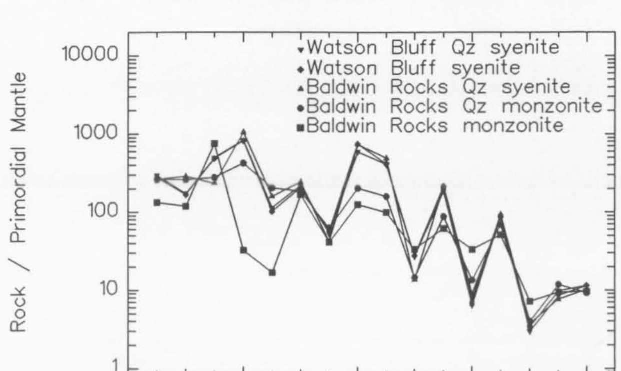

Figure 96. Spidergrams for average David Island plutonic rocks.

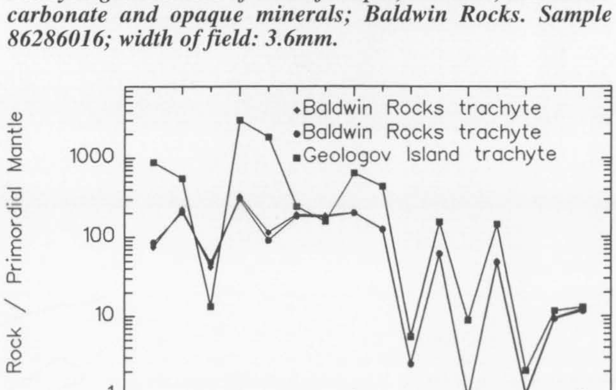

Figure 98. Spidergrams for trachyte dykes from Geologov Island and Baldwin Rocks.

Table 22. Chemical analyses of mafic dykes from Denman Glacier area, and metabasalt from moraines.

Sample no.	86286022	86286029	86285892	86286236	86286028	86286010
Locality	SW Baldwin Rocks	Cape Kennedy	Cape Charcot	Moraine (5km S of Dobrowol.)	Moraine (Cape Jones)	Moraine (Cape Jones N)
Lithology	Px–Bi–Hb–Pl granulite	Cp–Op–Pl granulite	Alkali gabbro	Metabasalt	Metabasalt	Metabasalt
SiO_2	47.40	49.30	46.90	45.70	48.80	48.70
TiO_2	2.83	2.50	1.70	3.44	2.42	2.13
Al_2O_3	16.27	15.58	14.48	14.65	13.74	13.68
Fe_2O_3	1.82	5.06	2.01	4.39	5.05	5.64
FeO	9.72	7.73	7.89	10.00	8.69	7.34
MnO	0.15	0.18	0.16	0.22	0.21	0.19
MgO	5.35	5.05	8.79	5.37	5.60	6.24
CaO	7.91	8.02	8.88	7.81	6.27	9.72
Na_2O	4.16	3.22	2.58	3.30	2.24	1.39
K_2O	1.47	0.90	2.31	1.16	3.92	0.74
P_2O_5	1.08	0.74	0.61	0.68	0.24	0.19
H_2O^+	–	–	1.08	2.55	2.30	2.88
H_2O^-	–	–	0.23	0.13	0.03	0.10
CO_2	–	–	1.23	0.22	0.15	0.65
LOI	1.69	1.38	–	–	–	–
Rest	0.42	0.54	0.90	0.31	0.40	0.31
Total	**100.27**	**100.20**	**99.75**	**99.93**	**100.06**	**99.90**
O=S,Cl	0.04	0.07	0.07	0.03	0.09	0.05
Total	**100.23**	**100.13**	**99.68**	**99.90**	**99.97**	**99.85**
	C.I.P.W. norms					
Q	–	0.33	–	–	–	5.50
Or	8.69	5.32	13.65	6.85	23.16	4.37
Ab	31.22	27.25	18.95	27.92	18.95	11.76
An	21.38	25.40	21.11	21.74	15.86	28.90
Ne	2.16	–	1.56	–	–	–
Di	8.90	7.93	15.36	10.43	11.35	14.92
Hy	–	22.32	–	4.91	7.06	22.65
Ol	15.20	–	18.63	13.18	12.15	–
Mt	2.75	2.97	2.34	3.37	3.20	3.00
Il	5.37	4.75	3.23	6.53	4.60	4.04
Ap	2.56	1.75	1.44	1.61	0.57	0.45
mg	49.7	46.3	65.5	44.7	47.0	51.3
	Trace elements in parts per million					
Ba	963	1485	3320	538	269	128
Rb	30	12	53	38	56	26
Sr	605	816	1146	262	241	313
Pb	14	14	43	8	6	9
Th	5	3	12	3	3	1
U	1.0	0.5	1.5	0.5	0.5	<0.5
Zr	297	153	225	240	172	139
Nb	24	21	24	10	12	9
Y	37	36	31	46	39	31
La	99	64	90	21	24	15
Ce	150	123	170	55	52	34
Nd	75	64	78	34	27	18
Sc	27	20	24	30	39	42
V	185	170	216	260	336	350
Cr	37	21	366	74	65	130
Ni	53	38	155	54	20	36
Cu	12	28	57	34	40	72
Zn	125	127	84	123	114	107
Ga	18	20	15	19	22	19
As	<0.5	<0.5	<0.5	<0.5	2.5	<0.5
S	800	1400	1140	700	1900	1100
Cl	–	155	570	–	–	–
K/Rb	407	623	362	253	581	236
Rb/Sr	0.050	0.015	0.046	0.145	0.232	0.083
Ce/Y	4.1	3.4	5.5	1.2	1.3	1.1
K/Zr	41	49	85	40	189	44
P/Zr	16	21	12	12	6.1	6.0
Nb/Zr	0.081	0.14	0.11	0.042	0.070	0.065
Nb/Nb*	0.35	0.48	0.32	0.39	0.19	0.53
Sr/Sr*	0.42	0.68	0.72	0.45	0.47	0.93

mg = atomic 100Mg/(Mg+0.85Fe(total))

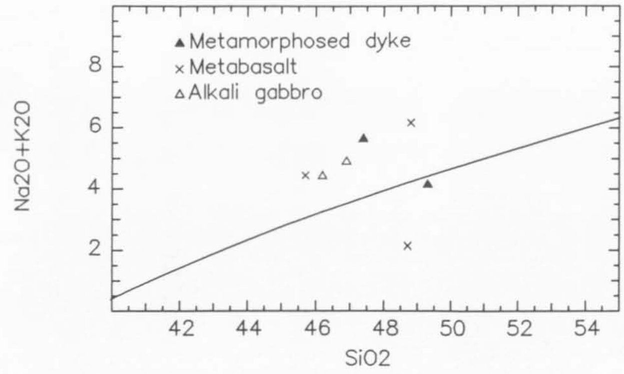

Figure 99. Alkalies-SiO_2 plot for mafic dykes from the Denman Glacier area and metabasalts. Boundary between alkaline and subalkaline fields after Irvine & Baragar (1971).

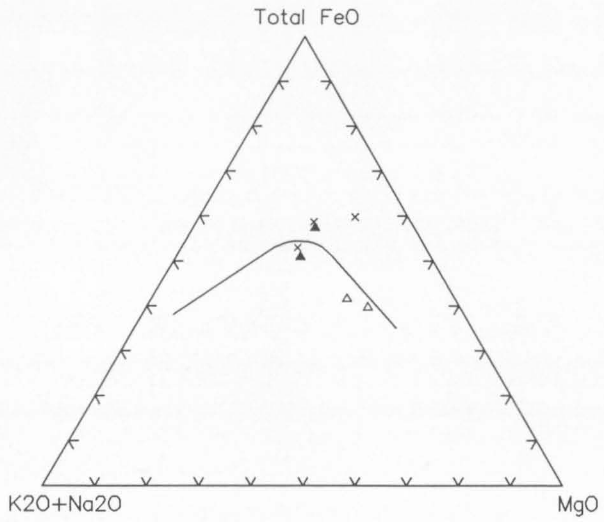

Figure 100. A–F–M diagram for mafic dykes from the Denman Glacier area and metabasalts. Boundary between tholeiitic and calc-alkaline (plus alkaline) fields after Irvine & Baragar (1971). Symbols as in Figure 99.

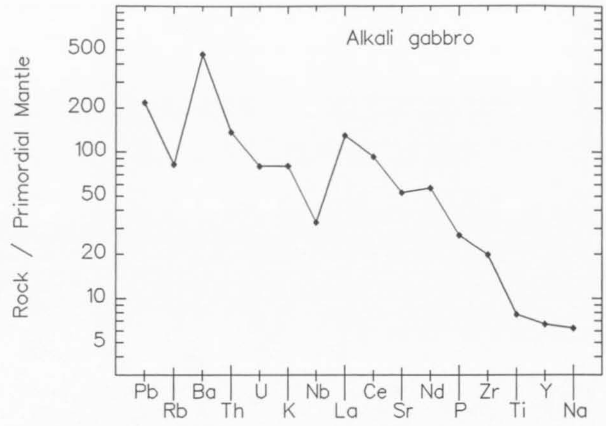

Figure 101. Spidergram for average alkali gabbro dyke from Cape Charcot.

Mount Amundsen and Mount Sandow

These small and isolated nunataks, about 110 km south of the Bunger Hills, were only examined from the air in 1986, as strong winds prevented helicopter landings. However, the rocks have been described in detail by Ravich et al. (1968), who assigned them to the Sandow Group (*NP–Ɛss*). Sandstone and metabasalt, presumed to be related, are quite abundant in moraines of the western Bunger Hills and, in particular, Cape Jones and the Obruchev Hills, although, apparently, not west of the Denman Glacier, which suggests a wide sub-glacial distribution to the south or southeast.

Sandow Group

Sediments

Ravich et al. (1968) published detailed sections of both Mounts Amundsen and Sandow. At Mount Sandow (Fig. 102), the strongly folded 130 m section comprises weakly metamorphosed pinkish or greenish-grey quartzitic sandstone, with subordinate interbedded conglomerate and reddish-brown siltstone and argillite, and a basal conglomerate, which unconformably overlies metabasalt ('greenschist'). Mount Amundsen consists of 80 m of arkosic sandstone with interbedded conglomerate, siltstone and argillite. Clastic material in the sandstone comprises quartz, plagioclase, K-feldspar, quartz-sericite schist, sericite-chlorite schist and microgranite. Metamorphic effects are largely confined to recrystallisation of quartz and intense sericitisation and saussuritisation of feldspar. Sericite is common in the sandstone matrix, as well as in the argillites, and clastic grains of tourmaline and zircon are widespread. Ravich et al. (1968) suggested a predominantly granitic source for the 'coastal-continental' (predominantly fluviatile, partly aeolian) sediments. They quoted a (?K-Ar) age of 610 Ma for sericite schist, apparently supported by microfossil determinations. Circular trace fossils, up to 20 cm across, of unknown affinity were found in a sandstone boulder in moraine at Cape Jones (Fig. 103).

Metabasalt

Eight metres of deformed and strongly altered metabasalt, exposed at the base of the sequence at Mount Sandow (Ravich et al. 1968), consists of chlorite-epidote-actinolite schist, with cross-cutting quartz, quartz-epidote and chlorite veins. In contrast, samples collected from moraines at Cape Jones and in the Bunger Hills are medium-grained (0.2–5 mm) with relict subophitic to intergranular textures, and are best termed metagabbro (Figs 104, 105). All contain abundant (10–20%) clinopyroxene, partly replaced by colourless to pale green amphibole, epidote, chlorite, ?prehnite and serpentine. Such alteration is extremely patchy on a centimetre scale. Relict olivine is present in one sample. Plagioclase (andesine) is more or less altered to sericite, and one rock contains plagioclase phenocrysts. Opaque minerals (5–7%) are partly replaced by leucoxene, and pyrite is conspicuous in hand specimen. Apatite is an accessory phase.

In spite of its alteration, many of the major primary chemical characteristics of the metabasalt are preserved. All samples are Hy-normative olivine or quartz tholeiite, although at least one (86286028) appears to have been strongly enriched in K_2O (Table 22, Figs 99, 100). Spidergram patterns are fairly consistent from Nb to Y (Fig. 106), but the two more evolved (low *mg**) samples have negative Sr anomalies, probably resulting from plagioclase fractionation. LILE (especially K) show much greater variation.

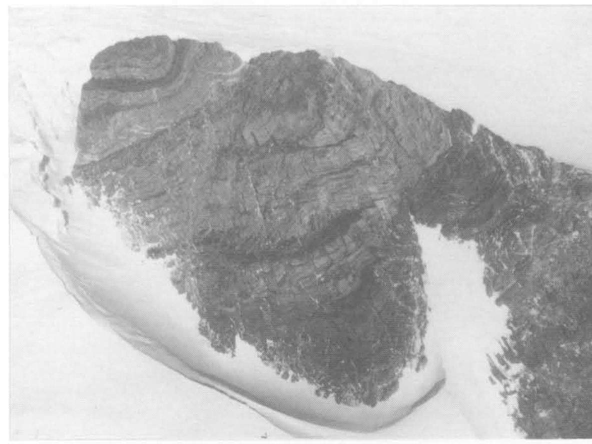

Figure 102. Mount Sandow, showing folded quartzitic sandstone, with interbedded conglomerate, siltstone, and argillite, unconformably overlying metabasalt. Height of nunatak about 150m.

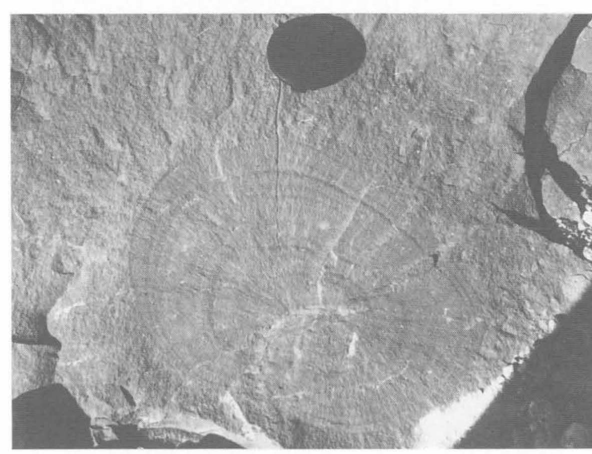

Figure 103. Possible trace fossil in pink sandstone boulder in moraine at Cape Jones.

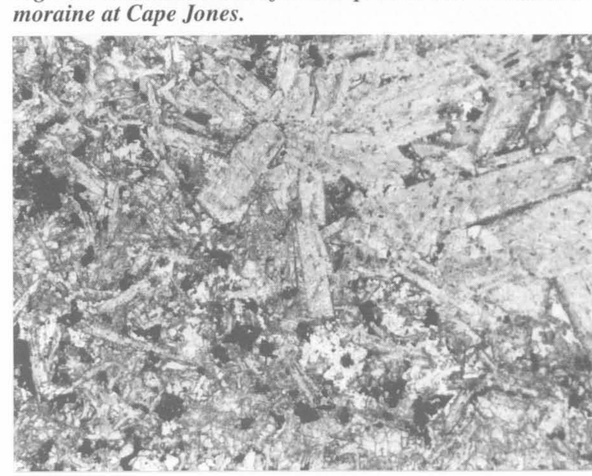

Figure 104. Metabasalt, showing sericitised plagioclase phenocrysts in an altered subophitic to intergranular groundmass containing relict clinopyroxene, pale green amphibole, chlorite, epidote, altered plagioclase, and opaque minerals; moraine at Cape Jones. Sample 86286028; width of field: 6.5mm.

The metabasalt was apparently derived from an enriched mantle source similar to that of the Bunger Hills dolerites (groups 3 and 4), showing similar variations in P/Zr, but probably having slightly higher Ce/Zr (see above).

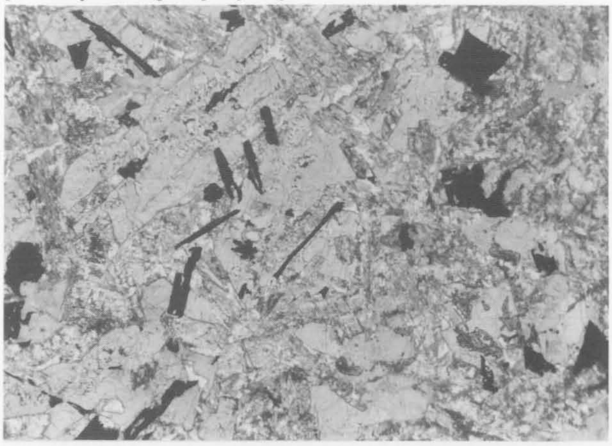

Figure 105. Metabasalt, showing subophitic texture with partly altered clinopyroxene, secondary chlorite and amphibole, sericitised plagioclase, and opaque minerals (including ilmenite and pyrite); moraine in southern Bunger Hills. Sample 86286236; width of field: 5.3mm.

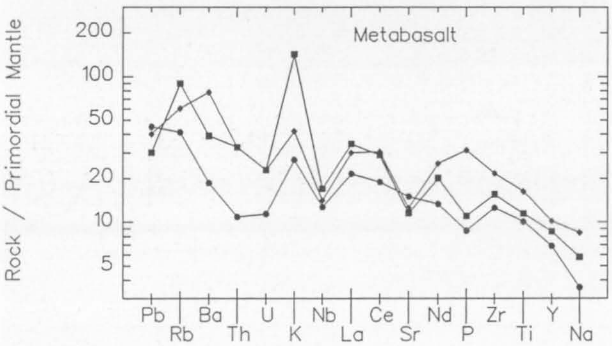

Figure 106. Spidergrams for metabasalts from moraines in Bunger Hills area.

Structural Geology

Bunger Hills area

The only detailed structural mapping in 1986 was carried out in the main Bunger Hills outcrops by geologists from the universities of Melbourne (Stüwe & Wilson 1990) and Adelaide (Ding & James 1991). This section therefore relies to a large extent on the data and interpretations of these authors, supplemented by our own observations in nearby parts of the area. Because the structural histories postulated in the above two papers differ in a number of important respects, we have attempted to reconcile them as far as possible to produce a consistent, although tentative, sequence of structural events. Clearly, more detailed mapping will be required if a definitive structural history is to be obtained.

The most fundamental disagreement is over the age of the major plutonic bodies relative to the deformation events, specifically the Paz Cove batholith and Algae Lake pluton. Stüwe & Wilson (1990) described two major ductile deformations, followed by a late doming (i.e. post-plutonic), and proposed that the Paz Cove batholith is of syn-D_1 age and the Algae Lake pluton is post-D_2. Ding & James (1991) postulated four fold phases and considered both bodies to be of pre or syn-D_4 age, their D_3-D_4 being more or less equivalent to D_2 of Stüwe & Wilson (1990).

We believe that both Bunger Hills intrusions are the same age and were emplaced during the last major deformation (our D_3). The two bodies have, within very narrow error limits, the same zircon U-Pb age (1170±3 Ma), whereas the metamorphic peak was significantly earlier (1190±15 Ma). As shown above, they are petrographically very similar. The only significant difference is that the Paz Cove batholith has a much stronger marginal foliation. However, we interpret this foliation to be of igneous origin, the rocks having a hypidiomorphic or allotriomorphic granular texture (Figs 40, 41), which contrasts with the granoblastic texture of the country rocks. The parallelism of the foliation in the plutons with the contacts would be a consequence of syn-deformational emplacement. In contrast to Stüwe and Wilson (1990), we have obtained virtually identical P-T estimates for the two bodies, using various methods (Table 6), and they are geochemically and isotopically indistinguishable.

D1 deformation

The earliest recognisable deformation (D_1) produced the dominant foliation (S_1) and associated structures during granulite-facies metamorphism (M_1). Stüwe & Wilson (1990) inferred that it was an intense flattening event, which resulted in high, but varied, degrees of boudinage of mafic and ultramafic layers (Fig. 107), and which they therefore attributed to crustal extension.

S_1 is generally parallel to the compositional layering, except at F_1 fold hinges, and is defined by discontinuous layers and lenses of mafic minerals and lensoid aggregates of quartz and feldspar. Textures are granoblastic interlobate in felsic gneisses, but polygonal in mafic and ultramafic rocks. In metasedimentary rocks the compositional layering presumably represents transposed sedimentary bedding, whereas in more massive orthogneiss units such layering may partly reflect the presence of a variety of now-deformed xenoliths. However, the well-defined compositional layering in F_1 fold hinges may well be a metamorphic feature (S_0), reflecting earlier tectonothermal activity.

F_1 folds are commonly mesoscopic intrafolial isoclines and are most common in more strongly layered gneiss (Fig. 108). Associated lineations (L_1) are defined either by the intersection of S_0 with S_1 or by a preferential alignment of acicular minerals (e.g. sillimanite), mineral aggregates, or small partial-melt bodies.

Figure 107. Mafic granulite boudins in felsic gneiss; northeast of Edgeworth David Base. (University of Melbourne photograph.)

Figure 108. F_1 folds in interlayered garnet-cordierite paragneiss and pyroxene gneiss, with garnet developed along the layer boundaries; southeastern Bunger Hills. (University of Melbourne photograph.)

D2 deformation

The predominant mesoscopic structures in the Bunger Hills area are open to tight or isoclinal, commonly asymmetric folds (F_2), which probably formed during a major shortening event (Stüwe & Wilson 1990) under granulite-facies conditions (M_2). The small separations of D_2 boudins (Fig. 109) and minor flattening component suggest a much smaller finite strain than during D_1.

F_2 fold hinges (Figs 110, 111) have highly variable orientations, owing to the effects of D_3; they commonly plunge west-southwest or east in the southern Bunger Hills, but more north or south near the Paz Cove batholith. The D_2 axial planar foliation (S_2) and lineation (L_2) are only weakly developed. F_2 folds are commonly nearly coplanar (but not coaxial) with F_1 folds (Fig. 112) and, according to Stüwe & Wilson (1990), interference patterns are mostly types 2 or 3 of Ramsay & Huber (1987) (Figs 113, 114).

Interference structures are well displayed on central Thomas Island, where F_1 isoclines are refolded by open to tight F_2 folds.

Figure 109. D_2 pegmatitic boudins in felsic orthogneiss; eastern Bunger Hills. (University of Melbourne photograph.)

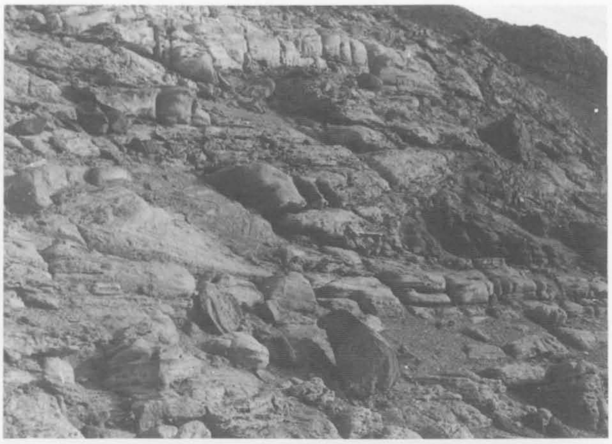

Figure 110. Recumbent isoclinal F_2 fold; east of Paz Cove. (University of Melbourne photograph.)

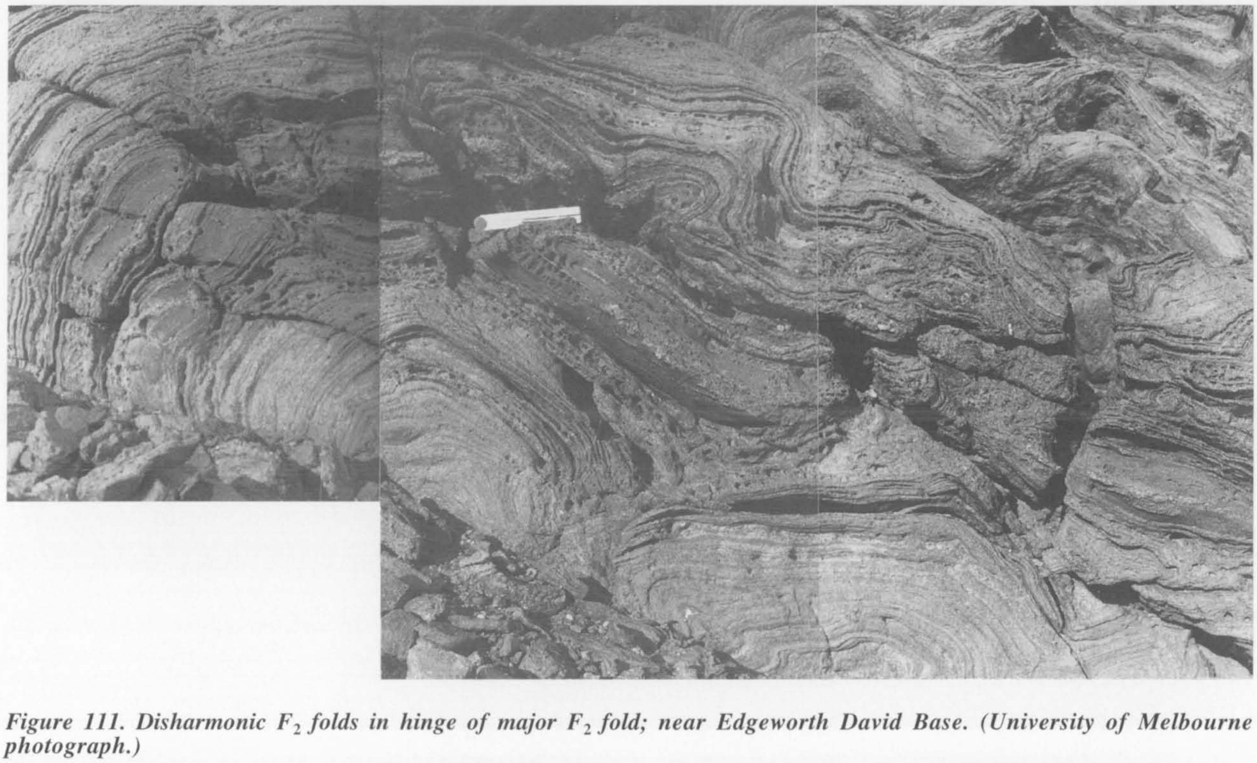

Figure 111. Disharmonic F_2 folds in hinge of major F_2 fold; near Edgeworth David Base. (University of Melbourne photograph.)

Both these fold phases have steeply plunging axes and steeply dipping axial planes where affected by east–west-trending major folds (F_3). Ding & James (1991) described two major F_2 folds in the southwestern and southeastern Bunger Hills, the former being associated with many tight recumbent parasitic folds.

D3 deformation

The regional strike in most of the Bunger Hills area is the result of a third major ductile deformation (D_3), still under granulite-facies conditions (M_3), which is thought to have been accompanied by emplacement of the Algae Lake and Paz Cove intrusions. F_3 folds are major upright structures, commonly asymmetric with shallow east or west-plunging axes (Figs 115–117). They clearly refold F_1 and F_2 structures on Thomas Island and elsewhere (Fig. 118). Two tight, upright, east–west-trending folds in the southwestern and southeastern Bunger Hills, attributed by Ding & James (1991) to F_3, have axes plunging at low angles (0–30°) to the west-southwest. Other major folds next to the Paz Cove batholith trend north–south to north-northwest–south-southeast, but may also have been formed during D_3. Their axial planes dip at 40–80° to the west or west-southwest and axes plunge at 30–80° to the west-northwest.

This varied orientation of F_3 folds is interpreted as due to deformation having been contemporaneous with emplacement of the two major Bunger Hills plutons, which would explain the presence of an igneous, rather than a metamorphic, foliation in these bodies. It is only near the Paz Cove batholith, which has the stronger marginal foliation, that the major F_3 folds have a roughly north–south trend. Elsewhere the dominant strike is west-southwest. Thus, D_4 of Ding & James (1991) does not appear to have been a regionally extensive deformation.

Plots of foliation orientation for other parts of the Bunger Hills area (including the Obruchev Hills) tend to define girdles consistent with regional folding about west-southwest-trending axes, suggesting that north-northwest–south-southeast compression was the main factor determining the regional strike (Fig. 119). Stüwe & Wilson (1990) also attributed the varied orientation of F_3 (their F_2) folds to the effects of the Paz Cove batholith, although they considered this body to have been emplaced during D_1. In contrast, Ding & James (1991) interpreted the north–south folds as a separate generation (F_4), on the basis of superimposed folding relationships with the west-southwest-trending F_3 folds. However, such relationships could be explained if the plutonic bodies were emplaced late in D_3, after the west-southwest-trending F_3 folds had started to form, so that D_3 and D_4 of Ding & James (1991) could represent two phases of a single progressive deformation (i.e. were essentially contemporaneous).

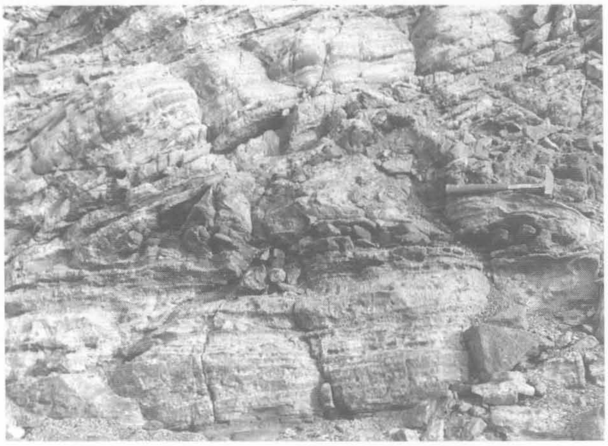

Figure 112. Coaxial F_1 (below hammer) and F_2 folds; east of Paz Cove. (University of Melbourne photograph.)

Figure 113. F_1 isocline folded by F_2 fold in interlayered mafic granulite and felsic orthogneiss; near Edgeworth David Base. (University of Melbourne photograph.)

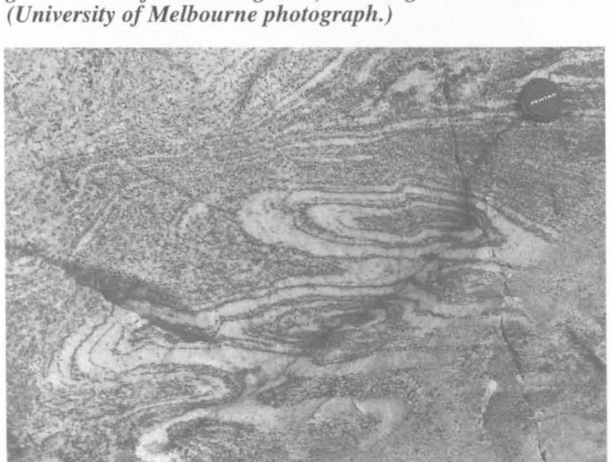

Figure 114. Probable F_1/F_2 interference pattern; south of Algae Lake. (University of Melbourne photograph.)

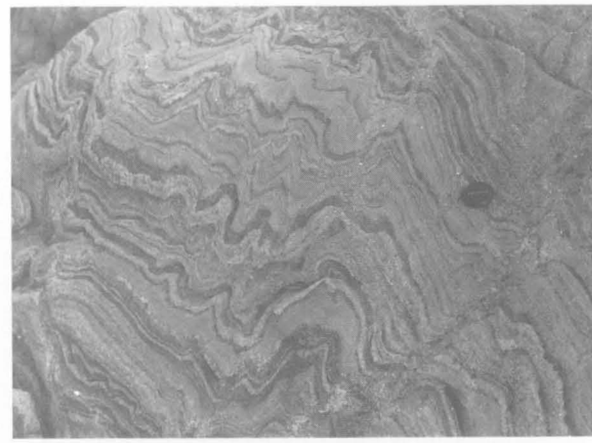

Figure 115. Minor F_3 folds; northeastern Bunger Hills. (University of Melbourne photograph.)

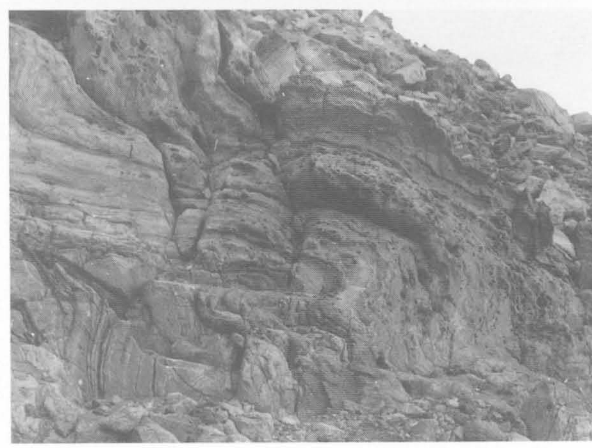

Figure 116. Asymmetric F_3 fold; near Edgeworth David Base. (University of Melbourne photograph.)

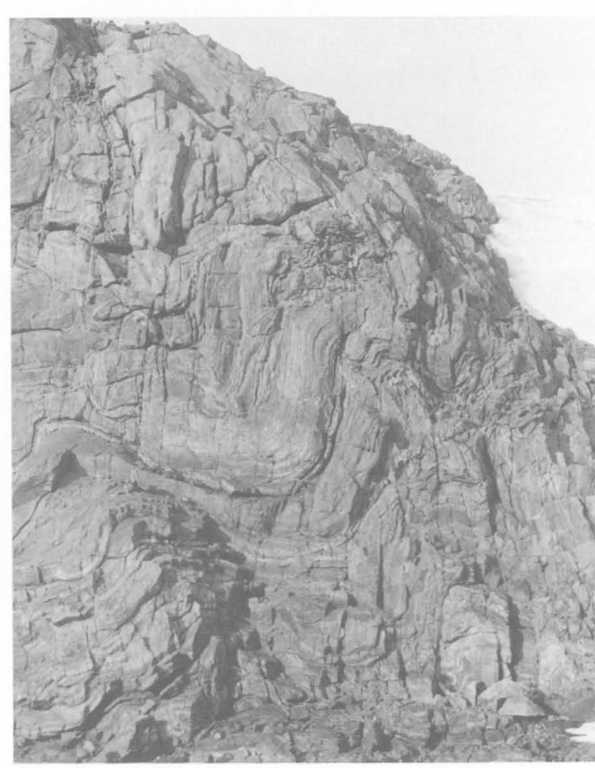

Figure 117. Asymmetric F_3 fold; near Edgeworth David Base. (University of Melbourne photograph.)

Much of the Booth Peninsula batholith (the unfoliated quartz monzodioritic and probably the granitic rocks) is about 20 Ma younger than the Bunger Hills plutons and clearly cuts D_3 structures (e.g. at eastern Thomas Island). Metamorphosed dykes that cut this body include probable syn-plutonic dykes, which have some chemical features (e.g. high Nb) in common with the quartz monzodioritic rocks. Undeformed amphibolite dykes described by Stüwe & Wilson (1990) from the Bunger Hills possibly belong to this suite. Group 1 dolerites might also be of similar age. However, subconcordant, folded and metamorphosed mafic dykes that cut the country rocks are presumably pre-D_3 (and possibly pre-D_2).

Figure 118. Tight F_2 folds on steep limb of major F_3 fold; near Edgeworth David Base. Height of cliff: about 30m. (University of Melbourne photograph.)

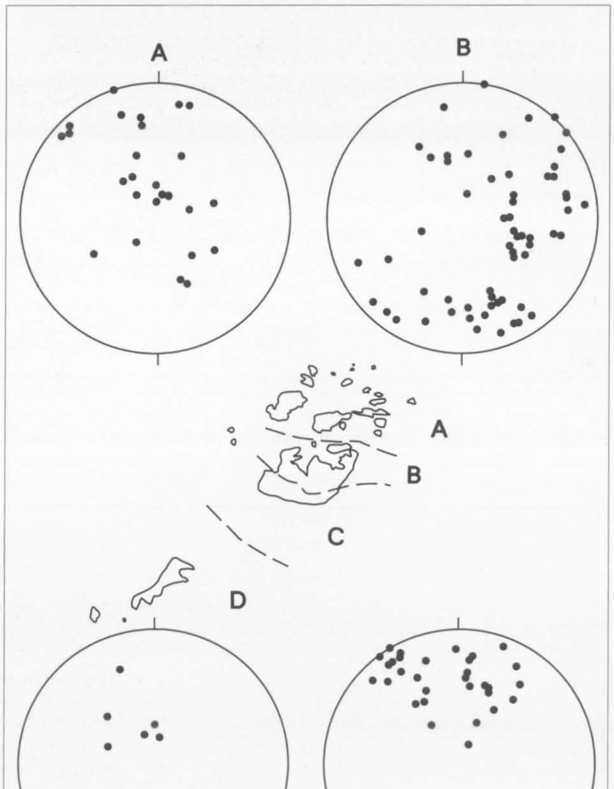

Figure 119. Stereographic plots of poles to foliations measured in four subareas (A to D) of the Obruchev Hills-Bunger Hills area.

Ding & James (1991) inferred a major post-D_3, pre-D_4 (their terminology) west-southwest–east-northeast-trending thrust in the southeastern Bunger Hills, which was taken to imply compression directed north-northwest. This is similar to the orientation of the stress field during our D_3, so the thrusting may have occurred as part of this event. However, the existence of this thrust was disputed by Stüwe & Wilson (1990), as the field evidence is equivocal and rapid uplift and subsequent reburial of the terrane would be implied. They postulated a post-D_3 (our terminology) regional asymmetric doming event, which was not recognised by Ding & James (1991). Clearly, more work is required to resolve this.

D4 deformation

The major ductile deformations described above were followed by a complex sequence of more localised brittle-ductile and brittle deformation (summarised as D_4). Several generations of retrograde shear zones, mylonites, and faults are present (Figs 120, 121). Stüwe & Wilson (1990) identified two major sets of steeply dipping shear zones, which trend 110° and 160° and are up to 15 km long and 50 m wide (but mostly 1–10 m). Both sets have dextral displacements and, therefore, do not form a conjugate set. Mylonitic fabrics were developed, commonly with mortar structures, and there is a strong penetrative foliation (Fig. 122). Extensive recrystallisation resulted in fine-grained polygonal aggregates. Garnet porphyroclasts were rounded and rotated, or fragmented (Fig. 123). Retrograde assemblages contain bluish-green hornblende, biotite, and chlorite, but in some places pyroxene is only slightly altered (Fig. 124). Earlier shear zones have a steeply plunging lineation, but late ultramylonites have a shallow lineation associated with the observed dextral displacement.

Tight minor folds with a strong axial planar foliation, defined by biotite, and lineation occur in shear zones in the southern Liberty Islands (4 km north of eastern Thomas Island). Felsic layers in gneiss near the shear zones were bleached during the associated retrogression (Fig. 120).

Many shear zones appear to be roughly contemporaneous with the intrusion of dolerite dykes at about 1140 Ma, and so cannot be much younger than the major ductile folding events and plutonic activity already described. However, age relationships between shear zones, pegmatites, and dolerite dykes are complex (Fig. 125). In the southeastern Highjump Archipelago, two sets of mylonites are cut by pink pegmatite veins that predate the dolerites. In contrast, mylonite zones at Mars Island are clearly younger than garnet + biotite-bearing pegmatites. Both mylonites and pegmatites are older than dolerite dykes at eastern Thomas Island, whereas other mylonite

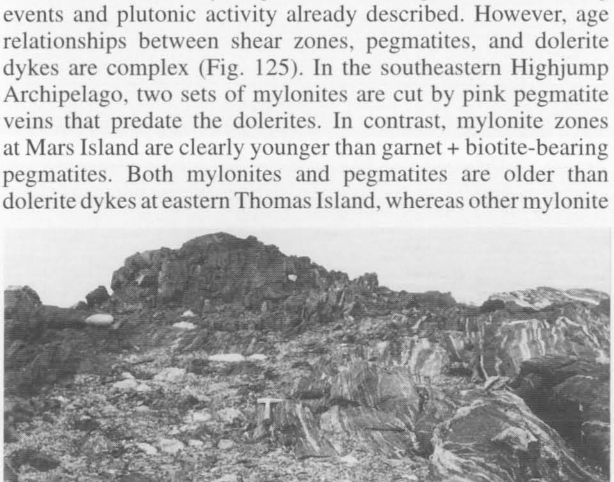

Figure 120. North-south trending retrograde shear zone in garnet paragneiss and mafic granulite; southern Liberty Islands. Note bleaching of felsic layers.

zones are clearly younger than the dykes, some of which have sheared margins. Deformation of metamorphosed mafic dykes in the northeastern Highjump Archipelago was associated with garnet formation.

Evidence for the contemporaneity of dyke emplacement and shear zone formation comes from the southern Liberty Islands, where a group 3E dolerite is cut by a shear zone, which is cut, in turn, by a second group 3E dyke. The two dykes are chemically identical and almost certainly belong to the same intrusive episode.

Pseudotachylite veins are commonly associated with the shear zones, and are interpreted as the result of reactivation under brittle, as opposed to brittle-ductile, conditions. The range of deformation structures in the shear zones (mylonite, ultramylonite, and pseudotachylite) and the presence of brittle faults suggest a change from plastic to brittle conditions during uplift. However, although some pseudotachylites clearly cut older shear zones (Stüwe & Wilson 1990), others appear to have been redeformed by ductile processes. A possible explanation of this is that during deformation the plastic strain

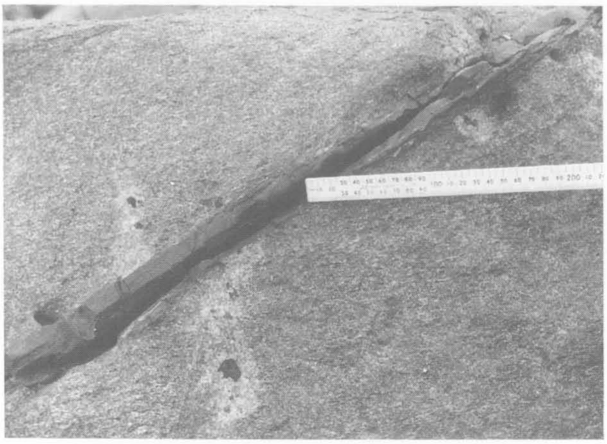

Figure 121. Ultramylonite zone cutting Paz Cove batholith. Note pegmatitic segregations in latter. (University of Melbourne photograph.)

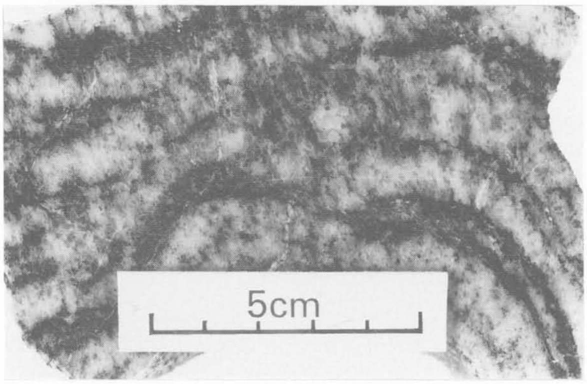

Figure 122. Hinge of isoclinal fold in shear zone of Figure 120, showing strong axial planar foliation (vertical in photo) defined by biotite grains.

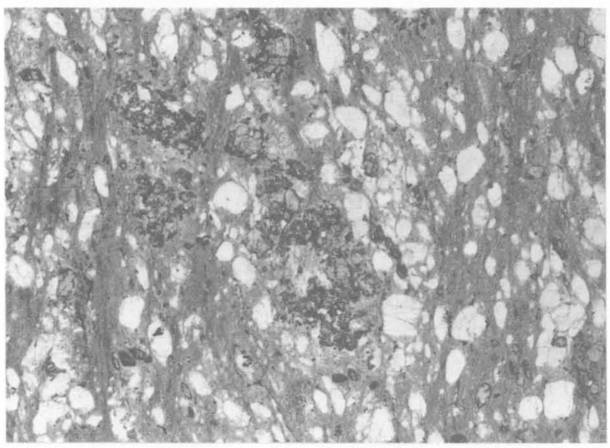

Figure 123. Gneiss from northeast-trending mylonite zone, showing porphyroclasts of plagioclase, garnet, and minor orthopyroxene in a very fine-grained biotite-rich matrix; Currituck Island. Sample 86285609; width of field: 6.5mm.

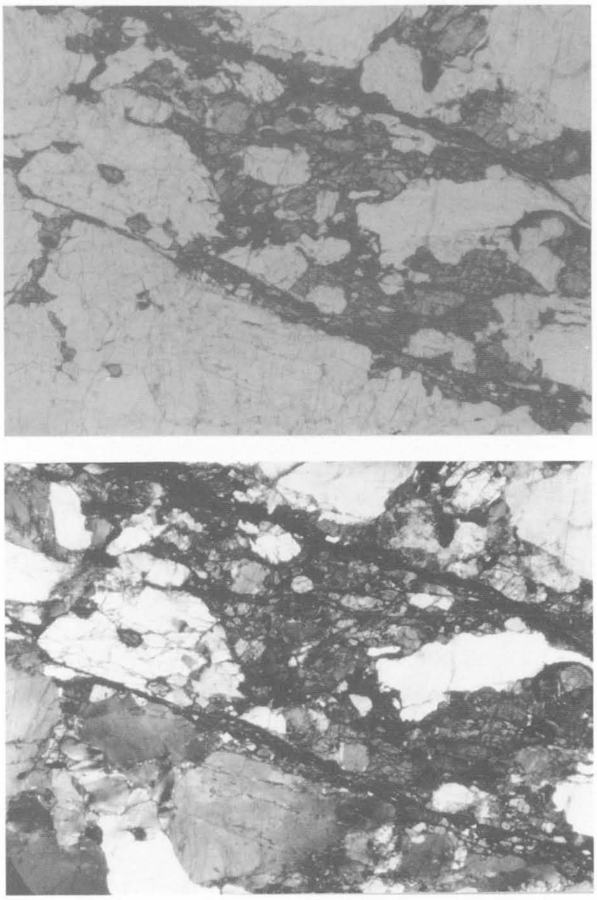

Figure 124. Thin ultramylonite zones cutting orthopyroxene granite of the Booth Peninsula batholith; 7 km east of Miles Island. Note little-altered orthopyroxene, and crushed and strained feldspar and quartz. Sample 86286277; cross polarised light in lower photo; width of field: 7mm.

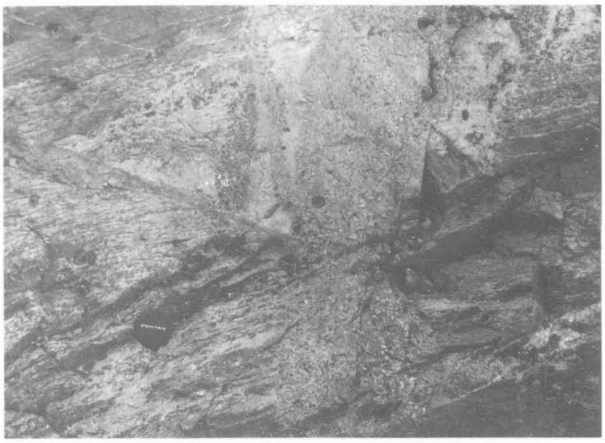

Figure 125. Pegmatite cutting ultramylonite zones; Bunger Hills. (University of Melbourne photograph.)

rate was not high enough to compensate for the applied stress, which therefore led to failure and pseudotachylite generation. The consequent stress drop could then have resulted in a return to plastic deformation (P. Marsh, University of Melbourne, personal communication 1989).

Denman Glacier area and Mounts Amundsen and Sandow

There was no opportunity for detailed structural observations in this area in 1986, as only a few hours were available for examining all the outcrops. The regional strike is roughly west-southwest, similar to that in the Bunger Hills.

Many outcrops west of the Denman Glacier have a particularly strong foliation. For example, garnet-biotite granite at Cape Harrison and Possession Rocks locally has a flaser structure. Similar granite interlayered with quartzite at Mount Barr-Smith has been deformed to an augen gneiss (Fig. 131). Garnet-quartz-feldspar gneiss at Mount Gist commonly has a cataclastic texture (Ravich et al. 1968). Metasediments at Jones Rocks have a strong lineation, defined by quartz rods, plunging south about 10°.

Rocks of the Sandow Group have variable orientations. Those at Mount Sandow dip east at 25–40°, whereas the dip at Mount Amundsen is 15–25° to the south-southeast (Ravich et al. 1968). From the air, the sediments at Mount Sandow appear to have been affected by open folds with shallow plunges.

Metamorphism

Bunger Hills area

Peak metamorphism

The metamorphic grade in most of the Bunger Hills area is intermediate-pressure granulite facies (Green & Ringwood 1967). Orthopyroxene is common in felsic rocks and orthopyroxene + clinopyroxene in mafic rocks throughout the area.

The usual assemblage in aluminous metasediments is

- garnet + sillimanite + cordierite ± biotite (+ K-feldspar + plagioclase + quartz + Fe-Ti oxide).

Well-crystallised primary biotite is common, but many rocks contain secondary biotite, in some cases rimming garnet. In many metapelites there is evidence for original coexisting spinel and quartz, although most of the spinel is now enclosed by grains of garnet, cordierite or sillimanite, which apparently represent reaction coronas (Stüwe & Powell 1989a). The assemblage

- garnet + cordierite + orthopyroxene ± biotite

is rare, and mostly occurs in migmatitic metapelites close to the Booth Peninsula batholith. Hence, the assemblage on the left of the reaction

- garnet + biotite + quartz → cordierite + orthopyroxene + K-feldspar + H_2O

(Winkler 1974) appears to have been stable in most of the Bunger Hills area (Fig. 34). Nevertheless, Clarke et al. (1989) pointed out that all these phases (together with spinel, rutile and ilmenite) may coexist because TiO_2 and Fe_2O_3 are normally present in addition to the components of the KFMASH (K_2O-FeO-MgO-Al_2O_3-SiO_2-H_2O) system. The assemblage corundum + magnetite + spinel may have been formed by an oxidation reaction

- spinel 1 + oxygen → spinel 2 + magnetite + corundum

during cooling (Ellis et al. 1980). Unlike in the Napier Complex (Sheraton et al. 1987c), none of the higher pressure and/or temperature associations — sillimanite + orthopyroxene, sapphirine + quartz, and osumilite (Hensen & Green 1973; Newton et al. 1974; Ellis et al. 1980) — has been found.

The high pressure assemblage

- garnet + orthopyroxene + clinopyroxene + plagioclase

is rare, but occurrences in subconcordant metamorphosed mafic dykes in the northeastern Highjump Archipelago suggest a reaction, apparently during deformation, such as

- orthopyroxene + anorthite → clinopyroxene + garnet + quartz.

Its presence in an olivine tholeiite (86285984: Table 10) is consistent with the observations of Green & Ringwood (1967, 1972) that garnet forms at pressures as low as 7–8 kb at 900°C in SiO_2-undersaturated (Ol-normative) compositions. A garnet-orthopyroxene-quartz-feldspar gneiss (86285979) from the same area contains two generations of garnet, one partly replacing orthopyroxene (Fig. 126), suggesting reactions such as

- orthopyroxene + anorthite → garnet + quartz, or
- aluminous orthopyroxene → garnet + orthopyroxene

(Green & Ringwood 1967). Such reaction coronas are consistent with near-isobaric cooling after the peak of metamorphism, as was the case in the Napier Complex (Ellis 1980; Harley 1985).

Similar high-pressure associations and coronas are rare in most of the Bunger Hills area, although garnet coronas surround orthopyroxene in the Paz Cove granite (Fig. 54) and garnet-bearing reaction zones occur locally around boudinaged mafic granulite layers (Stüwe & Powell 1989a). In contrast, symplectites of orthopyroxene + cordierite + plagioclase around garnet (Fig. 127) in a metapelite (86286263) from north of Raketa Island suggest a decompression reaction:

- garnet + quartz → cordierite + orthopyroxene + plagioclase.

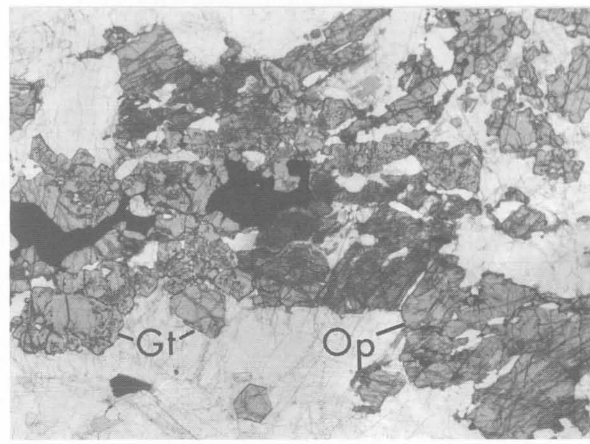

Figure 126. Garnet partly replacing orthopyroxene, which is slightly altered, in garnet-orthopyroxene-quartz-feldspar gneiss, consistent with near-isobaric cooling; northeastern Highjump Archipelago. Sample 86285979; width of field: 5.2mm.

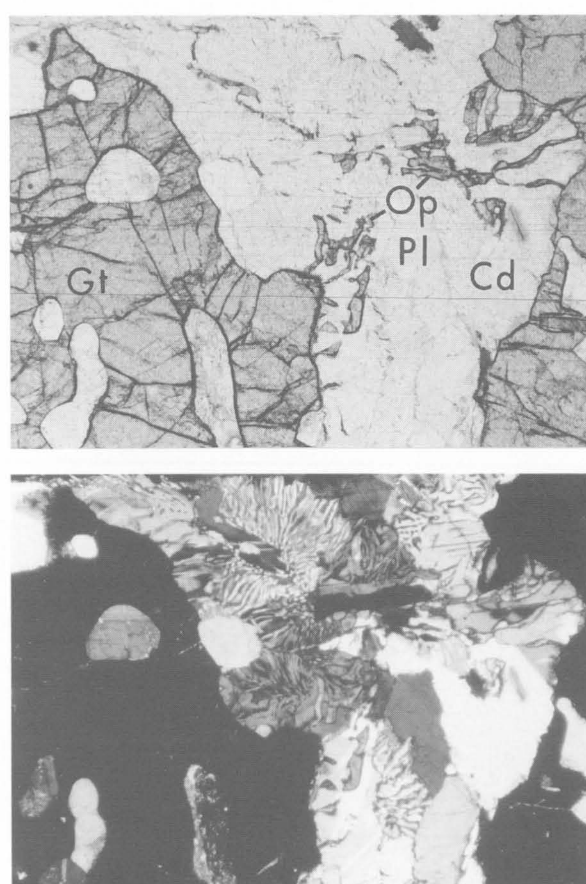

Figure 127. Symplectite of orthopyroxene+cordierite+plagioclase partly replacing garnet in orthopyroxene-biotite-garnet-plagioclase gneiss, suggesting decompression; 2km north of Raketa Island. Sample 86286263; cross-polarised light in lower photo; width of field: 2.0mm.

Pressure and temperature estimates for rocks from the Bunger Hills area are summarised in Table 23. The Wood & Banno (1973) two-pyroxene geothermometer is thought to overestimate temperatures for crustal granulites by about 50°C, and that of Wells (1977) possibly even more (Harley 1983), so that equilibration temperatures of about 800°C are probably more realistic. They would also be more consistent with those obtained using the graphical pyroxene geothermometer of Lindsley (1983) (~800°C, Fig. 128), the Al^{iv}-in-amphibole geothermometer of Blundy & Holland (1990) (~760°C), and the rather variable results of the garnet + orthopyroxene geothermometer of Harley (1984a) (700–800°C). Hence, the best estimate of peak metamorphic temperatures (during M_1) in the Bunger Hills is about 750–800°C. Temperatures in the northeastern Highjump Archipelago were apparently slightly lower (~700–750°C), although the data are not very consistent. The low temperature (627°C) obtained for granulite 86285984 using the Harley (1984a) method may be due to the garnet being of secondary origin, produced during cooling.

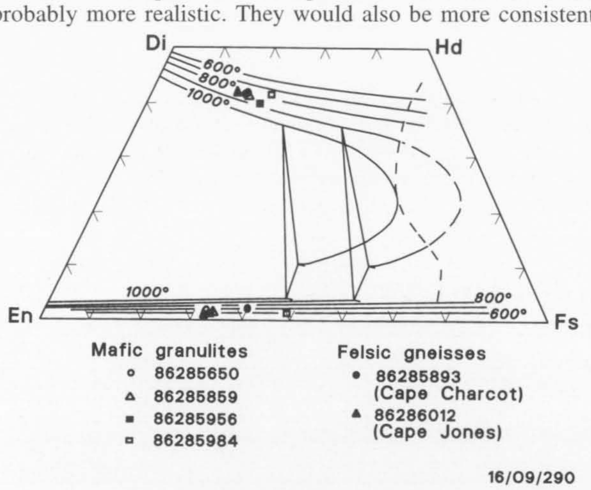

Figure 128. Pyroxene compositions for two pyroxene-bearing metamorphic rocks from the Bunger Hills area and Cape Charcot (Denman Glacier area), plotted on the graphical geothermometer of Lindsley (1983) for a pressure of 5kb.

Pressure estimates from the garnet + orthopyroxene geobarometers of Harley & Green (1982) and Harley (1984b) range from 2 kb to 6 kb, probably because rocks with high Kd^{Gt-Op}_{Fe-Mg} (e.g. 86285821, for which Kd = 2.9) give results which can be several kilobars too low (Harley 1984b). The higher pressures (~5 kb), obtained from rocks with low Kd values, are, therefore, probably the better estimates and are more consistent with pressures (mostly 5-6 kb) obtained using the Newton & Perkins (1982) orthopyroxene + garnet + plagioclase geobarometer. They are similar to the 4.7–5.2 kb (at 650–700°C) obtained using the method of Powell & Holland (1988), but slightly lower than the 6–7 kb quoted by Stüwe & Powell (1989a).

Hence, on the available data, the best P-T estimate for the Bunger Hills metamorphism is about 750–800°C and

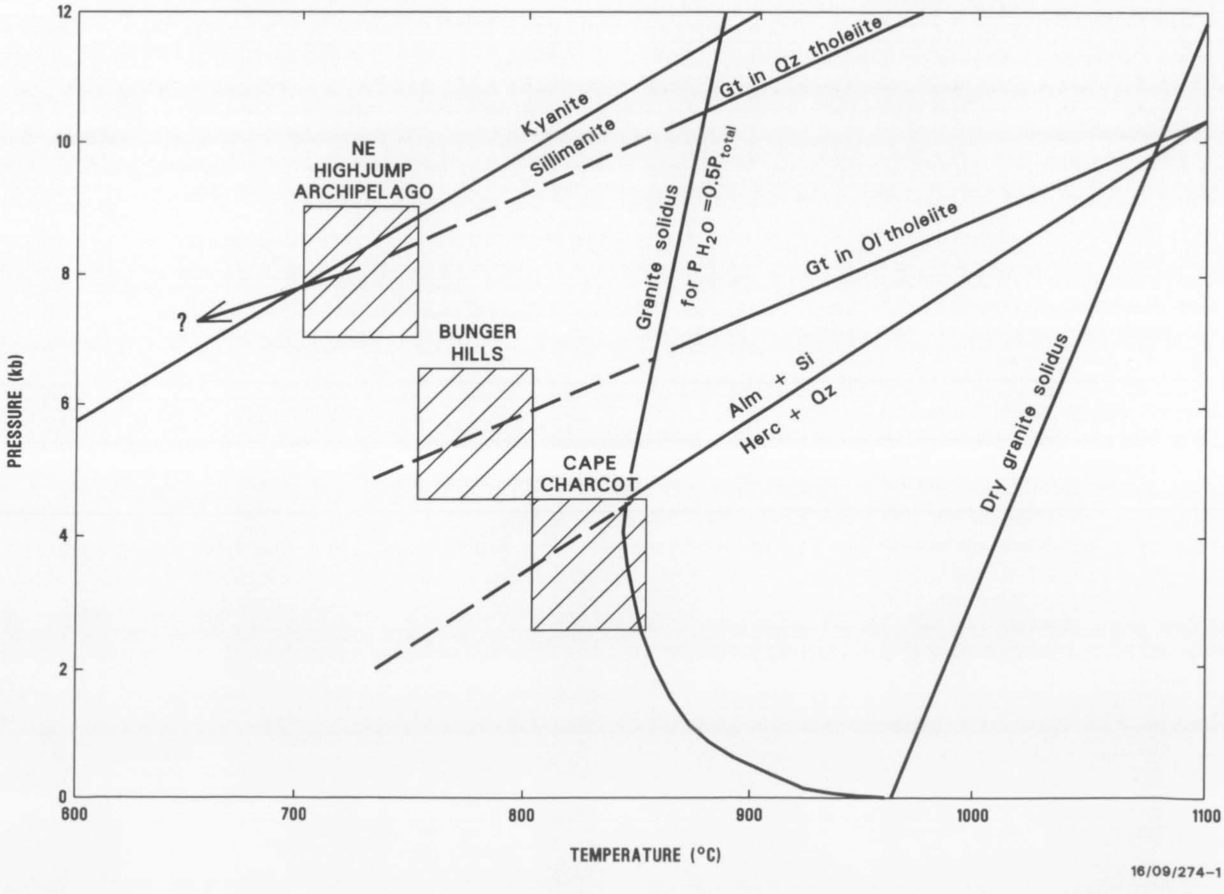

Figure 129. P-T diagram showing estimated peak conditions of metamorphism in the Bunger Hills and northeast Highjump Archipelago, and at Cape Charcot (Denman Glacier area), based on methods given in Table 23. Dry granite solidus after Huang & Wyllie (1975); estimated granite solidus for $P_{H2O} = 0.5P_{total}$ based on Cann (1970) and Huang & Wyllie (1975); appearance of garnet in mafic rocks of olivine tholeiite and quartz tholeiite compositions after Green & Ringwood (1967, 1972); kyanite-sillimanite boundary after Holdaway (1971); stability field of hercynite-rich spinel+quartz after Shulters & Bohlen (1989). Arrow indicates a possible near-isobaric cooling path for the northeastern Highjump Archipelago area. Alm, almandine; Herc, hercynite.

5–6 kb. Pressures in the northeastern Highjump Archipelago area were significantly higher at about 8 kb, assuming a temperature of 750°C (Table 23, Fig. 129), which is consistent with the stability of garnet in mafic granulites (Green & Ringwood 1967, 1972).

Stüwe & Powell (1989a) interpreted their P-T estimates (6–7 kb, 750°C) as reflecting a 'post-peak' event (M_2), equivalent in age to the Algae Lake pluton. They considered the presence of apparently relict spinel in metapelitic rocks to indicate the originally more widespread occurrence of the association spinel + quartz, which formed during an earlier 'peak' event (M_1) at about 4 kb and 800°C, and which was largely destroyed during subsequent compression in the reaction.

- spinel + quartz $\rightarrow$ garnet + cordierite + sillimanite.

This interpretation may not necessarily be correct, because some metapelites contain spinel either in contact with quartz or separated from it by only a very thin rim of cordierite (Figs 27, 29), and virtually all metapelites contain accessory amounts of spinel (< 1%). Such a widespread, but volumetrically minor, occurrence of spinel is difficult to reconcile with partial overprinting by higher pressure assemblages, which would be expected to result in much more variable modal spinel than is actually observed. In particular, spinel is just as abundant in migmatitic metapelites near the plutons, which, if the migmatisation was coeval with the plutonism, must have formed at pressures of at least 5 kb. Moreover, cordierite ± sillimanite ± garnet-bearing metapelites in the Windmill Islands, which equilibrated at about 760°C and 5.5–6.5 kb, also contain spinel (Blight & Oliver 1982). It therefore seems more likely that spinel was stable during the peak metamorphism.

The stability field of hercynite-rich spinel + quartz possibly extends to higher pressures than are indicated by experimental data (~ 3-4 kb at 800°C: Shulters & Bohlen 1989) if minor components such as Zn (i.e. gahnite) are present or oxygen fugacity is high (Hensen & Green 1971). The experimental data of Bertrand et al. (1991) show that spinel + quartz is stable at pressures as high as 9–10 kb at temperatures of 1000°C. Whether or not spinel formed during the lower pressure stage of a compressional event, we think the predominant assemblages (in mafic rocks and felsic orthogneiss, as well as metapelites) that produced the above P-T estimates were essentially formed about 20 Ma before emplacement of the plutonic rocks, during an event we term M_1. Nevertheless, at least some of the significant variations in the P-T estimates (Table 23) are probably due to partial re-equilibration between M_1-D_1 and M_3-D_3.

Estimated equilibration temperatures of the plutonic rocks (Table 6), emplaced during M_3-D_3, are very similar to those of the country rocks. The compositions of original pigeonite in some plutonic rocks are consistent with temperatures of 800–850°C (Fig. 45), rather than the considerably higher 940–1000°C postulated by Stüwe & Powell (1989a). The amphibole geothermometer of Blundy & Holland (1990) gives temperatures very similar to those obtained from pyroxene compositions. Pressures (~5–6 kb) are also very similar to those obtained for the country rocks, suggesting that there was no major uplift before emplacement of the plutonic rocks. Nevertheless, P-T estimates for core-rim pairs in the country rocks (Table 23) suggest a decrease in both temperature and pressure. The presence of retrograde shear zones of similar, or in some cases older, age to the 1140 Ma dolerite dykes

Table 23. Pressure–temperature estimates for Bunger Hills metamorphic rocks and dolerite dykes, and felsic gneiss from Cape Charcot (Denman Glacier area).

Sample	*Rock type*	*Locality*	*1*	*2*	*3*	*4*	*5*	*6*	*7*	*8*	*9*	*10*
			°C					*kb*				
86285979	Gt–Op–Qz–Kf–Pl gneiss	NE Highjump Arch.			671* 688*			6.7* 9.0*	6.3* 9.7*	8.1* 8.2*		
86285984	Gt–Op–Cp–Pl granulite	NE Highjump Arch.	813	788	627*		757	10.6*	6.5*	7.4*		
86286056	Op–Gt–Kf–Qz–Pl gneiss	E Miles Island			713			3.7	2.8	5.5		
86286261	Gt–Op–Pl–Qz gneiss	S Liberty Islands			773(r) 802(c)			2.4	4.6	5.7		
86285650	Cp–Op–Pl granulite	Thomas Island	848	840								
86285855	Gt–Op–Qz–Pl gneiss	Fuller Island			706 763			3.8 3.8	2.5 4.8	5.5 5.6		
86285859	Cp–Op–Pl granulite	Fuller Island	863	845								
86285871	Gt–OP–Pl–Kf–Qz gneiss	Aviatorov Peninsula			706 712			4.8 5.0	4.2 4.3	6.0 6.2		
86286072	Gt–Op–Qz–Pl gneiss	E of Paz Cove			797			4.6	7.1	7.0		
86285821	Gt–Op–Qz–Kf–Pl gneiss	Edgeworth David			692 745			2.5 2.5	–0.5 1.6	5.9 6.2		
86285679	Gt–Op–Kf–Qz–Pl gneiss	W of Lake Dolgoe			717(r) 740(c)			5.2(r) 5.2(c)	5.1(r) 5.9(c)	6.8(r) 6.9(c)		
86285956	Cp–Op–Pl granulite	SW Bunger Hills	852	839								
86286012	Cp–Op–Qz–Pl gneiss	Cape Jones	844	836		751 766					4.2 4.8	5.6 6.3
86285603	Group 2 dolerite	SE Currituck Island	1001– 1093	971– 1063								
86285913	Group 3A dolerite	Foster Island	797	778								
86285811	Group 4E dolerite	NE Obruchev Hills	778(r) 1057(c)	762(r) 944(c)								
86285893	Cp–Op–Qz–Pl gneiss	Cape Charcot	933	882		745*					3.5	4.8

r = rim, c = core.

1. Wells (1977).
2. Wood & Banno (1973).
3. Harley (1984a), assuming 5kb (*8kb). Temperatures are about 6°C higher at 6kb.
4. Blundy & Holland (1990), assuming 5kb (*3.5kb). Temperatures are about 15°C lower at 6kb.
5. Ellis & Green (1979), assuming 8kb.
6. Harley & Green (1982), assuming 800°C (*750°C). Pressures are about 1.8kb lower at 750°C.
7. Harley (1984b), assuming 800°C (*750°C). Pressures are 0.3–0.6kb higher at 750°C.
8. Newton & Perkins (1982), assuming 800°C (*750°C). Pressures are about 0.2kb lower at 750°C.
9. Johnson & Rutherford (1989).
10. Schmidt (1992).

also indicates some uplift into the zone of brittle-ductile deformation very soon after emplacement of the plutonic rocks.

Retrograde metamorphism

The effects of retrograde greenschist to amphibolite-facies metamorphism are widespread, particularly in the southeastern Bunger Hills. In some areas, retrogression was clearly associated with post-dolerite dyke shearing, which may have allowed water to get into relatively anhydrous rocks (Fig. 123). However, most altered rocks are virtually undeformed and in some mylonite zones pyroxene is little altered (Fig. 124). Generally, in retrograde mafic rocks pyroxene is replaced by pale green, fine-grained aggregates of hornblende or actinolite, with subordinate greenish-brown to brown biotite (particularly next to Fe-Ti oxide grains), and, locally, quartz, epidote and carbonate (Fig. 130). Dolerite dykes commonly retain a recognisable sub-ophitic texture.

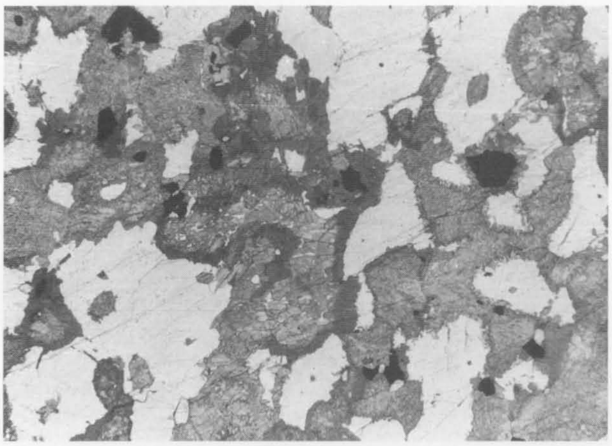

Figure 130. Retrogressed, but undeformed mafic granulite; east end of Algae Lake. Pyroxene is replaced by aggregates of pale green secondary amphibole, commonly rimmed by darker green to bluish-green amphibole, with minor epidote and brown biotite. Some primary olive-green hornblende survives. Sample 86286202; width of field: 5mm.

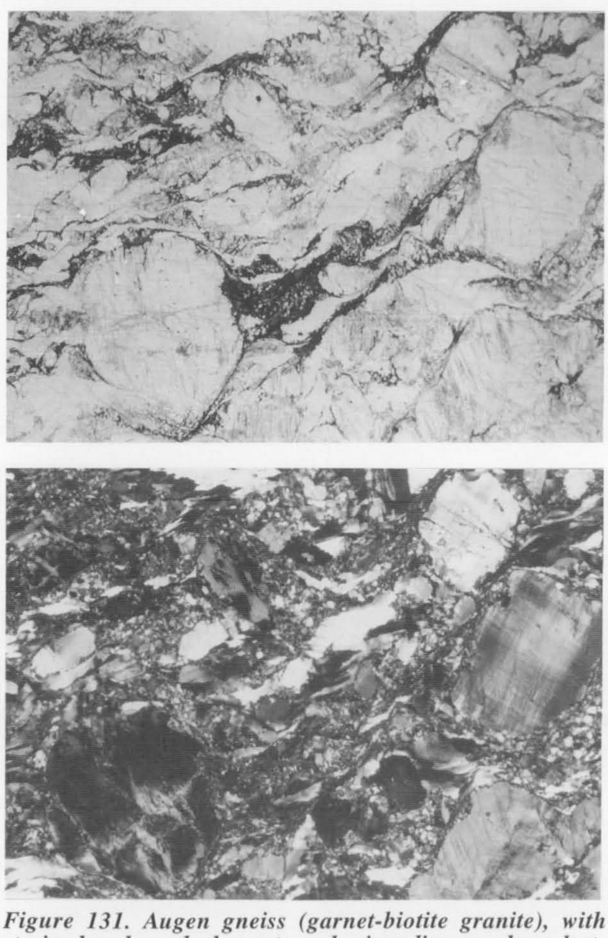

Figure 131. Augen gneiss (garnet-biotite granite), with strained and crushed quartz and microcline porphyroclasts enclosed in very fine-grained polygonal aggregates of quartz, feldspar, biotite, and minor garnet; Mount Barr-Smith. Sample 86286005; cross-polarised light in lower photo; width of field: 15mm.

Biotite is the most common alteration product of orthopyroxene in felsic gneiss, but yellowish-brown iddingsite is also widespread. Some pseudomorphs after orthopyroxene have cores of iddingsite and rims of pale green to colourless clinoamphibole, suggesting that the latter formed during an earlier retrogressive phase than the former. Some rocks show alteration of pyroxene to biotite (or chlorite) + quartz + epidote ± carbonate.

Other retrograde effects include chloritisation of biotite, sericitisation and saussuritisation of feldspar, and replacement of olivine (in mafic dykes) by ferruginous serpentine, rimmed by amphibole. Calc-silicate bodies are locally converted to phlogopite-tremolite schist. Cordierite in metapelites is locally replaced by biotite + sillimanite, and commonly by pinite. Although both reactions are consistent with an increase in P_{H2O} (Grant 1985), the former indicates a higher grade retrogression, implying at least two retrograde events.

The age of these retrogressions is unknown, but they clearly postdate the 1140 Ma dolerite dykes, and may be Neoproterozoic-Cambrian, when resetting of Rb-Sr isotopic systems occurred on a mineralogical scale (Sheraton et al. 1990).

Dolerites in the Obruchev Hills show evidence of a higher grade overprint (amphibolite to granulite-facies), but it is not known whether this occurred soon after emplacement or much later.

Denman Glacier area

Like the Bunger Hills area, the Denman Glacier area was metamorphosed at granulite facies. Orthopyroxene and clinopyroxene are widespread in felsic and mafic rocks. There are few diagnostic assemblages in metasediments, but garnet + biotite + sillimanite-bearing rocks crop out at Mounts Strathcona and Gist. The association sillimanite + muscovite at Mount Strathcona (Nockolds 1940) is presumably a retrograde effect. Garnet amphibolite inclusions in granite gneiss at Cape Harrison and Possession Rocks contain coexisting garnet and clinopyroxene.

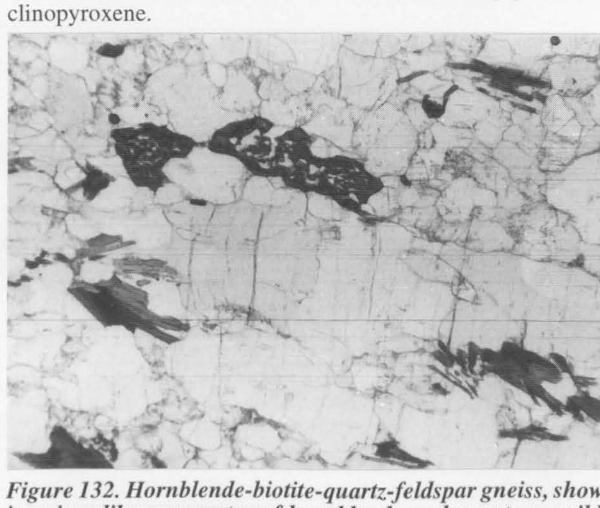

Figure 132. Hornblende-biotite-quartz-feldspar gneiss, showing sieve-like aggregates of hornblende and quartz, possibly replacing pyroxene, and preferred orientation of biotite; Jones Rocks. Sample 86285886; width of field: 2.7mm.

P-T estimates are only available for the Archaean two-pyroxene felsic orthogneiss from Cape Charcot, but they suggest slightly higher temperatures than for similar rocks in the Bunger Hills area (Table 23; Fig. 129). Allowing for the likely overestimates of the Wood & Banno (1973) and Wells (1977) geothermometers, an equilibration temperature of about 800–850°C for this rock is probable. The Johnson & Rutherford (1989) Al-in-hornblende geobarometer gives a relatively low pressure of 3.5 kb.

The effects of retrograde metamorphism are widespread in gneiss and many of the intrusive rocks, and are commonly associated with strong deformation. Granite at Mount Barr-Smith has been deformed to augen gneiss, with strongly aligned biotite and strained and recrystallised quartz and feldspar (Fig. 131). Orthopyroxene is partly replaced by cummingtonite in quartzite at Mount Strathcona. Felsic gneiss at Jones Rocks, like the diorite at Delay Point (Fig. 88), contains sieve-like aggregates of hornblende and quartz (Fig. 132), suggesting replacement of original pyroxene. The age of this apparent retrogression is not known for certain, but is most probably Neoproterozoic to Cambrian (500–600 Ma), when Pb loss from older zircon and growth of new zircon occurred in the Mount Charcot orthogneiss (Black et al. 1992b). It may also have been contemporaneous with greenschist-facies metamorphism of basalt at Mount Sandow.

Discussion

Geological history of the Bunger Hills area

Isotopic age data are summarised in Table 24 and a provisional geological history of the Bunger Hills area is given in Table 25.

The only indication of Archaean rocks in the area is an Y-depleted tonalite from the Obruchev Hills, which was emplaced about 2640 Ma ago. The earliest dated events in the Bunger Hills were emplacement of felsic igneous rocks (granodiorite) about 1500 and 1700 Ma ago. T_{DM}^{Nd} ages for these, and for 1150–1170 Ma plutonic rocks, are significantly older at 1840–2310 Ma (Table 8). However, the chemical compositions of all but one of these rocks suggest either direct mantle derivation (the gabbroic intrusives) or partial melting of a mafic source (the Y-depleted granodiorite), and the model ages may, therefore, reflect earlier mantle enrichment or melting, or crustal contamination, rather than generation of felsic crust (Rudnick 1990). Hence, in the absence of further isotopic data, the age of formation of felsic crust in the Bunger Hills (event 2 on Table 25) is uncertain. The limited data do, nevertheless, suggest that rocks in the Obruchev Hills and Bunger Hills formed at quite different times before both underwent high-grade metamorphism at about 1190 Ma.

Granulite-facies metamorphism, at least three deformations and emplacement of voluminous compositionally diverse suites of plutonic rocks all occurred within a period of 40 Ma or so. A similar situation has been reported for the Vestfold Block, where granulite-facies metamorphism, deformation and emplacement of various plutonic rocks all took place between 2526 and 2480 Ma ago (Black et al. 1991b). However, most of the analysed rocks there contain no isotopic evidence of a significantly older crustal history, although zircon cores in two orthogneisses from the northern Vestfold Block are up to 2800 Ma old. They differ in this respect from the Bunger Hills, where, on the basis of the limited data available, felsic crust appears to have formed in the Palaeo–Mesoproterozoic, well before the 1190 Ma granulite-facies metamorphism.

High-grade metamorphism and plutonism in the Bunger Hills were followed by a complex sequence of brittle-ductile deformation (formation of shear and mylonite zones), emplacement of minor granite and pegmatite bodies and intrusion of dolerite dykes of several chemically distinct suites (events 10–15 on Table 25). Many of these events apparently took place between emplacement of the plutonic rocks and the dolerite dykes, but granite/pegmatite emplacement and shear zone formation may have continued until (or resumed at) about 500 Ma. Rb-Sr and K-Ar isotopic systems were partly reset at about that time (Ravich et al. 1968; Sheraton et al. 1990) and, as discussed below, this may be correlated with the Ross orogeny of the Transantarctic Mountains (Elliot 1975) and the Pan-African orogeny elsewhere in Gondwana (Clifford 1974; Cooper 1990). Much of the retrograde metamorphism of both dolerite dykes and country rocks, which is particularly evident in the southeastern Bunger Hills, may be of similar Cambrian age. The only reasonably precisely dated event of this age in the Bunger Hills is the emplacement of alkaline mafic dykes about 500 Ma ago (Sheraton et al. 1990).

Table 24. Isotopic age determinations from the Bunger Hills-Obruchev Hills and Denman Glacier areas.

Locality	*Rock type*	*Method*	*Age (Ma)*	*Remarks*	*Reference*
NE Obruchev Hills	Tonalitic orthogneiss	U-Pb(Z)	2641^{+16}_{-14}	Emplacement age	Sheraton et al. (1992)
SW Bunger Hills	Granodioritic orthogneiss	U-Pb(Z-IM)	1699^{+19}_{-14}	Emplacement age	Sheraton et al. (1992)
Thomas Island	Granodioritic orthogneiss	U-Pb(Z-IM)	1521±29	Emplacement age	Sheraton et al. (1992)
Thomas Island	Granodioritic orthogneiss	U-Pb(Z-IM)	1190±15	Pb loss (high-grade metamorphism)	Sheraton et al. (1992)
NE Obruchev Hills	Tonalitic orthogneiss	U-Pb(Z-IM)	1040±53	Pb loss	Sheraton et al. (1992)
SW Bunger Hills	Granodioritic orthogneiss	U-Pb(Z-IM)	990^{+140}_{-170}	Pb loss	Sheraton et al. (1992)
SW of Algae Lake	Quartz monzogabbro	U-Pb(Z)	1171±3	Emplacement age	Sheraton et al. (1992)
E of Paz Cove	Quartz monzogabbro	U-Pb(Z)	1170±4	Emplacement age	Sheraton et al. (1992)
Booth Peninsula	Quartz monzodiorite	U-Pb(Z)	1151±4	Emplacement age	Sheraton et al. (1992)
Various Bunger Hills	Group 3A dolerites	Rb-Sr(WR)	1220±80	IR 0.7043±0.0006	Sheraton et al. (1990)
Mainly Obruchev Hills	Group 4E dolerites	Rb-Sr(WR)	1110±160	IR 0.7029±0.0003	Sheraton et al. (1990)
Geomorfologov Peninsula	Group 4D dolerite	Sm-Nd(Min)	1120±40	IR 0.51132±0.00005	Sheraton et al. (1990)
Thomas Island	Group 2 high-Mg dolerite	Rb-Sr(WR+Min)	645±121	IR 0.7057±0.0005 (reset age)	Sheraton et al. (1990)
NE Obruchev Hills	Group 4E dolerite	Rb-Sr(WR+Min)	550±24	IR 0.704±0.001 (reset age)	Sheraton et al. (1990)
Currituck Island	Group 2 high-Mg dolerite	Rb-Sr(WR+Min)	514±6	IR 0.7062±0.0007 (reset age)	Sheraton et al. (1990)
Miles Island	Alkali basalt	Rb-Sr(WR+Min)	502±12	IR 0.7168±0.0002	Sheraton et al. (1990)
N Taylor Islands	Trachybasalt	Rb-Sr(WR+Min)	502±7	IR 0.7085±0.0002	Sheraton et al. (1990)
Cape Charcot	Tonalitic orthogneiss	U-Pb(Z-IM)	3003±8	Emplacement age	Black et al. (1992b)
Cape Charcot	Tonalitic orthogneiss	U-Pb(Z-IM)	2889±9	New zircon growth (high-grade metamorphism)	Black et al. (1992b)
Mount Sandow	Sericite schist	?K-Ar	610		Ravich et al. (1968)
Cape Charcot	Tonalitic orthogneiss	U-Pb(Z-IM)	600, ?550	New zircon growth	Black et al. (1992b)
Cape Charcot	Tonalitic orthogneiss	U-Pb(Z-IM)	573±57	Pb loss	Black et al. (1992b)
Cape Charcot	Tonalitic orthogneiss	U-Pb(Z-IM)	567±49	Pb loss	Black et al. (1992b)
Watson Bluff	Syenite	U-Pb(Z)	516±1.5	Emplacement age	Black et al. (1992b)
David Island	"Granosyenite"	K-Ar	560, 470, 460		Ravich et al. (1968)
Baldwin Rocks	Trachyte dyke	K-Ar	330		Ravich et al. (1968)

IM, ion microprobe; IR, initial $^{87}Sr/^{86}Sr$ or $^{143}Nd/^{144}Nd$ ratio; Min, mineral; WR, whole rock; Z, zircon.

Regional correlations

The geological histories of the adjacent parts of the East Antarctic Shield are mostly poorly known and there is a dearth of modern geochronological data.

As has been shown, granulite-facies metamorphic rocks in the area west of the Denman Glacier differ from those of the Bunger Hills area in having only a small proportion of clearly sedimentary origin, and no unmetamorphosed dolerite dykes have been found. The only metamorphic rock to have been dated, a tonalitic orthogneiss from Cape Charcot, was emplaced about 3000 Ma ago and underwent high-grade metamorphism at about 2890 Ma; there is no evidence for metamorphism at 1190 Ma, but new zircon grew and Pb was lost from older zircon at 500-600 Ma (Black et al. 1992b). The Sandow Group (to the east of the present Denman Glacier) may have been deposited shortly before this time, in association with mafic intrusive and extrusive activity. Extensive syenitic to granitic plutons, with post-orogenic or anorogenic (A-type) chemical characteristics, were emplaced at 516 Ma. A-type magmatism in some other terranes appears to be an early manifestation of continental rifting (Anderson & Cullers 1978; Emslie 1978).

There are several possible explanations for the apparent lack of isotopic evidence for Mesoproterozoic metamorphism in the Denman Glacier area. The Neoproterozoic-Cambrian tectonothermal event was much more intense than in the Bunger Hills, and evidence of the earlier metamorphism may have been obliterated. However, this would make it difficult to explain the survival of evidence for Archaean igneous and metamorphic events. Alternatively, the Denman Glacier region may have been at a relatively high crustal level in the Mesoproterozoic, and any metamorphism of only low to medium grade. Finally, and perhaps most likely, the two areas may not have been juxtaposed at that time (Black et al. 1992b).

Although granulite-facies metamorphism apparently occurred in the Archaean, the time of the most extensive new zircon growth, T_{DM}^{Nd} model ages for other rocks in the area (intermediate to felsic intrusives and a garnet-biotite paragneiss) are much younger at 1600–2280 Ma (Table 21), indicating considerable continental crust formation and at least one period of high-grade metamorphism in post-Archaean times. It is possible that metadolerite xenoliths, some of which have relict igneous textures, in intermediate to felsic intrusives at Mount Strathcona (Ravich et al. 1968) and Mount Barr-Smith (Nockolds 1940) are the deformed equivalents of the Bunger

Table 25. Summary of the geological history of the Bunger Hills area.

	Approximate age (Ma)
1. Emplacement of oldest granitic rocks, predominantly tonalite (Obruchev Hills).	2640
2. ?Felsic crust formation.	~2000–2200
3. Deposition of sediments; emplacement of felsic intrusives/extrusives; ?high-grade metamorphism.	1500–1700
4. Emplacement of mafic and ultramafic bodies (dykes?), now boudinaged.	
5. Granulite-facies metamophism (M_1) at about 750-800°C and 5–6kb, and deformation (D_1); formation of present foliation, intrafolial folds (F_1), and lineation (L_1); emplacement of granitic rocks and migmatisation.	1190
6. Emplacement of mafic dykes (subconcordant granulites).	
7. Formation of open to tight or isoclinal, variably plunging, commonly asymmetric or recumbent folds (F_2) under granulite-facies conditions (M_2).	
8. Major asymmetric, open to tight, shallow plunging, upright folding (F_3) on WSW-trending axes; north or NNW-trending major folds may be of the same generation or may represent a slightly younger event (F_4); syn-deformational emplacement of Paz Cove and Algae Lake intrusions (predominantly quartz gabbro and quartz monzogabbro), probably still at granulite facies (M_3).	1170
9. Emplacement of quartz monzodioritic and probably granitic rocks of Booth Peninsula batholith; emplacement of syn-plutonic mafic granulite dykes; ?emplacement of flat-lying dolerite dykes (group 1 tholeiites) (these pre-date dolerites of event 13, but may post-date some or all of events 10–12).	1150
10. Formation of shear/mylonite zones of at least two sets.	
11. Emplacement of pink granites and pegmatites (biotite ± hornblende or garnet), possibly associated with the plutonic rocks.	
12. Formation of shear/mylonite zones (events 10–12 are probably of very similar age, and all probably associated with retrograde metamorphism).	
13. Emplacement of abundant NW-trending mafic dykes (group 2 magnesian dolerites, groups 3 and 4 dolerites, and probably picrite/ankaramites).	1140
14. Formation of shear/mylonite zones (at least some co-eval with mafic dyke emplacement).	
15. Emplacement of pink granites and pegmatites (muscovite + biotite); ?retrograde metamorphism (particularly in southeast Bunger Hills); possibly co-eval with some mylonites of event 14.	
16. Emplacement of east-trending alkali basalt and trachybasalt dykes (age relations with pink granites (15) not known). ?Final uplift towards the surface.	500
17. ?Emplacement of trachyte dykes (Geologov Island).	

Hills dolerites, but there are no chemical or isotopic data to confirm this. Indeed, gabbro and diorite at Cape Kennedy and Delay Point do not appear to be chemically related to the gabbroic plutons of the Bunger Hills.

A similar range of rock types near the Soviet base at Mirny (Fig. 133), about 250 km west of David Island, have been described in detail by Ravich et al. (1968). The granulite-facies country rocks consist mainly of interlayered tonalitic orthogneiss and mafic granulite, with minor garnet-bearing paragneiss. These are intruded, in turn, by commonly dyke-like gabbroic bodies (tholeiitic dolerite and gabbronorite), 'charnockites' (mainly orthopyroxene monzodiorite, quartz monzodiorite and granodiorite, and fayalite quartz monzonite and granite) and several generations of aplite and pegmatite.

The Mirny gabbroic bodies commonly have chilled margins and essentially igneous textures, although locally much recrystallised, and, hence, they postdate the peak of high-grade metamorphism. In this respect they resemble the Bunger Hills intrusions, which were emplaced shortly after the metamorphic peak. However, the gabbroic rocks are chemically different from either the Bunger Hills gabbroic plutons or dolerite dykes. They have much higher TiO_2 and P_2O_5 than the Bunger Hills gabbroic rocks, and, unlike most of the dykes, are strongly Hy-normative and have lower K_2O. They are also different from the Denman Glacier mafic intrusives, none of which has both the high TiO_2 and P_2O_5 of the Mirny rocks. In contrast, the fayalite quartz monzonite and granite appear, on major element data (Ravich et al. 1968), to be compositionally similar to the David Island quartz monzonite, and have given a similar Rb-Sr isochron age of 502±24 Ma (McQueen et al. 1972).

As in the Denman Glacier area, this igneous activity was accompanied by much resetting of the K-Ar system in the country rocks (Ravich et al. 1968). However, in the absence of definitive geochronological data, the ages of high-grade metamorphism and mafic intrusives at Mirny, as in the Denman Glacier area, are uncertain and regional correlations (Table 26) can only be tentative.

The nearest major outcrops east of the Bunger Hills are the Windmill Islands (Fig. 133), about 400 km distant and the site of Casey Station. The geology of this area has been described by Blight & Oliver (1977, 1982). The Windmill Metamorphics consist of amphibolite to granulite-facies metabasite, felsic orthogneiss, and cordierite±sillimanite±garnet-bearing metapelites. They are intruded by the Ardery Charnockite (mainly clinopyroxene-biotite-hornblende-orthopyroxene granite, granodiorite and quartz monzonite), emplaced between D_2 and D_3, the Ford Granite (porphyritic

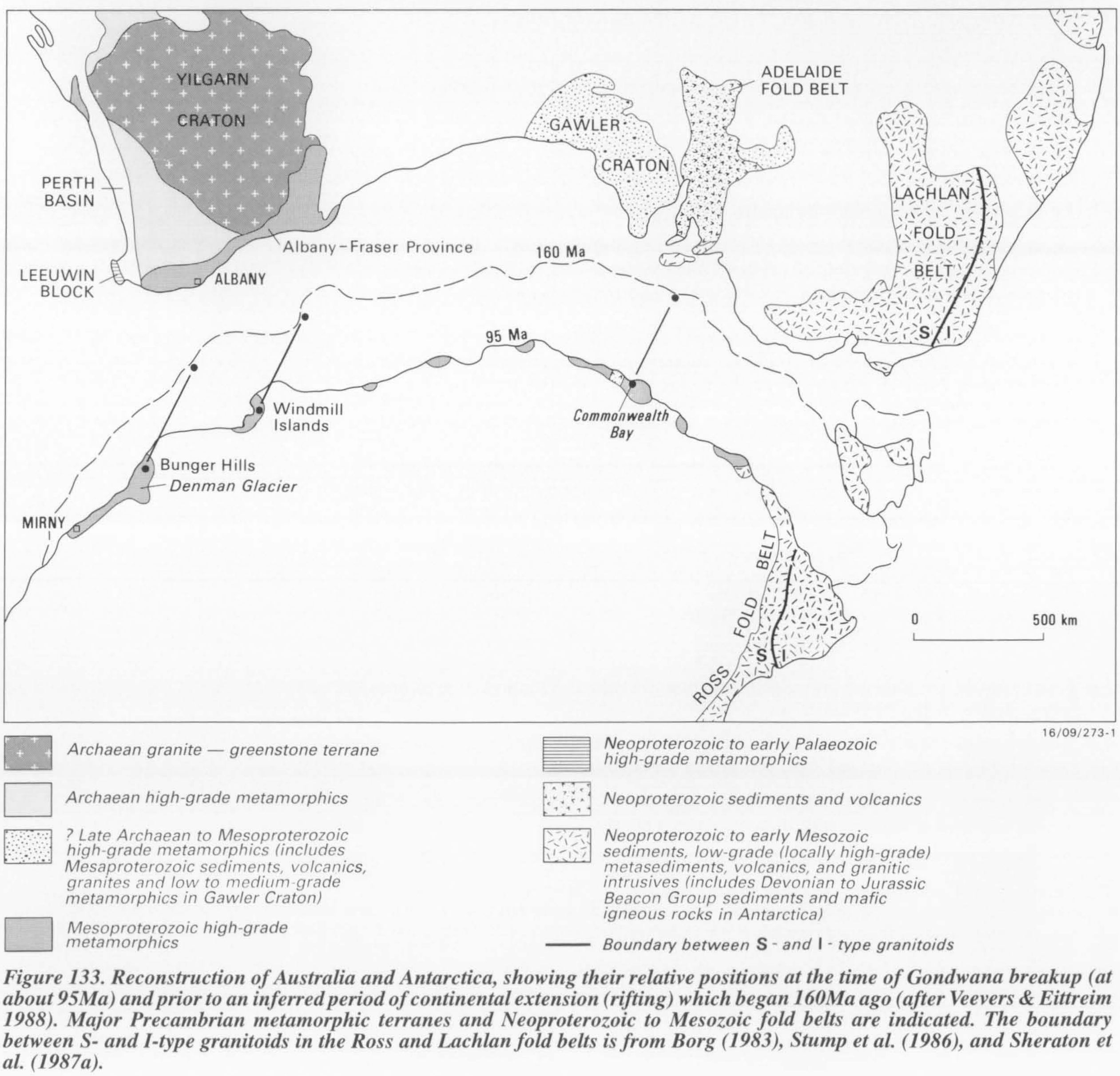

Figure 133. Reconstruction of Australia and Antarctica, showing their relative positions at the time of Gondwana breakup (at about 95Ma) and prior to an inferred period of continental extension (rifting) which began 160Ma ago (after Veevers & Eittreim 1988). Major Precambrian metamorphic terranes and Neoproterozoic to Mesozoic fold belts are indicated. The boundary between S- and I-type granitoids in the Ross and Lachlan fold belts is from Borg (1983), Stump et al. (1986), and Sheraton et al. (1987a).

hornblende-biotite granite), and various tholeiitic to alkaline mafic dykes (Blight & Oliver 1977).

Unfortunately, as in much of East Antarctica, reliable isotopic ages for the Windmill Islands are few, so that unambiguous correlations are presently impossible. Oliver et al. (1983) reported a lower concordia intercept zircon U-Pb age of 1275±21 Ma (interpreted as the age of metamorphism) and an upper intercept age of 2529±108 Ma (taken to represent a provenance age of the sediment) for a paragneiss. However, ages from conventional U-Pb dating of zircon can be geologically meaningless, particularly, as in this case, for 'reverse discordia' (see Black & Sheraton 1990). The younger age may, therefore, not be as accurate an estimate of the time of metamorphism as the error limits suggest, and the older age might also be in error. Williams et al. (1983) obtained U-Pb zircon ion-microprobe ages of 1450^{+70}_{-90} and 2990^{+230}_{-190} Ma for

Table 26. Provisional correlation of events in the Bunger Hills and Denman Glacier areas with those in the Windmill Islands and Albany Mobile Belt.

	Bunger Hills Area	Denman Glacier-Mirny Area	Windmill Islands	Albany Mobile Belt (AMB)	Age (Ma)
1.		Emplacement of granitic rocks (tonalite); ?high-grade metamorphism		Felsic crust formation; emplacement of granitic intrusives; deposition of sediments; high-grade metamorphism (northern part of AMB, adjacent to Yilgarn Craton).	2900–>3200
2.	Emplacement of granitic intrusives (mainly tonalite) (Obruchev Hills)		Felsic crust formation	Emplacement of granitic intrusives and volcanics; high-grade metamorphism and deformation (northern AMB)	2550–2750
3.				Emplacement of dolerite dykes	2410
4.	?Felsic crust formation	?Felsic crust formation		Felsic crust formation; ?deposition of sediments	~2000–2200
5.	?Deposition of sediments; emplacement of granitic intrusives; ?high-grade metamorphism	?Felsic crust formation	?Deposition of sediments: emplacement of granitic intrusives; high-grade metamorphism		~1450–1700
6.	Emplacement of mafic and ultramafic bodies			?Emplacement of dolerite dykes	
7.			?Metamorphism	Emplacement of tonalitic intrusives; ?high-grade metamorphism. Felsic crust formation at about this time in Leeuwin Block	~1290
8.	Granulite-facies metamorphism and deformation (D_1); emplacement of granitic intrusives		?Metamorphism	Granulite-facies metamorphism and deformation (D_1); emplacement of granitic intrusives and pegmatites	1190
9.	Emplacement of mafic dykes				
10.	Granulite-facies metamorphism and deformation (D_2)				
11	Major asymmetric folding (D_3); emplacement of gabbroic to quartz monzogabbroic intrusives under high-grade conditions		Emplacement of granitic intrusives (Ardery Charnockite); high-grade metamorphism		1170
12.	Emplacement of quartz monzodioritic and granitic intrusives, and flat-lying dolerites				1150
13.	Brittle deformation; emplacement of minor granitic bodies and pegmatites				
14.	Emplacement of abundant dolerite dykes				1140
15.			Emplacement of granitic intrusives (Ford Granite); uplift and cooling (closure of K-Ar and Rb-Sr systems in minerals); ?brittle deformation ?emplacement of dolerite dykes	Uplift and cooling (closure of K-Ar and Rb-Sr systems in minerals); ?brittle deformation;	~1060–1160
16.	Retrograde metamorphism; brittle deformation; emplacement of minor granitic bodies and pegmatites				
17.	Partial resetting of Rb-Sr and K-Ar systems in minerals	?Metamorphism (Denman Glacier). Greenschist-facies metamorphism (Mt Sandow). Resetting of K-Ar system (Mirny)	?Emplacement of dolerite dykes	Emplacement of granitic intrusives and dolerite dykes; granulite-facies metamorphism (in Leeuwin Block). Resetting of Rb-Sr and K-Ar systems (in adjacent parts of Yilgarn Craton)	~450–650
18.	Emplacement of alkaline mafic dykes	Emplacement of syenitic to granitic intrusives (David Island, Mirny)	?Emplacement of alkaline dykes		500–520
19.	?Emplacement of trachyte dykes	Emplacement of trachyte dykes			330

Data sources: Black et al. (1992a, b), Blight & Oliver (1977, 1982), Ding & James (1991), Fletcher et al. (1983), Myers (1990a,b), Oliver et al. (1983), Pidgeon (1990), Ravich et al. (1968), Sheraton et al. (1990, 1992), Stuwe & Powell (1989a), Stuwe & Wilson (1990), Wilde & Murphy (1990), Williams et al. (1983).

a paragneiss, the former being attributed to high-grade metamorphism. A Rb-Sr isochron age of 1477±73 Ma (Sr_i 0.7032±0.0004) was also reported for a tonalitic orthogneiss.

Emplacement of felsic igneous rocks was thus apparently coeval with high-grade metamorphism about 1500 Ma ago. However, it is probable that metamorphism continued at least until (or also occurred at) about 1200 Ma, as the Ardery Charnockite was emplaced at about that time (Rb-Sr isochron age of 1172±68 Ma: Tingey 1991), and possibly as late as 1070±36 Ma (Rb-Sr isochron age of the Ford Granite); biotite Rb-Sr and K-Ar ages are mostly between 1060 and 1160 Ma (Tingey 1991).

The age of the Windmill Islands dolerite dykes is unknown, but some appear to have been derived from a similar mantle source to some of the Bunger Hills dykes. The resemblance is not close enough to allow an unequivocal correlation, but, in view of the chemical heterogeneity of dykes in the Bunger Hills alone, this is not surprising. An alkali basalt dyke is quite different in composition to those in the Bunger Hills (Sheraton unpublished data) and is therefore probably unrelated.

There are thus marked geological and geochronological similarities with the Bunger Hills area (Table 26). Indeed, it is likely that emplacement of granitic rocks in the Bunger Hills about 1500–1700 Ma ago was also accompanied by metamorphism. However, in contrast to the Bunger Hills-Denman Glacier region, there appears to have been little resetting of Rb-Sr and K-Ar isotopic systems in the Windmill Islands rocks during the Cambrian.

Mesoproterozoic metamorphism in the East Antarctic Shield east of the Windmill Islands appears to have been much earlier than in the Bunger Hills. At Point Martin in Adélie Land, 2440 Ma granodioritic orthogneiss was intruded by 1700 Ma late granite veins (zircon U-Pb ion microprobe data: Menot et al. 1993), whereas at Point Geologie, amphibolite-facies migmatitic gneiss was metamorphosed about 1700 Ma ago (Monnier et al. 1993). Micas from pegmatite and orthogneiss in the Cape Denison area of Commonwealth Bay, George V Land (Fig. 133), have Rb-Sr ages mostly between 1300 and 1650 Ma (Tingey 1991), and granodioritic orthogneiss was emplaced much earlier (2366±33 Ma U-Pb zircon age: Oliver et al. 1983).

In contrast, high-grade metamorphism in the extensive Mesoproterozoic terrane west of the Bunger Hills (Fig. 1) was significantly later (Sheraton et al. 1987c). U-Pb zircon ion-microprobe ages of 1030 and 1000 Ma for granitic gneiss in the Prydz Bay area, Princess Elizabeth Land (Kinny et al. 1993), are similar to that of zircon growth (1025±56 Ma) in a 1250 Ma dolerite dyke in the Archaean Vestfold Block, just to the north (Black et al. 1991a). Zircon from high-grade gneiss in the Rayner Complex of Enderby Land crystallised somewhat later at 960-980 Ma, the time of emplacement of the late orogenic (between D_2 and D_3) Mawson Charnockite (Black et al. 1987; Young & Black 1991). Generally similar U-Pb zircon ion microprobe (L.P. Black, unpublished data) and Rb-Sr isochron (Tingey 1991) ages have been reported from the northern Prince Charles Mountains of MacRobertson Land.

Although comparable Rb-Sr isochron ages (1030–1130 Ma) have been reported for granulite-facies metamorphics in the Lützow-Holm Bay area of eastern Dronning Maud Land (Yoshida et al. 1983; Shibata et al. 1986), more recent ion microprobe U-Pb zircon dating has shown that the regional metamorphism in this area was only about 530 Ma ago (Shiraishi et al. 1992). However, Shiraishi & Kagami (1989) obtained a Sm-Nd isochron age of 999±164 Ma for metamorphics in the Sør Rondane Mountains to the west and magmatic activity and metamorphism occurred between 1130 and 1060 Ma (U-Pb zircon ages) in the Kottas Mountains of western Dronning Maud Land (Arndt et al. 1989). The latter may be correlated with the Kibaran metamorphics of southern Africa (Weber & Arndt 1991; Groenewald 1993).

It is noteworthy that the Bunger Hills metamorphic rocks are considerably younger than other, mostly Archaean, parts of the East Antarctic Shield cut by dolerite dyke swarms. All three well-documented Archaean cratonic blocks, the Napier Complex of Enderby Land (Sheraton et al. 1980, 1987c), the Vestfold Hills of Princess Elizabeth Land (Oliver et al. 1982; Collerson & Sheraton 1986; Black et al. 1991b) and the southern Prince Charles Mountains (Tingey 1982, 1991), contain dolerite dyke swarms (Fig. 1). The most abundant dolerites in the Vestfold Hills (Group II), correlated with geochemically similar dykes in the Napier Complex and southern Prince Charles Mountains (Sheraton et al. 1987b), were emplaced in two distinct episodes at 1241±5 and 1380±7 Ma ago (zircon U-Pb ion microprobe ages, Lanyon et al. 1993); other dykes are as old as 2240 Ma (Sheraton et al. 1987b; Lanyon et al. 1993).

Because such dykes are absent from the nearby ~1000 Ma high-grade terrane, except as deformed and metamorphosed relics, they have proved useful stratigraphic markers. However, it is clear from the Bunger Hills that the presence of dolerite dyke swarms does not necessarily indicate an Archaean age for the country rocks.

The Bunger Hills dykes are younger (~1140 Ma) than those in the Archaean cratons. They are also geochemically distinct from these, but were derived from generally similar mantle sources (Sheraton et al. 1990). It is noteworthy that mafic dykes in the Bunger Hills, Vestfold Block, and Napier Complex were emplaced relatively deep in the crust not long after high-grade metamorphism, although those in the last two areas are Palaeoproterozoic (~2240 Ma).

Gondwana reconstruction and tectonic synthesis

Gondwana reconstructions place the Bunger Hills area next to southwestern Australia. The Antarctica-Australia fit of Veevers (1990), based on satellite mapping of oceanic fracture zones, is shown in Figure 133. This reconstruction is similar to those of Sproll & Dietz (1969) and Smith & Hallam (1970), which were based on computer best fits of the 1000 and 500 fathom isobaths, respectively, but an inferred initial north-westerly spreading direction puts Tasmania roughly midway between Cape Adare (Antarctica) and Cape Howe (southeastern Australia). However, Veevers & Eittreim (1988) postulated, from structural and geophysical evidence, that a period of southwest-directed crustal extension occurred during pre-breakup rifting between 160 and 95 Ma ago. Their pre-160 Ma Gondwana reconstruction is also indicated in Figure 133.

This pre-rifting reconstruction is broadly consistent with many geological criteria, including the correlation of the early Palaeozoic Bowers Group of northern Victoria Land with the Dundas Trough of western Tasmania (Laird et al. 1977) and the correlation of distinct terranes and boundaries between S-type and I-type granitic rocks in northern Victoria Land and southeastern Australia (Fig. 133) (Borg 1983; Stump et al. 1986; Sheraton et al. 1987a; Flöttmann et al. 1993).

The juxtaposition of Palaeoproterozoic orthogneiss and Proterozoic mafic dykes of Commonwealth Bay with similar rocks in the southern part of the Gawler Craton in the Eyre Peninsula, South Australia (Oliver et al. 1983; Sheraton et al. 1989) is not as good as in the reconstruction at the time of breakup (95 Ma), but this might be due to the earlier crustal extension having been less extensive in this area than proposed by Veevers & Eittreim's (1988) model or, possibly, to a

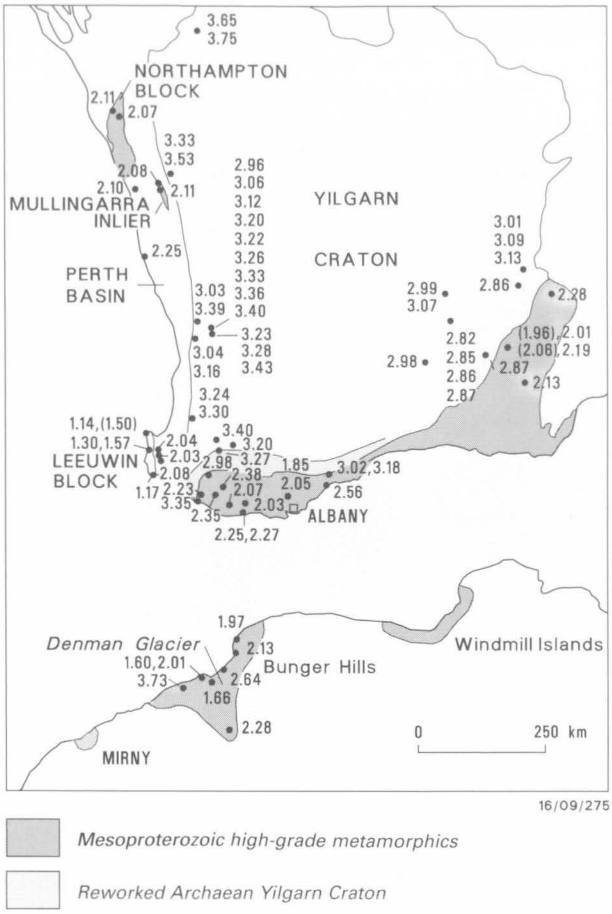

Figure 134. Pre-rifting reconstruction of southwestern Australia and the adjacent part of East Antarctica (from Figure 133), showing Mesoproterozoic metamorphic terranes and areas of reworked Archaean rocks in the northern part of the Albany Mobile Belt (after Beeson et al., 1988). T^{Nd}_{DM} model ages (in Ga) for felsic gneisses are indicated, using data from Black et al. (1992a, b), Fletcher et al. (1983, 1985, 1991), McCulloch (1987), McCulloch et al. (1883a, b), and Myers (1990b). Parameters used are $(^{143}Nd/^{144}Nd)_{DM} = 0.51317$, and $(^{147}Sm/^{144}Nd)_{DM} = 0.225$ (0.214 for Archaean rocks); $^{143}Nd/^{144}Nd$ was adjusted where necessary to allow for present day normalisation to $^{146}Nd/^{144}Nd$.

structural discontinuity in the rift zone. Certainly, continental breakup is likely to have been tectonically highly complex. For example, Willcox & Stagg (1990) have proposed, from geophysical data, a period of northwest–southeast crustal extension in the Great Australian Bight during the late Jurassic to early Cretaceous, whereas Harris & Li (1991) suggested, on structural evidence, that northeast–southwest extension may have occurred during the early Cretaceous (as well as the Cambrian) in the Albany Mobile Belt of southwestern Australia.

The Commonwealth Bay and Adélie Land metamorphic rocks can probably be correlated with those affected by the Kimban orogeny in the Gawler Craton, where metamorphism and emplacement of granitic and volcanic rocks occurred between 1580 and 1820 Ma ago (Parker & Lemon 1982; Webb et al. 1986). This event was followed by the much weaker Wartakan event, about 1450–1500 Ma ago, possibly coeval with high-grade metamorphism in the Windmill Islands and eastern Albany-Fraser Province (see below).

Overall, the Gondwana reconstruction of Veevers & Eittreim (1988) appears to fit the geological and geophysical evidence reasonably well, although, of course, it may yet be revised. It is therefore used as the basis for the following discussion and its implications for the geological evolution of the Bunger Hills-Denman Glacier region will be considered. It places the Bunger Hills about 400 km southwest of Albany at 160 Ma (Figs 133, 134), in this respect being somewhere between the two reconstructions discussed by Oliver et al. (1983) and Black et al. (1992b).

Recent U-Pb zircon ion-microprobe analyses of rocks from the western part of the Albany-Fraser Province (the Albany Mobile Belt) by Black et al. (1992a) have shown that amphibolite-granulite facies metamorphism and deformation (M_1-D_1), as well as several episodes of felsic magmatism, occurred within 10 Ma or so of 1190 Ma, i.e. essentially coeval with metamorphism and deformation in the Bunger Hills (M_1-D_1 and probably M_2-D_2). Granulite-facies metamorphism also occurred in the Musgrave Block of central Australia (Fig. 135) at about the same time (Gray 1978; Sun & Sheraton 1992).

The northern part of the Albany Mobile Belt consists partly of reworked Archaean (3000 Ma) gneiss of the southern Yilgarn Craton (Fig. 134) (Fletcher et al. 1983; Black et al. 1992a), although there is also evidence for a late Archaean component, probably correlating with further metamorphism and widespread felsic magmatism in the Yilgarn Craton (Wilde 1990; Myers 1990a). There are, however, some compositional differences between the northern Albany Mobile Belt — the Biranup Complex, which consists of intensely deformed tectonic slices of gneiss and gabbro — and the southern Yilgarn Craton (Myers 1990a).

Crust in the southern part of the Albany Mobile Belt is younger, T^{Nd}_{DM} model ages being mostly Palaeoproterozoic (1850–2350 Ma: Fletcher et al. 1983; Black et al. 1992a); tonalite was emplaced 1289±10 Ma ago, probably during high-grade metamorphism (Pidgeon 1990). Rb-Sr whole-rock isochron ages from the eastern part of the Albany-Fraser Province (the Fraser Range area) are older (1300–1700 Ma), and reflect a complex metamorphic history (Arriens & Lambert 1969; Bunting et al. 1976). Sm-Nd and Pb-Pb data for gabbro from the Fraser Complex indicate emplacement and metamorphism about 1300 Ma ago (Fletcher et al. 1991). These ages are generally comparable to those obtained from the Windmill Islands and consistent with the Veevers & Eittreim (1988) reconstruction of Gondwana (Fig. 135).

There are thus significant geological parallels between the Albany Mobile Belt and both the Bunger Hills and Windmill Islands (Table 26). The first two areas, at least, contain Archaean and Paleo–Mesoproterozoic protoliths and underwent high-grade metamorphism 1190 Ma ago, which was apparently the culmination of up to several hundred million years of metamorphism and felsic igneous activity. Paragneiss in the Windmill Islands contains Archaean detrital zircon (Oliver et al. 1983; Williams et al. 1983). In the Bunger Hills, mafic to felsic magmatism continued for 50 Ma or so after peak metamorphism, but, apparently, for no more than about 10 Ma in the Albany Mobile Belt. This phase of tectonic activity ended with the intrusion of dolerite dyke swarms in the Bunger Hills and possibly the Windmill Islands, but dykes of this age have not been found in the Albany Mobile Belt. Emplacement of the northwest-trending Boyagin dyke swarm, which is largely confined to the southwestern part of the Yilgarn Craton, was considered by Myers (1990b) to be related to Palaeoproterozoic–early Palaeozoic orogenic activity, and dolerite dykes in the Albany Mobile Belt itself were thought by Harris & Li (1991) to be of Cambrian age.

These similarities suggest that the Bunger Hills, Windmill Islands and the Albany-Fraser Province (orogen of Myers 1990a) once formed part of the same metamorphic belt. There are several possibilities for the nature of the tectonic event which caused this metamorphism. Myers (1990a) proposed

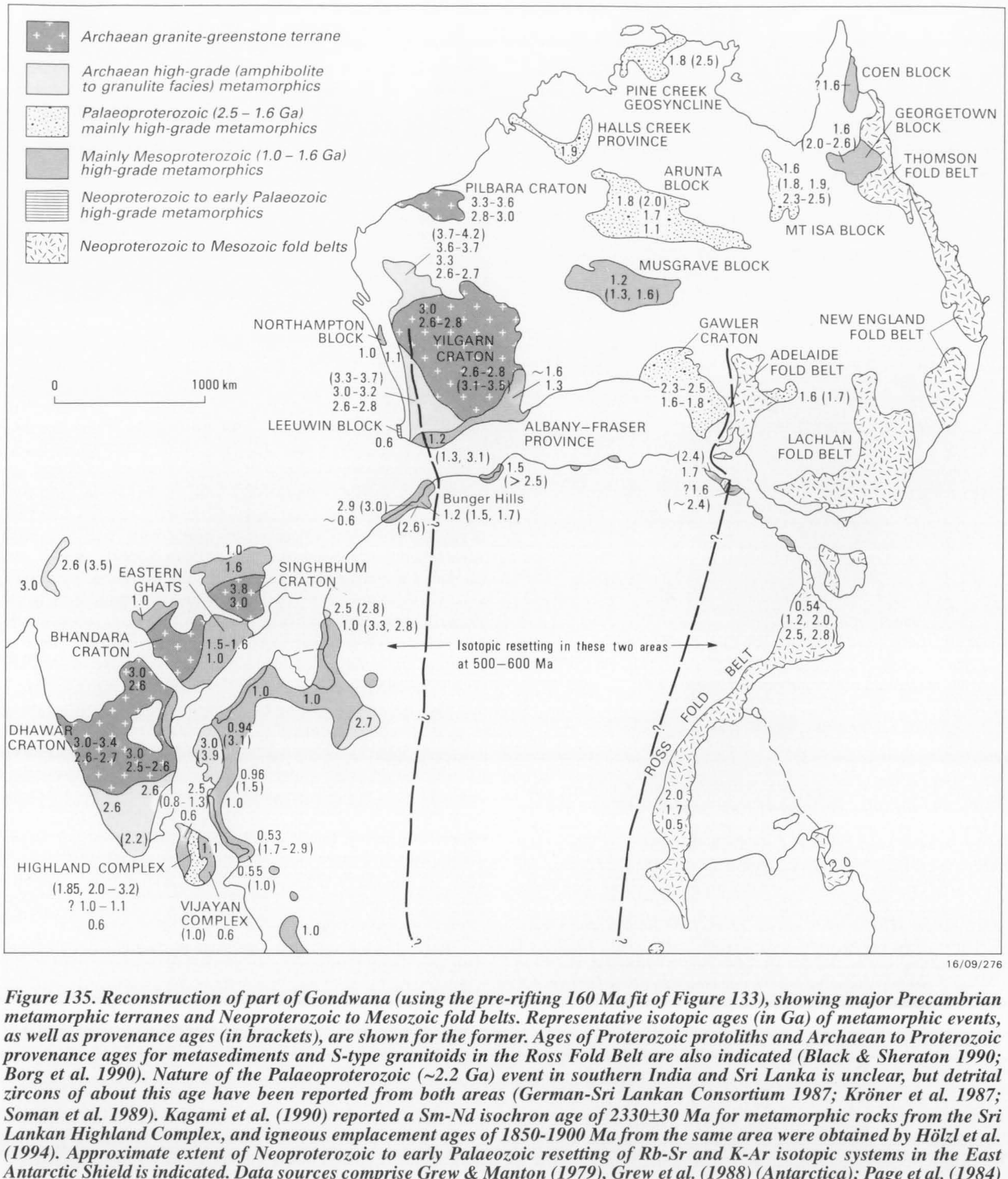

Figure 135. Reconstruction of part of Gondwana (using the pre-rifting 160 Ma fit of Figure 133), showing major Precambrian metamorphic terranes and Neoproterozoic to Mesozoic fold belts. Representative isotopic ages (in Ga) of metamorphic events, as well as provenance ages (in brackets), are shown for the former. Ages of Proterozoic protoliths and Archaean to Proterozoic provenance ages for metasediments and S-type granitoids in the Ross Fold Belt are also indicated (Black & Sheraton 1990; Borg et al. 1990). Nature of the Palaeoproterozoic (~2.2 Ga) event in southern India and Sri Lanka is unclear, but detrital zircons of about this age have been reported from both areas (German-Sri Lankan Consortium 1987; Kröner et al. 1987; Soman et al. 1989). Kagami et al. (1990) reported a Sm-Nd isochron age of 2330±30 Ma for metamorphic rocks from the Sri Lankan Highland Complex, and igneous emplacement ages of 1850-1900 Ma from the same area were obtained by Hölzl et al. (1994). Approximate extent of Neoproterozoic to early Palaeozoic resetting of Rb-Sr and K-Ar isotopic systems in the East Antarctic Shield is indicated. Data sources comprise Grew & Manton (1979), Grew et al. (1988) (Antarctica); Page et al. (1984) (Australia); Newton (1990), Rogers (1986), Sugden et al. (1990) (India); and Kagami et al. (1990) (Sri Lanka), together with other references quoted in the text.

a major continental collision event about 1200 Ma ago. The older protolith ages in the northern part of the Albany Mobile Belt, next to the Yilgarn Craton, are matched by Archaean rocks in the Obruchev Hills, southwest of the Bunger Hills. Evidence for collision in the Albany-Fraser Province includes tectonic interleaving of different crustal segments (Myers 1990a), a predominantly north to northwest-directed compressional deformation (Beeson et al. 1988; Black et al. 1992a), and increasing deformation towards the southern margin of the Yilgarn Craton (Harris et al. 1989a). Moreover, the last major regional deformation in the Bunger Hills (D_3) resulted from north-northwest-south-southeast compression, similar to that in the Albany-Fraser Province.

Stüwe & Powell (1989a) postulated that metamorphism in the Bunger Hills area took place during an extensional event, which was followed by compressive deformation caused by 'gravitational collapse'. They interpreted the apparently originally more widespread occurrence of coexisting spinel and quartz as reflecting an earlier metamorphic event at lower pressure (and possibly higher temperature) and, hence, deduced an anticlockwise P-T-time path for the area. Such an extensional model would imply essentially isobaric cooling after the metamorphic peak (Sandiford & Powell 1986; Bohlen 1987; Sandiford 1989a). In contrast, continental collision, which would be accompanied by major crustal thickening, is considered to produce a clockwise P-T-time path (England & Richardson 1977; Thompson & England 1984). In fact, as discussed above, we consider the petrographic evidence for an anticlockwise P-T-time path in the Bunger Hills to be inconclusive.

Although there is little evidence for the alternative clockwise path expected for a collisional model (i.e. no early high-pressure minerals or associations, such as kyanite), Bohlen (1987) has pointed out that the majority of granulite terranes contain no such evidence. A possible explanation is that many high-grade terranes may have been deep in the crust for a long time, so that any early mineral associations would have been destroyed, particularly during penetrative deformation (Harley et al. 1990). Ellis (1987) has postulated that granulites formed in the lower part of a doubly thickened crust would undergo only limited uplift before experiencing an extended period of near-isobaric cooling towards the base of a crust of normal thickness. In addition, more efficient detachment of thickened thermal boundary layers in the lithosphere beneath convergent orogens in the Precambrian, resulting from more vigorous mantle convection processes, may well have resulted in the obliteration of early high-pressure, low-temperature assemblages (Sandiford, 1989b).

Both collisional and crustal extension models have been invoked to explain the prolonged near-isobaric cooling of the Napier Complex (Sandiford 1985; Harley 1985; Ellis 1987; Harley et al. 1990). Either model would require a second orogenic cycle to uplift the lower crustal segment to the surface. Any early low-pressure event in the Bunger Hills may not have been directly related to the pervasive metamorphism (our M_1). Isotopic data show that felsic igneous activity (and presumably deformation and metamorphism) occurred over a period of several hundred million years up to 1200 Ma in the area. There is also evidence for a pre-D_1 layering (e.g. in F_1 fold hinges), which could well be of metamorphic origin. Moreover, the originally sub-horizontal (recumbent) foliation is not unequivocal evidence of extension, and could equally well have been formed during compression (Escher & Watterson 1974; Park 1981; Clarke 1988).

A third possibility is that high-grade metamorphism in the Bunger Hills area occurred in a continental arc tectonic environment (Andean or Cordilleran type of Pitcher 1982), which would have involved voluminous magmatism (Bohlen 1977), but relatively limited crustal thickening. In the Gondwana reconstruction used in Figures 133 and 134, the Bunger Hills are close to the line of the eastern edge of the Perth Basin (the Darling Fault), which marks the western limit of the Albany Mobile Belt. Hence, depending on the amount and direction of crustal extension and the consequent pre-rifting position of the Bunger Hills area relative to the Albany Mobile Belt, a continental collision (Himalayan or Hercynotype) tectonic setting for the Albany-Fraser Province and Windmill Islands may still be consistent with a continental arc environment for the Bunger Hills — although whether or not what is now the Australian continent extended significantly further west at that time is unknown. In this model, the subduction zone would have been oriented roughly east–west (in present-day terms), with a southerly dip.

The presence of abundant, largely mantle-derived plutonic rocks in the Bunger Hills is consistent with a continental arc setting (cf. Pitcher 1982), whereas granite (*s.s.*) plutons (presumably representing intracrustal melts) are more prominent in the Albany Mobile Belt and Windmill Islands. The Palaeoproterozoic model ages of granitic rocks in the Albany Mobile Belt (Fig. 134) (Fletcher et al. 1983; Black et al. 1992a) are consistent with this model. Moreover, the northeastern Highjump Archipelago apparently underwent metamorphism at significantly higher pressures than the rest of the Bunger Hills area, possibly due to a greater thickness of crust there.

There are significant analogies with the Cordilleran batholiths of the Andes, where the most voluminous (mafic to felsic) plutonism occurred during compressive deformation associated with active subduction, whereas predominantly mafic magmatic activity took place during periods of extension (Pichowiak et al. 1990; Soler & Bonhomme 1990). For example, in central Chile a pre-Andean (late Palaeozoic) phase of mostly tonalitic and granodioritic plutonism was followed by a transitional (Triassic to early Jurassic) phase of bimodal (leucogranite, gabbro) plutonism and dyke emplacement, and a final Andean (middle Jurassic to late Tertiary) phase, dominated by gabbro, diorite and tonalite (Parada 1990). The pre-Andean and Andean plutonism occurred in magmatic arcs developed during plate convergence, whereas the transitional phase was associated with an extensional regime.

Similarly, in the Bunger Hills, Y-depleted tonalitic to granodioritic magma, derived by melting of a mafic source (presumably subducted oceanic crust), was emplaced about 1700 Ma ago, and granodiorite at about 1500 Ma. Emplacement of voluminous mantle-derived gabbroic to granitic magmas at 1150–1170 Ma was clearly associated with compression, but a change to an extensional regime was marked by intrusion of dolerite dykes 1140 Ma ago. It is therefore quite possible that the 1200 Ma metamorphic peak (M_1-D_1) was also preceded by extension, as suggested by Stüwe & Powell (1989a).

There is some evidence for evolution of granitoids in the Bunger Hills from early (pre-M_1) tonalitic to granodioritic primitive arc type (low LILE, HFSE), through normal continental arc granite (higher LILE, low HFSE), to mature arc types (quartz monzodiorite with high LILE and HFSE), corresponding to an increasing within-plate component (Brown et al. 1984; Pearce et al. 1984). True within-plate granitoids (post-orogenic or anorogenic, commonly alkaline types) are apparently not represented (unless the rapakivi granites are such), but are present in the Denman Glacier area (the David Island batholith), albeit associated with a much younger tectonic event, as well as elsewhere in East Antarctica (Sheraton & Black 1988). The 1150–1170 Ma plutons appear to have been derived from much more isotopically enriched mantle source regions (perhaps with a higher subducted sedimentary component) than typical Andean batholiths (cf. Parada 1990; Soler & Rotach-Toulhoat 1990). However, this feature could be due to melting of enriched (sub-continental type) lithosphere associated with the continental crustal plates.

Although the presence of shear zones indicates some uplift before the intrusion of abundant dolerite dykes in the Bunger Hills 1140 Ma ago, extensive resetting of the Rb-Sr system on a mineralogical scale during the Cambrian suggests that final uplift towards the surface was delayed and that the Mesoproterozoic metamorphism was accompanied by only relatively limited crustal thickening. This contrasts with closure of the Rb-Sr and K-Ar systems within 100 Ma or so of high-grade metamorphism in the Windmill Islands and Albany Mobile Belt, consistent with relatively rapid post-collisional uplift in these areas. It is, of course, possible that resetting in the Bunger Hills was the result of early Palaeozoic igneous activity, although this would only be likely if the terrane was still deep in the crust.

Formation of the Bunger Hills metamorphics in a convergent tectonic regime is therefore considered to best fit the available geological constraints. Continental collision between the Yilgarn Craton and the East Antarctic Shield does not preclude the present Bunger Hills area from having been situated on an Andean plate margin at that time. Collisional terranes are, of course, likely to be tectonically and metamorphically complex, and P-T-time paths will vary considerably from place to place, particularly when there is extensive plutonic activity (Harley et al. 1990; Stüwe & Sandiford 1995).

The extensive Neoproterozoic-Cambrian plutonic activity in the Denman Glacier and Mirny areas indicates a major tectonothermal event, which may well have caused the eventual uplift of the Bunger Hills area. It may be correlated with high-grade metamorphism and magmatism that occurred in the Leeuwin Block (Fig. 134) between 550 and 600 Ma ago, based on zircon data for a felsic orthogneiss (Wilde & Murphy 1990). An event of this age in northwestern and central Australia was termed the Paterson orogeny by Myers (1990a), although in the extreme southwest of Australia it appears to have been largely confined to renewed activity in the Mesoproterozoic Pinjarra orogen.

The Veevers & Eittreim (1988) reconstruction (Fig. 135) places the Leeuwin Block next to the Denman Glacier area, which appears to define the eastern limit of major early Palaeozoic plutonism in this part of East Antarctic Shield. Moreover, this limit may also be marked by sedimentation and mafic igneous activity (the Sandow Group) of broadly similar age. The predominant foliation trend in the Leeuwin Block (and the Pinjarra orogen) is north–south (Myers 1990a,b), whereas it is north-northeast near Mirny (Ravich et al. 1968), and east-northeast in the Denman Glacier area, where many of the rocks have undergone considerable semi-brittle deformation. Hence, the Neoproterozoic–Cambrian event in the Denman Glacier and Mirny areas may well represent extension, to the south and west, of high-grade metamorphism in the Leeuwin Block.

There are, nevertheless, significant differences in the Precambrian histories of the two areas: T_{DM}^{Nd} model ages of rocks from the Leeuwin Block (1130–1570 Ma) are considerably younger than those from the Denman Glacier area (mostly 1600–2280 Ma, although Archaean orthogneiss is also present) (Myers 1990b; Black et al. 1992b), as well as those from the Bunger Hills and Albany Mobile Belt (Fig. 134). The Leeuwin Block protoliths may thus have been formed during the Mesoproterozoic Pinjarra orogeny of the extreme west of Western Australia (1000–1300 Ma; Myers 1990a,b). Black et al. (1992b) pointed out that these protoliths apparently formed at about the time of metasomatism of the source of the Bunger Hills dolerite dykes. Similarly, the protoliths of the Denman Glacier area rocks may have formed at about the same time as metasomatism of the mantle sources of the Bunger Hills gabbroic plutons and 500 Ma alkaline dykes, as well as being roughly coeval with felsic crust in the Albany-Fraser and Pinjarra orogens (Myers 1990b; Black et al. 1992a) and Bunger Hills.

It has already been pointed out that model ages (particularly those of mafic rocks) may be misleading, as a significant part of the LILE and LREE may have been derived from older subducted sedimentary material during magma generation above the subduction zone (Soler & Rotach-Toulhoat 1990). Nevertheless, even if the timing is not well constrained, there is evidence for several cycles of mantle metasomatism and felsic crust formation, which, if at least some of the David Island syenitic rocks are mantle derived, extended into the early Palaeozoic. It remains to be seen whether or not the equivalents (in terms of crustal formation ages) of the Leeuwin Block gneisses are present in Antarctica.

Myers (1990a) has pointed out that assembly of this part of Gondwana was probably not completed until the beginning of the Palaeozoic, possibly following breakup of an even larger supercontinent (Dalziel 1991). Thus, the Denman Glacier and Bunger Hills areas may represent distinct terranes that only moved together at about that time, thus accounting for their different lithologies and metamorphic histories.

According to Wilde & Murphy (1990), there was a change from compressional to extensional tectonics in the Leeuwin Block as early as 570 Ma ago, as indicated by the abundance of anorogenic (A-type) granitoids and metadolerite dykes. However, unlike the 516 Ma David Island A-type intrusions, those in the Leeuwin Block are foliated, and possibly not, therefore, truly anorogenic. Nevertheless, it is possible that the Perth Basin began to form at about this time. This major rift zone was certainly in existence by the early Silurian, and the Darling Fault Zone, which marks its eastern boundary, is much older (Myers, 1990b).

The proposed pre-breakup alignment of the Perth Basin and Denman Glacier (Fig. 134) suggests that the latter, which occupies a major trough (Drewry & Jordan 1983), may define a southerly extension of the Perth Basin rift. As has been shown, both structures define major geological discontinuities, whereas there are marked similarities in the geological histories of terranes to the east (Mesoproterozoic metamorphic rocks of the Bunger Hills area and Albany Mobile Belt) and west (Neoproterozoic–Cambrian metamorphic and plutonic rocks of the Denman Glacier area and Leeuwin Block). Such an alignment gives considerable support to the Veevers & Eittreim (1988) reconstruction, particularly because these are two of the very few major north–south trending structures that can be used to constrain Gondwana fits. The tectonic significance of the Sandow Group, which crops out immediately east of the Denman Glacier, is uncertain, but sedimentation in a 'coastal–continental' environment (Ravich et al. 1968) is consistent with continental collision followed by ensialic rifting.

Extensive Neoproterozoic-Cambrian ('Pan-African') resetting of K-Ar, Rb-Sr, and U-Pb systems, commonly accompanied by felsic magmatism (emplacement of granite and pegmatite), has been documented for large areas of the East Antarctic Shield, including the sector between 0° and 102°E (Ravich et al. 1968; Yoshida et al. 1983; Sheraton et al. 1987c; Moyes & Barton 1989; Tingey 1991; Shiraishi et al. 1992; Kinny et al. 1993). Metamorphic and felsic igneous activity at about 500–600 Ma was also common in Sri Lanka (Cooray 1984; Baur et al. 1991; Hölzl et al. 1994) and much of India (Sakar 1968; Grew & Manton 1986; Unnikrishnan-Warrier et al. 1995). The exact nature of this event, which apparently resulted in the final uplift of this part of East Antarctica (Harley 1988), is uncertain, although collision may again have been involved (Harris et al. 1989b). Clarke (1988) attributed the formation of late mylonite and shear zones in the Rayner Complex of Kemp Land to northward thrusting at this time. In Australia, this event seems to have been one of crustal extension, possibly related to the breakup of a Proterozoic supercontinent (Lindsay et al. 1987).

In contrast, as already noted, most K-Ar and Rb-Sr biotite ages from the Windmill Islands are between 1060 and 1160 Ma, and Rb-Sr ages of micas from the Commonwealth Bay area are mostly between 1300 and 1650 Ma (Tingey 1991). There is thus no evidence for Neoproterozoic–Cambrian resetting in these areas — the lower 'reverse discordia' intercept for felsic orthogneiss from Commonwealth Bay given by Oliver et al. (1983) may well be geologically meaningless. However, if greenschist-facies phyllite at Cape Hunter, west of Commonwealth Bay (Stillwell, 1918), is a correlative of the Meso–Neoproterozoic Adelaidean sediments (deformed and metamorphosed during the Cambro-Ordovician Delamerian orogeny) of South Australia, as proposed by Grew (1982), then Commonwealth Bay may have been close to the western limit of this metamorphic event in this part of the East Antarctic Shield. Stüwe & Oliver (1989) suggested that the grade of this metamorphism increases markedly east of Commonwealth Bay. The event was presumably related to the Ross orogeny in the Transantarctic Mountains (Elliot 1975; Grew 1982), a collisional terrane involving several microplates

(Weaver et al. 1984; Gibson & Wright 1985).

Similarly, the Bunger Hills may have been close to an eastern limit of Cambrian activity. Only partial resetting of the Rb-Sr system occurred (mineral-whole rock isochron ages of dolerite dykes range from about 1200 to 500 Ma: Sheraton et al. 1990) and igneous activity was much less intense at that time than in the area west of the Denman Glacier. In Australia, the geographical limits of such resetting (and associated geological activity) are relatively well constrained, being confined to the western margin of the Yilgarn Craton, near the Darling Fault (Myers 1990b), and to the area east of the Gawler Craton (the Adelaide Fold Belt, metamorphosed during the Cambro-Ordovician Delamerian orogeny) (Webb et al. 1986; Foden et al. 1991); these features correlate quite well with the proposed Gondwana reconstruction (Fig. 135).

Gondwana correlations

There are clearly considerable differences in the ages of Mesoproterozoic high-grade metamorphic events in the East Antarctic Shield, which range from a poorly constrained 1600–1700 Ma in the Commonwealth Bay area to about 1000 Ma in the western Rayner Complex of Enderby Land and in parts of Dronning Maud Land. Superficially, this might suggest a general decrease from east to west over about 4000 km, but geochronological data indicate a far more complex pattern. Several Archaean cratonic blocks and smaller relics are present, and T^{Nd}_{DM} model ages indicate a wide range of protolith ages throughout the shield.

Much of the Mesoproterozoic (~1000 Ma) terrane, from Princess Elizabeth Land to Enderby Land, preserves petrographic evidence for substantial (2–4 kb) post-peak decompression (Harley, 1988). Interpreted P-T-time paths are generally clockwise, although only a small, relatively late part of the overall P-T-time path is usually recorded. Early high-pressure associations (relict kyanite + staurolite enclosed in garnet) have been reported from the Lützow-Holm Complex of Dronning Maud Land (Motoyoshi 1990), but this area apparently underwent high-grade metamorphism during the Cambrian (Shiraishi et al. 1992). After decompression the Mesoproterozoic granulite terrane appears to have undergone near-isobaric cooling at middle crustal levels (3–5 kb) (Harley 1988; Stüwe & Powell 1989b).

This Mesoproterozoic P-T history can only be explained by major crustal thickening in a convergent tectonic regime — continental collision and/or continental arc. Clarke (1988) showed that deformation of the Rayner Complex in MacRobertson and Kemp Lands was due to westward thrusting against the stable craton of the Archaean Napier Complex, and Young & Ellis (1991) argued on geochemical grounds that the Mawson Charnockite was generated at pressures high enough to allow garnet fractionation. Moreover, Harley (1988) has shown that the gradients of the P-T-time paths commonly imply a heat budget enhanced by magmatic underplating. He also suggested that unusually rapid uplift in the Rauer Islands of Prydz Bay required extension of the previously thickened crust. Such a model fits the known geological history of the Bunger Hills quite well, although there is evidence for only limited uplift after voluminous, mantle-derived plutonic rocks were emplaced during compression in the area. However, the intrusion of a slightly younger dolerite dyke swarm suggests at least some subsequent extension. Presumably, the absence of coeval dolerite dyke swarms in the Albany Mobile Belt is because the terrane did not undergo extension at that time.

Mesoproterozoic ages comparable to those of East Antarctica have been reported from once contiguous parts of India and Sri Lanka (Fig. 135). The Grenville orogenic belt of North America is also of similar age (Park 1988; Connelly & Heaman 1993) and includes both mantle and crust-derived plutonic rocks of very similar age to those in the Bunger Hills (1130–1160 Ma: Emslie & Hegner 1993). Indeed, Moores (1991) suggested that the Grenville orogen may once have extended around the present coast of East Antarctica into India and Australia in a Neoproterozoic supercontinent, which eventually broke apart in the Neoproterozoic or early Palaeozoic, isolating North America (Laurentia) and resulting in formation of the Gondwana supercontinent (Dalziel 1991, 1992).

In India, granulite and charnockite from the Eastern Ghats and elsewhere in the northeast have been dated at about 1000 Ma (Sakar 1968; Grew & Manton 1986), although much of these areas is significantly older (Radhakrishna & Naqvi 1986), suggesting correlations with MacRobertson and Kemp Lands, and possibly also the Albany-Fraser Province (Harris 1993). It is therefore tempting to invoke collision of the Archaean to Palaeoproterozoic rocks of the Indian Shield with those of East Antarctica (the southern Prince Charles Mountains and Napier Complex) about 1000 Ma ago. If this was the case, then it is quite possible that the Bunger Hills were near a continental margin during and after collision between the Yilgarn and East Antarctic plates about 200 Ma earlier.

Further west, there are significant geological similarities between the Lützow-Holm Complex of Dronning Maud Land, and the Highland Complex of Sri Lanka (Yoshida 1988; Motoyoshi 1990; Yoshida et al. 1990). Both complexes were originally thought to be Mesoproterozoic (~1100 Ma), although derived from Archaean to Palaeoproterozoic protoliths (Shibata et al. 1986; German-Sri Lankan Consortium 1987; Kröner et al. 1987; Cooray 1991), but recent U-Pb zircon ion-microprobe dating has shown that both underwent high-grade (amphibolite-granulite facies) metamorphism in Neoproterozoic-Cambrian times: about 530 Ma ago in the Lützow-Holm Complex (Shiraishi et al. 1992) and 550–660 Ma ago in the Highland Series (Baur et al. 1991; Hölzl et al. 1994). The classic '*in situ* charnockitisation' in orthogneiss of the Highland Complex apparently occurred during the latter event. There is, however, some evidence for 1000-1100 Ma geological activity in both areas, including granitoid emplacement the Highland Complex (Kröner et al. 1987; Burton & O'Nions 1990) and ~1000 Ma zircon cores in some paragneiss from the Lützow-Holm Complex (Shiraishi et al. 1992).

Shiraishi et al. (1987) postulated a collisional plate tectonic model for the development of the Lützow-Holm and adjacent Yamato-Belgica Complexes, and Shiraishi et al. (1992) pointed out that this is the first reported occurrence of a Pan-African mobile belt in East Antarctica. There is also isotopic evidence (U-Pb zircon ages of granitic rocks) for a high-grade metamorphic event of Pan-African age in the Larsemann Hills area of Princess Elizabeth Land (Zhao et al. 1992; Dirks et al. 1993; Hensen & Zhou 1995). It is quite probable that the Denman Glacier-Mirny area represents another example of such a terrane, although further isotopic dating is needed to confirm this. Whether or not this terrane also evolved in a collision zone is uncertain, particularly as it is not known how far east (i.e. towards Australia) the Indian portion of Gondwana — in particular, the Meghalaya Province (Harris 1993) — extended at that time (Powell et al. 1988), but some sort of association, either direct or indirect, with collisional tectonics would explain the major subsequent uplift it experienced. Magmatic underplating may also have been an important factor (Stüwe & Sandiford 1993). The 'Pan-African' event was clearly of much greater significance in this part of Gondwana than was previously thought, having involved much more than relatively minor felsic magmatism and resetting of isotopic systems.

The tectonic significance of a further, older phase of granite and pegmatite emplacement about 770 Ma ago in the Rayner Complex of western Enderby Land (Black et al. 1987) is presently unclear, but this event may also have been quite widespread. Similar ages have been obtained for rocks from the Lützow-Holm Complex (Rb-Sr isochron ages, of uncertain reliability, for felsic gneiss: Shibata et al. 1986; Nakajima et al. 1988) and the Sri Lankan Highland Complex (771^{+17}_{-14} Ma U-Pb zircon ion microprobe age, interpreted as dating emplacement, for a granitic orthogneiss: Baur et al. 1991). Such ages are comparable to those of high-grade metamorphism in the Mozambique Belt of central Africa (Stern et al. 1992; Moseley 1993), which may also have been the time of breakup between Laurentia and Antarctica–Australia (Dalziel 1992).

There are thus systematic variations in the age of Mesoproterozoic metamorphism and magmatism and the intensity of the Neoproterozoic–early Palaeozoic event in East Antarctica, which can, to some extent, be correlated with events in once contiguous parts of Gondwana. Many of these geochronological data, as well as geological evidence, support the Antarctica-Australia reconstruction of Veevers & Eittreim (1988). Nevertheless, there are still significant uncertainties in the correlations, notably between the Denman Glacier area and southwestern Australia (cf. Black et al. 1992b) and between Commonwealth Bay and South Australia (cf. Oliver et al. 1983), which are exacerbated by poor outcrop on the Antarctic side. Many more isotopic ages, combined with structural, petrographic, geochemical and, in particular, marine geophysical studies, will be required before more definitive correlations and tectonic interpretations can be made. As more such data become available, the geological history of East Antarctica will certainly be shown to be far more complex than the above outline would suggest, as has been the case for other Precambrian shields, such as southern Africa (Cooper 1990), the Canadian Shield (Card 1990), and the Yilgarn Craton (Wilde 1990; Myers 1990a). It should eventually be possible to correlate metamorphic and magmatic activity in the East Antarctic Shield with major collisional and breakup events involving Precambrian continental plates prior to the formation of Gondwana. If Sri Lanka is 'the jewel in the crown of Gondwana' (Ellis 1988), then East Antarctica is surely the key piece of the Gondwana jigsaw, as Du Toit (1937) suggested in spite of general scepticism about continental drift at that time.

Acknowledgements

We gratefully acknowledge the considerable efforts of members of the Australian National Antarctic Research Expeditions 1986 summer party in the Bunger Hills, which ensured the success of the field program on which this *Bulletin* is based. Logistic support in the field was provided by the Antarctic Division, Department of the Arts, Sport, the Environment, Tourism and Territories.

We thank Puquan Ding, Dave Ellis, Paul Marsh, Alistair Stewart, Kurt Stüwe, and Chris Wilson as well as numerous colleagues at IGCP Project 236 (Precambrian Events in the Gondwana Fragments) meetings in Albany, Western Australia and Kandy, Sri Lanka, for invaluable discussions, and Kurt Stüwe and Chris Wilson (University of Melbourne) for permission to use photographs of the Bunger Hills area. Julie Haldane, Bill Pappas, and John Pyke carried out whole-rock chemical analyses, Andy Tindle analysed minerals in the plutonic rocks, Deborah O'Donoghue drafted some of the figures, and Margaret Russell and Dell Stafford typed early drafts of the manuscript. The *Bulletin* was reviewed by Andrew Glikson and Peter Williams.

References

Abbey, S., 1983. Studies in "standard samples" of silicate rocks and minerals, 1969–1982. *Geological Survey of Canada Paper*, 83–15.

Allègre, C.J., Treuill, M., Minster, J-F, Minster, B. & Albarède, F., 1977. Systematic use of trace elements in igneous processes. Part 1: Fractional crystallisation processes in volcanic suites. *Contributions to Mineralogy and Petrology*, 60, 57–75.

Anderson, J.L. & Cullers, R.L., 1978. Geochemistry and evolution of the Wolf River Batholith, a late Precambrian rapakivi massif in North Wisconsin. *Precambrian Research*, 7, 287–324.

Arndt, N.T., Chauvel, C., Todt, W., Tapfer, M. & Weber, K., 1989. Granulites in the Koltas Mountains, Antarctica: geology, geochronology and geochemistry (abstract). International Workshop on Antarctic Geochronology, Ludwig-Maximilians University, Munich, Germany, 6.

Arriens, P.A. & Lambert, I.B., 1969. On the age and strontium isotope geochemistry of granulite-facies rocks from the Fraser Range, Western Australia, and the Musgrave Ranges, central Australia. *Special Publication of the Geological Society of Australia*, 2, 377–388.

Baillie, P., 1984. A Palaeozoic suspect terrain in southeastern Australia and north Victoria Land, Antarctica (abstract). *Geological Society of Australia Abstracts*, 12, 43.

Barker, F., 1979. *Trodhjemites, dacites, and related rocks*. Elsevier, Amsterdam.

Baur, N., Kröner, A., Liew, T.C., Todt, W., Williams, I.S. & Hofmann, A.W., 1991. U-Pb isotopic systematics of zircons from prograde and retrograde transition zones in high-grade orthogneisses, Sri Lanka. *Journal of Geology*, 99, 527–545.

Bea, F., Fershtater, G. & Corretgé, L.G., 1992. The geochemistry of phosphorus in granite rocks and the effect of aluminium. *Lithos*, 29, 43–56.

Beard, J.S. & Lofgren, G.E., 1991. Dehydration melting and water-saturated melting of basaltic and andesitic greenstones and amphibolites at 1, 3, and 6.9 kb. *Journal of Petrology*, 32, 365–401.

Beeson, J., Delor, C.P. & Harris, L.B., 1988. A structural and metamorphic traverse across the Albany Mobile Belt, Western Australia. *Precambrian Research*, 40/41, 117–136.

Bertrand, K.J., 1967. A look at Operation Highjump twenty years later. *Antarctic Journal of the US*, 1, 5.

Bertrand, P., Ellis, D.J. & Green, D.H., 1991. The stability of sapphirine-quartz and hypersthene-sillimanite-quartz assemblages: an experimental investigation in the system $FeO-MgO-Al_2O_3-SiO_2$ under H_2O and CO_2 conditions. *Contributions to Mineralogy and Petrology*, 108, 55–71.

Black, L.P. & Sheraton, J.W., 1990. The influence of Precambrian source components on the U-Pb zircon age of a Palaeozoic granite from northern Victoria Land, Antarctica. *Precambrian Research*, 46, 275–293.

Black, L.P., Harley, S.L., Sun, S-S. & McCulloch, M.T., 1987. The Rayner Complex of East Antarctica: complex isotopic systematics within a Proterozoic mobile belt. *Journal of Metamorphic Geology*, 5, 1–26.

Black, L.P., Kinny, P.D. & Sheraton, J.W., 1991a. The difficulties of dating mafic dykes: an Antarctic example. *Contributions to Mineralogy and Petrology*, 109, 183–194.

Black, L.P., Kinny, P.D., Sheraton, J.W. & Delor, C.P., 1991b. Rapid production and evolution of late Archaean felsic crust in the Vestfold Block of East Antarctica. *Precambrian Research*, 50, 283–310.

Black, L.P., Harris, L.B. & Delor, C.P., 1992a. Reworking of Archaean and Palaeoproterozoic components during a progressive, Mesoproterozoic tectonothermal event in the Albany Mobile Belt, Western Australia. *Precambrian Research*, 59, 95–123.

Black, L.P., Sheraton, J.W., Tingey, R.J. & McCulloch, M.T., 1992b. New U-Pb zircon ages from the Denman Glacier area, East Antarctica, and their significance for Gondwana reconstruction. *Antarctic Science*, 4, 447–460.

Blight, D.F. & Oliver, R.L., 1977. The metamorphic geology of the Windmill Islands, Antarctica : a preliminary account. *Journal of the Geological Society of Australia*, 24, 239–262.

Blight, D.F. & Oliver, R.L., 1982. Aspects of the geologic history of the Windmill Islands, Antarctica. *In* Craddock, C. (Editor), *Antarctic geoscience*. University of Wisconsin Press, Madison, 445–454.

Blundy, J.D. & Holland, T.J.B., 1990. Calcic amphibole equilibria and a new amphibole-plagioclase geothermometer. *Contributions to Mineralogy and Petrology*, 104, 208–224.

Bohlen, S.R., 1987. Pressure-temperature time paths and a tectonic model for the evolution of granulites. *Journal of Geology*, 95, 617–632.

Borg, S.G., 1983. Petrology and geochemistry of the Queen Maud Batholith, central Transantarctic Mountains with implications for the Ross Orogeny. *In* Oliver, R.L., James, P.R. & Jago, J.B., (editors), *Antarctic earth science*. Australian Academy of Science, Canberra, 165–169.

Borg, S.G., DePaolo, D.J. & Smith, B.M., 1990. Isotopic structure and tectonics of the central Transantarctic Mountains. *Journal of Geophysical Research*, B5, 6647–6667.

Brown, G.C., Thorpe, R.S. & Webb, P.C., 1984. The geochemical charcteristics of granitoids in contrasting arcs and comments on magma sources. *Journal of the Geological Society of London*, 141, 413–426.

Bunting, J.A., De Laeter, J.R. & Libby, W.G., 1976. Tectonic subdivisions and geochronology of the northeastern part of the Albany-Fraser Province, Western Australia. *Geological Survey of Western Australia, Annual Report*, 1975, 117–126.

Burton, K.W. & O'Nions, R.K., 1990. Fe-Ti oxide chronometry, with implications for granulite formation. *Geochimica et Cosmochimica Acta*, 54, 2593–2602.

Cann, J.R., 1970. Upward movement of granitic magma. *Geological Magazine*, 107, 335–340.

Card, K.D., 1990. A review of the Superior Province of the Canadian Shield, a product of Archaean accretion. *Precambrian Research*, 48, 99–156.

Chappell, B.W. & White, A.J.R., 1974. Two contrasting granite types. *Pacific Geology*, 8, 173–174.

Clarke, G.L., 1988. Structural constraints on the Proterozoic reworking of Archaean crust in the Rayner Complex, MacRobertson and Kemp Land coast, East Antarctica. *Precambrian Research*, 40/41, 137–156.

Clarke, G.L., Powell, R. & Guiraud, M., 1989. Low-pressure granulite facies metapelitic assemblages and corona textures from MacRobertson Land, east Antarctica : the importance of Fe_2O_3 and TiO_2 in accounting for spinel-bearing assemblages. *Journal of Metamorphic Geology*, 7, 323–335.

Clifford, T.N., 1974. Review of African granulites and related rocks. *Geological Society of America Special Paper*, 156.

Cohen, A.S., O'Nions, R.K. & O'Hara, M.J., 1991. Chronology and mechanism of depletion in Lewisian granulites. *Contributions to Mineralogy and Petrology*, 106, 142–153.

Collerson, K.D. & Sheraton, J.W., 1986. Bedrock geology and crustal evolution of the Vestfold Hills. *In* Pickard, J. (editor), *Antarctic oasis*. Academic Press, Sydney, 21–62.

Collins, W.J., Beams, S.D., White, A.J.R. & Chappell, B.W., 1982. Nature and origin of A-type granites with particular reference to southeastern Australia. *Contributions to Mineralogy and Petrology*, 80, 189–200.

Connelly, J.N. & Heaman, L.M., 1993. U-Pb geochronological constraints on the tectonic evolution of the Grenville Province, western Labrador. *Precambrian Research*, 63, 123–142.

Cooper, M.R., 1990. Tectonic cycles in Africa. *Earth-Science Reviews*, 28, 321–364.

Cooray, P.G., 1991. The geology of Sri Lanka — problems and perspectives. *Journal of the Geological Society of Sri Lanka*, 3, 1–14.

Creaser, R.A., Price, R.C. & Wormald, R.J., 1991. A-type granites revisited: assessment of a residual–source model. *Geology*, 19, 163–166.

Dalziel, I.W.D., 1991. Pacific margins of Laurentia and East Antarctica-Australia as a conjugate rift pair: evidence and implications for an Eocambrian supercontinent. *Geology*, 19, 598–601.

Dalziel, I.W.D., 1992. Antarctica; a tale of two supercontinents? *Annual Review of Earth and Planetary Sciences*, 20, 501–526.

DePaolo, D.J., 1981. Trace element and isotopic effects of combined wallrock assimilation and fractional crystallisation. *Earth and Planetary Science Letters*, 53, 189–202.

Ding, P. & James, P.R., 1991. Structural evolution of the Bunger Hills area of East Antarctica. *In* Thomson, M.R.A., Crame, J.A. & Thomson, J.W. (editors), *The geological evolution of Antarctica*. Cambridge University Press, 13–17.

Dirks, P.H.G.M., Carson, C.J. & Wilson, C.J.L., 1993. The deformational history of the Larsemann Hills, Prydz Bay: the importance of the Pan-African (500 Ma) in East Antarctica. *Antarctic Science*, 5, 179–192.

Drewry, D.J. & Jordan, S.A., 1983. Sheet 3: Bedrock surface of Antarctica. *In* Drewry, D.J. (editor), *Antarctica: glaciological and geophysical folio*. Scott Polar Research Institute, University of Cambridge, Plate, 3.1.

Du Toit, A., 1937. *Our wandering continents*. Oliver & Boyd, Edinburgh.

Elliot, D.H., 1975. Tectonics of Antarctica: a review. *American Journal of Science*, 275A, 45–106.

Ellis, D.J., 1980. Osumilite-sapphirine-quartz granulites from Enderby Land, Antarctica: P-T conditions of metamorphism, implications for garnet-cordierite equilibria and the evolution of the deep crust. *Contributions to Mineralogy and Petrology*, 74, 201–210.

Ellis, D.J., 1987. Origin and evolution of granulites in normal and thickened crusts. *Geology*, 15, 167–170.

Ellis, D.J., 1988. The jewel in the crown of Gondwana. *Episodes*, 11, 45–46.

Ellis, D.J., & Green, D.H., 1979. An experimental study of the effect of Ca upon garnet-clinopyroxene Fe-Mg exchange equilibria. *Contributions to Mineralogy and Petrology*, 71, 13–22.

Ellis, D.J., Sheraton, J.W., England, R.N. & Dallwitz, W.B., 1980. Osumilite-sapphirine-quartz granulites from Enderby Land, Antarctica — mineral assemblages and reactions. *Contributions to Mineralogy and Petrology*, 72, 123–143.

Emslie, R.F., 1978. Anorthosite massifs, rapakivi granites, and Neoproterozoic rifting of North America. *Precambrian Research*, 7, 61–98.

Emslie, R.F., & Hegner, E., 1993. Reconnaissance isotopic geochemistry of anorthosite-mangerite-charnockite-granite (AMCG) complexes, Grenville Province, Canada. *Chemical Geology*, 106, 279–298.

England, P.C. & Richardson, S.W., 1977. The influence of erosion upon the mineral facies of rocks from different metamorphic environments. *Journal of the Geological Society of London*, 134, 201–213.

Escher, A. & Watterson, J., 1974. Stretching fabrics, folds and crustal shortening. *Tectonophysics*, 22, 223–231.

Fitton, J.G. & Upton, B.G.J., 1987. Alkaline igneous rocks. *Geological Society (London), Special Publication*, 30.

Fletcher, I.R., Wilde, S.A., Libby, W.G. & Rosman, K.J.R., 1983. Sm-Nd model ages from across the margins of the Archaean Yilgarn Block, Western Australia — II: southwest transect into the Proterozoic Albany-Fraser Province. *Journal of the Geological Society of Australia*, 30, 333–340.

Fletcher, I.R., Wilde, S.A. & Rosman, K.J.R., 1985. Sm-Nd model ages across the margins of the Archaean Yilgarn Block, Western Australia — III: the western margin. *Australian Journal of Earth Sciences*, 32, 73–82.

Fletcher, I.R., Myers, J.S. & Ahmat, A.L., 1991. Isotopic evidence on the age and origin of the Fraser Complex, Western Australia: a sample of Mid-Proterozoic lower crust. *Chemical Geology (Isotope Geoscience Section)*, 87, 197–216.

Flöttmann, T., Gibson, G.M. & Kleinschmidt, G., 1993. Structural continuity of the Ross and Delamerian orogens of Antarctica and Australia along the margin of the paleo-Pacific. *Geology*, 21, 319–322.

Foden, J., Turner, S. & Stewart, K., 1991. Isotopic constraints on the early evolution of the Gondwanan lithosphere in South Australia (abstract). Eighth international symposium on Gondwana, Hobart, Tasmania, 30.

German-Sri Lankan Consortium, 1987. The Precambrian basement of Sri Lanka: ancient segment of the deep continental crust (abstract). Precambrian events in the Gondwana fragments, IGCP 236 Meeting, Kandy, Sri Lanka, 26.

Gibson, G.M., & Wright, T.O., 1985. Importance of thrust faulting in the tectonic development of northern Victoria Land, Antarctica. *Nature*, 315, 480–483.

Grant, J.A., 1985. Phase equilibria in low-pressure partial melting of pelitic rocks. *American Journal of Science*, 285, 409–435.

Gray, C.M., 1978. Geochronology of granulite-facies gneisses in the western Musgrave Block, central Australia. *Journal of the Geological Society of Australia*, 25, 403–414.

Green, D.H. & Ringwood, A.E., 1967. An experimental investigation of the gabbro to eclogite transformation and its petrological applications. *Geochimica et Cosmochimica Acta*, 31, 767–833.

Green, D.H. & Ringwood, A.E., 1972. A comparison of recent experimental data on the gabbro-garnet granulite-eclogite transition. *Journal of Geology*, 80, 277–288.

Grew, E.S., 1982. The Antarctic margin. *In* Nairn, A.E.M., & Stehli, F.G. (editors), *The ocean basins and margins*. Vol. 6. Plenum, New York, 697–755.

Grew, E.S. & Manton, W.I., 1979. Archean rocks in Antarctica: 2.5 billion-year uranium-lead ages of pegmatites in Enderby Land. *Science*, 206, 443–445.

Grew, E.S. & Manton, W.I., 1986. A new correlation of sapphirine granulites in the Indo-Antarctic metamorphic terrain: Neoproterozoic dates from the Eastern Ghats Province of India. *Precambrian Research*, 33, 123–137.

Grew, E.S., Manton, W.I. & James, P.R., 1988. U-Pb data on granulite facies rocks from Fold Island, Kemp Coast, East Antarctica. *Precambrian Research*, 42, 63–75.

Groenewald, P.B., 1993. Correlation of cratonic and orogenic provinces in southeastern Africa and Dronning Maud Land, Antarctica. *In* Findlay, R.H., Unrug, R., Banks, M.R. & Veevers, J.J. (editors), *Gondwana eight*. Balkema, Rotterdam, 111–123.

Hamlyn, P.R. & Keays, R.R., 1986. Sulphur saturation and second-stage melts: application to the Bushveld platinum metal deposits. *Economic Geology*, 81, 1431–1445.

Harley, S.L., 1983. Regional geobarometry-geothermometry and metamorphic evolution of Enderby Land, Antarctica. *In* Oliver, R.L., James, P.R., & Jago, J.B. (Editors), *Antarctic earth science*. Australian Academy of Science, Canberra, 25–30.

Harley, S.L., 1984a. An experimental study of the partitioning of Fe and Mg between garnet and orthopyroxene. *Contributions to Mineralogy and Petrology*, 86, 359–373.

Harley, S.L., 1984b. Comparison of the garnet-orthopyroxene geobarometer with recent experimental studies, and applications to natural assemblages. *Journal of Petrology*, 25, 697–712.

Harley, S.L., 1985. Garnet-orthopyroxene bearing granulites from Enderby Land, Antarctica: metamorphic pressure-temperature-time evolution of the Archaean Napier Complex. *Journal of Petrology*, 26, 819–856.

Harley, S.L., 1988. Proterozoic granulites from the Rauer Group, East Antartica. I. Decompressional pressure-temperature paths deduced from mafic and felsic gneisses. *Journal of Petrology*, 29, 1059–1095.

Harley, S.L. & Green, D.H., 1982. Garnet-orthopyroxene barometry for granulites and peridotites. *Nature*, 300, 697–701.

Harley, S.L., Hensen, B.J. & Sheraton, J.W., 1990. Two-stage decompression in orthopyroxene-sillimanite granulites from Forefinger Point, Enderby Land, Antarctica: implications for the evolution of the Archaean Napier Complex. *Journal of Metamorphic Geology*, 8, 591–613.

Harris, L.B., 1993. Correlations of tectonothermal events between the Central Indian Tectonic Zone and the Albany Mobile Belt of Western Australia. *In* Findlay, R.H., Unrug, R., Banks, M.R. & Veevers, J.J. (editors), *Gondwana eight*. Balkema, Rotterdam, 165–180.

Harris, L.B. & Li, Z.X., 1991. Tectonic controls on Cambrian dolerite dyke emplacement in the Albany Mobile Belt, Western Australia (abstract). Eighth international symposium on Gondwana, Hobart, Tasmania, 41–42.

Harris, L., Delor, C., Beeson, J. & Standing, J., 1989a. The structural evolution of the Albany Fraser Province and Leeuwin Block, Western Australia (abstract). Australasian Tectonics. *Geological Society of Australia Abstracts*, 24, 67–68.

Harris, L., Delor, C., Beeson, J. & Standing, J., 1989b. A major Palaeozoic deformation event affecting Precambrian terrains of Australia and East Antarctica: implications for continental scale crustal shortening (abstract). Australasian Tectonics. *Geological Society of Australia Abstracts*, 24, 65–66.

Hensen, B.J. & Green, D.H., 1971. Experimental study of the stability of cordierite and garnet in pelitic compositions at high pressures and temperatures. I. Compositions with excess alumino-silicate. *Contributions to Mineralogy and Petrology*, 33, 309–330.

Hensen, B.J. & Green, D.H., 1973. Experimental study of the stability of cordierite and garnet in pelitic compositions at high pressures and temperatures. III. Synthesis of experimental data and geological applications. *Contributions to Mineralogy and Petrology*, 38, 151–166.

Hensen, B.J. & Zhou, B., 1995. A Pan-African granulite-facies metamorphic episode in Prydz Bay, Antarctica: evidence from Sm-Nd garnet dating. *Australian Journal of Earth Sciences*, 42, 249–258.

Holdaway, M.J., 1971. Stability of andalusite and the aluminium silicate phase diagram. *American Journal of Science*, 271, 97–131.

Hölzl, S., Hofmann, A.W., Todt, W. & Köhler, H., 1994. U-Pb geochronology of the Sri Lankan basement. *Precambrian Research*, 66, 123–149.

Huang, W.L. & Wyllie, P.J., 1975. Melting relations in the system $NaAlSi_3O_8$-$KAlSi_3O_8$-SiO_2 to 35 kilobars, dry and with excess water. *Journal of Geology*, 83, 737–748.

Irvine, T.N. & Baragar, W.R.A., 1971. A guide to the chemical classification of the common volcanic rocks. *Canadian Journal of Earth Sciences*, 8, 523–548.

James, R.S. & Hamilton, D.L., 1969. Phase relations in the system $NaAlSi_3O_8$-$KAlSi_3O_8$-$CaAl_2Si_2O_8$-SiO_2 at 1 kilobar water vapour pressure. *Contributions to Mineralogy and Petrology*, 21, 111–141.

Jenkins, R. & De Vries, J.L., 1967. *Practical X-ray spectrometry*. Philips, Eindhoven.

Johnson, M.C. & Rutherford, M.J., 1989. Experimental calibration of the aluminum-in-hornblende geobarometer with application to the Long Valley caldera (California) volcanic rocks. *Geology*, 17, 837–841.

Kagami, H., Owada, M., Osanai, Y. & Hiroi, Y., 1990. Preliminary geochronological study of Sri Lankan rocks. *In* Hiroi, Y. & Motoyoshi, Y. (editors), *Study of geologic correlation between Sri Lanka and Antarctica (1988–1989)*. Interim Report of Japan-Sri Lanka Joint Research, Chiba University, Japan, 55–70.

Kinny, P.D., Black, L.P. & Sheraton, J.W., 1993. Zircon ages and the distribution of Archaean and Proterozoic rocks in the Rauer Islands. *Antarctic Science*, 5, 193–206.

Kröner, A., Williams, I.S., Compston, W., Baur, N., Vitanage, P.W. & Perera, L.R.K., 1987. Zircon ion microprobe dating of high-grade rocks in Sri Lanka. *Journal of Geology*, 95, 775–791.

Laird, M.G., Cooper, R.A. & Jago, J.B., 1977. New data on the lower Palaeozoic sequence of northern Victoria Land, Antarctica, and its significance for Australian-Antarctic relations in the Palaeozoic. *Nature*, 265, 107–110.

Lambert, I.B. & Heier, K.S., 1968. Geochemical investigations of deep-seated rocks in the Australian Shield. *Lithos*, 1, 30–53.

Lanyon, R., Black, L.P. & Seitz. H-M., 1993. U-Pb zircon dating of mafic dykes and its application to the Proterozoic geological history of the Vestfold Hills, East Antarctica. *Contributions to Mineralogy and Petrology*, 115, 184–203.

Leake, B.E., 1978. Nomenclature of amphiboles. *Canadian Mineralogist*, 16, 501–520.

Le Maitre, R.W., 1984. A proposal by the IUGS Subcommission on the Systematics of Igneous Rocks for a chemical classification of volcanic rocks based on the total alkali silica (TAS) diagram. *Australian Journal of Earth Sciences*, 31, 243–255.

Lindsay, J.F., Korsch, R.J. & Wilford, J.R., 1987. Timing the breakup of a Proterozoic supercontinent: evidence from Australian intracratonic basins. *Geology*, 15, 1061–1064.

Lindsley, D.H., 1983. Pyroxene thermometry. *American Mineralogist*, 68, 477–493.

Luhr, J.R., Carmichael, I.S.I. & Varekamp, J.C., 1984. The 1982 eruptions of El Chichon Volcano, Chiapas, Mexico: mineralogy and petrology of the anhydrite-bearing pumices. *Journal of Volcanology and Geothermal Research*, 23, 69–108.

Martin, H., 1993. The mechanisms of petrogenesis of the Archaean continental crust — comparisons with modern processes. *Lithos*, 30, 373–388.

Mawson, D., 1915. *The home of the blizzard*. Heinemann, London.

McCulloch, M.T., 1987. Sm-Nd isotopic constraints on the evolution of Precambrian crust in the Australian continent. *In* Kröner, A. (editor), Proterozoic lithospheric evolution. *American Geophysical Union Geodynamics Series*, 17, 115–130.

McCulloch, M.T., Collerson, K.D. & Compston, W., 1983a. Growth of Archaean crust within the Western Gneiss Terrain, Yilgarn Block, Western Australia. *Journal of the Geological Society of Australia*, 30, 155–160.

McCulloch, M.T., Compston, W. & Froude, D., 1983b. Sm-Nd and Rb-Sr dating of Archaean gneisses, eastern Yilgarn Block, Western Australia. *Journal of the Geological Society of Australia*, 30, 149–153.

McQueen, D.M., Scharnberger, C.K., Scharon, L. & Halpern, M., 1972. Cambro-Ordovician paleomagnetic pole position and rubidium-strontium total rock isochron for charnockitic rocks from Mirnyy Station, East Antarctica. *Earth and Planetary Science Letters*, 16, 433–438.

Menot, R.P., Peucat, J.J., Monnier, O. & Fanning, M., 1993. Archaean and Palaeoproterozoic terrains in Terre Adélie (66.5°S, 141.25°E), East Antarctica (abstract). The Tectonics of East Antarctica, International Symposium, 13–14 October, 1993, Institute of Earth Sciences, University of Utrecht.

Menzies, M.A. & Wass, S.Y., 1983. CO_2 and LREE-rich mantle below eastern Australia: a REE and isotopic study of alkaline magmas and apatite-rich mantle xenoliths from the Southern Highlands Province, Australia. *Earth and Planetary Science Letters*, 65, 287–302.

Monnier, O., Menot, R.-P., Peucat, J.-J., Fanning, M. & Giret, A., 1993. The Terre Adélie basement revisited: recent data and new assumptions (French Polar Research Program 'GEOLETA') (abstract). The Tectonics of East Antarctica, International Symposium, 13–14 October, 1993, Institute of Earth Sciences, University of Utrecht.

Moores, E.M., 1991. Southwest U.S.-East Antarctica (SWEAT) connection: a hypothesis. *Geology*, 19, 425–428.

Moseley, P.N., 1993. Geological evolution of the Neoproterozoic 'Mozambique Belt' of Kenya. *Tectonophysics*, 221, 223–250.

Motoyoshi, Y., 1990. A review of P-T evolution of high-grade metamorphic terranes in East Antarctica. *In* Hiroi, Y. & Motoyoshi, Y. (editors), *Study of geologic correlation between Sri Lanka and Antarctica (1988–1989)*. Interim Report of Japan-Sri Lanka Joint Research, Chiba University, Japan, 132–139.

Moyes, A.B. & Barton, J.M., 1989. A review of isotopic data from western Dronning Maud Land, Antarctica (abstract). International Workshop on Antarctic Geochronology, Ludwig-Maximilians University, Munich, Germany, 35.

Myers, J.S., 1990a. Precambrian tectonic evolution of part of Gondwana, southwestern Australia. *Geology*, 18, 537–540.

Myers, J.S., 1990b. Pinjarra Orogen. *In* Geology and mineral resources of Western Australia. *Geological Survey of Western Australia Memoir* 3, 265–274.

Nakajima, T., Shibata, K., Shiraishi, K., Motoyoshi, Y. & Hiroi, Y., 1988. Rb-Sr whole rock ages of metamorphic rocks from eastern Queen Maud Land, East Antarctica (2): Tenmondai Rock and Rundvagshetta (abstract). Proceedings of the NIPR Symposium on Antarctic Geosciences, 2, 172.

Nelson, D.R. & McCulloch, M.T., 1989. Enriched mantle components and mantle recycling of sediments. *In* Ross, J. (editor), Kimberlites and related rocks, Vol. 1: Their composition, occurrence, origin and emplacement. *Geological Society of Australia, Special Publication* 14, 560–570.

Newton, R.C., 1990. The late Archaean high-grade terrain of south India and the deep structure of the Dharwar Craton. *In* Salisbury, M.H. & Fountain, D.M. (editors), *Exposed cross-sections of the continental crust.* Kluwer, Dordrecht, The Netherlands, 305–326.

Newton, R.C. & Perkins, D., 1982. Thermodynamic calibration of geobarometers based on the assemblages garnet-plagioclase-orthopyroxene(clinopyroxene)-quartz. *American Mineralogist*, 67, 203–222.

Newton, R.C., Charlu, T.V. & Kleppa, O.J., 1974. A calorimetric investigation of the stability of anhydrous magnesium cordierite with application to granulite facies metamorphism. *Contributions to Mineralogy and Petrology*, 44, 295–311.

Nockolds, S.R., 1940. Petrology of rocks from Queen Mary Land. *Australasian Antarctic Expedition Scientific Reports*, Series A, Volume IV, Part 2.

Norrish, K. & Chappell, B.W., 1977. X-ray fluorescence spectrometry. *In* Zussman, J. (editor), *Physical methods in determinative mineralogy*. Academic Press, London & New York, 201–272.

Norrish, K. & Hutton, J.T., 1969. An accurate X-ray spectrographic method for the analysis of a wide range of geological samples. *Geochimica et Cosmochimica Acta*, 33, 431–453.

Oliver, R.L., James, P.R., Collerson, K.D. & Ryan, A.B., 1982. Precambrian geological relationships in the Vestfold Hills, Antarctica. *In* Craddock,C. (editor), *Antarctic geoscience*. University of Wisconsin Press, Madison, 435–444.

Oliver, R.L., Cooper, J.A., & Truelove, A.J., 1983. Petrology and zircon geochronology of Herring Island and Commonwealth Bay and evidence for Gondwana reconstruction. *In* Oliver, R.L., James, P.R. & Jago, J.B. (editors), *Antarctic earth science*. Australian Academy of Science, Canberra, 64–68.

Page, R.W., McCulloch, M.T. & Black, L.P., 1984. Isotopic record of major Precambrian events in Australia. Precambrian geology, *Proceedings of the 27th International Geological Congress*, 5, 25–72.

Parada, M.A., 1990. Granitoid plutonism in central Chile and its geodynamic implications; a review. *In* Kay, S.M. & Rapela, C.W. (editors), Plutonism from Antarctica to Alaska. *Geological Society of America Special Paper* 241, 51–66.

Park, R.G., 1981. Origin of horizontal structure in high-grade Archaean terrains. *In* Glover, J.E. & Groves, D.I. (editors), Archaean geology. *Special Publication of the Geological Society of Australia* 7, 481–490.

Park, R.G., 1988. *Geological structures and moving plates.* Blackie, Glasgow.

Parker, A.J. & Lemon, N.M., 1982. Reconstruction of the Palaeoproterozoic stratigraphy of the Gawler Craton, South Australia. *Journal of the Geological Society of Australia*, 29, 221–238.

Pearce, J.A., Harris, N.B.W. & Tindle, A.G., 1984. Trace element discrimination diagrams for the tectonic interpretation of granitic rocks. *Journal of Petrology*, 25, 956–983.

Perkins, D. & Chipera, S.J., 1985. Garnet-orthopyroxene-plagioclase-quartz barometry: refinement and application to the English River subprovince and the Minnesota River Valley. *Contributions to Mineralogy and Petrology*, 89, 69–80.

Pichowiak, S., Buchelt, M. & Damm, K-W., 1990. Magmatic activity and tectonic setting of the early stages of the Andean cycle in northern Chile. *In* Kay, S.M., & Rapela, C.W. (editors), Plutonism from Antarctica to Alaska. *Geological Society of America Special Paper*, 241, 127–144.

Pidgeon, R.T., 1990. Timing of plutonism in the Proterozoic Albany Mobile Belt, southwestern Australia. *Precambrian Research*, 47, 157–167.

Pitcher, W.S., 1982. Granite type and tectonic environment. *In* Hsü, K.J. (editor), *Mountain-building processes.* Academic Press, London, 19–40.

Powell, R. & Holland, T.J.B., 1988. An internally consistent thermodynamic dataset with uncertainties and correlations: 3. Applications to geobarometry, worked examples and a computer program. *Journal of Metamorphic Geology*, 6, 173–204.

Powell, C.M., Roots, S.R. & Veevers, J.J., 1988. Pre-breakup continental extension in East Gondwanaland and the early opening of the eastern Indian Ocean. *Tectonophysics*, 155, 261–283.

Radhakrishna, B.P. & Naqvi, S.M., 1986. Precambrian continental crust of India and its evolution. *Journal of Geology*, 94, 145–166.

Ramsay, J.G. & Huber, M.I., 1987. *The techniques of modern structural geology. Volume 2: Folds andfractures.* Academic Press, London.

Rapp, R.P., Watson, E.B. & Miller, C.F., 1991. Partial melting of amphibolite/eclogite and the origin of Archean trondhjemites and tonalites. *Precambrian Research*, 51, 1–25.

Ravich, M.G., Klimov, L.V. & Solov'ev, D.S., 1968. *The Pre-Cambrian of East Antarctica.* Israel Program for Scientific Translations, Jerusalem.

Rock, N.M.S., 1984. Nature and origin of calc-alkaline lamprophyres minettes, vogesites, kersantites and spessartites. *Transactions of the Royal Society of Edinburgh: Earth Sciences*, 74, 193–227.

Rogers, J.J.W., 1986. The Dharwar Craton and the assembly of Peninsular India. *Journal of Geology*, 94, 129–143.

Rogers, J.J.W. & Greenberg, J.K., 1990. Late-orogenic, post-orogenic, and anorogenic granites: distinction by major-element and trace-element chemistry and possible origins. *Journal of Geology*, 98, 291–309.

Rollinson, H.R. & Windley, B.F., 1980. Selective elemental depletion during metamorphism of Archaean granulites, Scourie, NW Scotland. *Contributions to Mineralogy and Petrology*, 72, 257–263.

Rose, L.A., 1980. *Assault on eternity.* Naval Institute Press, Annapolis, Maryland.

Rudnick, R.L., 1990. Nd and Sr isotopic compositions of lower-crustal xenoliths from north Queensland, Australia: implications for Nd model ages and crustal growth processes. *Chemical Geology*, 83, 195–208.

Sakar, S.N., 1968. *Precambrian stratigraphy and geochronology of Peninsular India.* Dhanbad Publishers, India.

Sandiford, M., 1985. The metamorphic evolution of granulites at Fyfe Hills; implications for Archaean crustal thickness in Enderby Land, Antarctica. *Journal of Metamorphic Geology*, 3, 155–178.

Sandiford, M., 1989a. Horizontal structures in granulite terrains: a record of mountain building or mountain collapse? *Geology*, 17, 449–452.

Sandiford, M., 1989b. Secular trends in the thermal evolution of metamorphic terrains. *Earth and Planetary Science Letters*, 95, 85–96.

Sandiford, M. & Powell, R., 1986. Deep crustal metamorphism during continental extension: modern and ancient examples. *Earth and Planetary Science Letters*, 79, 151–158.

Saunders, A.D., Tarney, J. & Weaver, S.D., 1980. Transverse geochemical variations across the Antarctic Peninsula: implications for the generation of calc-alkaline magmas. *Earth and Planetary Science Letters*, 46, 344–360.

Saunders, A.D., Norry, M.J. & Tarney, J., 1991. Fluid influence on the trace element compositions of subduction zone magmas. *Philosophical Transactions of the Royal Society of London,* Series A, 335, 377–392.

Schmidt, M.W., 1992. Amphibole composition in tonalite as a function of pressure: an experimental calibration of the Al-in-hornblende barometer. *Contributions to Mineralogy and Petrology*, 110, 304–310.

Segalstad, T.M. & Larsen, A.O., 1978. Chevkinite and perrierite from the Oslo region, Norway. *American Mineralogist*, 63, 499–505.

Sheraton, J.W., 1982. Origin of charnockitic rocks of MacRobertson Land. *In* Craddock, C. (editor), *Antarctic geoscience*. University of Wisconsin Press, Madison, 489–497.

Sheraton, J.W. & Black, L.P., 1981. Geochemistry and geochronology of Proterozoic tholeiite dykes of East Antarctica: evidence for mantle metasomatism. *Contributions to Mineralogy and Petrology*, 78, 305–317.

Sheraton, J.W. & Black, L.P., 1983. Geochemistry of Precambrian gneisses: relevance for the evolution of the East Antarctic Shield. *Lithos*, 16, 273–296.

Sheraton, J.W. & Black, L.P., 1988. Chemical evolution of granitic rocks of the East Antarctic Shield, with particular reference to post-orogenic granites. *Lithos*, 21, 37–52.

Sheraton, J.W. & Collerson, K.D., 1984. Geochemical evolution of Archaean granulite-facies gneisses of the Vestfold Block and comparisons with other Archaean gneiss complexes in the East Antarctic Shield. *Contributions to Mineralogy and Petrology*, 87, 51–64.

Sheraton, J.W., Offe, L.A., Tingey, R.J. & Ellis, D.J., 1980. Enderby Land, Antarctica — an unusual Precambrian high-grade metamorphic terrain. *Journal of the Geological Society of Australia*, 27, 1–18.

Sheraton, J.W., Ellis, D.J. & Kuehner, S.M., 1985. Rare-earth element geochemistry of Archaean gneisses and evolution of the East Antarctic Shield. *BMR Journal of Australian Geology & Geophysics*, 9, 207–218.

Sheraton, J.W., Babcock, R.S., Black, L.P., Wyborn, D. & Plummer, C.C., 1987a. Petrogenesis of granitic rocks of the Daniels Range, northern Victoria Land, Antarctica. *Precambrian Research*, 37, 267–286.

Sheraton, J.W., Thomson, J.W. & Collerson, K.D., 1987b. Mafic dyke swarms of Antarctica. *In* Halls, H.C. & Fahrig, W.F. (editors), Mafic dyke swarms. *Geological Association of Canada Special Paper* 34, 419–432.

Sheraton, J.W., Tingey, R.J., Black, L.P., Offe, L.A. & Ellis, D.J., 1987c. Geology of an unusual Precambrian high-grade metamorphic terrane — Enderby and western Kemp Land, Antarctica. *Bureau of Mineral Resources, Australia, Bulletin* 223.

Sheraton, J.W., Oliver, R.L. & Stüwe, K., 1989. Geochemistry of Proterozoic amphibolite dykes of Commonwealth Bay, Antarctica, and possible correlations with mafic dyke swarms elsewhere in Gondwanaland. *Precambrian Research*, 44, 353–361.

Sheraton, J.W., Black, L.P., McCulloch, M.T. & Oliver, R.L., 1990. Age and origin of a compositionally varied mafic dyke swarm in the Bunger Hills, East Antarctica. *Chemical Geology*, 85, 215–246.

Sheraton, J.W., Black, L.P. & Tindle, A.G., 1992. Petrogenesis of plutonic rocks in a Proterozoic granulite-facies terrane — the Bunger Hills, East Antarctica. *Chemical Geology*, 97, 163–198.

Shibata, K., Yanai, K. & Shiraishi, K., 1986. Rb-Sr whole-rock ages of metamorphic rocks from eastern Queen Maud Land, East Antarctica. *Memoirs of the National Institute of Polar Research, Special Issue*, 43, 133–148.

Shiraish, K. & Kagami, H., 1989. Preliminary geochronological studies of granulites from the Sør Rondane Mountains, East Antarctica — a comparison of Rb-Sr and Sm-Nd ages (abstract). Proceedings of the NIPR Symposium on Antarctic Geosciences, 3, 152.

Shiraishi, K., Hiroi, Y., Motoyoshi, Y. & Yanai, K., 1987. Plate tectonic development of Neoproterozoic paired metamorphic complexes in eastern Queen Maud Land, East Antarctica. *In* McKenzie, G.W. (editor), *Gondwana six; structure, tectonics and geophysics.* American Geophysical Union Monograph 40, 309–318.

Shiraishi, K., Hiroi, Y., Ellis, D.J., Fanning, C.M., Motoyoshi, Y. & Nakai, Y., 1992. The first report of a Cambrian orogenic belt in East Antarctica — an ion microprobe study of the Lutzow-Holm Complex. *In* Yoshida, Y. (Editor), *Recent progress in Antarctic earth science.* Terra Scientific Publishing Company, Tokyo, 67–73.

Shulters, J.C. & Bohlen, S.R., 1989. The stability of hercynite and hercynite-gahnite spinels in corundum- or quartz-bearing assemblages. *Journal of Petrology*, 30, 1017–1031.

Skjerlie, K.P. & Johnston, A.D., 1993. Fluid-absent melting behavior of an F-rich tonalitic gneiss at mid-crustal pressures: implications for the generation of anorogenic granites. *Journal of Petrology*, 34, 785–815.

Smith, A.G., & Hallam, A., 1970. The fit of the southern continents. *Nature*, 225, 139–144.

Smithson, S.B. & Heier, K.S., 1971. K, U, and Th distribution between normal and charnockitic facies of a deep granite intrusion. *Earth and Planetary Science Letters*, 12, 325–326.

Soler, P. & Bonhomme, M.G., 1990. Relation of magmatic activity to plate dynamics in central Peru from Late Cretaceous to present. *In* Kay, S.M. & Rapela, C.W. (editors), Plutonism from Antarctica to Alaska. *Geological Society of America Special Paper*, 241, 173–191.

Soler, P. & Rotach-Toulhoat, N., 1990. Implications of the time-dependent evolution of Pb- and Sr-isotopic compositions of Cretaceous and Cenozoic granitoids from the coastal region on the lower Pacific slope of the Andes of central Peru. *In* Kay, S.M. & Rapela, C.W. (editors), Plutonism from Antarctica to Alaska. *Geological Society of America Special Paper*, 241, 161–172.

Soman, K., Narayanaswamy & Van Schmus, W.R., 1989. Zircon dating of south Kerala granulites (abstract). Gondwana fragments: Precambrian events and aspects of recent geology. IGCP 236 Meeting. Nairobi, Kenya, 26–27.

Sproll, W.P. & Dietz, R.S., 1969. Morphological continental drift of Australia and Antarctica. *Nature*, 222, 345–348.

Stern, R.J., Sultan, M. & Abdel-Salam, M.G., 1992. Comment and reply on 'Pacific margins of Laurentia and East Antarctica—Australia as a conjugate rift pair: evidence and implications for an Eocambrian supercontinent.' *Geology*, 20, 190–191.

Stillwell, F.L., 1918. The metamorphic rocks of Adelie Land. *Australasian Antarctic Expedition Scientific Reports*, Series A, Vol. III, Part I.

Streckeisen, A., 1976. To each plutonic rock its proper name. *Earth-Science Reviews*, 12, 1–33.

Streckeisen, A., 1979. Classification and nomenclature of volcanic rocks, lamprophyres, carbonatites and melilitic rocks: recommendations and suggestions of the IUGS Subcommission on the Systematics of Igneous Rocks. *Geology*, 7, 331–335.

Stump, E., White, A.J.R. & Borg, S.G., 1986. Reconstruction of Australia and Antarctica: evidence from granites and recent mapping. *Earth and Planetary Science Letters*, 79, 348–360.

Stüwe, K. & Oliver, R., 1989. Geological history of Adelie Land and King George V Land, Antarctica: evidence for a polycyclic metamorphic evolution. *Precambrian Research*, 43, 317–334.

Stüwe, K. & Powell, R., 1989a. Metamorphic evolution of the Bunger Hills, East Antarctica: evidence for substantial postmetamorphic peak compression with minimal cooling in a Proterozoic orogenic event. *Journal of Metamorphic Geology*, 7, 449–464.

Stüwe, K. & Powell, R., 1989b. Low-pressure granulite facies metamorphism in the Larsemann Hills area, East Antarctica: petrology and tectonic implications for the evolution of the Prydz Bay area. *Journal of Metamorphic Geology*, 7, 465–483.

Stüwe, K. & Sandiford, M., 1993. A preliminary model for the 500 Ma event in the East Antarctic Shield. *In* Findlay, R.H., Unrug, R., Banks, M.R. & Veevers, J.J. (editors), *Gondwana eight*. Balkema, Rotterdam, 125–130.

Stüwe, K. & Sandiford, M., 1995. A description of metamorphic PTt paths with implications for low-P high-T metamorphism. *Physics of the Earth and Planetary Interiors*, 88, 211–221.

Stüwe, K. & Wilson, C.J.L., 1990. Interaction between deformation and charnockite emplacement in the Bunger Hills, East Antarctica. *Journal of Structural Geology*, 12, 767–783.

Sugden, T.J., Deb, M. & Windley, B.F., 1990. The tectonic setting of mineralisation in the Proterozoic Aravalli-Delhi orogenic belt, NW India. *In* Naqvi, S.M. (editor), *Precambrian continental crust and its economic resources.* Elsevier, Amsterdam, 367–390.

Sun, S-S. & McDonough, W.F., 1989. Chemical and isotopic systematics of oceanic basalts: implications for mantle composition and processes. *In* Saunders, A.D. & Norry, M.J. (editors), Magmatism in ocean basins. *Geological Society Special Publication* 42, 313–345.

Sun, S-S., & Sheraton, J.W., 1992. Zircon U/Pb chronology, tectono-thermal and crust-forming events in the Tomkinson Ranges, Musgrave Block, Central Australia. *AGSO Research Newsletter*, 17, 9–11.

Tarney, J. & Saunders, A.D., 1979. Trace element constraints on the origin of cordilleran batholiths. *In* Atherton, M.P. & Tarney, J. (editors), *Origin of granitic batholiths: geochemical evidence*. Shiva, Nantwich, Cheshire, 90–105.

Tarney, J. & Weaver, B.L., 1987. Geochemistry and petrogenesis of Palaeoproterozoic dyke swarms. *In* Halls, H.C. & Fahrig, W.F. (editors), Mafic dyke swarms. *Geological Association of Canada Special Paper* 34, 81–94.

Tarney, J. & Windley, B.F., 1977. Chemistry, thermal gradients and evolution of the lower continental crust. *Journal of the Geology Society (London)*, 134, 153–172.

Tarney, J., Skinner, A.C. & Sheraton, J.W., 1972. A geochemical comparison of major Archaean gneiss units from northwest Scotland and East Greenland. *24th International Geological Congress*, Section, 1, 162–174.

Tarney, J., Wyborn, L.A.I., Sheraton, J.W. & Wyborn, D., 1987. Trace element differences between Archaean, Proterozoic and Phanerozoic crustal components — implications for crustal growth processes. *In* Ashwal, L.D. (editor), Workshop on the growth of continental crust. *Lunar and Planetary Institute, Technical Report* 88.02, 139–140.

Taylor, S.R. & McLennan, S.M., 1985. *The continental crust: its composition and evolution*. Blackwell Scientific Publications, Oxford.

Thompson, A.B. & England, P.C., 1984. Pressure-temperature-time paths of regional metamorphism II. Their inference and interpretation using mineral assemblages in metamorphic rocks. *Journal of Petrology*, 25, 929–955.

Tingey, R.J., 1982. The geologic evolution of the Prince Charles Mountains — an Antarctic Archean cratonic block. *In* Craddock, C. (editor), *Antarctic geoscience*. University of Wisconsin Press, Madison, 455–464.

Tingey, R.J., 1991. The regional geology of Archaean and Proterozoic rocks in Antarctica. *In* Tingey, R.J. (editor), *Geology of Antarctica*. Clarendon Press, Oxford, 1–73.

Tuttle, O.F. & Bowen, N.L., 1958. Origin of granite in the light of experimental studies in the system $NaAlSi_3O_8$-$KAlSi_3O_8$-SiO_2-H_2O. *Geological Society of America Memoir* 74.

Unnikrishnan-Warrier, C., Santosh, N. & Yoshida, M., 1995. First report of Pan-African Sm-Nd and Rb-Sr mineral isochron ages from regional charnockites of southern India. *Geological Magazine*, 132, 253–260.

Veevers, J.J., 1990. Antarctica-Australia fit resolved by satellite mapping of oceanic fracture zones. *Australian Journal of Earth Sciences*, 37, 123–126.

Veevers, J.J. & Eittreim, S.L., 1988. Reconstruction of Antarctica and Australia at breakup (95±5 Ma) and before rifting (160 Ma). *Australian Journal of Earth Sciences*, 35, 355–362.

Watson, E.B. & Harrison, T.M., 1983. Zircon saturation revisited: temperature and composition effects in a variety of crustal magma types. *Earth and Planetary Science Letters*, 64, 295–304.

Weaver, S.D., Bradshaw, J.D. & Laird, M.G., 1984. Geochemistry of Cambrian volcanics of the Bowers Supergroup and implications for the early Palaeozoic tectonic evolution of northern Victoria Land, Antarctica. *Earth and Planetary Science Letters*, 68, 128–140.

Webb, A.W., Thomson, B.P., Blissett, A.H., Daly, S.J., Flint, R.B. & Parker, A.J., 1986. Geochronology of the Gawler Craton, South Australia. *Australian Journal of Earth Sciences*, 33, 119–143.

Weber, K. & Arndt, N.T., 1991. Proterozoic link between Africa and Antarctica (abstract). *Eighth International Symposium on Gondwana, Hobart, Tasmania*, 90–91.

Wells, P.R.A., 1977. Pyroxene thermometry in simple and complex systems. *Contributions to Mineralogy and Petrology*, 62, 129–139.

Wendlandt, R.F., 1981. Influence of CO_2 on melting of model granulite facies assemblages: a model for the genesis of charnockites. *American Mineralogist*, 66, 1164–1174.

Whalen, J.B., Currie, K.L. & Chappell, B.W., 1987. A-type granites: geochemical characteristics, discrimination and petrogenesis. *Contributions to Mineralogy and Petrology*, 95, 407–419.

Wilde, S.A., 1990. Toodyay-Chittering. *3rd International Archaean Symposium, Perth, Australia, Excursion Guidebook* 4, 97–122.

Wilde, S.A. & Murphy, D.M.K., 1990. The nature and origin of Neoproterozoic high-grade gneisses of the Leeuwin Block, Western Australia. *Precambrian Research*, 47, 251–270.

Willcox, J.B. & Stagg, H.M.J., 1990. Australia's southern margin: a product of oblique extension. *Tectonophysics*, 173, 269–281.

Williams, I.S., Compston, W., Collerson, K.D., Arriens, P.A. & Lovering, J.F., 1983. A reassessment of the age of the Windmill Metamorphics, Casey area. *In* Oliver, R.L., James, P.R. & Jago, J.B. (editors), *Antarctic earth science*. Australian Academy of Science, Canberra, 73–76.

Winkler, H.G.F., 1974. *Petrogenesis of metamorphic rocks*. Springer-Verlag, Berlin.

Wolf, M.B. & Wyllie, P.J., 1994. Dehydration-melting of amphibolite at 10 kbar: the effects of temperature and time. *Contributions to Mineralogy and Petrology*, 115, 369–383.

Wood, B.J. & Banno, S., 1973. Garnet-orthopyroxene and orthopyroxene-clinopyroxene relationships in simple and complex systems. *Contributions to Mineralogy and Petrology*, 42, 109–124.

Yoshida, M., 1988. A reconnaissance geological survey of Sri Lanka and India 1985–1986, for comparing geology in Sri Lanka, India, and Antarctica. *Journal of Geosciences, Osaka City University*, 31, 1–17.

Yoshida, M. & Kizaki, K., 1983. Tectonic situation of Lützow-Holm Bay in East Antarctica and its significance in Gondwanaland. *In* Oliver, R.L., James, P.R. & Jago, J.B. (editors), *Antarctic earth science*. Australian Academy of Science, Canberra, 36–39.

Yoshida, M., Suzuki, M., Shirahata, H., Jokima, H. & Kizaki, K., 1983. A review of the tectonic and metamorphic history of the Lützow-Holm Bay region, East Antarctica. *In* Oliver, R.L., James, P.R. & Jago, J.B. (editors), *Antarctic earth science*. Australian Academy of Science, Canberra, 44–47.

Yoshida, M., Funaki, M. & Vitanage, P.W., 1990. Juxtaposition of India-Sri Lanka-Antarctica in Proterozoic to Mesozoic Gondwana. *In* Hiroi, Y. & Motoyoshi, Y., (Editors), *Study of geologic correlation between Sri Lanka and Antarctica (1988–1989)*. Interim Report of Japan-Sri Lanka Joint Research, Chiba University, Japan, 118–129.

Young, D.N. & Black, L.P., 1991. U-Pb zircon dating of Proterozoic igneous charnockites from the Mawson Coast, East Antarctica. *Antarctic Science*, 3, 205–216.

Young, D.N. & Ellis, D.J., 1991. The intrusive Mawson charnockites: evidence for a compressional plate margin setting of the Proterozoic mobile belt of East Antarctica. *In* Thomson, M.R.A., Crame, J.A. & Thomson, J.W. (editors), *The geological evolution of Antarctica*. Cambridge University Press, 25–31.

Zhao, J-X., Shiraishi, K., Ellis, D.J. & Sheraton, J.W., 1995. Geochemical and isotopic studies of syenites from the Yamato Mountains. East Antarctica: implications for the origin of syenitic magmas. Geochimica et Cosmochimica Acta, 59, 1363–1382.

Zhao, Y., Song, B., Wang, Y., Ren, L., Li, J. & Chen, T., 1992. Geochronology of the late granite in the Larsemann Hills, East Antarctica. *In* Yoshida, Y. (editor), *Recent progress in Antarctic earth science*. Terra Scientific Publishing Company, Tokyo, 155–161.

Appendix: Chemical analyses of rock samples from the Bunger Hills and Denman Glacier areas

Samples are listed in the same order in which they are described in the text.

Analytical methods

All analyses were carried out in AGSO's laboratories. Major and most trace elements were determined by X-ray fluorescence spectrometry (XRF) on Philips PW1404 or PW1450 equipment.

Major elements were measured on glass fusion discs using the method of Norrish & Hutton (1969). Calibration was against international and secondary rock standards, using SiO_2 and CaO blanks. Matrix corrections, with alpha factors for the rhodium tube, were applied to all major oxides (as well as S).

Na_2O was also analysed by atomic absorption spectrophotometry (AAS), the results agreeing well with those from XRF; averages are given in the listings. Ferrous iron (FeO) was determined separately by titration with standard potassium dichromate solution, and Fe_2O_3 estimated by difference. Loss on ignition (LOI) was measured by igniting about 5 g of sample at 1050°C. Quoted LOI values have been corrected for the FeO contents of the samples. Combined water (H_2O^+), moisture (H_2O^-), and total carbon (carbonate and carbon, quoted as CO_2) were determined gravimetrically.

Most trace elements (Ba, Rb, Sr, Pb, Th, U, Zr, Nb, Y, La, Ce, Nd, Pr, Sc, V, Cr, Sn, Ga, As, and Cl) were analysed by XRF on powder pellets, using the techniques of Norrish & Chappell (1977). Molybdenum, rhodium, and gold target X-ray tubes were used to give optimum excitation for different groups of elements. Synthetic standards were employed for calibration, except for Rb (NBS-70A and MA-N), Sr (AGV-1), V (AGV-1, BCR-1, and W-1), and Cr (PCC-1 and DTS-1).

Mass absorption corrections utilised the Compton scatter method for wavelengths less than 1.74Å (Fe absorption edge), and coefficients calculated from major element compositions for longer wavelengths. Empirical interfering-element corrections were made where necessary. Li, Ni, Cu, and Zn were determined with a Varian AA-975 spectrophotometer, Li being analysed by the method of standard addition. F was measured by specific ion electrode.

Estimated detection limits are given in Table I. Those for elements determined by XRF were calculated at the 95 percent confidence level for detection of peak above background, using the relation given by Jenkins & de Vries (1967):

$$\textit{detection limit} = \frac{3c}{(Rp-Rb)}\sqrt{\frac{Rb}{t}}$$

where, Rp = peak count rate (counts/sec),
Rb = background count rate (counts/sec),
t = background counting time (secs),
c = element concentration.

The detection limits given are twice these calculated theoretical values, and are considered to be more realistic. Detection limits for elements for which there are significant inter-element corrections (e.g., Ba, Ce, Sc, Y) are probably even higher.

Table A1. Detection limits (in weight percent for major oxides and ppm for trace elements).

SiO_2	0.006	Nb	2
TiO_2	0.008	Y	1
Al_2O_3	0.007	La	3
Fe_2O_3	0.005	Ce	4
MnO	0.004	Nd	2
MgO	0.006	Pr	3
CaO	0.0014	Sc	2
Na_2O	0.02	V	2
K_2O	0.0004	Cr	2
P_2O_5	0.003	Ni	2
Ba	5	Cu	2
Li	2	Zn	1
Rb	1	Sn	2
Sr	1	Ga	1
Pb	2	As	0.5
Th	2	S	12
U	0.5	F	200
Zr	2	C	14

Precision and accuracy

Precision of the XRF technique is generally good, as the effects of all but very short-term drift in machine conditions are practically eliminated by ratioing each measurement to a monitor standard. The precision (1σ level) for trace element analyses is typically ±3 per cent at the 30 to 100 ppm level. The corresponding precision for AAS analyses is between ±4 and ±6 percent.

Accuracy was assessed by analysing international rock standards. Comparisons of XRF and AAS results for two standard rocks (GSP-1 and BCR-1) are given in Table A2.

Table A2. Comparison of analyses of standard rocks with recommended values of Abbey (1983).

	GSP-1		*BCR-1*	
	AGSO	*Recom.*	*AGSO*	*Recom.*
SiO_2	67.97(0.29)*	67.32	54.42(0.16)	54.53
TiO_2	0.67(0.004)	0.66	2.26(0.015)	2.26
Al_2O_3	15.16(0.08)	15.28	13.51(0.06)	13.72
Fe_2O_3(t)	4.26(0.016)	4.28	13.29(0.03)	13.44
FeO	2.25	2.32	8.89	8.96
MnO	0.04	0.04	0.17	0.18
MgO	0.99(0.015)	0.97	3.53(0.012)	3.48
CaO	1.97(0.006)	2.03	6.97(0.06)	6.97
Na_2O	2.74	2.81	3.27(0.05)	3.30
K_2O	5.56(0.012)	5.51	1.71(0.010)	1.70
P_2O_5	0.28	0.28	0.36	0.36
Ba	1300	1300	702	680
Li	25	30	11	14
Rb	253	250	46	47
Sr	237	240	329	330
Pb	54	54	14	14
Th	104	105	6	6
U	2.0	2.1	1.5	1.7
Zr	507	500	187	185
Nb	25	?23	13	19
Y	28	29	37	40
La	165	195	29	27
Ce	391	360	55	53
Nd	187	?190	32	?26
Pr	46	?50	4	?7
Sc	8	7	31	33
V	49	54	416	420
Cr	11	12	6	15
Ni	7	9	7	10
Cu	30	33	17	16
Zn	91	105	117	125
Sn	8	?5	2	3
Ga	24	23	21	22
As	<0.5	<0.5	1.0	?0.8
S	400	?300	400	?400
F			500	500

* Standard deviation.

Bunger Hills Metamorphic Rocks

Sample number	86285643	86285604	86285910	86285916	86285938	86285981	86285613	86285625
Locality	Thomas Island SW	Currituck Island SE	1km S of Edgeworth David	Foster Island	5km SW of Dobrowol-ski	Highjump Archipel-ago NE	Currituck Island	Currituck Island S
Lithology	Bi-Op-Qz-Pl gneiss	Op-Qz-Kf gneiss	Op-Pl-Qz-Kf gneiss	Cp-Bi-Op-Qz-Pl gneiss	Bi-Op-Qz-Pl gneiss	Qz-Op-Pl gneiss	Op-Qz-Pl gneiss	Op-Qz-Pl gneiss
Classification	Undepleted tonalite	Undepleted granite	Undepleted granite	Depleted quartz diorite	Depleted quartz diorite	Depleted quartz diorite	Depleted tonalite	Depleted tonalite
SiO_2	68.00	74.10	69.70	58.20	55.40	55.10	64.60	60.00
TiO_2	.59	.48	.72	.60	.64	1.10	.55	.77
Al_2O_3	14.33	11.48	12.75	15.62	19.48	15.60	17.26	16.16
Fe_2O_3	2.54	1.39	2.71	.72	1.87	1.07	1.79	2.58
FeO	2.76	1.85	3.18	6.02	5.55	9.80	2.95	4.58
MnO	.09	.05	.06	.10	.13	.15	.11	.09
MgO	1.52	1.25	1.12	6.45	3.93	6.56	1.73	2.98
CaO	3.90	1.32	2.17	6.10	7.05	7.10	5.33	6.46
Na_2O	3.61	2.05	3.13	4.08	3.79	2.67	3.76	4.08
K_2O	.85	5.37	3.25	.60	.76	.41	1.34	1.05
P_2O_5	.15	.08	.11	.17	.30	.14	.11	.18
LOI	.83	.55	.79	.75	1.07	.81	.49	.54
Rest	.20	.23	.29	.27	.23	.19	.18	.37
Total	99.37	100.20	99.98	99.68	100.20	100.70	100.20	99.84
O=F,S,Cl	.02	.01	.01	.00	.01	.01	.01	.06
Total	99.34	100.19	99.96	99.67	100.19	100.69	100.19	99.77
	Trace elements in parts per million							
Ba	361	920	773	547	609	177	517	688
Rb	8	180	77	1	6	3	23	4
Sr	185	132	282	462	483	184	355	501
Pb	13	22	19	4	11	10	18	13
Th	1	6	26	<1	1	1	<1	<1
U	.50	1.00	.50	.50	.50	1.00	<.50	<.50
Zr	322	316	438	97	79	76	81	155
Nb	4	6	10	2	8	7	2	5
Y	26	17	25	11	22	23	16	28
La	21	39	80	13	29	21	16	33
Ce	45	63	163	26	54	38	30	65
Nd	19	19	60	13	23	19	12	28
Sc	15	8	10	19	21	39	12	19
V	46	22	37	114	85	256	67	130
Cr	12	5	29	442	74	150	8	40
Ni	9	7	7	145	17	48	22	36
Cu	16	5	10	16	9	16	24	102
Zn	60	35	71	76	99	134	58	44
Sn	<1	1	1	<1	1	<1	<1	1
Ga	17	12	20	21	24	19	17	19
S	500	200	300	100	300	200	300	1300

Bunger Hills Metamorphic Rocks

Sample number	86285651	86285693	86285695	86285806	86285807	86285820	86285928	86285958
Locality	Thomas Island C	Obruchev Hills SW	Obruchev Hills SW	Obruchev Hills NE	Obruchev Hills NE	1km S of Edgeworth David	S Taylor Islands	W end of Lake Dolgoe
Lithology	Op-Qz-Pl gneiss	Op-Qz-Pl gneiss	Cp-Op-Qz-Pl gneiss	Cp-Op-Qz-Pl gneiss	Op-Qz-Pl gneiss	Op-Qz-Pl gneiss	Cp-Op-Qz-Pl gneiss	Bi-Cp-Op-Qz-Pl gneiss
Classification	Depleted tonalite	Depleted tonalite	Depleted tonalite	Depleted tonalite	Depleted tonalite	Depleted tonalite	Depleted tonalite	Depleted tonalite
SiO_2	62.50	69.80	66.10	69.90	72.70	59.70	64.70	61.30
TiO_2	.72	.37	.50	.40	.28	.84	.77	.82
Al_2O_3	16.46	15.64	15.94	15.89	14.75	17.25	16.12	15.11
Fe_2O_3	2.39	1.05	1.33	1.41	.75	.45	1.62	.84
FeO	4.02	2.10	2.91	1.38	.85	6.87	3.62	6.46
MnO	.10	.05	.07	.03	.02	.12	.07	.11
MgO	3.81	1.39	2.09	.98	.82	3.41	2.25	3.95
CaO	4.58	3.80	5.25	3.88	3.59	6.20	5.61	7.01
Na_2O	3.67	4.38	4.00	4.67	4.29	3.04	3.95	2.51
K_2O	.87	.77	.85	.88	.70	.94	.67	.96
P_2O_5	.16	.09	.14	.12	.04	.17	.25	.13
LOI	.53	.58	.70	.39	.53	.89	.40	.86
Rest	.21	.17	.24	.19	.26	.18	.15	.25
Total	100.02	100.19	100.12	100.12	99.58	100.06	100.18	100.31
O=F,S,Cl	.00	.00	.02	.00	.01	.01	.00	.03
Total	100.02	100.19	100.10	100.11	99.56	100.05	100.18	100.27
	Trace elements in parts per million							
Ba	496	520	554	599	704	280	396	537
Rb	7	2	2	4	2	51	1	36
Sr	357	542	618	535	828	267	324	196
Pb	12	6	6	6	6	14	6	11
Th	8	<1	<1	<1	11	6	<1	6
U	.50	<.50	<.50	<.50	<.50	1.00	.50	1.00
Zr	137	82	99	169	148	106	145	92
Nb	5	1	3	2	1	7	5	5
Y	20	2	8	2	2	17	16	18
La	40	16	15	15	46	25	25	27
Ce	82	24	29	25	75	58	52	53
Nd	35	7	13	9	20	22	22	23
Sc	21	9	14	8	6	26	15	27
V	110	38	71	32	22	157	73	165
Cr	154	21	50	10	6	28	29	62
Ni	34	8	26	12	12	13	17	29
Cu	11	11	23	8	17	11	6	31
Zn	68	44	52	40	24	89	50	62
Sn	1	<1	<1	<1	<1	2	<1	1
Ga	18	16	18	19	15	21	19	19
S	100	100	500	100	300	300	<100	700

Bunger Hills Metamorphic Rocks

Sample number	86286009	86286012	86286096	86286210	86286238	86285600	86285623	86285873
Locality	Cape Jones	Cape Jones	Bunger Hills SE	Lake Mirror	5km S of Dobrowol-ski	Currituck Island SE	Currituck Island S	S of Parrot Island
Lithology	Hb-Op-Qz-Pl gneiss	Cp-Op-Qz-Pl gneiss	Bi-Op-Qz-Pl gneiss	Cp-Op-Qz-Pl gneiss	Bi-Op-Qz-Pl gneiss	Op-Qz-Mp gneiss	Op-Pl-Qz-Kf gneiss	Op-Kf-Qz-Pl gneiss
Classification	Depleted tonalite	Depleted tonalite	Depleted tonalite	Depleted tonalite	Depleted tonalite	Depleted granodior.	Depleted granodior.	Depleted granodior.
SiO_2	68.60	62.40	70.50	56.00	70.20	71.10	73.20	61.20
TiO_2	.47	.71	.36	1.06	.35	.33	.30	.81
Al_2O_3	15.72	16.58	15.25	15.71	15.36	14.83	13.66	16.99
Fe_2O_3	1.38	2.15	.94	.60	1.02	1.04	.89	.31
FeO	1.90	2.90	1.28	9.56	1.28	1.42	1.15	5.55
MnO	.04	.07	.02	.20	.03	.03	.02	.10
MgO	1.37	2.91	1.17	5.44	1.20	.94	.69	2.53
CaO	4.40	6.15	2.57	7.61	2.57	2.90	2.20	5.41
Na_2O	4.40	4.43	4.89	1.91	5.22	3.99	3.69	3.16
K_2O	.59	.87	1.40	.37	1.34	2.83	2.94	2.09
P_2O_5	.15	.22	.03	.16	.09	.13	.03	.20
LOI	.55	.74	.78	1.05	.54	.55	.99	1.12
Rest	.19	.29	.20	.25	.18	.21	.22	.30
Total	99.76	100.42	99.39	99.92	99.38	100.30	99.98	99.77
O=F,S,Cl	.02	.03	.00	.04	.00	.01	.02	.02
Total	99.74	100.38	99.39	99.88	99.38	100.29	99.96	99.75
	Trace elements in parts per million							
Ba	378	560	699	303	740	765	696	990
Rb	1	3	14	3	11	60	48	55
Sr	465	591	390	123	267	352	225	429
Pb	4	9	19	9	11	10	21	11
Th	<1	<1	21	<1	2	7	61	<1
U	<.50	<.50	<.50	.50	.50	.50	.50	.50
Zr	143	175	215	174	207	163	188	158
Nb	2	4	4	7	2	3	2	7
Y	5	13	2	28	6	6	3	10
La	18	23	55	18	22	35	62	40
Ce	31	47	83	36	38	59	102	70
Nd	13	25	22	17	13	18	26	23
Sc	10	18	6	33	7	7	4	19
V	46	97	32	190	34	23	22	92
Cr	14	60	6	129	13	11	4	34
Ni	10	33	9	84	8	9	9	21
Cu	30	37	6	24	4	19	36	17
Zn	45	66	33	101	37	26	22	118
Sn	1	2	<1	<1	<1	<1	2	<1
Ga	17	19	16	18	17	16	16	20
S	400	700	100	800	100	200	400	500

Bunger Hills Metamorphic Rocks

Sample number	86285960	86286094	86286200	86286208	86286209	86286235	86286254	86285665
Locality	W end of Lake Dolgoe	Bunger Hills SE	E end of Algae Lake	Lake Mirror	Lake Mirror	5km S of Dobrowol-ski	Husky Dog Island	Dieglman Island
Lithology	Op-Kf-Qz-Pl gneiss	Op-Kf-Qz-Pl gneiss	Op-Kf-Qz-Pl gneiss	Op-Pl-Qz-Kf gneiss	Op-Qz-Mp gneiss	Op-Qz-Pl gneiss	Bi-Op-Kf-Qz-Pl gneiss	Op-Qz-Mp gneiss
Classification	Depleted granodior.	Depleted granodior.	Depleted granodior.	Depleted granodior.	Depleted granodior.	Depleted granodior.	Depleted granodior.	Depleted granite
SiO_2	62.00	59.90	71.20	73.40	73.20	70.60	71.20	72.00
TiO_2	.70	.75	.36	.15	.17	.29	.15	.23
Al_2O_3	16.16	17.91	14.30	14.92	14.61	15.15	15.33	14.47
Fe_2O_3	1.17	1.28	1.29	.61	.76	1.18	.44	.57
FeO	4.82	3.94	1.68	.44	.50	1.02	1.04	1.15
MnO	.10	.10	.03	.01	.01	.02	.02	.02
MgO	3.42	3.33	1.40	.31	.38	.89	1.00	.67
CaO	3.85	4.70	2.89	1.34	1.87	1.93	2.04	1.52
Na_2O	3.71	4.46	4.06	4.98	5.19	5.35	4.95	3.84
K_2O	2.28	2.14	1.80	2.96	2.04	1.88	2.49	4.52
P_2O_5	.16	.15	.06	.04	.04	.05	.02	.11
LOI	.66	.99	.67	.40	.63	.80	.57	.53
Rest	.27	.30	.24	.19	.15	.20	.42	.25
Total	99.30	99.95	99.98	99.75	99.55	99.36	99.67	99.88
O=F,S,Cl	.00	.02	.00	.00	.00	.00	.05	.00
Total	99.29	99.93	99.97	99.75	99.55	99.35	99.62	99.88
	Trace elements in parts per million							
Ba	1088	959	1102	1183	755	958	1559	1414
Rb	56	24	11	39	16	15	23	68
Sr	412	521	365	235	257	227	846	203
Pb	13	23	12	13	11	15	26	23
Th	10	<1	22	1	7	5	<1	25
U	<.50	<.50	.50	<.50	<.50	.50	<.50	1.00
Zr	165	265	184	78	95	194	80	185
Nb	6	4	2	2	2	2	1	3
Y	11	4	3	1	4	2	1	12
La	40	22	47	12	15	34	18	55
Ce	77	34	79	18	24	58	28	95
Nd	29	10	21	5	8	16	7	29
Sc	20	12	6	4	3	5	8	5
V	107	88	27	7	11	23	15	18
Cr	28	25	8	<2	3	4	11	8
Ni	11	51	9	<2	2	3	11	4
Cu	9	22	2	4	1	4	73	8
Zn	66	76	35	15	17	27	20	15
Sn	<1	1	<1	<1	<1	<1	<1	<1
Ga	18	20	15	18	20	17	14	16
S	100	400	100	<100	<100	100	1000	<100

Bunger Hills Metamorphic Rocks

Sample number	86285801	86285904	86286217	86286241	86285628	86285844	86285858	86285870
Locality	Obruchev Hills C	1km S of Edgeworth David	Algae Lake NE	3km SE of Dobrowol-ski	Thomas Island N	Saturn Island	Fuller Island S	Aviatorov Peninsula S
Lithology	Op-Qz-Pl-Kf gneiss	Op-Pl-Qz-Kf gneiss	Bi-Op-Qz-Kf-Pl gneiss	Bi-Pl-Qz-Kf gneiss	Op-Kf-Pl-Qz gneiss	Bi-Op-Pl-Kf-Qz gneiss	Op-Qz-Pl gneiss	Cp-Op-Bi-Pl-Qz gneiss
Classification	Depleted granite	Depleted granite	Depleted granite	Depleted granite				
SiO_2	73.20	70.80	65.10	71.00	73.40	79.60	72.70	69.80
TiO_2	.21	.29	.57	.33	.73	.17	.36	.76
Al_2O_3	14.00	15.31	15.32	14.96	11.66	10.74	14.11	9.28
Fe_2O_3	.90	.75	1.42	.32	1.01	.62	.95	.84
FeO	.81	.84	3.35	1.04	3.25	1.12	1.48	4.02
MnO	.03	.02	.08	.01	.06	.03	.02	.10
MgO	.51	.51	2.41	.54	1.64	.94	1.30	5.17
CaO	2.28	1.90	2.91	2.03	2.68	1.32	5.14	7.36
Na_2O	3.10	3.80	2.91	2.87	3.02	2.16	2.49	.54
K_2O	3.92	4.85	4.31	5.72	1.77	2.67	.57	.58
P_2O_5	.06	.08	.18	.13	.10	.04	.01	.10
LOI	.48	.55	.96	.53	.49	.67	.58	1.37
Rest	.34	.34	.34	.36	.22	.19	.20	.15
Total	99.84	100.04	99.86	99.84	100.03	100.27	99.91	100.07
O=F,S,Cl	.00	.00	.02	.00	.01	.01	.02	.00
Total	99.83	100.04	99.84	99.84	100.01	100.26	99.89	100.07
	Trace elements in parts per million							
Ba	1902	1696	1369	2020	379	768	292	262
Rb	74	83	93	128	28	59	5	49
Sr	517	549	401	406	197	224	515	114
Pb	16	46	19	35	9	34	5	5
Th	4	35	7	11	23	<1	<1	1
U	<.50	.50	<.50	1.00	1.00	<.50	.50	1.00
Zr	141	219	194	275	400	102	201	290
Nb	<1	5	5	8	18	1	2	8
Y	4	3	12	11	19	7	2	21
La	35	60	53	40	79	37	12	18
Ce	52	100	97	74	159	62	22	39
Nd	14	27	34	26	59	18	7	20
Sc	5	5	14	4	9	7	8	17
V	17	18	70	15	43	19	64	81
Cr	5	4	34	3	16	25	22	103
Ni	10	4	13	5	11	18	9	26
Cu	5	12	24	5	13	11	15	4
Zn	17	31	55	31	42	24	22	49
Sn	<1	<1	<1	<1	1	1	<1	1
Ga	13	18	15	16	16	11	15	11
S	100	<100	400	<100	300	200	500	100

Bunger Hills Metamorphic Rocks

Sample number	86285608	86285610	86285639	86285669	86285673	86285679	86285684	86285819
Locality	Currituck Island	Currituck Island	Thomas Island SW	Dieglman Island	Dieglman Island N	W of Lake Dolgoe	4km S of Edgeworth David	1km S of Edgeworth David
Lithology	Gt-Pl-Qz-Kf gneiss	Gt-Pl-Qz-Kf gneiss	Bi-Gt-Kf-Pl-Qz gneiss	Gt-Bi-Pl-Kf-Qz gneiss	Gt-Kf-Pl-Qz gneiss	Gt-Op-Kf-Qz-Pl gneiss	Gt-Qz-Pl gneiss	Bi-Gt-Pl-Qz gneiss
Classification								
SiO_2	73.10	63.80	68.90	77.50	65.70	61.80	76.60	69.80
TiO_2	.50	.76	.68	.17	.54	.68	.24	.66
Al_2O_3	12.71	12.89	15.21	11.58	13.55	16.42	12.77	14.09
Fe_2O_3	.91	4.97	.99	.24	2.65	1.19	.28	.74
FeO	2.62	9.22	2.88	1.26	7.51	5.41	1.90	4.34
MnO	.09	.29	.05	.03	1.50	.11	.05	.10
MgO	.90	2.44	1.67	1.29	2.51	4.63	.75	1.98
CaO	1.72	1.00	2.83	1.31	2.74	3.86	1.64	3.47
Na_2O	1.62	1.20	3.13	2.10	1.44	3.22	3.88	2.62
K_2O	4.59	3.27	2.49	3.71	1.26	1.89	1.05	1.33
P_2O_5	.11	.11	.05	.01	.20	.09	.06	.10
LOI	.39	.33	.61	.75	.33	.80	.30	.82
Rest	.19	.24	.31	.22	.25	.23	.11	.21
Total	99.45	100.52	99.80	100.17	100.18	100.33	99.63	100.26
O=F,S,Cl	.00	.00	.02	.00	.00	.01	.00	.02
Total	99.45	100.52	99.78	100.17	100.17	100.32	99.62	100.24
	Trace elements in parts per million							
Ba	921	847	956	794	1266	633	212	311
Rb	149	102	57	83	23	40	9	52
Sr	110	140	330	43	132	354	183	232
Pb	22	20	22	43	18	11	20	16
Th	<1	17	27	20	7	13	7	12
U	.50	1.00	.50	2.00	<.50	1.00	.50	1.00
Zr	197	250	263	393	184	148	182	267
Nb	6	7	7	14	9	5	3	6
Y	32	37	14	32	32	19	12	22
La	27	43	93	69	37	42	34	42
Ce	48	86	196	136	78	81	67	87
Nd	16	33	74	53	28	28	24	32
Sc	8	12	9	4	10	19	7	16
V	31	80	61	2	52	114	14	110
Cr	16	135	26	2	63	49	2	64
Ni	7	34	14	6	12	19	2	13
Cu	4	8	17	9	5	10	6	16
Zn	21	49	61	48	44	62	16	54
Sn	<1	2	1	2	1	<1	1	<1
Ga	12	14	16	16	14	18	13	17
S	<100	100	400	100	100	300	100	400

Bunger Hills Metamorphic Rocks

Sample number	86285825	86285854	86285856	86285871	86285899	86285907	86285961	86285982
Locality	1km E of Edgeworth David	Fuller Island S	Fuller Island S	Aviatorov Peninsula S	Paz Cove SE	1km S of Edgeworth David	W of Lake Dolgoe	Highjump Archipel-ago NE
Lithology	Bi-Gt-Kf-Qz gneiss	Bi-Gt-Op-Qz-Pl gneiss	Bi-Gt-Pl-Qz-Kf gneiss	Gt-Op-Pl-Kf-Qz gneiss	Bi-Gt-Qz-Pl gneiss	Bi-Gt-Pl-Qz-Kf gneiss	Bi-Gt-Pl-Qz-Kf gneiss	Gt-Qz-Pl gneiss
Classification								
SiO_2	75.60	61.50	72.10	69.00	64.00	69.70	73.70	75.00
TiO_2	.53	.79	.25	.93	1.77	.61	.13	.06
Al_2O_3	11.28	17.87	14.50	12.80	15.51	14.20	14.41	14.04
Fe_2O_3	.35	.89	.21	1.16	.96	.31	.19	.27
FeO	3.32	5.00	2.34	4.97	7.78	3.67	1.67	1.74
MnO	.08	.04	.09	.10	.25	.06	.03	.05
MgO	1.39	3.11	.99	2.24	2.01	2.27	.61	.76
CaO	.33	3.80	1.90	2.37	2.66	1.52	1.58	3.04
Na_2O	1.26	3.84	3.11	2.11	3.30	2.24	3.25	3.30
K_2O	5.65	2.18	3.72	3.38	1.00	4.46	4.06	1.41
P_2O_5	.04	.04	.07	.15	.12	.06	.07	.04
LOI	.42	.71	.51	.55	.53	.75	.34	.33
Rest	.24	.28	.15	.36	.31	.25	.18	.08
Total	100.49	100.05	99.94	100.12	100.20	100.10	100.22	100.12
O=F,S,Cl	.01	.01	.00	.03	.02	.00	.00	.00
Total	100.48	100.04	99.93	100.09	100.18	100.10	100.22	100.12
	Trace elements in parts per million							
Ba	778	683	487	1011	210	922	932	225
Rb	157	74	98	80	34	156	69	33
Sr	148	468	202	122	179	269	247	171
Pb	22	22	31	12	26	30	25	22
Th	20	31	12	21	109	17	9	<1
U	1.00	1.00	1.50	1.50	4.00	1.50	.50	1.00
Zr	259	119	90	442	510	210	55	61
Nb	6	12	4	40	41	9	3	<1
Y	33	11	17	95	57	15	18	32
La	46	85	32	95	168	42	27	14
Ce	86	196	69	197	369	83	56	26
Nd	32	82	27	82	148	31	20	9
Sc	8	15	9	12	25	9	5	12
V	61	117	35	67	121	73	7	10
Cr	72	49	8	20	24	61	7	18
Ni	14	10	3	20	7	19	4	11
Cu	12	7	6	23	15	12	5	7
Zn	33	96	32	115	84	59	16	12
Sn	<1	<1	<1	<1	1	<1	<1	<1
Ga	12	24	16	22	20	17	16	14
S	200	200	100	600	400	100	<100	<100

Bunger Hills Metamorphic Rocks

Sample number	86285995	86286056	86286069	86286074	86286249	86286252	86286262	86285606
Locality	Raketa Island	Miles Island E	Paz Cove NE	Paz Cove NE	Zabytyy Island	Husky Dog Island	Samoylov-icha Islands	Currituck Island
Lithology	Op-Gt-Qz-Pl gneiss	Op-Gt-Kf-Qz-Pl gneiss	Gt-Kf-Qz-Pl gneiss	Gt-Bi-Kf-Qz-Pl gneiss	Gt-Op-Qz-Pl gneiss	Gt-Op-Kf-Qz-Pl gneiss	Gt-Bi-Pl-Kf-Qz gneiss	Si-Gt pelite
Classification								
SiO_2	68.50	65.40	60.20	66.30	66.40	67.60	72.60	72.20
TiO_2	.44	.96	2.26	1.21	.31	.73	.74	1.00
Al_2O_3	13.55	14.74	17.06	14.09	16.46	14.48	12.37	13.69
Fe_2O_3	1.34	.76	1.15	1.16	.72	1.74	1.69	1.98
FeO	7.56	5.97	9.56	5.81	3.56	3.28	3.06	4.43
MnO	.33	.13	.29	.14	.08	.09	.12	.12
MgO	3.35	2.98	2.04	1.55	2.52	2.33	1.67	2.21
CaO	1.10	3.49	4.24	3.89	3.88	2.40	2.06	.20
Na_2O	2.52	2.71	1.98	2.14	2.84	3.74	2.53	.83
K_2O	1.12	1.67	.99	2.01	2.20	2.42	1.57	3.17
P_2O_5	.02	.03	.03	.36	.06	.05	.03	.02
LOI	.45	.69	.45	.92	.69	.75	.73	.27
Rest	.12	.33	.40	.39	.23	.25	.21	.25
Total	100.40	99.86	100.65	99.97	99.95	99.86	99.38	100.37
O=F,S,Cl	.00	.05	.03	.02	.01	.01	.00	.00
Total	100.39	99.81	100.62	99.94	99.94	99.85	99.38	100.36
	Trace elements in parts per million							
Ba	295	561	1654	1732	650	670	657	841
Rb	9	48	14	46	60	40	32	107
Sr	135	317	424	312	591	338	308	48
Pb	11	12	17	16	15	17	12	12
Th	2	11	<1	<1	8	<1	5	5
U	.50	.50	<.50	<.50	.50	<.50	1.00	1.00
Zr	149	203	149	299	84	233	232	464
Nb	4	10	21	15	4	9	8	13
Y	25	14	193	29	18	15	14	24
La	32	50	33	37	32	35	27	26
Ce	55	105	54	69	60	68	56	46
Nd	17	39	17	34	22	19	19	14
Sc	11	16	41	19	11	13	10	11
V	44	128	132	101	68	93	94	98
Cr	43	95	18	24	16	135	123	111
Ni	7	24	21	8	12	46	32	12
Cu	1	32	25	15	15	9	14	3
Zn	31	92	43	80	48	61	44	42
Sn	<1	<1	<1	1	<1	1	1	<1
Ga	12	20	15	17	18	16	12	17
S	100	1100	600	500	200	200	<100	100

Bunger Hills Metamorphic Rocks

Sample number	86285607	86285631	86285634	86285638	86285642	86285659	86285662	86285691
Locality	Currituck Island	Thomas Island N	Thomas Island N	Thomas Island SW	Thomas Island SW	Thomas Island E	Thomas Island E	1km S of Edgeworth David
Lithology	Si-Gt pelite	Si-Bi-Gt pelite	Cd-Si-Gt pelite	Bi-Si-Gt pelite	Bi-Cd-Gt pelite	Gt-Cd pelite	Gt-Cd pelite	Cd-Gt-Bi-Si pelite
Classification								
SiO_2	56.30	68.80	58.00	68.10	66.40	66.30	67.60	66.30
TiO_2	1.54	.98	.94	.76	.94	.95	.70	.82
Al_2O_3	23.45	13.97	20.63	15.93	15.46	16.24	16.03	16.73
Fe_2O_3	3.49	2.37	3.90	1.73	3.53	2.83	3.25	2.80
FeO	7.79	4.73	6.14	4.93	3.98	4.32	2.76	4.18
MnO	.11	.12	.41	.21	.18	.24	.10	.16
MgO	3.09	2.66	3.69	2.71	2.76	2.46	1.70	2.64
CaO	2.07	.92	.98	1.46	1.63	.87	1.75	.55
Na_2O	1.00	1.32	.37	.69	1.80	1.74	2.68	.80
K_2O	.31	2.59	3.91	2.21	2.54	3.22	2.27	3.70
P_2O_5	.05	.03	.10	.05	.04	.03	.04	.04
LOI	.76	.58	.82	.76	1.08	.84	.75	1.15
Rest	.24	.26	.30	.25	.28	.26	.27	.33
Total	100.20	99.33	100.19	99.79	100.62	100.30	99.90	100.20
O=F,S,Cl	.01	.01	.00	.01	.00	.00	.01	.03
Total	100.19	99.32	100.19	99.78	100.61	100.30	99.89	100.17
	Trace elements in parts per million							
Ba	244	712	1213	889	789	881	851	1063
Rb	10	99	201	123	107	89	80	127
Sr	82	107	79	87	155	145	328	158
Pb	7	11	18	13	13	31	22	19
Th	7	11	19	19	13	1	13	18
U	<.50	.50	1.00	.50	.50	1.00	1.00	1.00
Zr	265	372	176	203	281	357	236	241
Nb	19	9	11	12	9	10	8	10
Y	32	41	45	18	30	29	15	32
La	33	49	44	41	52	35	57	48
Ce	66	98	86	82	109	58	117	94
Nd	28	36	33	31	41	16	40	34
Sc	26	16	20	11	16	14	10	14
V	194	103	150	115	111	102	69	95
Cr	430	144	129	89	256	119	73	104
Ni	52	42	51	46	55	34	28	39
Cu	13	29	7	28	2	7	11	29
Zn	75	48	90	87	62	77	50	58
Sn	1	3	3	<1	2	2	4	2
Ga	32	15	25	24	18	21	22	21
S	200	200	100	200	100	100	200	600

Bunger Hills Metamorphic Rocks

Sample number	86285852	86285868	86285876	86285895	86285963	86286063	86286214	86286251
Locality	Fuller Island	Aviatorov Peninsula S	2km SE of Dobrowol-ski	Paz Cove SE	6km S of Edgeworth David	Vertolet-nyy Peninsula	Algae Lake NE	Zabytyy Island
Lithology	Sp-Gt-Cd pelite	Bi-Gt-Cd pelite	Si-Gt-Cd pelite	Si-Gt-Cd pelite	Si-Gt-Cd pelite	Gt-Si-Cd pelite	Bi-Si-Gt pelite	Bi-Gt-Cd pelite
Classification								
SiO_2	57.40	66.50	64.80	75.30	70.00	67.80	65.70	77.60
TiO_2	1.34	.92	1.16	.82	.93	.76	.96	1.04
Al_2O_3	20.81	14.08	16.28	12.89	15.46	15.58	17.09	10.23
Fe_2O_3	5.43	1.01	3.39	.98	.97	2.59	.53	1.30
FeO	8.01	6.24	5.65	5.53	5.71	3.60	6.66	3.29
MnO	.44	.12	.31	.07	.09	.12	.11	.06
MgO	4.46	3.38	3.09	3.12	3.61	1.96	2.31	1.84
CaO	.50	.52	.98	.07	.24	1.02	.49	.81
Na_2O	.59	.90	1.22	.18	.25	1.91	.91	1.02
K_2O	.40	4.87	2.41	.15	1.24	3.62	4.68	1.57
P_2O_5	.02	.03	.02	.02	.03	.05	.04	.01
LOI	.91	1.17	.66	.61	1.07	1.04	.78	.81
Rest	.18	.30	.29	.11	.17	.24	.25	.17
Total	100.49	100.04	100.26	99.85	99.77	100.29	100.51	99.75
O=F,S,Cl	.01	.02	.00	.00	.01	.00	.01	.00
Total	100.48	100.02	100.25	99.85	99.76	100.29	100.50	99.75
	Trace elements in parts per million							
Ba	109	962	945	184	379	769	759	329
Rb	14	155	76	18	40	117	145	57
Sr	62	133	178	11	31	153	76	75
Pb	4	21	15	2	5	28	22	8
Th	1	3	10	3	3	19	10	6
U	<.50	1.50	<.50	.50	1.00	1.00	1.00	.50
Zr	217	297	358	267	240	300	320	399
Nb	4	10	9	11	8	8	13	13
Y	5	36	46	27	31	31	46	17
La	14	25	49	9	11	57	44	27
Ce	24	40	93	16	19	112	85	55
Nd	8	13	31	8	8	41	27	20
Sc	16	15	21	10	15	10	14	8
V	212	116	121	100	131	83	102	82
Cr	217	96	157	101	99	95	90	76
Ni	64	19	45	19	26	35	35	25
Cu	19	22	10	3	22	8	13	4
Zn	143	76	66	34	64	60	55	47
Sn	<1	<1	4	<1	<1	2	<1	3
Ga	39	18	21	16	21	19	22	16
S	200	500	100	<100	200	<100	200	100

Bunger Hills Metamorphic Rocks

Sample number	86286264	86286270	86285645
Locality	N of Rocket Island	Mars Island	Thomas Island NW
Lithology	Gt-Si-Bi-Cd pelite	Bi-Cd pelite	Bi-Gt-Pl quartzite
Classification			
SiO_2	85.10	76.20	82.50
TiO_2	.37	.13	.94
Al_2O_3	7.72	12.16	6.35
Fe_2O_3	.25	.65	.73
FeO	1.33	1.09	4.55
MnO	.02	.03	.09
MgO	1.05	1.55	1.96
CaO	.41	.48	.90
Na_2O	.63	1.32	.41
K_2O	1.62	4.64	.52
P_2O_5	.01	.01	.03
LOI	.84	.81	.55
Rest	.12	.46	.20
Total	99.47	99.53	99.73
O=F,S,Cl	.00	.08	.04
Total	99.47	99.45	99.68
	Trace elements in parts per million		
Ba	408	1771	143
Rb	69	108	24
Sr	96	72	27
Pb	8	142	4
Th	13	19	5
U	1.00	1.50	<.50
Zr	200	108	192
Nb	8	7	13
Y	25	4	19
La	21	34	19
Ce	42	55	35
Nd	16	13	14
Sc	5	<3	10
V	20	3	118
Cr	19	<2	75
Ni	6	5	21
Cu	5	24	18
Zn	22	165	47
Sn	1	2	<1
Ga	8	13	7
S	<100	1700	900

Bunger Hills Igneous Rocks

Sample number	86286231	86286232	86285932	86285944	86285937	86285942	86285947	86285953
Locality	Grace Rocks	Grace Rocks	4km SW of Dobrowolski	2km SW of Dobrowolski	5km SW of Dobrowolski	2km SW of Dobrowolski	2km SW of Dobrowolski	6km SW of Dobrowolski
Lithology	Cp-Op quartz monzonite	Cp-Op quartz monzogabb.	Bi-Cp-Op quartz gabbro	Hb-Cp-Op quartz gabbro	Bi-Cp-Op quartz monzogabb.	Hb-Cp-Op quartz monzogabb.	Hb-Cp-Op quartz monzogabb.	Bi-Cp-Op quartz monzogabb.
Intrusion			Algae Lake pluton	Algae Lake pluton	Algae Lake pluton	Algae Lake pluton	Algae Lake pluton	Algae Lake pluton
SiO_2	58.40	56.70	52.00	54.80	56.10	58.60	58.80	53.60
TiO_2	1.92	2.10	.77	.73	1.54	1.86	1.79	2.79
Al_2O_3	13.74	14.14	17.14	18.67	15.34	14.34	14.93	15.78
Fe_2O_3	2.78	3.67	1.34	1.52	3.61	2.11	1.93	2.85
FeO	7.41	7.20	7.90	7.05	7.18	7.64	7.31	8.54
MnO	.20	.22	.18	.16	.24	.18	.18	.21
MgO	2.72	3.24	7.28	3.81	3.92	2.75	2.90	3.43
CaO	5.75	6.17	8.82	8.15	6.74	5.98	6.01	6.63
Na_2O	2.07	2.66	2.12	2.68	2.17	2.04	2.21	2.32
K_2O	3.05	2.35	.86	1.37	1.78	2.76	2.78	2.22
P_2O_5	.54	.54	.14	.17	.35	.54	.49	.96
H_2O+	-	-	-	-	-	-	-	-
H_2O-	-	-	-	-	-	-	-	-
CO_2	-	-	-	-	-	-	-	-
LOI	.94	.95	1.66	1.07	.90	.81	.76	.80
Rest	.48	.46	.37	.34	.38	.47	.43	.49
Total	100.00	100.40	100.58	100.52	100.25	100.08	100.52	100.62
O=F,S,Cl	.07	.06	.08	.05	.05	.06	.05	.07
Total	99.93	100.34	100.50	100.47	100.20	100.02	100.48	100.55
	Trace elements in parts per million							
Ba	1626	1334	416	690	848	1397	1343	1156
Li	-	-	-	-	-	-	-	-
Rb	69	55	14	31	48	68	60	50
Sr	373	375	376	572	389	353	366	484
Pb	17	16	7	11	13	17	17	16
Th	<1	<1	<1	1	4	1	<1	2
U	<.50	1.00	.50	<.50	.50	1.00	.50	.50
Zr	147	294	67	92	181	281	319	238
Nb	14	15	3	5	10	17	17	19
Y	36	44	15	20	36	42	37	45
La	36	47	19	35	38	56	52	59
Ce	81	98	34	63	79	118	106	134
Nd	41	46	14	24	37	54	50	66
Sc	26	27	32	28	30	27	25	27
V	189	203	151	120	194	166	155	207
Cr	27	38	243	55	71	38	49	65
Ni	9	11	21	22	17	5	6	10
Cu	20	19	23	17	28	13	15	23
Zn	112	121	91	89	105	120	112	149
Sn	<1	<1	2	1	<1	<1	<1	<1
Ga	17	17	18	22	18	21	19	21
As	-	-	-	-	-	-	-	-
S	1000	1200	1400	1100	500	700	500	500
F	400	-	300	-	600	600	500	1000
Cl	-	-	-	-	-	-	-	-

Bunger Hills Igneous Rocks

Sample number	86285962	86285933	86285934	86286071	86286081	86286082	86286227	86286242
Locality	6km S of Edgeworth David	4km SW of Dobrowolski	4km SW of Dobrowolski	Paz Cove NE	Krylatyy Peninsula	Krylatyy Peninsula	Paz Cove SW	Paz Cove E
Lithology	Cp-Bi-Op quartz monzogabb.	Hb-Op quartz monzonite	Hb-Op quartz monzonite	Op quartz gabbro	Cp-Bi-Op quartz gabbro	Cp-Op quartz gabbro	Cp-Bi-Op quartz gabbro	Cp-Bi-Op quartz gabbro
Intrusion	Algae Lake pluton	Algae Lake pluton	Algae Lake pluton	Paz Cove batholith	Paz Cove batholith	Paz Cove batholith	Paz Cove batholith	Paz Cove batholith
SiO_2	56.30	59.60	59.40	49.20	56.10	52.80	54.40	54.10
TiO_2	2.51	1.91	1.98	1.68	.55	.76	1.06	1.56
Al_2O_3	14.91	14.46	14.56	17.86	16.57	16.27	15.90	17.48
Fe_2O_3	2.73	2.68	2.51	2.53	.75	.93	1.15	1.63
FeO	7.87	5.94	6.16	10.81	8.16	8.68	8.71	7.80
MnO	.20	.17	.16	.24	.20	.19	.20	.17
MgO	3.01	2.28	2.31	6.98	5.76	6.34	5.82	4.08
CaO	5.62	4.72	4.85	7.53	7.92	9.46	8.09	7.89
Na_2O	2.25	2.20	2.21	1.86	1.98	2.02	1.96	2.06
K_2O	2.89	3.79	3.64	.30	.84	.79	1.36	1.75
P_2O_5	.72	.61	.63	.42	.11	.12	.25	.25
H_2O+	-	-	-	-	-	-	-	-
H_2O-	-	-	-	-	-	-	-	-
CO_2	-	-	-	-	-	-	-	-
LOI	.82	1.20	1.12	.67	1.07	1.26	1.07	1.12
Rest	.50	.50	.46	.41	.24	.27	.32	.33
Total	100.33	100.06	99.99	100.49	100.25	99.89	100.29	100.22
O=F,S,Cl	.07	.06	.03	.07	.03	.04	.02	.03
Total	100.26	100.00	99.96	100.42	100.22	99.85	100.26	100.18
	Trace elements in parts per million							
Ba	1295	1369	1394	218	392	465	842	830
Li	-	-	-	-	-	-	-	-
Rb	77	110	110	4	36	16	37	46
Sr	413	343	360	614	274	274	394	456
Pb	20	25	26	13	9	6	9	13
Th	5	9	10	3	4	1	3	2
U	.50	1.00	1.00	1.00	.50	1.00	.50	.50
Zr	286	427	573	230	106	86	131	155
Nb	19	20	19	16	5	3	7	11
Y	48	51	50	32	22	27	32	26
La	63	76	74	55	26	19	32	34
Ce	137	160	160	113	47	34	62	67
Nd	64	71	71	52	21	14	28	27
Sc	26	21	22	46	31	36	33	29
V	188	140	145	242	139	156	200	170
Cr	47	32	35	178	150	168	190	57
Ni	9	5	7	29	10	11	17	10
Cu	21	14	16	29	13	14	14	14
Zn	143	122	130	150	87	86	95	104
Sn	<1	2	<1	<1	<1	<1	<1	1
Ga	21	19	19	26	16	16	18	22
As	-	-	-	-	-	-	-	-
S	600	300	700	1400	600	900	500	700
F	900	1000	-	-	-	-	-	-
Cl	-	-	-	-	-	-	-	-

Bunger Hills Igneous Rocks

Sample number	86285896	86286066	86286068	86286083	86286218	86286221	86286228	86286245
Locality	Paz Cove SE	Paz Cove NE	Paz Cove NE	Krylatyy Peninsula	Geologov Island	Geologov Island	Paz Cove SW	Paz Cove E
Lithology	Hb-Cp-Op quartz monzogabb.	Hb-Cp-Op quartz monzogabb.	Hb-Cp-Op quartz monzogabb.	Cp-Bi-Op quartz monzogabb.	Cp-Hb-Op quartz monzogabb.	Cp-Op quartz monzogabb.	Cp-Hb-Op quartz monzogabb.	Hb-Cp-Op quartz monzogabb.
Intrusion	Paz Cove batholith	Paz Cove batholith	Paz Cove batholith	Paz Cove batholith	Paz Cove batholith	Paz Cove batholith	Paz Cove batholith	Paz Cove batholith
SiO_2	57.40	58.60	58.50	58.00	58.40	58.60	57.80	58.80
TiO_2	1.81	1.11	1.62	1.29	2.01	1.81	1.59	1.99
Al_2O_3	13.88	14.32	14.64	15.39	14.00	13.99	14.40	13.64
Fe_2O_3	2.35	1.44	1.42	1.28	1.64	3.01	1.47	2.43
FeO	8.46	8.98	7.75	7.86	8.56	7.41	8.18	8.17
MnO	.20	.22	.18	.19	.21	.20	.19	.21
MgO	3.19	3.28	3.13	3.71	2.65	2.80	3.36	1.74
CaO	6.73	7.24	5.77	6.23	5.72	6.01	6.26	6.00
Na_2O	2.12	1.88	2.01	2.05	2.19	1.77	2.17	2.10
K_2O	2.32	1.76	3.13	2.71	2.43	2.52	2.82	2.87
P_2O_5	.45	.28	.50	.34	.57	.36	.43	.78
H_2O+	-	-	-	-	-	-	-	-
H_2O-	-	-	-	-	-	-	-	-
CO_2	-	-	-	-	-	-	-	-
LOI	.88	.93	.85	.88	.91	1.02	.88	.91
Rest	.42	.32	.41	.35	.42	.38	.40	.44
Total	100.21	100.36	99.91	100.28	99.71	99.88	99.95	100.08
O=F,S,Cl	.04	.04	.03	.02	.04	.04	.04	.06
Total	100.16	100.32	99.88	100.25	99.67	99.84	99.91	100.03
	Trace elements in parts per million							
Ba	1304	896	1361	1129	1255	1170	1197	1293
Li	-	-	-	-	-	-	-	-
Rb	57	43	86	85	62	67	78	80
Sr	369	349	341	346	366	346	341	348
Pb	15	12	18	16	18	15	20	17
Th	1	<1	1	5	2	<1	4	<1
U	<.50	<.50	<.50	1.00	<.50	.50	1.00	<.50
Zr	236	155	367	237	334	240	294	252
Nb	14	6	16	12	19	16	14	21
Y	43	35	43	37	44	42	39	58
La	54	35	61	51	67	41	64	67
Ce	112	68	129	108	137	87	131	144
Nd	48	31	59	46	61	36	56	68
Sc	30	35	25	25	28	29	28	28
V	202	160	146	143	179	165	173	138
Cr	22	16	47	61	26	23	36	2
Ni	4	3	5	5	3	3	4	3
Cu	14	15	18	12	15	16	13	11
Zn	120	105	118	111	127	119	120	137
Sn	1	<1	<1	<1	2	1	3	<1
Ga	19	18	18	18	20	18	19	20
As	-	-	-	-	-	-	-	-
S	900	800	600	500	800	800	800	600
F	-	-	-	-	-	-	-	600
Cl	-	-	-	-	-	-	-	-

Bunger Hills Igneous Rocks

Sample number	86285968	86286272	86285845	86285847	86285850	86286274	86286042	86285814
Locality	Booth Peninsula W	Booth Peninsula W	Black Island	Black Island	Fuller Island N	Booth Peninsula	Thomas Island E	Booth Peninsula
Lithology	Bi-Hb-Cp-Op gabbro	Bi-Cp-Op gabbro	Bi-Cp-Op quartz gabbro	Bi-Cp-Op quartz gabbro	Bi-Cp-Op quartz gabbro	Bi-Cp-Op quartz gabbro	Hb-Cp-Op quartz monzogabb.	Hb-Cp-Op quartz monzonite
Intrusion	Booth Peninsula batholith	Booth Peninsula batholith	Booth Peninsula batholith	Booth Peninsula batholith	Booth Peninsula batholith	Booth Peninsula batholith	Booth Peninsula batholith	Booth Peninsula batholith
SiO_2	51.10	51.00	52.30	53.00	54.80	52.00	57.70	52.60
TiO_2	.47	.73	.99	1.11	1.19	.70	1.47	2.86
Al_2O_3	16.42	17.95	17.12	15.39	15.74	16.31	14.88	15.14
Fe_2O_3	.81	.89	1.38	1.75	1.88	1.40	1.39	1.24
FeO	8.09	7.52	7.56	8.62	8.14	9.14	8.11	10.90
MnO	.19	.18	.17	.22	.20	.23	.19	.23
MgO	9.08	7.68	6.14	5.68	5.11	7.06	3.15	2.61
CaO	8.53	10.28	10.23	8.95	7.60	9.56	6.68	6.18
Na_2O	2.65	2.15	2.30	2.04	2.06	2.21	2.30	2.98
K_2O	.98	.69	.82	1.19	1.67	.51	2.52	3.14
P_2O_5	.06	.10	.22	.28	.23	.14	.38	1.13
H_2O+	-	-	-	-	-	-	-	-
H_2O-	-	-	-	-	-	-	-	-
CO_2	-	-	-	-	-	-	-	-
LOI	1.64	1.11	1.08	2.13	1.48	1.06	.88	1.24
Rest	.26	.27	.30	.30	.32	.26	.42	.56
Total	100.28	100.55	100.61	100.66	100.42	100.58	100.07	100.81
O=F,S,Cl	.02	.04	.05	.05	.04	.03	.04	.07
Total	100.25	100.51	100.56	100.61	100.38	100.55	100.03	100.74
	Trace elements in parts per million							
Ba	248	268	439	513	726	397	1331	1520
Li	-	-	-	-	-	-	-	-
Rb	26	13	15	39	45	7	66	43
Sr	272	283	361	313	322	384	423	454
Pb	6	4	7	9	12	6	18	12
Th	<1	1	<1	<1	1	<1	1	<1
U	<.50	<.50	<.50	<.50	<.50	.50	<.50	<.50
Zr	46	48	76	103	165	51	269	552
Nb	5	4	4	6	7	3	10	61
Y	16	15	18	25	27	20	42	55
La	14	12	20	25	34	16	51	74
Ce	24	25	39	51	70	25	100	155
Nd	10	9	17	24	29	10	45	74
Sc	33	31	35	38	30	35	28	26
V	144	147	212	158	170	171	167	107
Cr	510	319	133	145	95	211	44	8
Ni	49	43	33	15	23	30	5	5
Cu	19	26	25	15	22	18	12	18
Zn	90	76	79	113	105	91	105	130
Sn	-	-	-	-	-	-	1	<1
Ga	16	15	18	18	20	18	21	21
As	<.50	.50	<.50	<.50	<.50	<.50	-	-
S	500	500	1000	1000	800	700	900	600
F	-	400	-	-	-	-	-	1000
Cl	-	-	-	-	-	-	-	-

Bunger Hills Igneous Rocks

Sample number	86285815	86286051	86286052	86285817	86285972	86285816	86285828	86285830
Locality	Booth Peninsula	Miles Island W	Miles Island W	Booth Peninsula	Booth Peninsula W	Booth Peninsula	Booth Peninsula E	Booth Peninsula E
Lithology	Hb-Cp-Op quartz monzonite	Hb-Cp-Op quartz monzodior.	Bi-Hb-Op quartz monzodior.	Bi-Hb-Op quartz monzonite	Hb-Cp-Op quartz monzonite	Cp-Op-Hb granite	Cp-Op granite	Hb-Cp-Op granite
Intrusion	Booth Peninsula batholith	Booth Peninsula batholith	Booth Peninsula batholith	Booth Peninsula batholith	Booth Peninsula batholith	Booth Peninsula batholith	Booth Peninsula batholith	Booth Peninsula batholith
SiO_2	53.50	53.30	51.90	57.10	60.00	61.50	60.90	60.10
TiO_2	2.72	2.95	3.35	1.65	1.31	1.67	1.62	1.72
Al_2O_3	14.53	13.88	14.55	14.86	13.93	13.54	13.71	14.28
Fe_2O_3	1.67	2.94	2.02	2.72	2.57	2.10	1.82	1.77
FeO	10.94	10.62	11.61	9.16	8.33	7.07	7.14	7.26
MnO	.23	.26	.26	.24	.20	.16	.15	.16
MgO	2.36	2.43	2.76	1.32	.94	1.53	1.93	1.96
CaO	6.05	6.34	6.45	4.74	4.64	4.79	5.19	5.41
Na_2O	2.78	2.33	2.51	2.79	2.60	2.67	2.55	2.68
K_2O	2.80	2.64	2.34	3.71	3.56	3.26	3.15	3.15
P_2O_5	.95	1.26	1.24	.92	.49	.59	.44	.47
H_2O+	-	-	-	-	-	-	-	-
H_2O-	-	-	-	-	-	-	-	-
CO_2	-	-	-	-	-	-	-	-
LOI	1.13	.79	1.04	.96	1.00	.83	1.12	.99
Rest	.47	.63	.41	.47	.51	.43	.39	.44
Total	100.13	100.37	100.44	100.64	100.08	100.14	100.11	100.39
O=F,S,Cl	.04	.08	.03	.02	.05	.05	.03	.05
Total	100.09	100.29	100.41	100.62	100.04	100.09	100.08	100.34
	Trace elements in parts per million							
Ba	1380	2120	1475	1946	1914	1324	1436	1495
Li	-	-	-	-	-	-	-	-
Rb	38	44	34	48	34	47	70	69
Sr	438	453	429	414	401	259	247	262
Pb	11	14	12	12	8	12	19	18
Th	<1	1	<1	<1	1	1	<1	<1
U	.50	1.00	.50	<.50	.50	.50	.50	<.50
Zr	657	438	217	608	680	493	370	382
Nb	61	58	60	61	52	26	16	17
Y	55	58	49	49	43	54	56	56
La	67	82	65	50	31	49	46	49
Ce	138	174	142	104	70	108	101	105
Nd	62	78	65	54	35	55	49	51
Sc	29	32	30	21	19	21	24	23
V	97	111	125	33	27	99	120	120
Cr	6	3	7	<2	<2	8	15	15
Ni	5	<2	3	<2	<2	4	5	5
Cu	21	18	21	18	17	16	15	14
Zn	133	156	152	125	121	112	106	104
Sn	<1	<1	<1	1	<1	<1	<1	<1
Ga	20	18	20	21	21	21	19	20
As	-	-	-	-	-	-	-	-
S	800	900	600	500	700	400	600	600
F	-	800	-	-	300	600	-	400
Cl	-	-	-	-	-	-	-	-

Bunger Hills Igneous Rocks

Sample number	86285831	86285835	86285837	86285975	86285986	86285987	86285989	86286276
Locality	Booth Peninsula E	Geomorfol-ogov Peninsula	Countess Peninsula	Booth Peninsula W	Highjump Archipel-ago SE	Highjump Archipel-ago SE	Highjump Archipel-ago SE	7km E of Miles Island
Lithology	Cp-Op granite	Hb-Cp-Op granite	Hb-Cp-Op granite	Bi-Hb-Op granite	Bi-Cp-Hb granite	Hb-Cp-Op granite	Hb-Px granite	Cp-Op granite
Intrusion	Booth Peninsula batholith	Booth Peninsula batholith	Booth Peninsula batholith	Booth Peninsula batholith	Booth Peninsula batholith	Booth Peninsula batholith	Booth Peninsula batholith	Booth Peninsula batholith
SiO_2	60.80	59.80	59.20	63.40	61.00	60.50	65.30	60.70
TiO_2	1.79	1.80	1.88	1.45	1.78	1.82	1.38	1.70
Al_2O_3	14.09	14.20	14.01	13.56	13.37	13.46	13.27	14.06
Fe_2O_3	2.05	1.73	2.13	1.76	2.45	2.25	2.59	1.92
FeO	6.98	7.61	7.70	7.00	7.21	7.80	4.84	6.94
MnO	.15	.17	.17	.17	.18	.19	.14	.15
MgO	1.94	2.16	2.09	1.06	1.91	2.05	1.05	1.91
CaO	5.40	5.65	5.59	3.65	4.99	5.20	3.42	5.41
Na_2O	2.77	2.59	2.67	2.24	2.13	2.25	2.00	2.63
K_2O	3.07	2.79	2.79	4.20	3.61	3.43	4.89	3.03
P_2O_5	.48	.46	.52	.60	.47	.49	.45	.45
H_2O+	-	-	-	-	-	-	-	-
H_2O-	-	-	-	-	-	-	-	-
CO_2	-	-	-	-	-	-	-	-
LOI	.75	.78	.66	.72	.91	.69	.64	.76
Rest	.40	.44	.38	.46	.41	.41	.39	.43
Total	100.67	100.18	99.79	100.27	100.42	100.54	100.36	100.09
O=F,S,Cl	.03	.05	.02	.04	.03	.03	.01	.05
Total	100.63	100.13	99.77	100.24	100.39	100.51	100.35	100.04
	Trace elements in parts per million							
Ba	1367	1415	1356	1774	1510	1517	1650	1454
Li	-	-	-	-	-	-	-	-
Rb	58	57	59	65	97	91	138	70
Sr	252	267	259	304	273	284	260	262
Pb	16	18	17	15	22	21	26	17
Th	<1	<1	<1	<1	1	1	2	1
U	<.50	.50	1.00	.50	<.50	<.50	.50	<.50
Zr	413	351	404	606	349	340	473	328
Nb	19	18	18	43	17	17	22	16
Y	60	54	60	40	57	55	49	56
La	51	48	53	41	63	61	69	48
Ce	111	104	115	85	131	130	147	101
Nd	55	49	54	41	59	59	70	48
Sc	23	24	24	18	27	27	19	24
V	124	125	139	38	141	139	71	126
Cr	16	20	17	2	14	16	3	17
Ni	5	6	5	<2	4	4	<2	8
Cu	17	16	14	13	14	14	10	14
Zn	105	108	114	109	120	117	112	105
Sn	<1	1	<1	1	1	2	<1	<1
Ga	21	20	19	20	19	19	18	19
As	-	-	-	-	-	-	-	-
S	700	600	500	400	600	600	200	500
F	-	500	-	400	-	-	-	500
Cl	-	-	-	-	-	-	-	-

Bunger Hills Igneous Rocks

Sample number	86286277	86286281	86286058	86286060	86286061	86286088	86286089	86285827
Locality	7km E of Miles Island	6km E of Miles Island	Vertolet-nyy Peninsula	Vertolet-nyy Peninsula	Vertolet-nyy Peninsula	Krylatyy Peninsula	Krylatyy Peninsula	Booth Peninsula E
Lithology	Hb-Cp-Op granite	Hb-Cp-Op granite	Op-Gt granite	Op granite	Hb-Op granite	Hb-Op-Gt granite	Hb-Op granite	Hb-Op monzodior-ite dyke
Intrusion	Booth Peninsula batholith	Booth Peninsula batholith	Paz Cove batholith	Paz Cove batholith	Paz Cove batholith	Paz Cove batholith	Paz Cove batholith	
SiO_2	60.30	60.90	63.80	64.00	64.60	66.70	65.40	47.50
TiO_2	1.72	1.54	1.32	1.25	1.40	.81	1.06	1.88
Al_2O_3	13.89	14.36	13.86	13.92	13.27	13.25	13.04	15.76
Fe_2O_3	1.84	2.06	2.07	1.85	1.81	1.82	2.27	6.29
FeO	7.02	6.28	6.23	5.98	6.17	4.58	5.52	11.82
MnO	.16	.15	.17	.15	.15	.12	.15	.33
MgO	1.81	1.72	1.25	1.19	1.49	.58	.77	2.04
CaO	5.36	5.26	3.47	3.59	3.92	2.74	3.17	6.02
Na_2O	2.54	2.69	2.10	2.30	2.12	1.97	2.06	3.17
K_2O	3.10	3.16	4.02	4.16	3.89	5.61	4.97	2.58
P_2O_5	.51	.42	.54	.47	.48	.29	.41	1.41
H_2O+	-	-	-	-	-	-	-	-
H_2O-	-	-	-	-	-	-	-	-
CO_2	-	-	-	-	-	-	-	-
LOI	1.05	.70	.75	.78	.86	.68	.61	.87
Rest	.37	.40	.44	.42	.45	.49	.45	.62
Total	99.67	99.64	100.02	100.06	100.61	99.64	99.88	100.29
O=F,S,Cl	.01	.03	.03	.02	.04	.01	.03	.11
Total	99.66	99.62	99.99	100.04	100.57	99.63	99.86	100.18
	Trace elements in parts per million							
Ba	1592	1594	1894	1973	1709	2740	1851	1264
Li	-	-	-	-	-	-	-	-
Rb	67	67	100	100	96	150	138	33
Sr	273	278	281	294	298	277	239	375
Pb	18	18	18	21	20	26	26	11
Th	<1	<1	<1	1	<1	1	<1	<1
U	1.00	.50	.50	.50	.50	<.50	1.00	1.50
Zr	380	349	357	351	333	451	544	711
Nb	18	15	25	20	18	18	21	59
Y	57	51	33	31	43	45	51	75
La	52	47	45	48	50	56	59	78
Ce	114	99	92	105	109	110	129	176
Nd	54	48	38	50	54	52	60	87
Sc	24	22	23	21	23	17	20	30
V	133	116	70	70	99	12	25	17
Cr	16	13	10	8	11	<2	<2	<2
Ni	6	8	3	3	3	<2	<2	<2
Cu	8	13	17	19	15	12	12	24
Zn	110	99	104	102	103	98	118	204
Sn	<1	2	<1	<1	<1	<1	<1	<1
Ga	20	19	18	18	17	17	18	25
As	-	-	-	-	-	-	-	-
S	200	200	300	400	400	200	100	1200
F	-	400	400	-	500	-	500	1200
Cl	-	-	-	-	-	-	-	-

Bunger Hills Igneous Rocks

Sample number	86286266	86286267	86286256	86285617	86285676	86285834	86286041	86286222
Locality	Mars Island	Mars Island	Husky Dog Island	Currituck Island W	Currituck Island W	Geomorfol-ogov Peninsula	Thomas Island E	Geologov Island
Lithology	Cp-Op Qz gabbro dyke	Cp-Op Qz gabbro dyke	Op granite dyke	Bi-Mus granite	Bi-Mus granite	Hb-Bi granite	Bi granite	Trachyte dyke
Intrusion								
SiO_2	50.70	53.90	64.60	74.80	74.60	72.50	70.80	58.70
TiO_2	3.46	3.22	1.15	.05	.14	.24	.54	.43
Al_2O_3	13.27	13.65	13.24	13.56	13.63	13.98	13.86	18.01
Fe_2O_3	4.97	8.68	5.04	.50	.69	.47	1.19	1.98
FeO	12.20	7.55	3.78	.25	.59	1.17	1.07	2.41
MnO	.36	.33	.16	.03	.03	.03	.04	.11
MgO	2.28	2.12	.80	.12	.19	.47	.75	1.09
CaO	7.79	7.20	3.47	.77	.98	2.01	1.18	1.74
Na_2O	1.72	1.16	2.15	3.51	3.31	2.31	2.31	5.04
K_2O	.81	.75	3.68	5.05	5.02	5.49	6.38	6.71
P_2O_5	.89	.81	.46	.01	.03	.02	.08	.19
H_2O+	-	-	-	-	-	-	-	.72
H_2O-	-	-	-	-	-	-	-	.14
CO_2	-	-	-	-	-	-	-	2.25
LOI	1.07	.76	1.05	.83	.96	.78	1.02	-
Rest	.44	.38	.45	.14	.19	.33	.48	.59
Total	99.96	100.51	100.03	99.62	100.36	99.80	99.70	100.11
O=F,S,Cl	.08	.05	.02	.00	.00	.00	.01	.02
Total	99.88	100.45	100.01	99.62	100.36	99.80	99.69	100.08
	Trace elements in parts per million							
Ba	745	745	2140	113	363	1976	2360	92
Li	-	5	-	-	-	-	-	-
Rb	6	13	60	604	507	116	140	344
Sr	487	465	315	52	111	269	455	114
Pb	6	8	11	115	86	28	47	175
Th	<1	1	<1	45	96	2	56	273
U	1.00	<.50	.50	20.00	9.50	1.00	.50	40.00
Zr	271	199	560	97	137	290	411	1593
Nb	58	50	20	60	31	4	7	112
Y	64	66	34	22	13	8	18	53
La	33	39	32	6	47	22	103	453
Ce	77	85	62	11	92	28	214	794
Nd	48	46	28	5	31	7	78	208
Sc	33	32	20	4	5	7	6	5
V	129	116	29	<2	3	9	33	11
Cr	6	6	<2	<2	<2	<2	<2	<2
Ni	4	6	<2	2	2	<2	3	<2
Cu	20	14	17	<1	3	3	26	2
Zn	165	148	106	16	15	25	21	64
Sn	<1	1	<1	7	6	<1	<1	-
Ga	20	20	17	30	28	15	11	19
As	-	-	-	-	-	-	-	7.00
S	1630	990	400	<100	100	100	200	500
F	-	-	-	-	-	-	-	-
Cl	130	225	-	-	-	-	-	-

Bunger Hills Igneous Rocks

Sample number	86285640	86285970	86285984	86285996	86286040	86286044	86286045	86285678
Locality	Thomas Island S	Booth Peninsula W	Highjump Archipel-ago NE	Highjump Archipel-ago NE	Thomas Island E	Obryvistyy Island	Obryvistyy Island	W of Lake Dolgoe
Lithology	Px-Pl granulite	Px-Hb-Pl granulite	Hb-Px-Pl granulite	Hb-Px-Pl granulite	Px-Pl granulite	Bi-Px-Pl granulite	Px-Pl granulite	Quartz tholeiite dyke
Classification	Metadyke	Metadyke	Metadyke	Metadyke	Metadyke	Metadyke	Metadyke	Group 1
SiO_2	50.50	47.10	48.80	49.60	49.50	53.50	46.80	51.90
TiO_2	.51	1.61	1.91	1.84	1.53	1.16	2.32	1.77
Al_2O_3	17.46	15.47	13.50	14.64	16.69	14.47	15.32	15.20
Fe_2O_3	1.89	1.61	2.62	2.71	3.93	1.35	4.40	1.82
FeO	7.55	10.17	11.90	9.53	9.13	6.97	9.66	8.58
MnO	.18	.19	.22	.19	.19	.16	.25	.15
MgO	8.30	7.90	6.88	6.63	8.03	7.09	7.28	5.35
CaO	11.00	9.05	11.18	11.01	8.67	7.48	9.96	8.48
Na_2O	1.33	2.99	2.36	2.45	.91	1.15	2.21	3.38
K_2O	.20	1.13	.37	.56	.29	1.48	.36	.86
P_2O_5	.05	.32	.21	.16	.24	1.60	.62	.36
H_2O+	-	-	-	-	-	-	-	-
H_2O-	-	-	-	-	-	-	-	-
CO_2	-	-	-	-	-	-	-	-
LOI	1.00	2.20	.70	.83	.91	1.21	1.09	2.16
Rest	.28	.33	.27	.39	.28	2.00	.42	.36
Total	100.25	100.07	100.92	100.54	100.30	99.62	100.69	100.37
O=F,S,Cl	.06	.04	.03	.09	.04	.25	.08	.07
Total	100.19	100.02	100.88	100.45	100.25	99.37	100.61	100.31
	Trace elements in parts per million							
Ba	197	385	114	172	293	8730	400	364
Rb	4	21	2	13	20	84	6	15
Sr	234	371	199	306	173	2380	342	628
Pb	4	4	4	5	8	12	9	5
Th	<1	2	<1	<1	<1	10	<1	<1
U	.50	<.50	.50	<.50	1.00	1.50	<.50	1.00
Zr	29	140	112	121	110	406	266	106
Nb	<1	24	9	8	10	14	20	22
Y	22	25	32	28	31	32	33	21
La	6	23	15	12	19	94	36	16
Ce	16	41	32	32	44	199	76	37
Nd	8	21	18	19	22	88	36	23
Pr	-	-	-	-	-	-	-	-
Sc	30	35	49	37	41	31	41	19
V	160	198	413	309	252	171	291	117
Cr	270	246	126	163	88	245	94	122
Ni	23	135	63	55	110	110	56	49
Cu	47	28	74	83	76	172	58	31
Zn	70	102	113	94	103	108	121	115
Sn	-	-	-	-	-	-	-	-
Ga	16	16	18	19	19	15	20	20
As	<.50	<.50	<.50	<.50	<.50	<.50	<.50	<.50
S	1160	900	700	1810	900	5000	1700	1190
F	-	-	-	-	-	-	-	-
Cl	75	-	-	115	-	-	-	270

Bunger Hills Igneous Rocks

Sample number	86285682	86285690	86285860	86285905	86285964	86286237	86285603	86285644
Locality	W of Lake Dolgoe	1km S of Edgeworth David	Fuller Island	1km S of Edgeworth David	1km N of Edgeworth David	5km S of Dobrowol-ski	Currituck Island SE	Thomas Island S
Lithology	Quartz tholeiite dyke	Quartz tholeiite dyke	Olivine tholeiite dyke	Quartz tholeiite dyke	Olivine tholeiite dyke	Quartz tholeiite dyke	High-Mg Ol tholeiite dyke	High-Mg Ol tholeiite dyke
Classification	Group 1	Group 1	Group 1	Group 1	Group 1	Group 1	Group 2	?Group 2
SiO_2	52.30	51.60	48.90	50.70	49.60	53.00	49.10	49.20
TiO_2	1.72	1.69	2.28	1.71	2.11	1.56	2.47	1.63
Al_2O_3	15.20	14.98	14.40	14.76	14.63	14.97	9.87	14.63
Fe_2O_3	2.66	3.81	2.87	2.59	3.21	1.85	2.93	3.02
FeO	8.03	7.03	8.40	8.16	8.10	9.00	10.31	8.93
MnO	.15	.16	.16	.15	.16	.16	.19	.19
MgO	5.49	5.52	5.83	5.28	5.98	5.64	12.57	8.64
CaO	8.51	8.17	7.57	8.27	8.10	8.11	8.94	9.23
Na_2O	3.42	3.35	3.26	3.18	3.46	3.27	1.83	2.83
K_2O	.84	.78	1.83	.78	1.35	.63	.90	.49
P_2O_5	.36	.35	.56	.34	.50	.26	.24	.19
H_2O+	-	-	1.07	.68	-	-	-	-
H_2O-	-	-	.04	.13	-	-	-	-
CO_2	-	-	2.24	2.53	-	-	-	-
LOI	1.31	2.05	-	-	2.46	1.18	.81	1.24
Rest	.33	.35	.53	.42	.50	.32	.56	.32
Total	100.32	99.84	99.94	99.68	100.16	99.95	100.72	100.54
O=F,S,Cl	.05	.06	.09	.10	.09	.06	.04	.06
Total	100.27	99.78	99.85	99.58	100.06	99.89	100.68	100.48
	Trace elements in parts per million							
Ba	354	313	495	330	543	245	278	102
Rb	15	14	40	15	25	11	26	9
Sr	627	580	857	571	877	495	337	327
Pb	3	4	24	5	7	3	7	4
Th	1	<1	2	<1	2	<1	3	<1
U	.50	<.50	<.50	<.50	.50	<.50	1.50	.50
Zr	102	96	157	100	136	83	200	100
Nb	22	22	41	23	37	16	11	10
Y	22	20	22	20	22	19	28	18
La	16	17	22	14	24	12	20	8
Ce	35	32	54	35	50	27	55	26
Nd	22	19	32	20	32	17	32	16
Pr	-	-	-	-	-	-	-	-
Sc	19	24	18	21	17	18	29	24
V	117	125	112	119	113	112	315	174
Cr	116	144	136	128	142	164	1139	319
Ni	46	57	67	50	75	63	372	170
Cu	28	37	34	31	32	34	85	60
Zn	111	111	164	118	129	114	109	104
Sn	-	-	-	-	-	-	-	-
Ga	19	20	20	20	20	21	19	18
As	<.50	.50	1.00	1.00	<.50	<.50	<.50	<.50
S	980	1180	1140	1930	1670	1130	405	1100
F	-	-	-	-	-	-	-	-
Cl	245	270	1320	265	495	185	1000	110

Bunger Hills Igneous Rocks

Sample number	86285654	86285655	86285656	86286201	77284736	86285902	86285913	86285936
Locality	Thomas Island E	Thomas Island E	Thomas Island E	E end of Algae Lake	5km E of Dobrowolski	Paz Cove SE	Foster Island	5km SW of Dobrowolski
Lithology	High-Mg Ol tholeiite dyke	High-Mg Ol tholeiite dyke	High-Mg Ol tholeiite dyke	High-Mg Ol tholeiite dyke	Olivine tholeiite dyke	Quartz tholeiite dyke	Quartz tholeiite dyke	Quartz tholeiite dyke
Classification	Group 2	Group 2	Group 2	Group 2	Group 3A	Group 3A	Group 3A	Group 3A
SiO_2	48.60	48.50	47.80	46.30	47.20	48.60	47.40	48.80
TiO_2	3.32	2.95	2.88	2.76	3.68	3.63	3.74	3.67
Al_2O_3	11.74	10.70	10.59	10.64	15.59	14.13	15.81	14.25
Fe_2O_3	3.41	2.56	2.12	3.53	3.67	3.67	5.62	3.38
FeO	10.67	11.65	11.97	10.39	10.22	10.62	8.68	10.84
MnO	.19	.20	.20	.19	.20	.22	.21	.22
MgO	7.69	10.10	10.95	12.08	4.07	4.67	4.09	4.80
CaO	9.64	9.10	8.42	8.23	8.01	7.81	8.23	7.90
Na_2O	2.30	2.00	2.03	1.75	3.15	2.71	3.08	2.87
K_2O	1.35	1.29	1.34	.97	1.64	1.62	1.59	1.59
P_2O_5	.32	.32	.33	.29	.64	.56	.62	.53
H_2O+	-	-	-	-	.95	-	-	-
H_2O-	-	-	-	-	.20	-	-	-
CO_2	-	-	-	-	.22	-	-	-
LOI	1.01	1.07	.93	2.04	-	1.53	.71	1.02
Rest	.40	.48	.52	.72	.30	.46	.44	.47
Total	100.64	100.92	100.08	99.89	99.74	100.23	100.22	100.34
O=F,S,Cl	.03	.04	.04	.13	.02	.09	.08	.10
Total	100.61	100.88	100.04	99.76	99.72	100.14	100.13	100.24
	Trace elements in parts per million							
Ba	415	408	384	336	579	632	651	579
Rb	38	36	39	27	47	51	45	48
Sr	490	435	425	375	277	226	288	225
Pb	11	10	11	8	12	14	13	13
Th	4	5	5	5	6	7	6	6
U	.50	.50	.50	1.00	1.00	1.50	.50	<.50
Zr	270	271	287	243	292	292	297	279
Nb	17	16	17	15	19	16	16	15
Y	34	34	35	31	57	57	56	57
La	33	29	31	21	41	34	42	31
Ce	73	68	68	59	91	81	90	72
Nd	44	40	42	36	47	44	51	41
Pr	-	-	-	-	-	-	-	-
Sc	30	27	26	25	30	29	25	27
V	348	317	299	288	238	288	226	281
Cr	383	770	985	978	24	47	28	50
Ni	122	238	345	598	38	50	33	53
Cu	87	102	126	126	28	39	50	36
Zn	109	114	116	116	142	149	141	142
Sn	-	-	-	-	-	-	-	-
Ga	21	20	20	19	22	21	21	21
As	<.50	1.00	.50	<.50	1.00	<.50	<.50	<.50
S	410	690	675	2630	500	1750	1560	2030
F	-	-	-	-	-	-	-	-
Cl	225	155	140	140	-	155	165	120

Bunger Hills Igneous Rocks

Sample number	86285948	86286059	86286077	86286234	86286244	86285998	86286054	86286279
Locality	2km SW of Dobrowolski	Vertoletnyy Peninsula	Krylatyy Peninsula	5km S of Dobrowolski	Paz Cove E	Zabytyy Island N	Miles Island E	7km E of Miles Island
Lithology	Quartz tholeiite dyke	Quartz tholeiite dyke	Olivine tholeiite dyke	Olivine tholeiite dyke	Olivine tholeiite dyke	Quartz tholeiite dyke	Olivine tholeiite dyke	Olivine tholeiite dyke
Classification	Group 3A	Group 3A	Group 3A	Group 3A	Group 3A	Group 3B	Group 3B	?Group 3B
SiO_2	47.10	48.90	47.40	47.70	47.40	46.30	46.60	47.20
TiO_2	3.85	3.63	3.73	3.68	3.71	3.50	3.08	2.77
Al_2O_3	15.60	14.17	15.61	15.95	15.66	14.15	14.92	14.34
Fe_2O_3	5.88	2.77	2.99	3.42	3.43	5.89	5.49	3.42
FeO	8.69	11.43	11.19	10.32	10.62	9.53	9.07	10.98
MnO	.22	.22	.21	.20	.21	.25	.23	.25
MgO	4.17	4.52	4.28	4.00	4.06	5.27	5.78	5.41
CaO	8.25	8.04	8.23	8.25	8.26	8.56	8.57	8.87
Na_2O	3.03	2.77	3.09	3.06	3.04	2.81	2.74	2.85
K_2O	1.59	1.67	1.61	1.61	1.64	1.35	1.31	1.31
P_2O_5	.61	.57	.63	.61	.63	.63	.53	.71
H_2O+	-	-	-	-	-	-	-	-
H_2O-	-	-	-	-	-	-	-	-
CO_2	-	-	-	-	-	-	-	-
LOI	.99	1.05	.94	1.05	.94	.98	1.29	1.21
Rest	.47	.48	.52	.44	.51	.49	.48	.51
Total	100.45	100.22	100.43	100.29	100.11	99.71	100.09	99.83
O=F,S,Cl	.10	.11	.13	.09	.12	.11	.11	.11
Total	100.35	100.12	100.30	100.20	99.99	99.60	99.98	99.72

Trace elements in parts per million

Ba	639	626	623	634	648	442	452	609
Rb	45	53	45	46	45	29	31	21
Sr	281	224	282	285	281	301	312	291
Pb	13	12	12	13	13	9	9	9
Th	6	8	7	5	6	1	2	1
U	.50	1.00	<.50	1.00	1.00	1.00	.50	.50
Zr	304	298	314	310	301	314	268	414
Nb	17	17	18	17	18	17	16	16
Y	59	59	60	58	60	56	49	61
La	37	37	36	39	38	26	23	27
Ce	83	80	85	85	86	64	59	65
Nd	47	47	50	48	49	38	38	46
Pr	-	-	-	-	-	-	-	-
Sc	23	26	22	23	23	30	27	31
V	231	275	212	213	212	349	290	269
Cr	32	46	31	22	23	89	77	78
Ni	44	51	48	39	40	38	54	39
Cu	29	40	29	25	27	43	41	38
Zn	148	144	143	139	140	138	123	134
Sn	-	-	-	-	-	-	-	-
Ga	23	22	22	23	22	22	20	21
As	<.50	<.50	1.00	<.50	<.50	<.50	<.50	<.50
S	2000	2080	2460	1730	2410	2090	2230	2190
F	-	-	-	-	-	-	-	-
Cl	125	105	145	95	115	150	135	145

Bunger Hills Igneous Rocks

Sample number	86285660	86285841	86286215	86286219	86286259	86286260	86285646	86285666
Locality	Thomas Island E	Saturn Island	Algae Lake NE	Geologov Island	Liberty Islands S	Liberty Islands S	Thomas Island N	Dieglman Island
Lithology	Olivine tholeiite dyke	Olivine tholeiite dyke	Olivine tholeiite dyke	Olivine tholeiite dyke	Olivine tholeiite dyke	Quartz tholeiite dyke	Olivine dolerite dyke	Olivine dolerite dyke
Classification	Group 3C	Group 3C	Group 3D	Group 3D	Group 3E	Group 3E	Group 4A	Group 4A
SiO_2	45.30	45.60	45.30	45.00	48.50	49.10	45.60	46.50
TiO_2	4.06	4.11	4.16	4.19	2.70	2.67	3.27	3.21
Al_2O_3	13.59	13.66	12.60	12.25	13.02	13.23	15.78	15.98
Fe_2O_3	3.62	2.83	4.04	2.78	2.45	5.14	3.74	3.15
FeO	12.44	13.09	12.37	13.81	13.63	11.10	10.71	11.22
MnO	.27	.28	.28	.29	.29	.29	.21	.21
MgO	4.95	4.82	4.46	4.64	2.78	2.86	6.20	6.23
CaO	8.48	8.50	8.26	8.37	6.21	6.28	8.35	8.53
Na_2O	2.79	2.88	2.87	2.75	3.53	3.54	3.14	2.88
K_2O	1.61	1.64	1.83	1.84	2.64	2.75	.91	.91
P_2O_5	1.13	1.12	2.33	2.40	1.68	1.71	.43	.44
H_2O+	-	-	-	-	-	-	-	-
H_2O-	-	-	-	-	-	-	-	-
CO_2	-	-	-	-	-	-	-	-
LOI	1.17	1.44	1.21	.98	1.49	.76	1.29	.82
Rest	.52	.55	.58	.52	.64	.60	.47	.38
Total	99.93	100.52	100.29	99.82	99.56	100.03	100.10	100.46
O=F,S,Cl	.11	.12	.13	.11	.12	.11	.13	.08
Total	99.82	100.40	100.16	99.71	99.43	99.92	99.97	100.38
	Trace elements in parts per million							
Ba	669	656	858	676	1524	1457	341	323
Rb	38	38	41	41	48	51	18	19
Sr	303	301	274	263	345	343	292	296
Pb	12	12	11	12	15	15	6	6
Th	2	3	3	2	3	2	1	1
U	.50	1.50	<.50	<.50	1.00	.50	.50	1.00
Zr	384	398	477	483	471	496	203	212
Nb	22	23	18	18	41	41	11	11
Y	70	71	82	81	85	88	42	40
La	47	43	44	41	62	63	19	14
Ce	106	103	107	106	131	136	41	42
Nd	67	66	78	78	83	82	25	25
Pr	-	-	-	-	-	-	-	-
Sc	29	31	34	34	18	21	24	25
V	282	282	199	202	35	29	226	234
Cr	28	26	2	2	<2	<2	74	76
Ni	27	28	9	8	<2	<2	80	82
Cu	34	33	33	33	21	22	38	65
Zn	148	154	165	170	177	179	116	117
Sn	-	-	-	-	-	-	-	-
Ga	24	23	21	20	23	23	20	19
As	<.50	<.50	<.50	<.50	<.50	<.50	<.50	<.50
S	2080	2350	2640	2190	2250	2030	2420	1590
F	-	-	-	-	-	-	-	-
Cl	175	230	110	105	430	345	200	125

Bunger Hills Igneous Rocks

Sample number	86285667	86285864	86285865	86285877	86285929	86285939	86286087	86286097
Locality	Dieglman Island	Aviatorov Peninsula N	Aviatorov Peninsula N	2km SE of Dobrowol-ski	S Taylor Islands	5km SW of Dobrowol-ski	Krylatyy Peninsula SW	Bunger Hills SE
Lithology	Olivine dolerite dyke	Olivine dolerite dyke	Olivine dolerite dyke	Olivine dolerite dyke	Olivine dolerite dyke	Olivine dolerite dyke	Olivine dolerite dyke	Olivine dolerite dyke
Classification	Group 4A	Group 4A	Group 4A	Group 4A	Group 4A	Group 4A	Group 4A	Group 4A
SiO_2	45.90	45.70	45.40	45.60	45.90	45.00	45.60	45.30
TiO_2	3.26	3.36	2.90	3.05	3.33	3.10	3.20	3.25
Al_2O_3	15.91	15.85	16.47	16.83	15.98	16.05	16.03	15.92
Fe_2O_3	2.83	3.71	3.69	3.97	4.36	5.64	3.33	3.35
FeO	11.59	10.83	9.65	9.04	9.83	8.61	11.01	11.05
MnO	.21	.21	.19	.18	.19	.20	.21	.20
MgO	6.27	5.79	6.38	5.84	5.80	6.11	6.12	6.07
CaO	8.49	8.44	8.53	8.79	8.48	8.52	8.62	8.50
Na_2O	3.06	3.10	3.08	3.15	3.23	3.12	3.10	3.01
K_2O	.92	.92	.82	.83	1.01	.80	.86	.88
P_2O_5	.44	.45	.39	.40	.43	.38	.42	.44
H_2O+	-	-	-	-	-	-	-	-
H_2O-	-	-	-	-	-	-	-	-
CO_2	-	-	-	-	-	-	-	-
LOI	.92	1.47	2.41	2.05	1.45	1.84	1.49	1.85
Rest	.43	.40	.35	.42	.51	.55	.38	.38
Total	100.23	100.23	100.26	100.15	100.50	99.92	100.37	100.20
O=F,S,Cl	.11	.09	.07	.10	.13	.16	.08	.08
Total	100.12	100.14	100.18	100.04	100.37	99.75	100.28	100.12
	Trace elements in parts per million							
Ba	345	346	290	322	359	301	311	330
Rb	18	19	16	15	22	16	17	18
Sr	294	295	307	313	290	296	293	285
Pb	7	6	6	6	5	4	5	6
Th	1	1	1	<1	3	1	2	<1
U	.50	.50	.50	.50	<.50	.50	<.50	.50
Zr	210	210	187	191	218	192	202	206
Nb	12	9	11	10	10	10	10	10
Y	43	44	36	39	42	40	41	42
La	15	17	12	15	14	14	14	13
Ce	44	42	35	41	42	39	41	43
Nd	26	27	23	26	28	24	26	25
Pr	-	-	-	-	-	-	-	-
Sc	24	23	23	24	27	21	23	26
V	227	223	200	207	251	225	220	253
Cr	74	70	65	62	74	63	68	73
Ni	80	77	105	95	82	91	85	84
Cu	37	42	35	35	44	38	39	42
Zn	119	115	111	109	135	123	119	125
Sn	-	-	-	-	-	-	-	-
Ga	19	19	19	20	20	19	19	21
As	<.50	<.50	<.50	<.50	<.50	<.50	.50	<.50
S	2090	1820	1440	2030	2470	3100	1640	1570
F	-	-	-	-	-	-	-	-
Cl	120	110	95	155	425	385	115	75

Bunger Hills Igneous Rocks

Sample number	86285872	86285966	86285997	86286075	86286076	86286048	86286050	77284739
Locality	S of Parrot Island	1km N of Edgeworth David	Highjump Archipel- ago SE	Paz Cove NE	Paz Cove NE	Miles Island W	Miles Island W	Thomas Island E
Lithology	Olivine dolerite dyke	Olivine dolerite dyke	Olivine dolerite dyke	Olivine dolerite dyke	Olivine dolerite dyke	Olivine dolerite dyke	Olivine dolerite dyke	Olivine dolerite dyke
Classification	Group 4B	Group 4B	?Group 4B	Group 4B	Group 4B	Group 4C	Group 4C	Group 4D
SiO_2	44.60	44.90	44.70	44.70	44.60	46.80	46.60	44.00
TiO_2	3.67	4.00	3.74	3.30	3.56	2.40	2.59	3.67
Al_2O_3	15.45	15.27	15.16	15.65	15.49	16.14	15.68	14.92
Fe_2O_3	2.84	4.20	4.37	2.69	3.62	3.89	2.91	4.67
FeO	12.34	11.54	11.34	11.90	11.55	9.20	10.32	11.39
MnO	.23	.22	.22	.21	.22	.21	.21	.22
MgO	6.15	5.66	5.61	6.91	6.47	6.38	6.11	5.71
CaO	8.86	8.48	8.17	8.98	8.85	8.84	8.75	8.19
Na_2O	3.14	3.01	3.27	2.96	2.90	2.91	2.92	3.06
K_2O	.90	1.11	1.05	.79	.85	.95	.99	1.28
P_2O_5	.72	.79	.60	.62	.70	.31	.34	.67
H_2O+	-	-	-	-	-	-	-	.76
H_2O-	-	-	-	-	-	-	-	.12
CO_2	-	-	-	-	-	-	-	.39
LOI	1.18	.62	1.56	1.11	.94	1.83	1.70	-
Rest	.47	.44	.50	.46	.40	.45	.70	.41
Total	100.55	100.24	100.29	100.28	100.15	100.31	99.82	99.46
O=F,S,Cl	.12	.10	.13	.13	.09	.12	.24	.08
Total	100.43	100.14	100.16	100.16	100.06	100.20	99.58	99.38
	Trace elements in parts per million							
Ba	344	478	442	295	291	321	327	335
Rb	16	16	21	14	14	14	15	29
Sr	320	312	290	327	320	366	356	333
Pb	7	5	8	6	6	5	6	9
Th	1	<1	1	<1	<1	<1	1	3
U	1.00	<.50	<.50	1.00	.50	.50	<.50	.50
Zr	246	250	255	208	252	191	208	303
Nb	10	10	11	9	10	11	12	18
Y	46	44	47	40	44	34	36	51
La	16	16	20	15	15	15	16	35
Ce	48	44	51	40	43	35	39	79
Nd	32	31	35	28	29	24	24	43
Pr	-	-	-	-	-	-	-	-
Sc	25	25	24	25	27	26	27	32
V	251	266	263	218	236	247	261	322
Cr	77	49	67	68	71	75	72	43
Ni	67	60	58	93	82	65	55	49
Cu	55	38	42	50	48	42	42	37
Zn	112	130	127	105	115	104	107	138
Sn	-	-	-	-	-	-	-	-
Ga	21	20	21	20	21	20	21	23
As	<.50	.50	<.50	<.50	<.50	<.50	<.50	1.00
S	2370	2040	2570	2450	1770	2240	4720	1600
F	-	-	-	-	-	-	-	-
Cl	125	70	125	135	105	175	165	-

Bunger Hills Igneous Rocks

Sample number	77284741	86285657	86285812	86285818	86285833	86285839	86285840	86285971
Locality	Thomas Island E	Thomas Island E	Booth Peninsula	Booth Peninsula	Geomorfol-ogov Peninsula	Saturn Island	Saturn Island	Booth Peninsula W
Lithology	Olivine dolerite dyke	Olivine dolerite dyke	Olivine dolerite dyke	Olivine dolerite dyke	Olivine dolerite dyke	Olivine dolerite dyke	Olivine dolerite dyke	Olivine dolerite dyke
Classification	Group 4D	?Group 4D	Group 4D	Group 4D	Group 4D	Group 4D	Group 4D	Group 4D
SiO_2	44.00	46.80	45.00	44.80	44.90	44.20	43.90	44.70
TiO_2	3.71	2.97	3.89	3.91	4.00	3.70	3.77	3.97
Al_2O_3	14.91	16.44	14.17	14.20	14.33	15.01	15.10	14.43
Fe_2O_3	5.60	3.00	2.96	3.22	3.57	3.94	4.18	2.83
FeO	10.28	10.72	12.86	12.59	12.32	11.75	11.74	13.31
MnO	.21	.23	.25	.25	.25	.24	.24	.25
MgO	5.56	4.24	5.48	5.43	5.14	5.73	5.90	5.35
CaO	8.11	7.76	8.22	8.34	8.05	8.27	8.36	8.10
Na_2O	3.08	3.64	2.96	3.00	3.06	3.06	3.03	3.06
K_2O	1.29	1.73	1.39	1.36	1.45	1.25	1.17	1.46
P_2O_5	.68	.75	.76	.78	.80	.67	.63	.76
H_2O+	1.07	-	-	-	-	-	-	-
H_2O-	.26	-	-	-	-	-	-	-
CO_2	.40	-	-	-	-	-	-	-
LOI	-	1.60	1.64	1.58	1.63	1.69	1.44	1.43
Rest	.45	.44	.55	.57	.53	.51	.49	.57
Total	99.61	100.32	100.13	100.03	100.03	100.02	99.95	100.22
O=F,S,Cl	.10	.08	.14	.15	.12	.12	.12	.14
Total	99.51	100.24	100.00	99.88	99.91	99.90	99.83	100.08
	Trace elements in parts per million							
Ba	344	550	494	477	489	380	352	483
Rb	30	40	33	32	36	29	27	34
Sr	325	373	298	305	310	332	341	310
Pb	8	10	8	9	12	9	8	10
Th	2	3	2	2	2	1	<1	2
U	1.00	.50	.50	1.00	1.00	.50	<.50	<.50
Zr	306	377	340	334	355	329	305	362
Nb	19	23	20	20	20	19	18	20
Y	52	62	59	58	62	54	52	60
La	32	32	36	33	36	28	24	35
Ce	72	81	82	81	87	68	62	86
Nd	41	51	52	53	56	43	39	53
Pr	-	-	-	-	-	-	-	-
Sc	36	24	28	28	27	28	26	27
V	332	205	314	302	304	313	298	308
Cr	43	24	65	55	48	46	38	47
Ni	49	26	42	44	40	53	53	43
Cu	32	25	38	38	35	38	38	38
Zn	131	132	142	145	146	144	131	150
Sn	-	-	-	-	-	-	-	-
Ga	22	23	22	23	23	22	22	24
As	1.00	1.00	<.50	<.50	<.50	<.50	<.50	.50
S	2000	1460	2620	2830	2410	2350	2300	2730
F	-	-	-	-	-	-	-	-
Cl	-	330	190	200	175	235	220	220

Bunger Hills Igneous Rocks

Sample number	86285973	86285977	86285802	86285803	86285811	86285832	77284734	77284735
Locality	Booth Peninsula W	Booth Peninsula W	Obruchev Hills C	Obruchev Hills C	Obruchev Hills NE	Geomorfol-ogov Peninsula	Dobrowol-ski	Dobrowol-ski
Lithology	Olivine dolerite dyke	Olivine dolerite dyke	Olivine dolerite dyke	Olivine dolerite dyke	Olivine dolerite dyke	Olivine dolerite dyke	Olivine dolerite dyke	Olivine dolerite dyke
Classification	Group 4D	Group 4D	Group 4E	Group 4E	Group 4E	?Group 4E	Group 4	?Group 4
SiO_2	43.90	44.90	45.50	45.00	44.90	44.40	45.90	47.80
TiO_2	4.09	3.98	3.24	3.34	3.82	3.08	1.55	1.90
Al_2O_3	14.13	14.18	15.35	15.04	14.74	15.73	15.94	17.53
Fe_2O_3	3.49	2.13	3.98	4.79	3.75	2.77	1.74	2.54
FeO	12.81	14.02	10.40	10.16	11.85	10.84	11.11	8.93
MnO	.25	.25	.24	.24	.26	.22	.18	.15
MgO	5.47	5.43	6.92	6.71	5.97	6.45	10.55	5.82
CaO	8.27	8.32	9.29	9.03	9.00	9.51	7.64	8.55
Na_2O	2.98	2.89	2.97	2.94	3.17	3.14	2.80	3.16
K_2O	1.34	1.40	.73	.73	.82	.87	.76	1.36
P_2O_5	.75	.81	.42	.43	.49	.51	.33	.29
H_2O+	-	-	-	-	-	-	.71	1.51
H_2O-	-	-	-	-	-	-	.12	.21
CO_2	-	-	-	-	-	-	.28	.61
LOI	2.03	1.12	1.00	.82	1.12	1.75	-	-
Rest	.58	.53	.40	.29	.45	.40	.21	.21
Total	100.09	99.96	100.44	99.52	100.34	99.67	99.82	100.57
O=F,S,Cl	.15	.12	.09	.04	.10	.08	.02	.01
Total	99.94	99.83	100.35	99.49	100.24	99.59	99.80	100.56
	Trace elements in parts per million							
Ba	439	458	146	113	247	393	264	393
Rb	31	32	6	7	15	26	17	29
Sr	308	297	298	295	265	359	278	296
Pb	9	9	5	3	6	5	5	9
Th	1	3	<1	<1	<1	<1	1	2
U	<.50	1.00	.50	.50	1.00	1.00	<.50	.50
Zr	347	354	281	289	301	246	149	123
Nb	19	22	12	11	16	10	8	7
Y	58	60	49	51	60	48	30	28
La	29	32	13	12	20	15	19	13
Ce	75	77	40	43	49	40	36	29
Nd	47	50	29	30	34	28	21	16
Pr	-	-	-	-	-	-	-	-
Sc	28	31	32	32	33	29	21	26
V	332	316	309	323	330	226	87	149
Cr	53	71	104	106	120	113	37	99
Ni	44	43	69	71	58	60	252	109
Cu	39	40	45	48	44	43	23	7
Zn	152	153	113	122	135	99	98	98
Sn	-	-	-	-	-	-	-	-
Ga	23	23	23	22	24	21	16	20
As	<.50	.50	<.50	<.50	<.50	<.50	.50	.50
S	2860	2380	1810	670	1940	1640	400	200
F	-	-	-	-	-	-	-	-
Cl	235	160	85	85	185	100	-	-

Bunger Hills Igneous Rocks

Sample number	77284740	86285991	86286049	86286091	86286223	86285954	86286085	86285688
Locality	Thomas Island E	Highjump Archipel-ago SE	Miles Island W	Krylatyy Peninsula SW	Geologov Island	Lake Polyans-kogo	Krylatyy Peninsula	2km SW of Edgeworth David
Lithology	Olivine dolerite dyke	Olivine dolerite dyke	Olivine dolerite dyke	Olivine dolerite dyke	Olivine basalt dyke	Picrite basalt dyke	Picrite basalt dyke	Ankaramite dyke
Classification	Group 4	Group 4	Group 4	Group 4				
SiO_2	44.80	46.80	44.30	45.30	48.60	42.60	34.30	41.90
TiO_2	3.29	2.24	4.84	1.68	1.29	2.40	3.96	2.68
Al_2O_3	15.31	15.50	14.18	15.81	13.59	8.79	4.21	10.41
Fe_2O_3	4.06	3.20	5.03	1.75	3.62	3.46	6.89	3.98
FeO	11.29	9.65	11.79	11.45	5.67	9.47	8.75	10.42
MnO	.23	.21	.25	.19	.15	.18	.20	.20
MgO	5.21	7.23	4.72	10.70	8.95	15.59	20.60	12.41
CaO	7.97	10.29	8.03	7.73	8.35	8.78	9.53	10.10
Na_2O	3.33	2.58	3.25	2.68	2.20	2.09	.16	2.43
K_2O	1.49	.55	1.25	.65	2.27	1.47	1.69	1.06
P_2O_5	1.07	.23	.92	.27	.64	.41	.51	.39
H_2O+	.98	-	-	-	1.57	1.95	2.89	.79
H_2O-	.13	-	-	-	.11	.08	.07	.02
CO_2	.42	-	-	-	1.43	1.77	4.59	2.17
LOI	-	1.28	1.11	1.62	-	-	-	-
Rest	.39	.38	.52	.34	1.21	.70	.64	.67
Total	99.97	100.14	100.19	100.17	99.65	99.74	98.99	99.63
O=F,S,Cl	.06	.09	.14	.06	.15	.08	.10	.13
Total	99.90	100.05	100.05	100.10	99.50	99.66	98.89	99.51

Trace elements in parts per million

Ba	416	198	392	249	3720	1012	471	337
Rb	35	6	25	15	69	43	65	22
Sr	344	316	268	281	1278	517	268	629
Pb	9	2	7	6	68	11	11	5
Th	3	<1	3	<1	40	6	9	2
U	1.00	<.50	.50	.50	4.00	.50	1.00	<.50
Zr	337	131	377	132	272	201	219	216
Nb	21	8	16	6	13	47	108	32
Y	63	33	66	28	31	22	17	21
La	42	8	24	11	172	57	60	34
Ce	100	26	67	29	290	114	126	75
Nd	55	17	47	18	121	57	65	34
Pr	-	-	-	-	-	-	-	-
Sc	27	34	30	15	23	29	20	27
V	266	295	261	107	183	309	259	321
Cr	33	121	<2	205	349	734	663	669
Ni	37	65	28	271	118	503	622	339
Cu	29	55	36	27	25	70	109	88
Zn	141	94	154	105	98	112	107	114
Sn	-	-	-	-	-	-	-	-
Ga	23	20	23	16	15	16	15	20
As	1.00	<.50	<.50	.50	<.50	.50	30.00	<.50
S	1300	1770	2670	1140	1170	1330	1870	2350
F	-	-	-	-	1400	-	-	-
Cl	-	100	130	255	1380	685	290	410

Bunger Hills Igneous Rocks

Sample number	86285823	86285824	86286046	86286067	86285611	86285637	86285677	86285912
Locality	1km E of Edgeworth David	1km E of Edgeworth David	Obryvistyy Island NW	Paz Cove NE	Currituck Island N	Thomas Island SW	W of Lake Dolgoe	1km SE of Edgeworth David
Lithology	Ankaramite dyke	Ankaramite dyke	Ankaramite dyke	Ankaramite dyke	Alkali Ol basalt dyke	Alkali Ol basalt dyke	Alkali Ol basalt dyke	Alkali Ol basalt dyke
Classification								
SiO_2	43.90	42.80	41.60	42.20	46.20	47.30	46.10	45.90
TiO_2	1.82	2.85	3.50	2.63	.91	1.16	.93	1.47
Al_2O_3	7.33	10.43	9.96	10.32	11.75	16.95	12.96	13.98
Fe_2O_3	2.57	3.15	5.17	2.40	2.84	3.65	3.43	3.36
FeO	9.78	11.58	9.35	10.87	5.96	4.69	3.98	4.98
MnO	.18	.21	.19	.20	.14	.13	.14	.14
MgO	16.58	13.37	8.85	13.88	13.49	6.63	12.49	7.30
CaO	12.47	10.04	10.81	9.94	7.62	8.16	6.91	8.49
Na_2O	1.50	2.22	2.81	2.25	1.58	2.94	1.91	2.58
K_2O	.55	.87	2.12	1.13	4.30	2.34	4.89	5.14
P_2O_5	.18	.29	.70	.39	.70	.63	.95	1.19
H_2O+	.49	.68	.96	1.13	1.94	1.19	1.88	1.04
H_2O-	.05	.08	.06	.05	.08	.14	.10	.11
CO_2	1.60	.63	2.40	1.76	.34	3.18	1.68	2.61
LOI	-	-	-	-	-	-	-	-
Rest	.63	.61	.75	.73	1.52	1.05	1.58	1.77
Total	99.63	99.81	99.23	99.88	99.37	100.14	99.93	100.06
O=F,S,Cl	.09	.11	.14	.14	.19	.08	.10	.14
Total	99.54	99.70	99.08	99.74	99.18	100.06	99.83	99.91
	Trace elements in parts per million							
Ba	184	247	793	293	4840	3950	6060	6820
Rb	10	17	56	20	129	69	213	180
Sr	329	526	733	639	1892	1526	1621	2410
Pb	4	6	7	5	36	89	110	100
Th	<1	1	7	1	13	50	76	42
U	<.50	<.50	2.00	1.50	2.50	5.00	10.00	6.00
Zr	125	190	318	229	212	262	406	408
Nb	15	24	73	34	9	12	12	28
Y	16	18	32	22	29	31	39	32
La	13	22	51	32	94	226	166	194
Ce	35	49	107	69	163	370	301	334
Nd	22	30	55	40	78	146	140	142
Pr	-	-	-	-	-	-	-	-
Sc	34	26	23	24	19	22	18	21
V	286	328	237	284	153	155	126	167
Cr	1260	626	328	918	1082	20	890	360
Ni	534	375	214	363	239	58	363	84
Cu	127	83	103	65	56	15	42	48
Zn	82	110	154	101	84	81	76	94
Sn	-	-	-	-	-	-	-	-
Ga	14	20	20	19	12	15	11	13
As	<.50	<.50	.50	.50	<.50	1.50	2.00	3.50
S	1780	2150	2610	2050	3460	1230	1050	1790
F	-	-	-	700	-	-	-	-
Cl	255	340	640	335	775	1010	2070	2460

Bunger Hills Igneous Rocks

Sample number	86285917	86285918	86285921	86285922	86285957	86286055	77284730	86285919
Locality	N Taylor Islands	N Taylor Islands	N Taylor Islands	N Taylor Islands	Lake Dolgoe W	Miles Island E	SW Bunger Hills	N Taylor Islands
Lithology	Alkali Ol basalt dyke	Alkali Ol basalt dyke	Alkali Ol basalt dyke	Alkali Ol basalt dyke	Alkali Ol basalt dyke	Alkali Ol basalt dyke	Trachy-basalt dyke	Trachy-basalt dyke
Classification								
SiO_2	48.70	48.30	46.00	46.20	45.00	47.30	50.50	50.10
TiO_2	1.01	1.10	1.05	1.05	.92	1.01	1.46	1.16
Al_2O_3	13.22	14.29	11.06	11.16	12.23	12.23	17.67	15.31
Fe_2O_3	1.57	1.84	2.23	2.28	3.21	2.72	2.59	1.65
FeO	6.33	5.59	6.31	6.44	4.27	4.90	4.79	4.17
MnO	.13	.12	.13	.14	.13	.12	.13	.07
MgO	10.47	9.56	12.36	13.13	12.98	11.05	4.04	5.21
CaO	8.79	7.28	8.60	8.02	6.82	9.79	6.14	7.26
Na_2O	2.03	2.12	1.53	1.54	1.75	1.61	3.06	2.81
K_2O	3.36	4.92	3.76	3.80	4.78	3.78	5.88	5.59
P_2O_5	.64	.91	.77	.77	.95	.63	1.15	.98
H_2O+	1.67	1.45	2.04	1.79	1.84	1.68	.39	.92
H_2O-	.07	.05	.23	.07	.03	.14	.03	.18
CO_2	.79	.67	2.72	2.45	2.74	1.68	-	2.25
LOI	-	-	-	-	-	-	-	-
Rest	1.05	1.08	1.30	1.30	1.76	1.27	1.11	1.69
Total	99.83	99.28	100.09	100.14	99.41	99.91	98.94	99.35
O=F,S,Cl	.08	.06	.10	.10	.09	.13	.00	.04
Total	99.75	99.22	99.99	100.04	99.32	99.78	98.94	99.31
	Trace elements in parts per million							
Ba	3860	4240	4360	4470	7280	4510	5150	7220
Rb	114	189	142	139	213	128	213	107
Sr	893	1280	1245	1268	1507	1057	2060	4250
Pb	46	25	66	64	102	36	104	49
Th	23	58	42	42	76	36	96	55
U	4.50	7.50	5.00	6.00	9.00	5.00	11.00	6.50
Zr	234	340	328	327	392	221	468	317
Nb	13	21	13	13	12	12	25	20
Y	27	25	31	31	40	28	30	22
La	75	118	210	215	203	133	266	242
Ce	136	212	347	360	371	225	450	401
Nd	63	102	146	151	176	100	170	167
Pr	-	-	-	-	-	-	45	-
Sc	22	20	25	23	24	23	12	12
V	154	127	183	176	170	166	127	110
Cr	760	637	1104	953	1231	1043	82	207
Ni	188	194	330	376	394	112	47	180
Cu	36	46	60	60	49	29	58	76
Zn	74	71	77	84	70	65	83	88
Sn	-	-	-	-	-	-	1	-
Ga	14	14	11	12	11	11	18	16
As	<.50	<.50	.50	1.00	1.50	1.50	4.50	<.50
S	820	890	1640	1600	795	1190	-	480
F	-	-	-	-	-	1400	-	-
Cl	1620	685	855	860	2210	540	-	695

Bunger Hills Igneous Rocks

Sample number	86285920	86285949	86285952	86285687	86285931	86285878	86286230	86286285
Locality	N Taylor Islands	Lake Dolgoe E	6km SW of Dobrowol-ski	3km SW of Edgeworth David	S Taylor Islands	Moraine	Moraine	Moraine
Lithology	Trachy-basalt dyke	Trachy-basalt dyke	Trachy-basalt dyke	Trachy-andesite dyke	Trachy-andesite dyke	Bi granite	Bi-Hb granite	Bi-Hb granite
Classification						Rapakivi	Rapakivi	Rapakivi
SiO_2	48.80	49.40	51.00	53.10	53.90	69.90	65.60	67.50
TiO_2	1.23	1.26	1.42	1.45	1.50	.45	.70	.71
Al_2O_3	14.73	16.51	18.12	18.27	18.41	14.44	15.56	14.40
Fe_2O_3	2.23	3.00	2.46	2.72	3.04	.44	1.04	1.16
FeO	3.94	4.50	4.69	4.62	4.44	1.94	3.02	3.18
MnO	.07	.12	.12	.09	.09	.04	.07	.07
MgO	5.31	5.76	3.68	2.71	2.54	.99	.73	.76
CaO	7.87	6.72	5.80	5.36	5.45	1.36	2.79	2.38
Na_2O	2.62	2.65	2.94	3.44	3.67	2.83	3.00	2.89
K_2O	5.16	5.69	6.06	4.45	4.68	6.15	5.84	5.74
P_2O_5	.98	1.06	1.01	.83	.85	.14	.24	.20
H_2O+	1.49	.85	.93	.93	.52	-	-	-
H_2O-	.20	.07	.11	.06	.04	-	-	-
CO_2	3.66	.61	.36	.51	.04	-	-	-
LOI	-	-	-	-	-	1.31	.69	.86
Rest	1.54	1.07	1.26	1.03	1.06	.27	.35	.34
Total	99.83	99.27	99.96	99.57	100.23	100.26	99.63	100.19
O=F,S,Cl	.04	.04	.03	.07	.05	.00	.00	.00
Total	99.79	99.23	99.93	99.50	100.18	100.26	99.63	100.19
	Trace elements in parts per million							
Ba	6890	4390	5820	3620	4050	947	1581	1117
Rb	96	224	212	136	145	389	259	322
Sr	3410	1419	1729	1613	1635	107	176	139
Pb	39	108	109	59	51	68	42	48
Th	49	82	96	51	54	44	17	42
U	8.00	12.00	14.00	5.50	5.00	4.00	3.00	5.50
Zr	276	498	604	525	542	306	404	585
Nb	18	24	31	31	32	15	17	23
Y	20	35	36	37	37	51	54	75
La	219	203	322	177	182	54	60	94
Ce	350	353	532	328	319	106	126	200
Nd	145	146	207	116	124	40	51	78
Pr	-	-	-	-	-	-	-	-
Sc	13	14	14	18	12	7	12	11
V	118	128	150	131	121	22	32	35
Cr	215	204	81	<2	<2	2	3	<2
Ni	191	78	40	21	22	2	3	7
Cu	72	57	63	25	31	17	7	9
Zn	84	106	92	102	95	38	61	71
Sn	-	-	-	-	-	6	3	7
Ga	17	17	18	21	20	19	20	18
As	<.50	149.00	3.00	3.00	2.50	-	-	-
S	395	500	570	725	350	100	100	<100
F	-	-	-	-	-	-	-	-
Cl	770	475	165	1360	1500	-	-	-

Denman Glacier Metamorphic Rocks

Sample number	86285893	86285885	86286001	86286002
Locality	Cape Charcot	Jones Rocks	Mount Strathcona	Mount Strathcona
Lithology	Cp-Op-Qz-Pl gneiss	Bi-Pl-Qz-Kf gneiss	Gt-Bi-Pl-Kf-Qz gneiss	Gt-Bi-Pl quartzite
Classification	Depleted tonalite			
SiO_2	69.00	79.20	72.40	87.60
TiO_2	.30	.30	.50	.45
Al_2O_3	14.04	10.91	12.28	5.27
Fe_2O_3	1.01	.13	.67	.62
FeO	2.65	.52	3.25	2.34
MnO	.06	.01	.18	.06
MgO	2.10	.48	1.38	1.16
CaO	4.10	.91	1.11	.69
Na_2O	4.34	2.16	1.58	.50
K_2O	1.02	4.93	5.19	.76
P_2O_5	.05	.02	.06	.02
LOI	-	.31	.70	.60
Rest	.21	.13	.25	.10
Total	98.88	100.01	99.55	100.17
O=F,S,Cl	.00	.00	.00	.01
Total	98.87	100.01	99.55	100.16

Trace elements in parts per million

Ba	586	577	1191	84
Li	5	-	-	-
Rb	10	158	194	49
Sr	522	79	97	19
Pb	17	18	32	4
Th	<1	4	21	7
U	<.05	.50	1.00	<.50
Zr	175	145	229	162
Nb	2	6	9	7
Y	8	4	41	19
La	12	13	39	16
Ce	22	21	84	32
Nd	11	7	30	11
Sc	12	5	16	7
V	60	37	20	50
Cr	78	11	14	52
Ni	32	7	5	15
Cu	9	2	5	9
Zn	51	15	51	30
Sn	4	1	3	<1
Ga	18	13	12	7
S	100	<100	100	200

Denman Glacier Igneous Rocks

Sample number	86286030	86286031	86285888	86285890	86285793	86286006	86286013	86286014
Locality	Cape Kennedy	Cape Kennedy	Delay Point	Delay Point	Mount Strathcona	Cape Harrison	Possession Rocks	Baldwin Rocks
Lithology	Op leuco-gabbro	Op leuco-gabbro	Hb-Cp-Bi diorite	Bi-Hb diorite	Bi-Hb quartz gabbro	Gt granite gneiss	Gt-Bi granite gneiss	Cp-Op-Hb monzonite
Intrusion								David Is. batholith
SiO_2	52.80	52.00	50.20	49.40	49.20	71.30	68.60	55.60
TiO_2	.68	.90	1.87	1.89	3.13	.39	.55	1.33
Al_2O_3	19.04	18.47	17.42	16.42	16.97	13.83	15.33	16.49
Fe_2O_3	1.27	1.39	2.64	4.48	2.99	.49	.63	1.61
FeO	6.24	6.64	5.77	5.86	10.28	2.71	2.43	7.79
MnO	.12	.12	.12	.13	.21	.08	.03	.14
MgO	6.79	7.08	4.30	4.26	3.10	.29	.68	1.16
CaO	7.79	7.72	8.68	7.22	8.76	2.15	2.40	4.50
Na_2O	3.46	3.32	3.41	3.68	2.79	2.55	2.87	3.77
K_2O	.67	.69	1.52	2.48	.94	5.06	5.09	4.81
P_2O_5	.09	.14	1.25	1.32	.40	.14	.17	.68
H_2O+	-	-	-	.82	-	-	-	-
H_2O-	-	-	-	.11	-	-	-	-
CO_2	-	-	-	.32	-	-	-	-
LOI	1.26	1.57	2.31	-	1.29	.26	.58	1.09
Rest	.33	.34	.84	.94	.28	.37	.29	1.01
Total	100.54	100.38	100.33	99.33	100.34	99.62	99.65	99.98
O=F,S,Cl	.04	.04	.12	.03	.03	.00	.00	.06
Total	100.50	100.33	100.21	99.30	100.31	99.62	99.65	99.93
	Trace elements in parts per million							
Ba	539	556	1947	3840	463	1300	1090	5730
Rb	8	10	41	97	15	158	211	79
Sr	907	876	1580	1624	385	163	168	792
Pb	6	7	28	41	7	62	40	27
Th	<1	1	9	11	1	66	47	3
U	.50	1.00	1.00	2.00	<.50	1.00	1.50	.50
Zr	42	47	201	486	93	343	268	522
Nb	4	4	18	34	18	17	13	25
Y	7	8	35	58	21	102	30	39
La	18	17	128	215	15	217	102	85
Ce	29	32	266	429	33	407	253	176
Nd	11	13	105	166	17	206	88	77
Sc	19	19	24	26	36	16	8	22
V	72	90	181	176	362	6	25	<2
Cr	134	145	39	7	5	<2	10	<2
Ni	67	80	32	30	8	<2	2	<2
Cu	18	18	25	40	19	4	7	7
Zn	72	78	105	119	120	35	73	109
Sn	<1	<1	<1	2	<1	<1	<1	<1
Ga	18	19	22	20	22	20	22	23
As	-	-	-	-	-	-	-	-
S	900	900	1100	700	600	<100	<100	600
F	-	-	1600	-	-	-	-	700
Cl	-	-	-	-	-	-	-	-

Denman Glacier Igneous Rocks

Sample number	86286015	86286018	86286020	86286021	86286024	86286033	86286023	86286016
Locality	Baldwin Rocks	Baldwin Rocks W	Baldwin Rocks W	Baldwin Rocks W	Watson Bluff	Watson Bluff	Watson Bluff	Baldwin Rocks
Lithology	Ol-Cp-Op monzonite	Bi-Hb quartz monzonite	Hb-Bi quartz monzonite	Hb-Bi quartz syenite	Op-Cp-Hb syenite	Px-Bi-Hb syenite	Op-Cp-Hb quartz syenite	Trachyte dyke
Intrusion	David Is. batholith	David Is. batholith	David Is. batholith	David Is. batholith	David Is. batholith	David Is. batholith	David Is. batholith	
SiO_2	54.00	65.70	63.80	62.20	59.50	60.10	60.90	65.20
TiO_2	1.66	.76	.93	.78	.77	.67	.63	.22
Al_2O_3	15.70	14.90	14.85	16.44	17.43	18.63	18.20	15.75
Fe_2O_3	2.20	1.39	1.37	1.76	1.50	1.45	1.33	3.16
FeO	9.66	3.51	4.78	3.44	4.76	3.46	3.38	1.73
MnO	.18	.07	.09	.11	.12	.09	.09	.12
MgO	1.25	.67	.92	.73	.56	.62	.49	.21
CaO	4.61	2.46	2.72	2.17	3.13	3.27	2.93	.72
Na_2O	3.62	3.63	3.52	3.92	4.22	4.61	4.37	4.79
K_2O	4.52	5.08	5.16	6.75	5.80	5.65	6.06	5.34
P_2O_5	.77	.27	.32	.16	.19	.20	.14	.02
H_2O+	-	-	-	-	-	-	-	1.24
H_2O-	-	-	-	-	-	-	-	.41
CO_2	-	-	-	-	-	-	-	1.39
LOI	.93	.75	.90	.88	.65	.67	.61	-
Rest	.82	.57	.51	.67	.90	.81	.81	.25
Total	99.92	99.76	99.87	100.01	99.53	100.23	99.94	100.55
O=F,S,Cl	.03	.04	.01	.03	.02	.02	.00	.01
Total	99.88	99.72	99.86	99.99	99.51	100.21	99.93	100.54
	Trace elements in parts per million							
Ba	4530	1923	1908	1611	3010	3680	3400	290
Rb	71	164	162	180	104	106	109	141
Sr	607	305	309	289	516	649	568	52
Pb	26	51	53	52	56	55	59	15
Th	3	37	41	96	111	39	76	30
U	<.50	5.00	4.00	3.50	2.50	2.00	2.50	2.50
Zr	601	711	806	1030	1082	838	969	541
Nb	34	39	51	30	48	33	38	132
Y	45	50	56	34	52	35	38	43
La	91	139	146	518	744	301	417	143
Ce	187	277	305	894	1004	516	747	230
Nd	89	112	125	284	393	182	249	83
Sc	26	12	13	19	12	12	12	2
V	<2	25	32	7	6	8	5	1
Cr	<2	<2	<2	<2	<2	<2	<2	<2
Ni	<2	<2	<2	<2	<2	<2	<2	<2
Cu	10	5	6	2	4	2	3	6
Zn	137	87	110	70	121	99	89	73
Sn	<1	2	2	<1	<1	<1	<1	-
Ga	25	23	25	19	25	26	24	20
As	-	-	-	-	-	-	-	<.50
S	700	100	200	200	100	100	100	145
F	-	900	-	400	300	300	-	-
Cl	-	-	-	-	-	-	-	90

Denman Glacier Igneous Rocks

Sample number	86286017	86285892	86285894	86286022	86286029	86286010	86286028	86286236
Locality	Baldwin Rocks	Cape Charcot	Cape Charcot	SW Baldwin Rocks	Cape Kennedy	Moraine (Cape Jones N)	Moraine (Cape Jones)	Moraine (5km S of Dobrowols)
Lithology	Trachyte dyke	Alkali gabbro dyke	Alkali gabbro dyke	Px-Bi-Hb-Pl granulite	Px-Pl granulite	Metabasalt	Metabasalt	Metabasalt
Intrusion				Metadyke	Metadyke			
SiO_2	64.20	46.90	46.20	47.40	49.30	48.70	48.80	45.70
TiO_2	.21	1.70	1.59	2.83	2.50	2.13	2.42	3.44
Al_2O_3	15.20	14.48	13.68	16.27	15.58	13.68	13.74	14.65
Fe_2O_3	3.90	2.01	2.39	1.82	5.06	5.64	5.05	4.39
FeO	1.98	7.89	7.68	9.72	7.73	7.34	8.69	10.00
MnO	.12	.16	.16	.15	.18	.19	.21	.22
MgO	.30	8.79	10.58	5.35	5.05	6.24	5.60	5.37
CaO	.72	8.88	9.03	7.91	8.02	9.72	6.27	7.81
Na_2O	4.51	2.58	2.28	4.16	3.22	1.39	2.24	3.30
K_2O	5.13	2.31	2.14	1.47	.90	.74	3.92	1.16
P_2O_5	.02	.61	.57	1.08	.74	.19	.24	.68
H_2O+	1.09	1.08	1.17	-	-	2.88	2.30	2.55
H_2O-	.73	.23	.19	-	-	.10	.03	.13
CO_2	1.15	1.23	1.10	-	-	.65	.15	.22
LOI	-	-	-	1.69	1.38	-	-	-
Rest	.25	.90	.88	.42	.54	.31	.40	.31
Total	99.51	99.75	99.64	100.27	100.20	99.90	100.06	99.93
O=F,S,Cl	.01	.07	.07	.04	.07	.05	.09	.03
Total	99.50	99.68	99.57	100.23	100.13	99.85	99.96	99.89
	Trace elements in parts per million							
Ba	334	3320	3100	963	1485	128	269	538
Rb	130	53	50	30	12	26	56	38
Sr	52	1146	1067	605	816	313	241	262
Pb	17	43	44	14	14	9	6	8
Th	28	12	13	5	3	1	3	3
U	2.00	1.50	2.00	1.00	.50	<.50	.50	.50
Zr	525	225	217	297	153	139	172	240
Nb	127	24	23	24	21	9	12	10
Y	42	31	29	37	36	31	39	46
La	142	90	92	99	64	15	24	21
Ce	226	170	165	150	123	34	52	55
Nd	83	78	75	75	64	18	27	34
Sc	2	24	26	27	20	42	39	30
V	1	216	204	185	170	350	336	260
Cr	<2	366	491	37	21	130	65	74
Ni	<2	155	218	53	38	36	20	54
Cu	4	57	54	12	28	72	40	34
Zn	93	84	84	125	127	107	114	123
Sn	-	-	-	-	-	-	-	-
Ga	19	15	15	18	20	19	22	19
As	<.50	<.50	<.50	<.50	<.50	<.50	2.50	<.50
S	130	1140	1090	800	1400	1100	1900	700
F	-	-	-	-	-	-	-	-
Cl	80	570	505	-	155	-	-	-

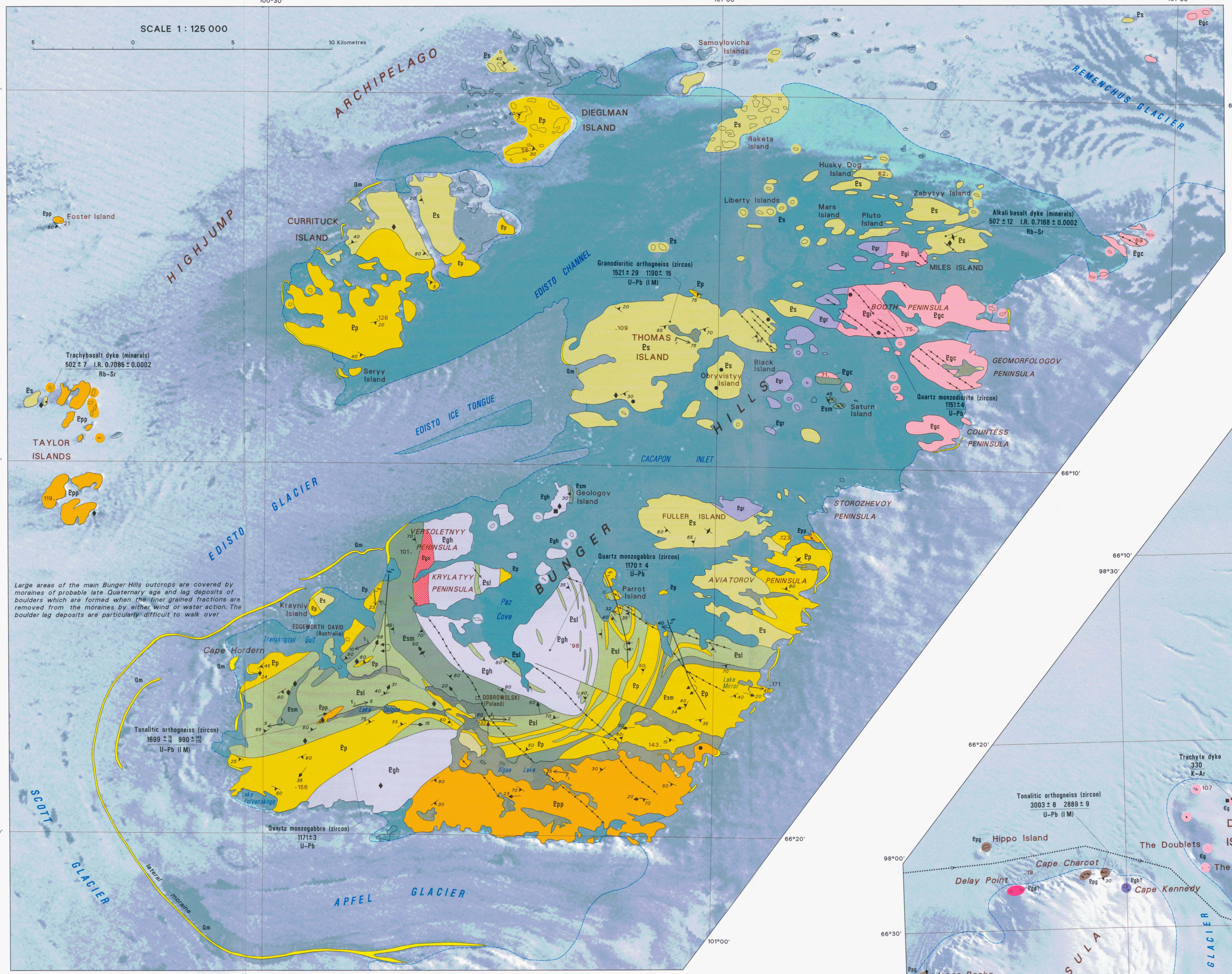

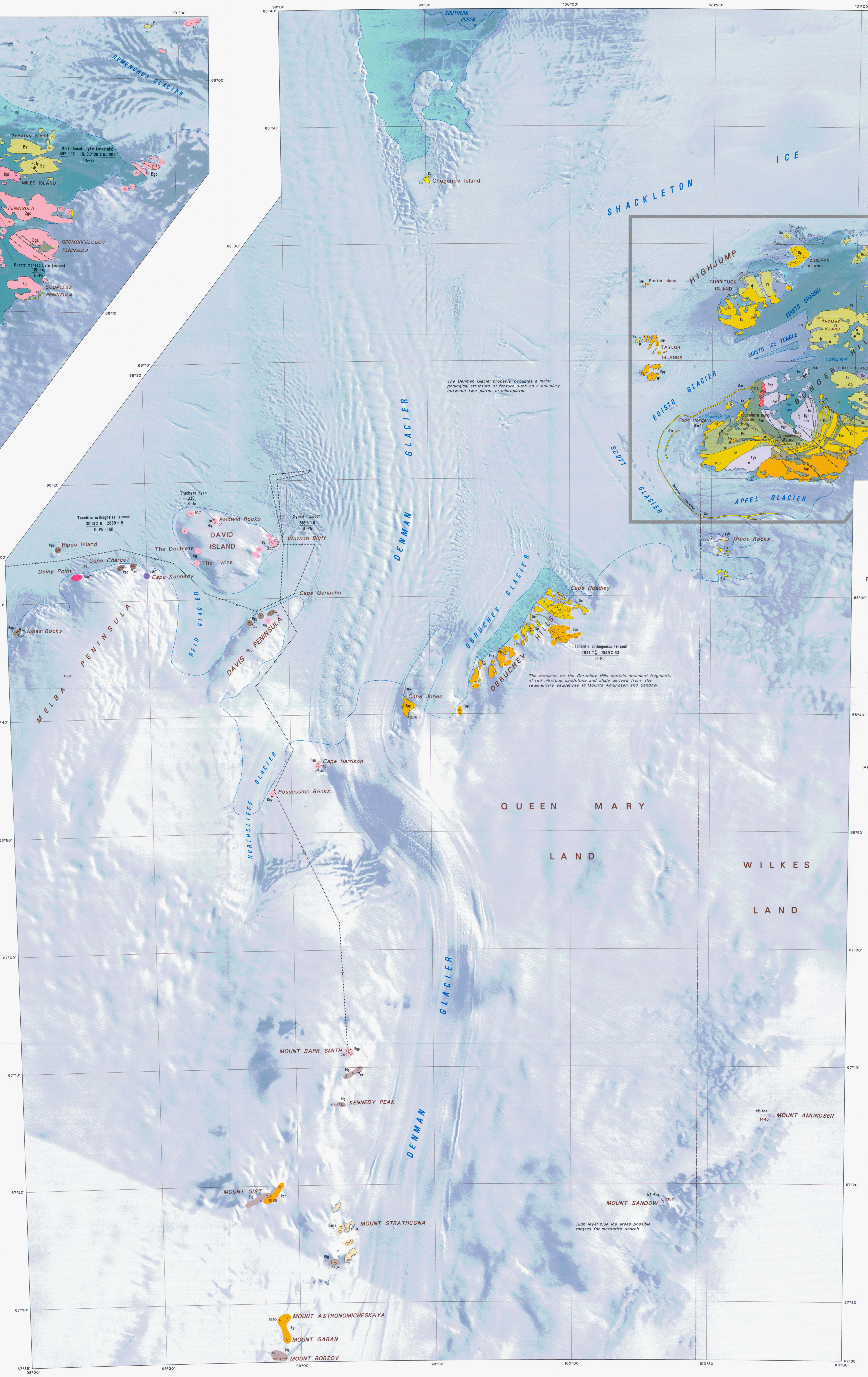

BEDROCK GEOLOGY OF THE BUNGER HILLS–DENMAN GLACIER REGION

AUSTRALIAN ANTARCTIC TERRITORY

by J.W. Sheraton and R.J. Tingey

1994

SCALE 1:250 000

5 0 5 10 15 20 25 Kilometres

LAMBERT CONFORMAL CONIC PROJECTION WITH TWO STANDARD PARALLELS (66°00'S and 67°20'S)

LATITUDE OF ORIGIN: 0°, LONGITUDE OF ORIGIN: 100°

GEOLOGY
1911–14 by A.D.Watson, Australasian Antarctic Expedition (AAE), Leader Sir Douglas Mawson
1956–57 by M.G.Ravich, D.S.Solov'ev and others, Soviet Antarctic Expeditions (SAE)
1986 by P.Ding[1], P.Marsh[2], J.W.Sheraton[3], K.Stüwe[2], R.J.Tingey[3], C.J.Wilson[2]
1 University of Adelaide, 2 University of Melbourne, 3 Australian Geological Survey Organisation
Compiled 1990–91 by J.W.Sheraton
Project initiation and map concept by R.J.Tingey

CARTOGRAPHY
Design and production by L.M.Highet, D.J.Kennedy and J.A.Gallagher, Cartographic Services Unit, AGSO, using Intergraph graphics applications

IMAGE PROCESSING
Digital base created by P.Bierwirth, AGSO, and N.Young, Australian Antarctic Division, from Multi Spectral Scanner (MSS) data from the LANDSAT scenes indicated on the key map below using AGSO's International Imaging System (IIS)

LANDSAT (originally ERTS) imagery courtesy of United States National Aeronautics and Space Administration Distributed through the United States Geological Survey's EROS Data Center and by the EOSAT company

This map is accompanied by a text publication: Sheraton, J.W., Tingey, R.J. Oliver, R.L., and Black, L.P., 1994, Geology of the Bunger Hills–Denman Glacier Region, Antarctica. Australian Geological Survey Organisation, *Bulletin 244*

It is recommended that this map be referred to as: Sheraton, J.W., and Tingey, R.J., 1994 – *Bedrock Geology of the Bunger Hills–Denman Glacier Region* (1 : 250 000 scale map), Australian Geological Survey Organisation, Canberra

Printed by Mercury–Walch Pty Ltd, Hobart, Australia

Published by the Australian Geological Survey Organisation, Department of Primary Industries and Energy, Canberra. Issued under the authority of the Minister for Primary Industries and Energy

SATURN ISLAND

THE BUNGER HILLS–DENMAN GLACIER REGION

The Bunger Hills–Denman Glacier region was first visited in November 1912 by a sledging party from the Australasian Antarctic Expedition's Western Base on the western edge of the Shackleton Ice Shelf. Frank Wild led the sledging party along the route indicated on the map in order to explore the country east of the Western Base. The severely crevassed and broken surface of the Denman Glacier near David Island proved impassable and the party turned south and reached Mount Barr–Smith. The outcrops now known as the Bunger Hills were sighted from Watson Bluff and named the Hordern Islands (later changed to Cape Hordern); Mounts Amundsen, Sandow, and Strathcona were sighted from Mount Barr–Smith.

The Bunger Hills were first visited in 1947 during "Operation Highjump" led by Admiral Richard E. Byrd USN, the largest ever Antarctic expedition. They are named after Lieutenant Commander Bunger USN who landed his Martin Mariner seaplane on an area of seawater near Thomas Island. Originally named the Bunger Oasis by the USN's public relations unit who applied flamboyant terms such as "polar fairyland" and "Shangri–la"; a stark contrast to the bleak, windy conditions experienced by the 1986 ANARE party. Bunger and his crew collected some rock specimens and in the follow up "Operation Windmill" in 1948 a party was landed by helicopter on Thomas Island to establish survey control for the aerial photography acquired during "Highjump".

The Russian (formerly Soviet) Antarctic Expedition (SAE) established Mirny Station near the western edge of the Shackleton Ice Shelf in the early 1950s. The Bunger Hills–Denman Glacier region was an obvious target for investigation and the SAE made wide ranging geological, geophysical and survey traverses during this decade. A permanent station (Oasis) was built on the northern shore of Algae Lake in 1956 and it was renamed Dobrowolski when transferred to Polish control in 1959.

The fieldwork for the investigations described in the accompanying AGSO Bulletin was done between mid January and early March 1986. Previous SAE studies provided an informative basis for these investigations. The 1986 ANARE party was equipped with two Hughes 500 and one Bell 206 Jet Ranger helicopters, and used them to establish the Edgeworth David summer base camp on the eastern shore of Transkriptsii Gulf in the southwest of the Bunger Hills and to make geological traverses from the base. The SAE had acquired good quality aerial photography in the 1950s but this was unavailable to the 1986 ANARE field geologists. However the excellent SAE published 1 : 50 000 map sheets enabled them to accurately locate themselves to within 50m on the ground. Black and white and colour aerial photography was acquired during the 1986 season by 2 x 70mm cameras mounted in a helicopter. Several black and white films were processed at the field base and some prints became available late in the season.

This map presents geological information on a base map derived from Landsat imagery which provides a graphic and appropriate impression of the terrain from which the bedrock outcrops protrude.

LANDSAT IMAGERY KEY

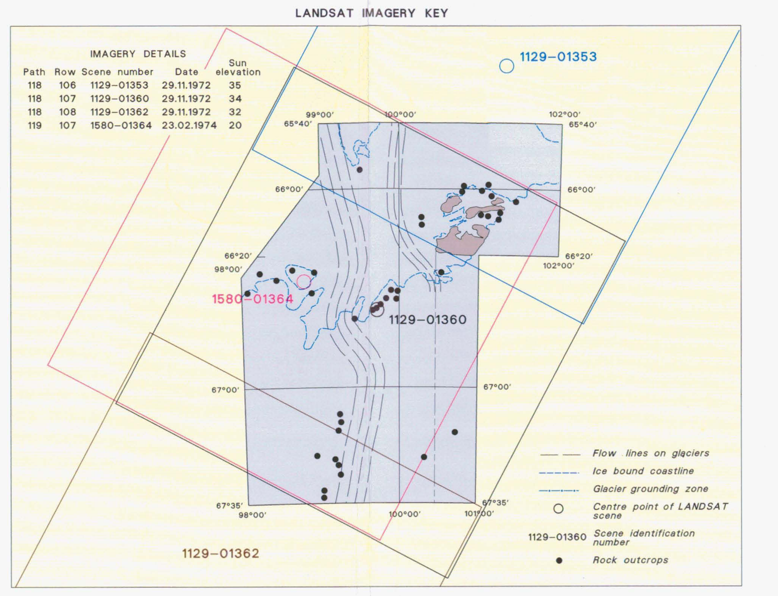

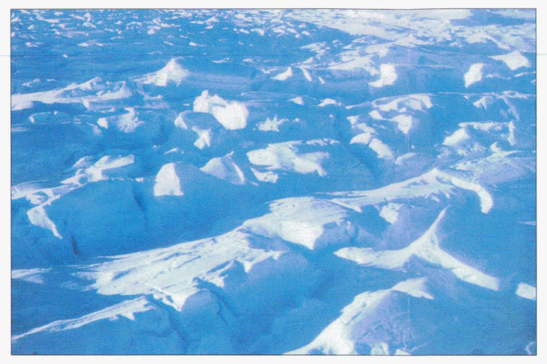

DENMAN GLACIER

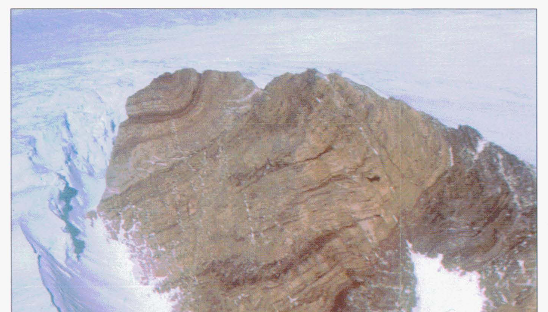

MOUNT SANDOW

ICE NOMENCLATURE

DIGITAL DATA

LEGEND

CAINOZOIC	QUATERNARY	Qm	Moraines, mostly ice–cored on tops or flanks of glaciers
PALAEOZOIC	CARBONIFEROUS?	■	Trachyte dykes (K–Ar age 330Ma)
	CAMBRIAN	◆	Alkaline mafic dykes (alkali basalt, trachybasalt, and trachyandesite: Rb–Sr isochron age 502 ± 10Ma)
	CAMBRIAN	Єg	Clinopyroxene–orthopyroxene–hornblende syenite, quartz syenite, and monzonite, biotite–hornblende quartz monzonite of David Island (zircon U–Pb age 516 ± 1.5Ma)
PROTEROZOIC	NEOPROTEROZOIC –CAMBRIAN	NP–Єss	Sandow Group: quartzitic and arkosic sandstones; subordinate conglomerate, siltstone, argillite, and metabasalt
		Pgm?	Biotite–hornblende quartz gabbro, clinopyroxene–biotite–orthopyroxene quartz monzodiorite of Mount Strathcona
		Pgd?	Hornblende–biotite–clinopyroxene diorite of Delay Point
		Pgb?	Biotite–orthopyroxene gabbro (leuconorite) of Cape Kennedy
		Pgg	Gneissose biotite and biotite–garnet granite
		Pgt	Porphyritic garnet–orthopyroxene–biotite tonalite and granodiorite
		Ppg	Clinopyroxene–biotite–orthopyroxene–quartz–feldspar gneiss and hornblende–biotite quartz–feldspar gneiss (tonalitic to granitic orthogneiss); minor metasediments and mafic to ultramafic granulite
		Plg	Layered garnet–biotite–quartz–feldspar gneiss, pelitic and psammitic gneiss (sillimanite–garnet–biotite–quartz–feldspar gneiss and impure quartzite); minor orthopyroxene–biotite–quartz–feldspar gneiss
			Major dolerite dykes (numerous smaller dykes, of at least four distinct suites, are also present in outcrops east of the Denman Glacier: mean Sm–Nd and Rb–Sr isochron age 1140Ma)
		●	Folded mafic granulite dykes
		Pgc	Hornblende–clinopyroxene–orthopyroxene granite
		Pgi	Hornblende–clinopyroxene–orthopyroxene quartz monzodiorite and quartz monzonite (zircon U–Pb age 1151±4Ma)
		Pgh	Hornblende–clinopyroxene–orthopyroxene quartz gabbro and quartz monzogabbro (zircon U–Pb age 1171±4Ma)
		Pgo	Garnet–orthopyroxene granite
		Pgr	Biotite–clinopyroxene–orthopyroxene gabbro and quartz gabbro
		Pp	Orthopyroxene–quartz–feldspar gneiss (tonalitic to granitic orthogneiss); minor biotite–garnet–quartz–feldspar gneiss, metasediments, and mafic granulite
		Ppp	Orthopyroxene–quartz–plagioclase gneiss (tonalitic orthogneiss); minor granitic orthogneiss, biotite–garnet–quartz–feldspar gneiss, metasediments, and mafic granulite
		Ps	Layered biotite–garnet–quartz–feldspar gneiss and pelitic gneiss; subordinate orthopyroxene–quartz–feldspar gneiss and mafic granulite; minor psammitic gneiss
		Psm	Migmatitic pelitic gneiss (biotite–sillimanite–garnet–quartz–feldspar cordierite gneiss); minor biotite–garnet–quartz–feldspar gneiss, orthopyroxene–quartz–feldspar gneiss, and mafic granulite
		Psl	Layered biotite–garnet–quartz–feldspar gneiss; subordinate pelitic and psammitic gneiss, orthopyroxene–quartz–feldspar gneiss, and mafic granulite; rare calc–silicate rocks

Geological boundary

Geological boundary, position approximate

Lineament

Rock outcrop–absence of geological colour indicates outcrop has not been visited

F_2 40 Plunge of F_2 fold axes

F_3 32 Overturned antiform showing plunge

F_3 32 Overturned synform showing plunge

F_3 folding episode

40 Strike and dip of foliation

Vertical foliation

23 Trend and plunge of lineation

Selected structural data after Ding and James, 1991

Where multiple structural elements have been observed at a single locality symbols are combined on the map

.1445 Elevation in metres

Sub–territorial boundary

Coastline

Ice bound coastline

Grounding zone of glacier

Route of 1912 sledging party – Australasian Antarctic Expedition

GEOCHRONOLOGY

1171± 3 Age in Ma

U–Pb Isotopic system

(I M) Ion microprobe

Ar– Argon K–Potassium Pb– Lead

Rb– Rubidium Sr– Strontium U– Uranium

I.R. 0.7085 ± 0.0002 Initial ratio $^{87}Sr/^{86}Sr$

MAP LOCALITY

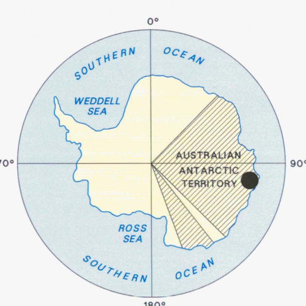

INDEX TO 1:1 000 000 MAP SHEETS

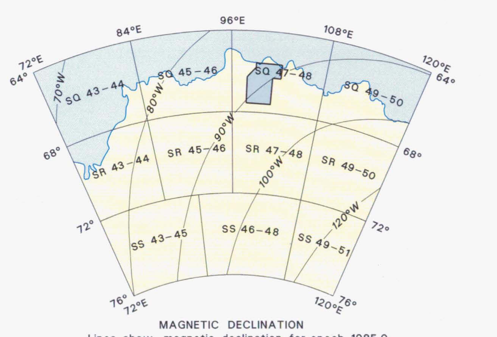

MAGNETIC DECLINATION

BEDROCK GEOLOGY OF THE BUNGER HILLS–DENMAN GLACIER REGION

AUSTRALIAN ANTARCTIC TERRITORY

FIRST EDITION 1994